

**Investigation of Bio-MOFs for Energetic and Biomedical Applications: From an Atomic
Point of View**

by

İlknur Eruçar Fındıkçı

A Dissertation Submitted to the
Graduate School of Sciences and Engineering
in Partial Fulfillment of the Requirements for
the Degree of

Doctor of Philosophy

In

Chemical and Biological Engineering



August, 2016

**Investigation of Bio-MOFs for Energetic and Biomedical Applications: From an Atomic
Point of View**

Koç University

Graduate School of Sciences and Engineering

This is to certify that I have examined this copy of a doctoral dissertation by

İlknur Eruçar Fındıkçı

and have found that it is complete and satisfactory in all respects,
and that any and all revisions required by the final
examining committee have been made.

Committee Members:

Assoc. Prof. Dr. Seda Keskin Avcı

Assist. Prof. Dr. Alper Uzun

Assoc. Prof. Dr. E. Murat Sözer

Prof. Dr. Ş. Birgül Tantekin Ersolmaz

Prof. Dr. M. Göktuğ Ahunbay

Date: _____

*To my beloved mom and father,
Selma-Necmi Eruçar
and
Sinan Fındıkçı
for always standing behind me with their love and support.*

ABSTRACT

Metal organic frameworks (MOFs) offer a great promise for gas storage and separation applications since they have large surface areas, low densities, well-defined pores and tailorable structural properties. Recently, a new group of MOFs called bio-MOFs which are composed of bio-compatible metal cations and organic linkers such as amino acids, nucleobases and sugars has been synthesized. Due to their permanent porosity and chemical functionality, bio-MOFs are ideal materials for gas separation and biomedical applications. However, research on bio-MOFs is just starting and there is a lack of information about the adsorption and transport properties of guest molecules within the pores of bio-MOFs. Molecular level understanding of properties of bio-MOFs is highly useful to accelerate the design and development of these new materials.

In this thesis, potentials of bio-MOFs in energetic applications for separation of gas mixtures (CO_2/N_2 , CO_2/H_2 , CO_2/CH_4 and CH_4/H_2) were investigated. Separation of these gas mixtures has economic and environmental impacts. CO_2/CH_4 and CO_2/N_2 separations are important for natural gas purification and flue gas separation. CO_2/H_2 and CH_4/H_2 separations are important for H_2 recovery from refineries. Atomically-detailed simulations were performed to assess adsorption-based and membrane-based gas separation performances of 10 different bio-MOFs. A good agreement was found between experiments and molecular simulations for single-component adsorption isotherms of several gases in different bio-MOFs. Adsorption selectivity, diffusion selectivity, membrane selectivity and gas permeability of MOFs were calculated using atomically-detailed simulations to identify the most promising adsorbent and membrane materials. Gas separation performances of bio-MOFs were compared with those of various MOFs, zeolites and polymers. Membrane selectivity and gas permeability of bio-MOFs were computed considering flexibility of the structures in molecular simulations for the first time in the literature. The permeability and selectivity predictions obtained from molecular simulations were then compared with the data of experimentally fabricated bio-MOF membranes. A good agreement between molecular simulations and experiments for bio-MOF-1 membrane was found. The effects of temperature and pressure on the selectivity were also investigated. Performances of two promising bio-MOFs as fillers in polymers were investigated for mixed matrix membrane (MMM) applications. Bio-MOFs enhanced the CO_2 permeability of pure polymer without making any significant change in the CO_2 selectivity when they were incorporated into a widely studied polymer, Matrimid. Results showed that several bio-MOFs outperform widely studied MOFs

and zeolites both in adsorption-based and membrane-based gas separations. Bio-MOF-1, bio-MOF-11 and bio-MOF-12 were identified as promising adsorbents and membranes especially for natural gas purification.

In the second part of this thesis, molecular simulations were performed to investigate storage and release of an analgesic and anti-inflammatory drug, ibuprofen and two cosmetic molecules, caffeine (lipo-reducer) and urea (hydrating agent) in bio-compatible MOFs. First, the results of molecular simulations were compared with the experimentally available data for ibuprofen, caffeine and urea uptakes of MOFs. Motivated from the good agreement between molecular simulations and experiments, molecular simulations were extended for 24 different bio-compatible MOFs and their ibuprofen, caffeine and urea storage performances were predicted. Bio-MOF-100 and MOF-74 material series were identified as promising candidates for drug/cosmetic molecule storage. These bio-compatible MOFs outperformed widely studied drug storage materials. Diffusion of drug molecules in bio-compatible MOFs using molecular dynamics simulations was investigated considering the flexibility of the MOFs and the presence of water for the first time in the literature. Slow diffusion of drug molecules in MOFs' pores suggested that MOFs can be strong alternatives to traditional nanoporous materials for drug storage and delivery.

This study provides information about the adsorption and diffusion properties of gas and drug molecules in bio-MOFs. Results showed that bio-MOFs can be promising materials for adsorption-based and membrane-based gas separations and for drug storage and delivery applications.

ÖZETÇE

Metal organik yapılar (MOFlar) geniş yüzey alanlarına, düşük yoğunluklara, iyi tanımlanmış gözeneklere ve ayarlanabilir yapısal özelliklere sahip olduklarından dolayı gaz depolama ve ayırma uygulamaları için oldukça umut vaat ederler. Yakın zamanda, yeni bir MOF grubu olan biyo-MOFlar, biyolojik-uyumlu metal iyonları ve aminoasitler, nükleobazlar ve şekerler gibi organik bağlayıcılar kullanılarak sentezlenmiştir. Biyo-MOFlar kalıcı gözeneklilikleri ve kimyasal fonksiyonellikleri sebebi ile gaz ayırma uygulamaları ve biyomedikal uygulamalar için potansiyel malzemelerdir. Fakat biyo-MOF araştırmaları henüz başlangıç aşamasındadır ve biyo-MOFların gözenekleri içindeki misafir moleküllerinin adsorpsiyonu ve taşınım özellikleri hakkında bilgi eksikliği vardır. Biyo-MOFların özelliklerinin moleküler düzeyde anlaşılması, bu malzemelerin tasarımını ve gelişimini hızlandırmak için oldukça yararlı olacaktır.

Bu tezde, ilk olarak biyo-MOFların enerji uygulamalarındaki potansiyelleri gaz karışımlarının (CO_2/N_2 , CO_2/H_2 , CO_2/CH_4 ve CH_4/H_2) ayırımı için incelenmiştir. Bu gazların ayrılması ekonomik ve çevresel öneme sahiptir. CO_2/CH_4 ve CO_2/N_2 ayırmaları doğal gazın saflaştırılması ve baca gazı ayırımı için önemlidir. CO_2/H_2 ve CH_4/H_2 ayırmaları rafinerilerden H_2 kazanımı için önemlidir. Bu çalışmada 10 farklı biyo-MOFun adsorpsiyon ve membran-temelli gaz ayırma performanslarını değerlendirmek için atomik düzeyde detaylı simülasyonlar yapılmıştır. Deneyler ile moleküler simülasyonlar farklı biyo-MOFlar içindeki çeşitli gazların adsorpsiyon izotermeleri için iyi bir uyum göstermiştir. MOFların adsorpsiyon seçiciliği, difüzyon seçiciliği, membran seçiciliği ve gaz geçirgenliği potansiyeli yüksek adsorbent ve membran malzemelerini belirleyebilmek için atomik düzeyde detaylı simülasyonlar kullanılarak hesaplanmıştır. Biyo-MOFların gaz ayırma performansları çeşitli MOFların, zeolitlerin ve polimerlerinki ile karşılaştırılmıştır. Biyo-MOFların membran seçiciliği ve gaz geçirgenliği moleküler simülasyonlarda yapıların esnekliği göz önüne alınarak literatürde ilk kez hesaplanmıştır. Moleküler simülasyonlar ile tahmin edilen geçirgenlik ve seçicilik değerleri deneysel olarak sentezlenmiş biyo-MOF membranların sonuçları ile karşılaştırılmıştır. Biyo-MOF-1 membranı için deneyler ile moleküler simülasyonlar oldukça yakın sonuç vermiştir. Gaz seçiciliğinde sıcaklık ve basıncın etkileri ayrıca araştırılmıştır. Potansiyeli yüksek olan iki biyo-MOF malzemesinin polimer membranlardaki dolgu performansı karışık yataklı membran (MMM) uygulamaları için incelenmiştir. Biyo-MOFlar, yaygın olarak çalışılan polimer membrana (Matrimid)

eklendiklerinde, polimerin CO₂ seçiciliğinde önemli bir değişiklik yapmadan saf polimerin CO₂ geçirgenliğini arttırmıştır. Sonuçlar adsorpsiyon ve membran-temelli gaz ayırmada birkaç biyo-MOFun yaygın olarak çalışılan MOFlardan ve zeolitlerden üstün olduğunu göstermiştir. Biyo-MOF-1, biyo-MOF-11 ve biyo-MOF-12 özellikle doğal gazın saflaştırılması için potansiyeli yüksek adsorbentler ve membranlar olarak belirlenmiştir.

Tezin ikinci kısmında, biyolojik-uyumlu MOFlarda analjezik ve antiinflamatuvar bir ilacın, ibuprofenin, ve iki kozmetik molekülünün, kafein (yağ-giderici) ve ürenin (hidratlaştıran etken), depolanmasını ve salınımını araştırmak için moleküler simülasyonlar yapılmıştır. İlk olarak, moleküler simülasyonların sonuçları MOFların ibuprofen, kafein ve üre depolamaları için mevcut deneysel veriler ile karşılaştırılmıştır. Deneyle moleküler simülasyonlar arasındaki iyi uyumdan ötürü, moleküler simülasyonlar 24 farklı biyolojik-uyumlu MOF için genişletilmiştir ve onların ibuprofen, kafein ve üre depolama performansları tahmin edilmiştir. Biyo-MOF-100 ve MOF-74 malzeme serileri ilaç/kozmetik molekül depolama için potansiyel adaylar olarak belirlenmiştir. Bu biyolojik-uyumlu MOFlar, yaygın olarak çalışılan ilaç depolama malzemelerini performans olarak geçmiştir. Biyolojik-uyumlu MOFlar içindeki ilaç moleküllerinin difüzyonu moleküler dinamik simülasyonları kullanılarak, MOFların esnekliği ve suyun varlığı göz önünde bulundurularak literatürde ilk kez araştırılmıştır. İlaç moleküllerinin MOFların gözenekleri içindeki yavaş difüzyonu MOFların ilaç depolama ve salınım uygulamaları için geleneksel nanogözenekli malzemelere göre güçlü birer alternatif olduklarını göstermiştir.

Bu çalışma, biyo-MOFların gözenekleri içindeki gaz ve ilaç moleküllerinin adsorpsiyon ve difüzyon özellikleri hakkında bilgi sağlamaktadır. Sonuçlar, bu malzemelerin hem adsorpsiyon ve membran-temelli gaz ayırma işlemleri için hem de ilaç depolama ve salınım uygulamaları için potansiyeli yüksek malzemeler olduklarını göstermiştir.

ACKNOWLEDGEMENTS

Doktora sürecim boyunca pek çok mükemmel insanı tanıma fırsatım oldu. Her birine bu satırlarda, kendi ana dilimde en içten şekilde teşekkür etmek istiyorum.

Öncelikle tez danışmanım olan değerli hocam Doç. Dr. Seda Keskin Avcı'ya teşekkürlerimi sunmak istiyorum. Kendisinin ilk doktora öğrencisi olmanın onurunu taşıyorum. Birlikte geçirdiğimiz altı yıl boyunca kendisinden çok şey öğrendim. Her zaman anlayışlı, güler yüzlü ve içten tavırları ile yardımına hazırды. Her zaman yanımda olmanızı temenni ediyorum. Doktora sürecimde gerek fikirlerinizle, gerekse içten duruşunuzla yanımda olduğunuz için sonsuz teşekkürlerimi sunuyorum. NEMO'nun bir parçası olduğum için çok şanslıyım. O kadar uzun zaman olmuş ki şu an ayrılacak olmak beni üzüyor. Sizden aldığım ilham ile yoluma devam edip ben de kendi öğrencilerimi yetiştirmek için sabırsızlanıyorum. Umarım ben de onlara sizin gibi mükemmel bir danışmanlık yapabilirim. Bu bayrağı sizden teslim aldığım için çok mutluyum.

Tez jürimde yer alan sevgili hocam, Doç. Dr. Alper Uzun'a en içten teşekkürlerimi sunmak istiyorum. Her zaman benim potansiyelime inandığı ve sorularıma en içten şekilde yanıt verdiği için çok teşekkür ediyorum. Tez jürimde olan değerli hocam Doç. Dr. Murat Sözer'e çok teşekkür ediyorum. Her zaman motive edici, içten dilekleri ile yanımda oldu. Daha iyi sunum yapabilmem ve kendimi geliştirebilmem için değerli fikirlerinden yardım aldım. Bu süreçte sizinle çalıştığım için çok şanslıyım. Tez jürimde olmayı kabul eden İstanbul Teknik Üniversitesi'ndeki değerli hocalarım Prof. Dr. Ş. Birgül Tantekin Ersolmaz'a ve Prof. Dr. M. Göktuğ Ahunbay'a çok teşekkür ediyorum.

Doktora sürecim boyunca Koç Üniversitesi'nde çok kıymetli hocalar ile çalışma fırsatı buldum. Sevgili hocam Burak Erman'a sonsuz teşekkürlerimi sunuyorum. Burak Hocam'dan aldığım ilk Termodinamik dersinde kendisinden ders dinleyecek olmanın verdiği heyecanla odaklanamadığımı hatırlıyorum© Ne zaman işin içinden çıkmadığım bir problem olsa sorabildiğim, her zaman bana temel kaynakları öneren kıymetli Hocam'a çok teşekkür ediyorum. Yine doktora dönemimde ders alarak tanıdığım sevgili Levent Hocam'a çok teşekkür ediyorum. Ders anlatış şekli, konuyu mükemmel şekilde özetlemesi ve bağlantı kurması ile ileride hazırlamayı planladığım derslerde bana ilham vermiştir.

Doktora dönemim boyunca 2211-Yurt İçi Doktora Burs Programı kapsamında sağladığı destekten ötürü TÜBİTAK (Türkiye Bilimsel ve Teknolojik Araştırma Kurumu) Bilim İnsanı Destekleme Daire Başkanlığı'na teşekkür ederim. 2211-C Öncelikli Alanlar Doktora Bursiyeri olmanın onurunu taşıyorum.

Sevgili NEMO'nun üyelerine teşekkür etmek istiyorum. Sadece iki kişi olarak başladığımız bu maceramıza katılan ama şu an doktoralarını yurt dışında yapan tüm geçmiş NEMO üyelerine öncelikle teşekkür etmek istiyorum. Özellikle Tuğba'yı çok özlediğimi belirtmek istiyorum. Birlikte geçirdiğimiz güzel günlerimiz hep aklımda. Aydın, Yeliz ve Tuğba ile birlikte olan çalışmalarımızı da hiç unutmadım. İyi ki bu yolda sizi tanıdım. Çiğdem'ciğim sen benim her zaman küçük kız kardeşim olarak kalacaksın. Melek kalbin ile her zaman herkesin yardımına koşan NEMO'nun gülen yüzüsün. Bu yıl aramıza katılan ve çok sevdiğim Pelin Kınık'a, Burak Koyutürk'e, Zeynep Sümer'e ve Vahid Nozari'ye çok teşekkür ediyorum. Hepsini öyle çok seviyorum ki, iyi ki varsınız. Her zaman yanımda olduğunuz için çok teşekkür ediyorum. Birlikte geçirdiğimiz güzel günlerimizi, konferans

maceralarımızı hep hatırlayacağım. Neyse ki bu yıl da birlikte Amerika'ya gidiyoruz☺ Yaşasın!

Bu süreçte tanıdığım ve çok sevdiğim değerli arkadaşlarıma da çok teşekkür etmek istiyorum. Elda'cığım neşeli sohbetlerimiz için ve her zaman bana verdiği destek için çok teşekkür ediyorum. Sevgili Benay'a, Didar'a ve Özge'ye teşekkür ediyorum. Benay'cığım her zaman gülen yüzün ile NEMO'nun yanında oldun. Birlikte çok güzel zamanlar geçirdik. Beni evinizde sürekli misafir ettiğiniz için ayrıca hepinize (Benay, Çiğdem, Özge, Didar, Özlem) çok teşekkür ediyorum. Koç Üniversitesi'ndeki değerli arkadaşlarım Zeynep Ülker Demir'e, Zehra Önen'e, Ayşenur Kibar Asaly'e de çok teşekkür ediyorum. Doktora için bizden ayrılan, bu yola birlikte çıktığım sevgili dostum Buse Aras'a da sevgilerimi iletiyorum. Her zaman bize yardımcı olan Fen Bilimleri Enstitü çalışanlarına, Emine Hanım'a, Elif Hanım'a, sevgili Gözde'ye, Derya Hanım'a, sevgili Türkan'a ve Ayşe Abla'ya çok teşekkür ediyorum. Bu günlere kadar yanımda olan ve bana destek veren değerli dostlarım Nurcan ve Şebnem'e de teşekkür ediyorum.

Son olarak kıymetli aileme teşekkürlerimi sunmak istiyorum. Sevgili annem ve babam Selma-Necmi Eruçar'a ve kardeşim İlker Eruçar'a teşekkür ediyorum. Her zaman doktora yapmamı destekleyip arkamda oldular. Onların emekleri olmasaydı asla doktoramı yapamazdım. Her zaman benimle gurur duyan, hasta yatağında dahi yanındakilere akademik başarılarımı anlatan canım dedeciğim Hüseyin Eruçar'a da teşekkürlerimi sunuyorum. Bu günümü görebilseydi eminim çok mutlu olurdu. Doktora sürecimde yeni bir ailem daha oldu. Sevgili annem ve babam Gülsen-Ali Fındıkçı'ya, kardeşlerim Sena, Sertan ve Sibel Ablam'a da çok teşekkür ediyorum. Sevgili Sinem'i de unutmuyorum. Sibel ve Nedim Kaçar'a ayrıca TÜBİTAK bursumda bana kefil oldukları için çok teşekkür ediyorum. Son olarak değerli eşim Sinan Fındıkçı'ya çok teşekkür ediyorum. Onun sevgisi, yardımı, ilgisi ve desteği ile bu zorlu süreci tamamlamanın mutluluğu içerisindeyim. Yol arkadaşım, iyi ki varsın.

Son olarak emeği geçen, bu süreçte yanımda olan herkese çok teşekkür ediyorum.

TABLE OF CONTENTS

Abstract	iii
Özetçe	v
Acknowledgements	vii
List of Tables	xi
List of Figures	xii
Nomenclature	xv
Chapter 1: Introduction	1
Chapter 2: Literature Review	7
2.1 Metal Organic Frameworks (MOFs)	7
2.2 Gas Storage Applications of MOFs	11
2.3 Gas Separation Applications of MOFs	18
2.3.1 Adsorption-based Gas Separation	18
2.3.2 Membrane-based Gas Separation	24
2.4 Biomedical Applications of MOFs	33
Chapter 3: Computational Methods	38
3.1 Theoretical Background of Molecular Simulations	38
3.1.1 Grand Canonical Monte Carlo (GCMC) Simulations	41
3.1.2 Equilibrium Molecular Dynamics (EMD) Simulations	44
3.2 Molecular Simulations of Thin-Film MOF Membranes	45
3.3 Computational Modeling of MOF-Based MMMs	48
3.4 Molecular Simulations of Drug/Cosmetic Molecules	51
Chapter 4: Modeling of Bio-MOFs for Gas Separations	56
4.1 Modeling of Bio-MOFs for CO₂/CH₄ Separations	56
4.1.1 Computational Details	57
4.1.2 Validation of the Accuracy of Molecular Simulations	62
4.1.3 Adsorption-based Gas Separations	66
4.1.4 Membrane-based Gas Separations	68
4.2 Evaluation of Bio-MOFs for Other Gas Separations	76
4.2.1 Adsorption-based and Membrane-based Gas Separations	77
4.2.2 Investigation of Temperature and Pressure Effects	82
4.2.3 Investigation of Bio-MOFs for MMM Applications	84
Chapter 5: Efficient Storage of Drug and Cosmetic Molecules in Bio-MOFs	89
5.1 Computational Details	89
5.2 Comparison of Simulations with the Experimental Data	92
5.3 Ibuprofen, Caffeine and Urea Uptake and Diffusion in Bio-Compatible MOFs	96
Chapter 6: Conclusion	107
Bibliography	112

Appendix A: Modeling of Bio-MOFs for Gas Separations.....	129
Appendix B: Efficient Storage of Drug/Cosmetic Molecules in Bio-Compatible MOFs	141
Vita.....	151



LIST OF TABLES

Table 4.1 Structural properties of bio-MOFs.....	58
Table 4.2 Interaction potential parameters used for gas molecules	61
Table 4.3 Self-diffusion of gas coefficients, CO ₂ permeabilities and permeation selectivities of bio-MOFs (CO ₂ /CH ₄ :50/50, at 10 bar and 300 K)	69
Table 4.4 Permeability and selectivity data of pure MOF membranes for H ₂ /CH ₄ separation.....	85
Table 4.5 Permeability and selectivity data of pure MOF membranes for CO ₂ /CH ₄ separation.....	85
Table 4.6 Permeability and selectivity data of pure MOF membranes for H ₂ /CO ₂ separation.....	85
Table 4.7 Permeability and selectivity data of pure MOF membranes for CO ₂ /N ₂ separation.....	85
Table A.1 Diffusion coefficients of CO ₂ for rigid bio-MOF-1, -11, -12 and -13.....	135
Table B.1 Structural properties of bio-compatible MOFs	141
Table B.2 Data for comparison of our predicted ibuprofen uptake with the experiments and other simulation data available in the literature	145

LIST OF FIGURES

Figure 1.1 General classification of porous solids: polymers for porous organic solids; zeolites for porous inorganic solids and MOFs for porous hybrid solids.....	3
Figure 2.1 (a)The structure of cubic MOF-5 (IRMOF-1): ZnO ₄ tetrahedra (blue tetrahedra) joined by benzene dicarboxylate linkers (O:red and C:gray). The pores (8 Å×12 Å) are shown as a yellow sphere. (b)The topology of the structure (primitive cubic net). (c)The structure shown as the envelopes of the ZnO ₄ tetrahedra (red truncated tetrahedron) and benzene dicarboxylate (blue slat)	8
Figure 2.2 Examples for isorecticular metal organic frameworks (IRMOFs).....	9
Figure 2.3 Number of articles on different potential applications of MOFs	9
Figure 2.4 Examples of MOFs constructed from biocompatible organic linkers. Metal polyhedral are in pink, gray, gray, blue, or orange (for Bi, Mg, Zn, Cu and Fe, respectively) and carbon atoms in black, respectively	10
Figure 2.5 Schematic representation of MOF manufacturing process for bio-applications	11
Figure 2.6 Schematic representation of working capacity and unused amount of gas at isothermal conditions.....	12
Figure 2.7 CO ₂ storage in 125 MOFs at 298 K and 1 bar	17
Figure 2.8 (a)Simple volumetric apparatus, the valve train itself serves as the reference volume. (b)Volumetric apparatus with separate pressure vessel to act as a reference volume. (c)Gravimetric instrument	19
Figure 2.9 (a)Schematic view of the excess and absolute adsorption on a two-dimensional rectangular surface. (b)Total adsorption for porous materials.....	20
Figure 2.10 Number of publications featuring the terms "metal organic framework", "gas separation" in their topics and "membrane" in titles, Accessed: 2016-04-12 at Web of Science	27
Figure 2.11 Ibuprofen delivery in several porous MOFs and MCM-41.....	34
Figure 3.1 The schematic representations of exchange move	42
Figure 3.2 Geometry optimization of ibuprofen.....	52
Figure 3.3 Conformer analysis for ibuprofen molecule.....	55
Figure 4.1 Configurations of bio-MOF-13. Connolly surface diagrams were prepared using 1 Å probe molecule. The inner (outer) surfaces of the cavities are shown in blue (gray)	59
Figure 4.2 Configurations of bio-MOF-14. Connolly surface diagrams were prepared using 1 Å probe molecule. The inner (outer) surfaces of the cavities are shown in blue (gray)	60
Figure 4.3 Comparison of experiments and our molecular simulations for single-component adsorption isotherm of (a)CO ₂ at 298 K in bio-MOFs-11, -12, -13 and -14	

(b)H ₂ at 77 K (squares) and 87 K (circles) in bio-MOF-11 (c)N ₂ at 298 K in bio-MOFs-11, -12 and -13.....	65
Figure 4.4 Comparison of adsorption selectivities and working capacities of bio-MOFs with other MOFs and zeolites for CO ₂ /CH ₄ :50/50 separation at 10 bar and 300 K.....	67
Figure 4.5 Comparison of CO ₂ /CH ₄ permeation selectivity and CO ₂ permeability of bio-MOFs with other MOFs and zeolites at 10 bar and 300 K. (CO ₂ /CH ₄ :50/50) Closed (open) symbols represent the results of rigid (flexible) EMD simulation	70
Figure 4.6 Comparison of experiments and molecular simulations for bio-MOF-1, bio-MOF-13 and bio-MOF-14 membranes in CO ₂ /CH ₄ (50/50) separation. Feed pressure is 2.4 bar and temperature is 298 K for bio-MOF-1, 295 K for bio-MOFs-13 and -14. Simulation results for rigid bio-MOF-13 (configuration I) and rigid bio-MOF-14 (configuration III) were not shown since gas diffusion was not measurable in these materials.....	74
Figure 4.7 Comparison of adsorption selectivities and delta loading capacities of MOFs and zeolites for CH ₄ /H ₂ separation	77
Figure 4.8 Comparison of adsorption selectivities and delta loading capacities of MOFs and zeolites for CO ₂ /H ₂ separation	78
Figure 4.9 Comparison of adsorption selectivities and delta loading capacities of MOFs and zeolites for CO ₂ /N ₂ separation	79
Figure 4.10 Comparison of permeation selectivities and CH ₄ permeabilities of MOFs and zeolites for CH ₄ /H ₂ separation	80
Figure 4.11 Comparison of permeation selectivities and CO ₂ permeabilities of MOFs and zeolites for CO ₂ /H ₂ separation	81
Figure 4.12 Comparison of permeation selectivities and CO ₂ permeabilities of MOFs and zeolites for CO ₂ /N ₂ separation	81
Figure 4.13 Investigation of temperature and pressure effects on (a)CH ₄ /H ₂ , (b)CO ₂ /CH ₄ , (c)CO ₂ /H ₂ and (d)CO ₂ /N ₂ selectivities of bio-MOF-11	83
Figure 4.14 Investigation of temperature and pressure effects on (a)CH ₄ /H ₂ , (b)CO ₂ /CH ₄ , (c)CO ₂ /H ₂ and (d)CO ₂ /N ₂ selectivities of WODFOL.....	84
Figure 4.15 Comparison of membrane selectivity and CO ₂ permeability of MOF membranes with polymeric membranes for (a)CO ₂ /CH ₄ and (b)CO ₂ /N ₂ separations. The data of pure MOF membrane and matrimid were also shown	87
Figure 5.1 Comparison of our predicted ibuprofen uptake with the experiments and other simulation data available in the literature	94
Figure 5.2 Comparison of our predicted caffeine and urea uptakes with the experiments and other simulation data available in the literature.....	96
Figure 5.3 Predicted ibuprofen uptake of MOFs. Current limit was set based on experimental ibuprofen uptake of MIL-101(Cr)	97
Figure 5.4 Correlations between predicted ibuprofen uptakes of MOF-74 series and their calculated (a)pore volumes (b)largest cavity diameters (LCDs)	98
Figure 5.5 Predicted caffeine uptake in MOFs. Current limit was set based on experimental caffeine uptake of MIL-100(Fe)	99

Figure 5.6 Predicted urea uptake in MOFs. Current limit was set based on experimental urea uptake of MIL-100(Fe)	100
Figure 5.7 (a)MSD and (b)RDF analyses of ibuprofen diffusion in MIL-101(Cr)	101
Figure 5.8 MSD of (a)ibuprofen, (b)caffeine and (c)urea in bio-MOF-100.....	102
Figure 5.9 Comparison of ibuprofen diffusion in bio-MOF-100, -102 and RAVXIX....	105
Figure A.1 (a-h)Unit cell structures of bio-MOFs given A along X, B in XY plane	132
Figure A.2 N ₂ uptakes in bio-MOF-14.	133
Figure A.3 CO ₂ and CH ₄ uptakes in bio-MOF-1	134
Figure A.4 Mean square displacements (MSD) vs. t graphs for rigid bio-MOF-1, -11, -12 and -13 (configuration II)	135
Figure A.5 Total free volume analysis of bio-MOFs	137
Figure A.6 Pore size analysis of bio-MOFs-1, -11, -12, IZUMUM, NUDKON, OFUSAL, PESTUD and WODFOL	138
Figure A.7 Pore size analysis of bio-MOF-13	139
Figure A.8 Pore size analysis of bio-MOF-14.....	140
Figure B.1 Conformation of ibuprofen molecules in (a)MOF-74 and (b)RAVWES.....	146
Figure B.2 Conformation of ibuprofen in MIL-101(Cr)	146
Figure B.3 MSDs of ibuprofen in bio-MOF-11. Data for Bei et al. is taken from the literature.....	147
Figure B.4 Pore size analysis of bio-MOF-100 during MD simulations.....	148
Figure B.5 MD snapshots of urea diffusion in bio-MOF-100 in the presence of water. Water molecules are shown in white circles	149
Figure B.6 RDF analyses of (a,b)ibuprofen, (c)caffeine and (d)urea in bio-MOF-100 ..	149
Figure B.7 Conformation of ibuprofen in bio-MOF-100	150
Figure B.8 Conformation of caffeine in bio-MOF-100	150
Figure B.9 Conformation of urea in bio-MOF-100	150

NOMENCLATURE

- AARE: The percentage average absolute relative error
- ARPA-E: Advanced Research Projects Agency-Energy
- Å: Angstrom
- CBAC: Connectivity-based atom contribution
- CCDC: Cambridge Crystallographic Data Centre
- CH₄: Methane
- CO: Carbon monoxide
- CO₂: Carbon dioxide
- COF: Covalent organic frameworks
- COM: Center of mass
- CPU: Central processing unit
- DFT: Density functional theory
- D_o: Corrected diffusivity
- DOE: The U.S. Department of Energy
- D_s: Self-diffusivity
- D_t: Transport diffusivity
- EMD: Equilibrium molecular dynamics
- EQeq: Extended charge equilibration method
- g: Gram
- GCMC: Grand canonical Monte Carlo
- IAS: Ideal adsorption selectivity
- IDS: Ideal diffusion selectivity
- IMS: Ideal membrane selectivity
- K: Kelvin
- kJ: Kilojoules
- LCD: Largest cavity diameter
- LPD: Limiting pore diameter
- MAS: Mixture adsorption selectivity
- MDS: Mixture diffusion selectivity
- MMM: Mixed matrix membranes
- MMS: Membrane's mixture selectivity

MOF: Metal organic framework
 N: Number of molecules
 ns: Nanosecond
 P: Pressure or permeability
 PCN: Porous coordination network
 P_{MMM} : Permeability of MMM
 $P_{polymer}$: Permeability of polymer
 ps: Picoseconds
 PSA: Pressure swing adsorption
 QeQ: Charge equilibration method
 Qst: Isosteric heat of adsorption
 r: Distance between molecule pairs
 REPEAT: Repeating electrostatic potential extracted atomic method
 S_{ads} : Adsorption selectivity
 S_{diff} : Diffusion selectivity
 S_{perm} : Permeation selectivity
 STP: Standard temperature and pressure
 T: Temperature
 TSA: Temperature swing adsorption
 UFF: Universal force field
 V: Volume
 ZIF: Zeolitic imidazolate framework
 Γ : Thermodynamic correction factor
 ΔN : Working capacity
 ε : Energetic potential parameter
 ε_0 : Permittivity of free space
 μ : Chemical potential
 σ : LJ size parameter
 ϕ : Volume fraction of filler in MMM

Chapter 1

INTRODUCTION

"*When it rains, it pores.*" Professor Geoffrey Ozin from the University of Toronto explains his thoughts on the future of porous materials with this phrase.[1] The porous materials have gained significant attention over the last three decades due to their ability to interact with atoms or molecules at their surfaces and throughout the bulk material.[2] These materials have potential in a large number of applications including adsorption, separation, purification, catalysis, drug storage and delivery.[3, 4] The pore sizes of the porous materials can be classified according to the International Union of Pure and Applied Chemistry (IUPAC): micropores (≤ 2 nm), mesopores (in the range of 2 nm and 50 nm) and macropores (>50 nm). It is important to note that "nanoporous materials" are commonly used to refer a group of porous materials that have pore diameters between 1-100 nm.[5]

The porous materials can be generally divided into two groups: organic and inorganic materials.[4] Organic porous materials have highly voided structures and lack of order. Porous polymers[6] and activated carbons[7] are well-known examples of this group. Porous polymeric materials are rigid and highly voided structures and they are generally prepared by solution casting, sintering and phase separation methods.[6] These materials are generally used in industrial membrane applications because they provide high gas permeability (the rate of fluid flow per unit area of the membrane per unit driving force such as concentration or pressure) but low selectivity (the ratio of permeability of the two competing components) because of the indistinct voids which limit their size selective property.[6] Activated carbons are produced from carbon-rich materials (such as coal) and they have high surface areas (400-

3000 m²/g).[7] Activated carbons are commonly used in various gas separation and purification applications such as air separation, natural gas purification, flue gas separation and removal of trace impurity.[7]

Inorganic porous materials such as zeolites have highly ordered structures and exhibit better thermal and mechanical stabilities at high temperatures compared to polymeric materials.[8] Inorganic porous materials are commonly used in gas separation and catalysis applications. They can be also used as membrane reactors because they are chemically inert and have good wear resistance.[9] Although inorganic materials possess good separation characteristics, they are not able to compete with the polymeric materials for large-scale commercial use since they are significantly expensive than the polymeric materials. It is also challenging to fabricate large, defect-free inorganic membranes for gas separation applications because inorganic materials are generally brittle and difficult to process. Another problem of inorganic materials is the lack of tunable pore sizes which hinders their usage in separation of large molecules such as hydrocarbons.[10]

Combining the advantages of organic and inorganic porous materials, metal organic frameworks (MOFs) have been recently synthesized. The illustration of porous solids is shown in Figure 1.1. MOFs are a relatively new group of nanoporous materials which are composed of metal ions or clusters connected by organic linkers to create highly porous networks. The advent of MOFs was triggered in 1999 by Yaghi et al.[11] who synthesized a crystalline three-dimensional framework called MOF-5. The surface area of MOF-5 (3631 m²/g) was reported to be much higher than the zeolite with the highest surface area, zeolite Y (904 m²/g)[12] and activated carbons (526-2386 m²/g).[13] The "building block approach" was developed to synthesize large families of isorecticular MOFs having the same topology with different pore sizes and surface areas.[14] This approach has received widespread attention in recent years since it provided the opportunity to synthesize numerous materials, over 50,000, with different chemical compositions and functionalities.[15] Theoretically unlimited numbers of MOFs can be synthesized by changing the combination of organic linkers and metal-ions.[16] Crystal structures of thousands of synthesized MOFs are deposited in a large database, Cambridge Crystallographic Data Centre (CCDC).[15] Several MOF families have been reported such as zeolitic imidazolate frameworks (ZIFs), porous coordination networks (PCNs), covalent organic frameworks (COFs). MOFs have gained

considerable attention as promising nanoporous materials due to their exceptional physical and chemical properties such as very large surface areas ($500\text{-}6500\text{ m}^2/\text{g}$), high pore volumes ($1\text{-}4\text{ cm}^3/\text{g}$), tunable pore sizes ($1\text{-}98\text{ \AA}$) and reasonable thermal and mechanical stabilities.[17] These outstanding properties of MOFs have been tested in many applications including gas storage,[18] gas separation,[19] drug storage[20], drug delivery,[21] catalysis[4] and sensing.[22] Among these different applications, gas separation has received significant interest due to the tunable pore sizes of MOFs. MOFs have been used to fabricate defect-free, thin-film membranes and tested for gas separation applications in addition to being used as filler particles in polymers to make mixed matrix membranes (MMM).[23]



Figure 1.1 General classification of porous solids: polymers for porous organic solids; zeolites for porous inorganic solids and MOFs for porous hybrid solids.[3]

MOFs have been intensively studied for gas storage and gas separation applications during the past decades.[18] Considerable efforts have been devoted to search for clean energy carriers such as hydrogen (H_2) and methane (CH_4) because of the depletion of fossil fuels. H_2 can be recovered from refineries by separation of CH_4/H_2 mixture. The gas mixture is generally 50% H_2 at 5-10 bar and the impurities are C1-C5 hydrocarbons. Among these hydrocarbons, CH_4 represents the smallest of the impurities and the van der Waals forces between CH_4 and the surface of a porous material is the weakest.[24] Therefore, separation of CH_4/H_2 mixtures is considered as the most difficult separation to achieve in refinery off-gas separation processes. Our group recently examined adsorption-based and membrane-based

CH₄/H₂ separation performances of MOFs and reported that significant number of MOFs exhibit higher adsorption-based and membrane-based CH₄/H₂ selectivities compared to well-known traditional zeolites.[25, 26]

Developing efficient methods for storage of carbon dioxide (CO₂) is significant because of the global warming problem. The combustion of oil, coal and natural gas causes CO₂ emission. Today carbon capture and sequestration technologies play an important role in all over the world due to economic and environmental concerns.[27] In order to capture CO₂, several industrial processes such as post-combustion (CO₂/N₂) and pre-combustion of the fuel (CO₂/H₂), and natural gas purification (CO₂/CH₄) are considered.[28] Extensive studies have been conducted on gas storage and gas separation performances of MOFs and many MOFs were identified as promising adsorbents or membranes due to their very large surface areas, pore volumes and chemical tunability.[19, 29, 30]

Recently, MOFs have been used in biomedical applications including drug storage, drug delivery and imaging.[21, 31, 32] Efficient drug storage is required to improve the drug bio-distribution, the biological half-life of the active species and therapeutic effect of the drug.[33] Lipids, polymeric nanoparticles, metal clusters and carbon structures have been tested as drug storage materials in the past.[33] However, these materials have several limitations such as low drug loading capacities (<5 wt%), rapid drug release and toxicity.[34] MOFs have been recently studied as alternative drug storage materials due to their large pore volumes. The first group of MOFs which was investigated as potential candidates for drug storage was the MILs (Materials of Institut Lavoisier) due to their large pore sizes (25-34 Å) and high surface areas (3100-5900 m²/g).[35] However, practical usage of MILs in drug storage and delivery is limited due to the presence of toxic Cr metal in the framework. In order to decrease the toxic effects of organic linkers and metals, bio-molecules such as amino acids, nucleobases and sugars are used as linker molecules and bio-compatible metal cations are chosen to construct bio-MOFs.[36] An and co-workers[37] synthesized bio-MOF-1, the first member of bio-MOF family, using adenine as a biomolecular ligand and zinc salts as metal centers. They reported that bio-MOF-1 shows promise for storage and release of cationic drug molecules due its anionic character. This was the first potential biomedical application of a MOF constructed with biomolecular building blocks.

Bio-MOFs are new and promising materials for both gas separation and biomedical applications due to their permanent porosity, chemical functionality and structure-tunability. The storage capacities of bio-MOFs exceed those of many traditional materials due to their large pore sizes. Additionally, tuning the host-guest interactions with the organic linkers and non-toxic metals of bio-MOFs enables one to control diffusion of gas and drug molecules through the pores by changing the pore size, flexibility and interconnectivity.[38] These superior properties improved the practical applications of bio-MOFs. However, the research on bio-MOFs is just starting and there is a lack of information in the literature specifically for gas separation and biomedical applications of bio-MOFs. Molecular level understanding of properties of bio-MOFs is crucial to accelerate the design and development of these new materials. Computational studies are highly required to identify the most promising materials prior to extensive experimental efforts. Molecular simulation studies can direct the experimental researchers to focus on more promising materials for a target application.

In this thesis, we aim to unlock the potential of bio-MOFs in adsorption-based and membrane-based gas separations and biomedical applications. Section 2 reviewed the current literature on gas storage, gas separation and bio-medical applications of MOFs. Section 3 discussed molecular simulation techniques, Grand Canonical Monte Carlo (GCMC), configurational bias Monte Carlo (CBMC) and Equilibrium Molecular Dynamics (EMD), which were used to investigate adsorption and diffusion of gas molecules and drug molecules in bio-MOFs. Gas permeation models used to study MMMs are also reviewed in Section 3. Section 4 discussed the potential of bio-MOFs in energetic applications for CO₂ separation from CO₂/CH₄, CO₂/N₂ and CO₂/H₂ mixtures and H₂ separation from CH₄/H₂ mixture. The accuracy of the molecular modeling methods was discussed by comparing predictions of the computational methodologies with the experimental measurements for both adsorption-based and membrane-based separations in Section 4. Several parameters such as adsorption selectivity, working capacity, membrane selectivity and gas permeability were also discussed in Section 4. The CO₂ separation performances of bio-MOFs were compared with those of various MOFs, zeolites and polymers in order to assess potential of bio-MOFs and effects of structure flexibility on the predicted membrane performance of bio-MOFs were also discussed. The effects of temperature and pressure on the selectivity were also investigated. Performances of two promising bio-MOFs as fillers in polymers were investigated for MMM

applications. Section 5 examined the drug/cosmetic molecule storage and release performances of bio-compatible MOFs. The effects of structure flexibility and presence of water on the diffusion of drug and cosmetic molecules were investigated. Additionally, effects of MOFs' structural properties such as pore volume and pore size on the drug storage and diffusion were examined to provide information on the materials' structure-performance relationships in Section 5. Finally, Section 6 discussed the main outcomes of this thesis and the opportunities and challenges of using computational approaches to assess potential of bio-MOF membranes in both energetic and bio-medical applications were addressed.



Chapter 2

LITERATURE REVIEW

Metal organic frameworks (MOFs) have recently gained significant attention due to their highly porous and functional structures. In this chapter, general background on MOFs and their potentials in gas separation and bio-medical applications was given.

2.1. Metal Organic Frameworks (MOFs)

The history of metal organic frameworks (MOFs) dates back to 1965 when Tomic[39] prepared a polymer solution composed of 3 ligands and selected metal-ions such as Zn, Ni, Al and Fe. MOFs are robust and crystalline materials that are composed of metal ligand complexes such as Zn^{2+} , Co^{2+} , Ni^{2+} , Cu^{2+} , Cd^{2+} , Fe^{2+} , Mg^{2+} , Al^{3+} and Mn^{2+} connected with organic linkers such as benzene-dicarboxylate (BDC), polycarboxylate (BTB) and imidazole. MOFs are self-assembled structures where metal ions link to organic ligands by a typical coordination bond. The development of MOF synthesis has been mainly driven by Yaghi and co-workers[40] with the concept of "reticular synthesis" in solvothermal reactions at relatively low temperatures (below 300 °C). This method consists of assembling rigid molecular building blocks to obtain predetermined ordered structures.[40] It is an affective design strategy to produce or manipulate MOFs for desired functions and applications. MOF-5 (IRMOF-1) (isoreticular metal organic framework), one of the most widely studied MOF in the literature can be given as an example. Figure 2.1 illustrates the topology of MOF-5. Octahedral secondary building units (SBU) containing four ZnO_4 tetrahedra with a common vertex and six carboxylate C atoms are joined by benzene links to construct cubic, porous MOF-5. Conceptual design of MOFs using different SBUs provides synthesis of

predetermined networks and their pore sizes and chemical functionalities can be directly controlled during synthesis. This results in theoretically infinite number of structures having different physical and chemical characteristics.

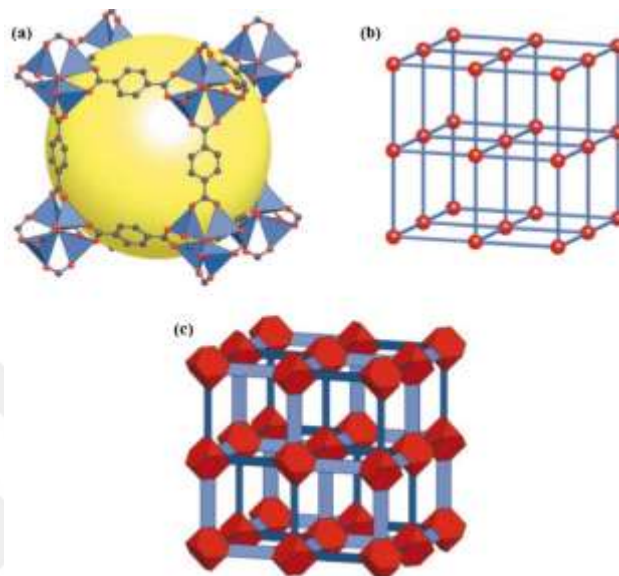


Figure 2.1 (a) The structure of cubic MOF-5 (IRMOF-1): ZnO_4 tetrahedra (blue tetrahedra) joined by benzene dicarboxylate linkers (O:red and C:gray). The pores ($8 \text{ \AA} \times 12 \text{ \AA}$) are shown as a yellow sphere. (b) The topology of the structure (primitive cubic net). (c) The structure shown as the envelopes of the ZnO_4 tetrahedra (red truncated tetrahedron) and benzene dicarboxylate (blue slat).[40]

Figure 2.2 shows the series of IRMOFs which have the same framework topology (octahedral Zn-O-C clusters that exhibit a cubic structure). The pore sizes of MOFs change from 3.8 to 28.8 \AA based on the length of organic linkers. This large variety of structures makes MOFs promising candidates in especially gas storage and separation applications due to their highly porous and functional nature. Besides gas storage and gas separation applications, MOFs have been also considered as promising materials in many areas including catalysis, chemical sensing, nonlinearoptics/ferroelectricity and biomedical imaging and drug delivery.[41] Figure 2.3 illustrates the potential applications of MOFs considering the growth of the number of publications. As can be seen from Figure 2.3, the MOF research on "adsorption" has the maximum number of publications with a total of 2776 articles from year 1998 to 2014. Gas storage and separation applications of MOFs have a total of 762 and 953 articles, respectively. Research on the drug storage and delivery applications of MOFs is a relatively new area and has the minimum total article number, 99.[42]

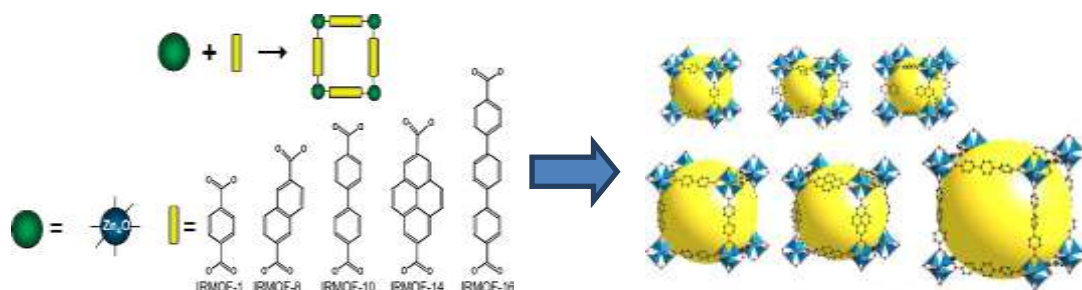


Figure 2.2 Examples for isoreticular metal organic frameworks (IRMOFs)[43]

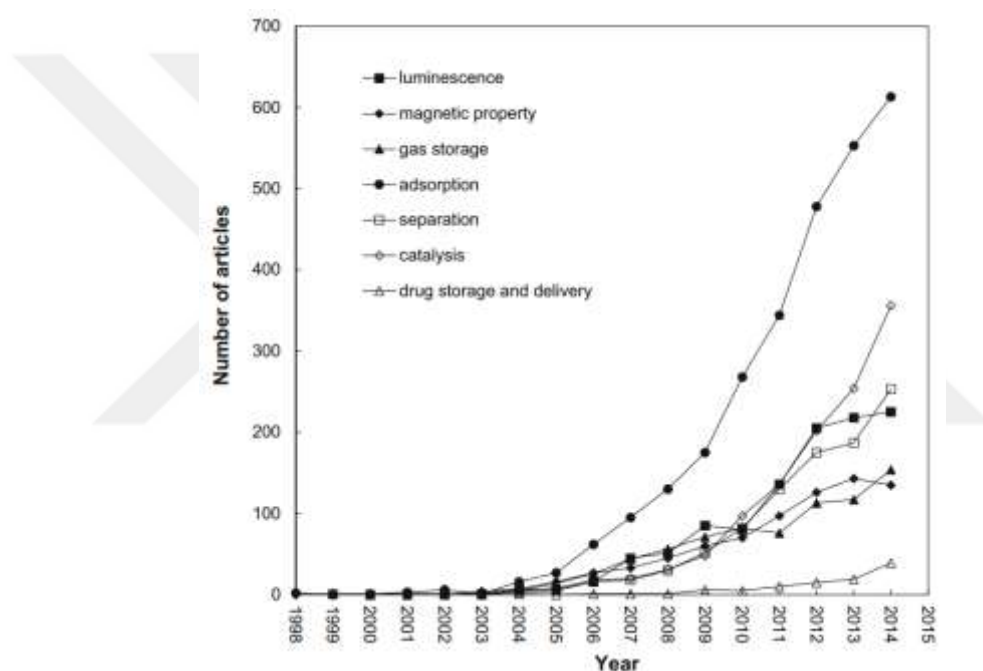


Figure 2.3 Number of articles on different potential applications of MOFs[42]

Recently, biomolecules such as amino acids, nucleobases and sugars as linker molecules and biocompatible metal cations have been used to construct bio-MOFs.[36] Using biomolecular building blocks, Rosi and co-workers[37] synthesized bio-MOF-1 as the first member of bio-MOF group using adenine as a biomolecular ligand and zinc salts as metal centers. The research on bio-MOFs is at the beginning and there are just nine adenine-based bio-MOFs (1, 11, 12, 13, 14, 100, 101, 102, 103) that have been synthesized in the literature to date. MOFs constructed from different biocompatible organic linkers such as the iron(III) gallate, fumarate, cyclodextrin or muconate were also available in the literature.[34] Figure 2.4

shows the structures of MOFs which are built from various bio-compatible organic linkers such as aspartate, fumarate and muconate.

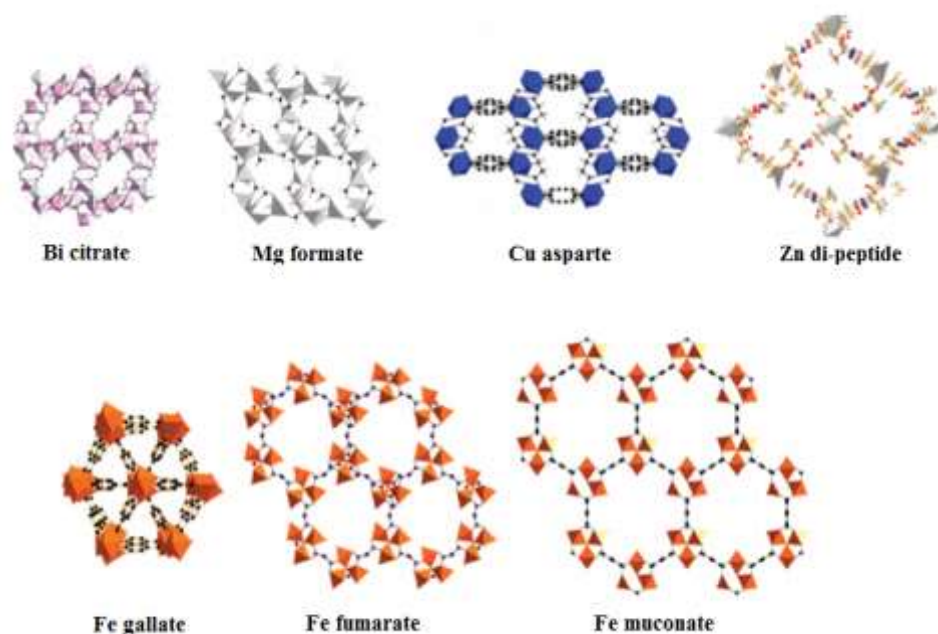


Figure 2.4 Examples of MOFs constructed from biocompatible organic linkers. Metal polyhedra are in pink, gray, gray, blue, or orange (for Bi, Mg, Zn, Cu and Fe, respectively) and carbon atoms in black, respectively.[34]

The schematic representation of MOF synthesis for bio-applications is shown in Figure 2.5. MOFs are initially synthesized using metallic precursor and organic linkers and then activation and characterization procedures are performed. The bio-application of MOFs can be divided into two categories: the bioactive molecules such as drugs, cosmetics, enzymes and toxins can be incorporated within the pores of MOFs and bioactive molecules such as cations and organic ligands can be directly used to synthesize MOFs which are also known as bio-MOFs.[33] For example, bio-MOF-1 (Zn-adeninate) contains both a bioactive cation and an endogenous ligand.[37] Several excellent reviews discuss the biological and medical application of bio-MOFs in detail.[33, 38, 44, 45] Since bio-MOFs have regular porosity and chemical functionality, they were investigated not only for biomedical applications, but also for gas storage and gas separation applications.[46, 47]

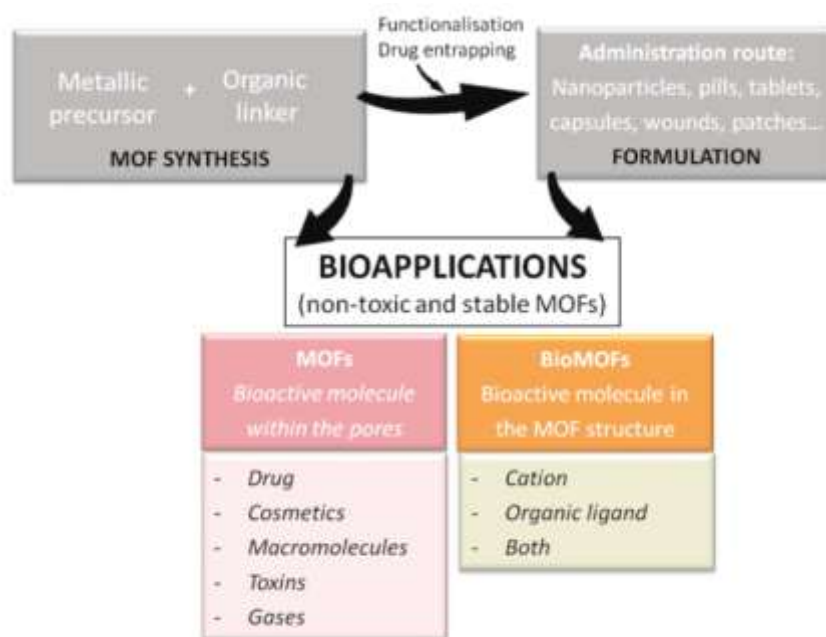


Figure 2.5 Schematic representation of MOF manufacturing process for bio-applications.[33]

2.2. Gas Storage Applications of MOFs

With an increasing need for clean and efficient energy systems, H_2 and CH_4 have been considered as an ideal energy carriers.[18] Especially in automotive industry, H_2 and CH_4 gases have been investigated for on board gas storage. H_2 has almost triple energy density that of gasoline per mass unit and generates zero emission. CH_4 is the main component of natural gas and it has the highest H to C ratio of any fossil fuel and therefore combustion of CH_4 produces less amount of CO and CO_2 . [18] However, storage of these gases using conventional methods such as compression or liquefaction is challenging because of the requirement of extremely high pressures (200 bar) or low temperatures (77 K). [48] Adsorption process is used for gas storage applications because this method is based on physisorption of gas molecules within the porous material. Due to the van der Waals interactions, gas molecules are adsorbed within the pores of materials at moderate temperatures and pressures.

To evaluate gas storage capacities of the solid porous materials ARPA-E (Advanced Research Projects Agency-Energy) target set by the U.S. Department of Energy (DOE) is used. For example, the DOE target for on-board H_2 storage systems is reported as 5.5 wt%

and 40 g/L by 2017.[49] The DOE target was recently set to 350 cm^3 (STP:standard temperature and pressure)/ cm^3 for CH_4 storage assuming a 25% loss in volumetric capacity due to packing and pelletization of adsorbent in a fuel tank.[50] Development of porous materials to meet the DOE target for gas storage is currently an active research area. Herein, it is important to note that a promising adsorbent should have both high storage and deliverable capacity. The deliverable capacity which is also known as working capacity is defined as the amount of gas that can be delivered when the adsorption pressure is decreased to a specified desorption pressure.[50] Generally, 5 bar is used as desorption pressure since natural gas powered internal combustion engines work at this operating pressure. 35 bar or 65 bar is assumed as the adsorption pressure because these pressures can be achievable with a typical single-stage or two-stage compressors.[51] Schematic representation of working capacity and unused amount of gas at isothermal conditions is given in Figure 2.6. As can be seen, to increase the working capacity of an adsorbent, it is required to maximize the gas storage at adsorption pressure and minimize the gas storage at the desorption pressure.

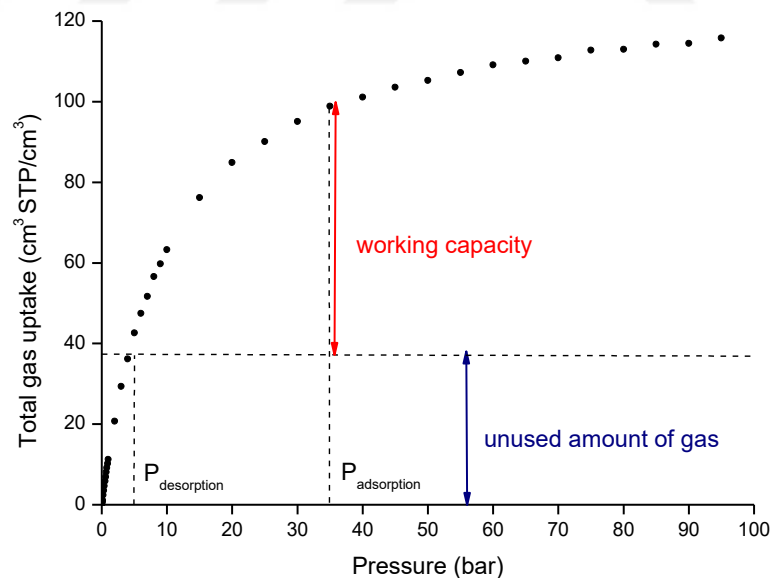


Figure 2.6 Schematic representation of working capacity and unused amount of gas at isothermal conditions

Recent studies investigate whether MOFs can meet the DOE targets. Due to high porosity and large surface area, MOFs have the excellent potential in H_2 storage. For example,

MOF-177 has a H₂ saturation uptake of 11 wt% at about 100 atm and 77 K.[49] H₂ storage has been widely studied both experimentally and theoretically in the literature and there are several reviews on H₂ adsorption in MOFs.[52-55] Langmi et al.[56] summarized the best H₂ storage results reported in the literature at both 77 K and room temperature together with the surface area of MOFs. Based on their data, total volumetric H₂ uptake capacities at 77 K were found in the range of 40-60 g/L (6-15 wt%) for MOFs. However, the best H₂ storage capacities of MOFs at room temperature are in the range of 0.5-1 wt% and volumetric capacities are less than 15 g/L.[56] Results showed that H₂ uptakes at room temperature are below the DOE target because of the weak interaction between H₂ molecules and the framework. It was also stated that at low pressures pore size has a considerable effect on H₂ uptake in MOFs but at high pressures H₂ uptake is dependent on both surface area and pore volume of the MOFs. Several strategies such as incorporation of metal ions and catenation have been investigated to optimize the storage of H₂ in MOFs at room temperature.[56]

Due to the very large number of synthesized MOFs in the literature, it is not practical to examine H₂ storage capacities of each MOF using experimental methods. Theoretical modeling and molecular simulations play a key role to predict gas storage capacities of a large number of MOFs in a reasonable computing time. Basdogan and Keskin[57] reviewed the molecular simulation studies of MOFs for H₂ storage. They showed that molecular simulations provide the atomic-level information about H₂-MOF interactions. This knowledge is very important for developing new design strategies to enhance H₂ uptake in MOFs. For example, Han et al.[58] identified the adsorption mechanism of H₂ in MOFs using molecular simulations. They found that the favorable H₂ adsorption sites are the organic linkers of MOFs. Moreover, they showed that H₂ uptake in MOFs increases by changing the aromatic organic linkers. In another study,[59] molecular simulations showed that interpenetration of MOFs which is the self-assembly of two separate frameworks enhances H₂ adsorption at low temperature and low pressure due to the decrease in pore sizes of MOFs and increase in heat of adsorption. Results showed that molecular simulations can provide theoretical insights into the adsorption mechanisms inside MOFs.

Different porous materials such as zeolites, silica gels and activated carbons were studied to investigate CH₄ storage.[60] However, practical applications of these materials are not feasible because of the structural limitations. For example, zeolites have low surface area

(<1000 m²/g) and they are extremely hydrophilic which decreases their CH₄ adsorption capacity due to moisture adsorption. Zeolite packing is also one of the problems to implement these materials for the on-board fuel storage of vehicles.[60] Activated carbons have high CH₄ storage capacities (50-160 cm³ (STP)/cm³) but they have low packing densities that decrease the volumetric CH₄ uptake capacity of these materials.[51] Although silica gels have high packing densities, their surface areas are not so high to increase the gas uptake capacity. CH₄ storage performance of different types of MOFs has been assessed and some MOFs have been identified as promising adsorbents due to their chemical functionalities and high porosities. In 2002, Eddaoudi et al.[14] synthesized IRMOF-6 and reported that this MOF has an uptake of 240 cm³ (STP)/g at 298 K and 36 atm. This MOF showed much higher CH₄ uptake than other crystalline materials such as zeolite 5A (87 cm³(STP)/cm³) and other coordination frameworks (up to 213 cm³ (STP)/g).[14] After this pioneering work, thousands of MOFs were synthesized and a large family of MOFs were further investigated for CH₄ storage.[51] Mason et al.[50] and He et al.[51] reviewed experimental CH₄ uptake data in MOFs. Based on their results, there are several CH₄ adsorption isotherm data reported for the same material and the CH₄ uptake capacities are varying in a range depending on the activation procedure of the MOF and the measurement technique.[50] For example, Ni-MOF-74 has total CH₄ uptakes at 35 bar and 298 K ranging between 208 and 230 cm³ (STP)/cm³. There are also some cases where CH₄ uptakes in the same MOF have been reported for different experimental conditions. HKUST-1, for example, has total CH₄ uptakes ranging between 89 and 227 cm³ (STP)/cm³ at 18 bar and 35 bar (both at room temperature), respectively. These results show that in order to compare the storage performance of different types of MOFs accurately, it is important to use the same experimental methodology including activation techniques and measurements of high pressure CH₄ isotherms.

He et al.[51] reported 153 experimental CH₄ uptake data of MOFs together with MOFs' crystal density, pore volume and surface area. The highest total volumetric CH₄ uptake (267 cm³ (STP)/cm³) has been reported for HKUST-1 at 298 K and 65 bar.[61] If the packing density is ignored, HKUST-1 can reach the DOE's new volumetric target at 65 bar (263 cm³ (STP)/cm³). It is important to note that the packing density of a MOF affects the storage capacity of materials. Due to the loss of porosity, the total volumetric uptake may decrease with increasing density. Therefore, accurate determination of the packing density of

a MOF is important for practical storage applications. Similar to HKUST-1, Ni-MOF-74 shows also high CH₄ storage performance (260 cm³ (STP)/cm³ at 298 K and 65 bar).[50] In these MOFs, Cu²⁺ and Ni²⁺ are the favorable binding sites which directly affect their storage performance. As discussed above, the comparison for the storage performances of materials by just considering uptake capacities is not enough since delivery capacities of porous materials provide a better understanding about the realistic performance of adsorbents. For example, although Ni-MOF-74 has comparable CH₄ storage capacity with HKUST-1, it (142 cm³ (STP)/cm³) has less delivery capacity than HKUST-1 (190 cm³ (STP)/cm³) at 298 K (storage at 65 bar and delivery at 5 bar). This can be attributed to weaker interaction of CH₄ molecules with HKUST-1 than those with Ni-MOF-74 at the delivery pressure. This can be directly observed from their isosteric heat of adsorption (Q_{st}). HKUST-1 (17 kJ/mol) has lower Q_{st} value than Ni-MOF-74 (20.6 kJ/mol) which also explains the higher delivery capacity of HKUST-1. Several reviews discuss CH₄ storage in MOFs.[50, 51, 62]

To date many computational studies were performed to predict CH₄ storage in MOFs.[63] Recently, large-scale computational studies of MOFs were performed.[64, 65] These studies provide the gas uptake data of a large number of MOFs and using this large data the structure-property relations can be described to forecast the storage performance of MOFs without detailed calculations or experimental methods. Additionally, hypothetical MOFs can be designed and investigated for gas separation applications. For example, Wilmer et al.[64] screened a database of 137,953 hypothetical MOFs for CH₄ storage and they found that volumetric CH₄ storage density increases linearly with volumetric surface area. They also revealed that the optimal gravimetric surface area is in the range of 2000-3000 m²/g. Methyl-functionalized MOFs were found to be top performers in terms of CH₄ storage capacity.[64] Similarly, Fernandez et al.[66] reported the first large-scale, quantitative structure-property relationship (QSPR) analysis of ~ 130,000 hypothetical MOFs for CH₄ storage. They showed that the void fraction and the dominant pore diameter are highly correlated with CH₄ storage in MOFs. Recently, Chung et al.[67] constructed a MOF database, known as the computation-ready, experimental (CoRE) MOF database and this database contains over 4700 MOF structures which are experimentally synthesized and suitable for molecular simulations. Using this database, they found that MIL-53(Al) has the maximum CH₄ storage capacity. They also showed that the structure-property correlations for CH₄ storage are similar for hypothetical

MOFs and experimentally reported MOFs. With increasing the efficiency of simulation algorithms, high-throughput screening studies are highly useful to predict gas storage in MOFs and uncover the adsorption mechanism of gas molecules.

Apart from H₂ and CH₄ storage, the demand for developing efficient methods for capture and storage of CO₂ has been increasing rapidly due to the global warming. The most widely used conventional method for CO₂ separation is absorption of CO₂ in aqueous solutions of alkanolamines. However, this method is expensive because of the solvent exchange process for the regeneration.[68] MOFs can offer great promise for CO₂ storage applications because there is generally no chemical bond formation between adsorbates and adsorbents which requires less energy for regeneration comparing to conventional methods.[69] An and co-workers[46] reported a cobalt-adenine MOF, bio-MOF-11, which shows high CO₂ uptake capacity (4.06 mmol/g MOF at 1 bar and 298 K) due to the strong interactions between adenine and CO₂ molecules. This strong interaction was attributed to the presence of Lewis-basic sites, including an amino group and pyrimidine nitrogens and narrow pore dimensions of bio-MOF-11 that leads to the strong confinement of CO₂ molecules. The CO₂ adsorption capacity of bio-MOF-11 at atmospheric pressure and room temperature was reported to be higher than that of many other widely studied MOFs including IRMOF-1, CuBTC, ZIF-69, CUK-1.[70] Sumida et al.[28] reviewed both high pressure (>5 bar) and low pressure (~1 bar) CO₂ adsorption in MOFs and reported that the volumetric CO₂ adsorption capacity for MOF-177 is 320 cm³ (STP)/cm³ at 35 bar. This uptake capacity is 9 times higher than the quantity stored in an empty tank at the same pressure and also higher than traditional zeolites such as zeolite 13X.[28] Schoedel et al.[71] recently reviewed CO₂ capture in MOFs. Figure 2.7 shows the relationship between surface area and CO₂ uptake in a total of 125 MOFs including MOFs containing open metal sites, without open metal sites, amine functionalized and paddlewheel (square SBU). As shown in Figure 2.7, Mg-MOF-74 has the highest CO₂ uptake (37.9 wt%, (193 cm³ (STP)/cm³)) at 1 bar and room temperature. This was attributed to strong interaction between CO₂ molecules and the framework which has open metal sites.[71] There are several review articles on CO₂ storage in MOFs in the literature. [28, 69, 71]

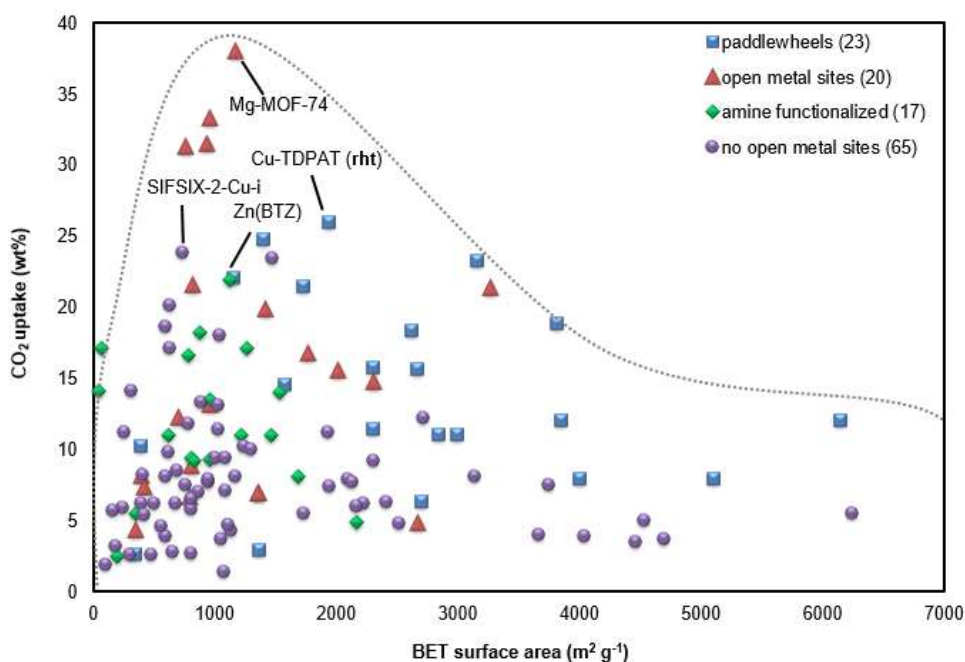


Figure 2.7 CO₂ storage in 125 MOFs at 298 K and 1 bar[71]

A large number of computational studies have been reported for CO₂ uptake in MOFs. Babarao and Jiang[72] performed molecular simulations to examine the effects of the metal oxide, organic linker and functional group on CO₂ storage in a series of isorecticular MOFs (IRMOF-1, Mg-IRMOF-1, Be-IRMOF-1, IRMOF-1(NH₂)₄, IRMOF-10, IRMOF-13 and IRMOF-14). They showed that CO₂ uptake capacity of IRMOFs can be tuned by varying the metal oxide, organic linker and functional group. For example, adding a functional group into IRMOF-1 to construct IRMOF-1(NH₂)₄ increased the CO₂ uptake at low pressures due to the enhanced CO₂ affinity.[72] Their results also showed that two physical parameters, the free volume and accessible surface area of MOFs can be tuned by changing the organic linkers and these parameters affect gas uptake at high pressures. IRMOF-10 and IRMOF-14 which have longer and bigger organic linkers than IRMOF-1 exhibited the top performing materials at 50 bar and room temperature. The same group also investigated CO₂ storage in 3D, 2D and 1D (D: dimensional) COFs using molecular simulations.[73] COFs, which are a sub class of MOFs consisted of light elements such as B, C, O and H, and organic linkers are covalently bonded with boron-oxide clusters. Their results showed that 3D-COFs, COF-105 (82 mmol/g) and COF-108(96 mmol/g) exhibited exceptionally high CO₂ storage capacity and exceeded the experimentally reported highest capacity in MOF-177 (33 mmol/g) at 30 bar and 300 K.

They also discussed that free volume, porosity, accessible surface area and the framework density are highly correlated with the gravimetric and volumetric CO₂ uptake at 300 K and 30 bar.[72] In another study, Liu et al.[74] described the adsorption mechanism of CO₂ molecules in two ZIFs, ZIF-68 and ZIF-69 using conventional simulation techniques. ZIFs are a sub class of MOFs which resemble zeolites. Their results showed that the small pores formed by the imidazolate ligands are the preferential adsorption sites for CO₂ molecules.[74] Current literature review suggests that MOFs are highly useful adsorbents for gas storage applications and molecular simulations can be used to describe the adsorption mechanisms of gas molecules inside MOFs and screen a large number of MOFs to identify the promising ones.

2.3. Gas Separation Applications of MOFs

Gas separation using MOFs has been generally studied in two categories: equilibrium-based gas separations and kinetic-based gas separations.[75] In equilibrium-based gas separations, MOFs are used as adsorbents and the selectivity of an equilibrium-based separation is governed by the adsorption affinity of the MOF for one gas species relative to other. In kinetic-based separations, MOFs are used as membranes and the selectivity is controlled by the combination of adsorption and diffusion where the latter is determined by different transport rates of the gas species through membrane's pores. In the following sections, both adsorption-based and membrane-based gas separation applications of MOFs were discussed.

2.3.1 Adsorption-based Gas Separation

Adsorption-based gas separation processes have been gained significant attention in chemical and petrochemical industries in the past two decades.[76] The process is based on physical adsorption of gas molecules under a high pressure and a low temperature, and desorption at a reduced pressure and an increased temperature. Temperature swing adsorption (TSA) and pressure swing adsorption (PSA) processes are used in practical applications. In TSA process, the adsorbent is regenerated by heating whereas in PSA process, the adsorbent is regenerated by lowering the pressure.[76] Gas separation occurs based on the following mechanisms: (1) molecular sieving effect: some of the molecules can enter the pores where they are adsorbed while others cannot due to size or shape exclusion, (2) the thermodynamic

equilibrium effect: preferential adsorption of some components due to different adsorbate-surface and adsorbate packing interactions, (3) the kinetic effect: some components can enter and be adsorbed on the pores faster than others due to different diffusing rates.[30]

The amount of adsorbed gas can be measured by using either the Sieverts apparatus based on the volumetric measurement method or microbalance based on the gravimetric method.[51] Figure 2.8 provides the schematic view of both volumetric and gravimetric method. In volumetric method, the change in pressure within a sealed system containing the adsorbate and adsorbent is measured to determine the amount of adsorbed gas. The adsorbed gas amount is then calculated by using an equation of state to mimic real gas behavior at the desired pressure and temperature. In the gravimetric method, the mass of the adsorbed gas is directly measured by using a microbalance.[62] Both methods can be used to obtain gas adsorption isotherms.

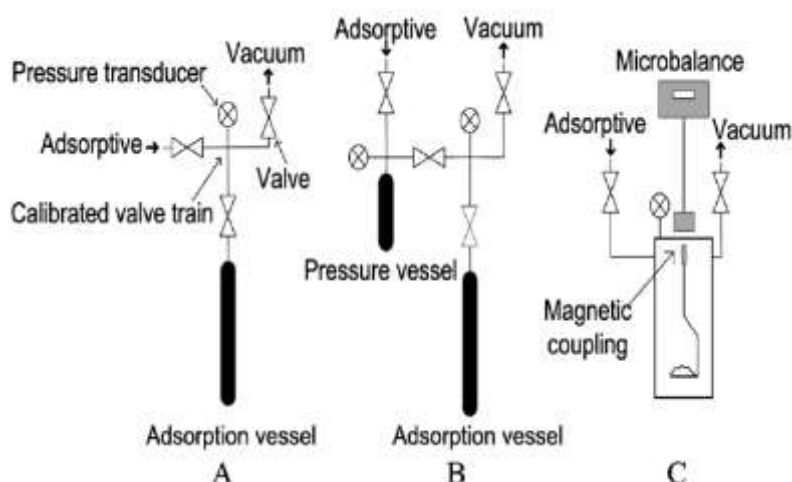


Figure 2.8 (a) Simple volumetric apparatus, the valve train itself serves as the reference volume. (b) Volumetric apparatus with separate pressure vessel to act as a reference volume. (c) Gravimetric instrument.[62]

In the literature, *absolute*, *excess* and *total* adsorption terms are commonly used to express gas uptake in a porous MOF. Gas adsorption within MOFs is dependent on the weak dispersive forces. The distance between gas molecules and surface of the porous material affects the strength of the interaction. If the separation distance is very large, attractive forces of the surface can be negligible and free gas molecules are only present in the system.[50]

Herein, Gibbs dividing surface can be defined as shown in Figure 2.9. This surface divides the free volume into two states: adsorbed gas region (green) or bulk gas region (blue). Since it is not possible to know the exact location of this red boundary, experiments report *excess* adsorption. Excess adsorption gives the amount of adsorbed gas which is in contact with the framework. *Absolute* adsorption, on the other hand gives the amount of adsorbed gas which is in contact with both the framework and bulk region. The presence of bulk gas molecules is considered when the gas-solid interactions are absent. For gas storage applications in MOFs, it is more convenient to use *total* adsorption. As can be seen in Figure 2.9 (b), total adsorption is calculated by the summation of excess amount and the amount of gas within in the pore of the material.

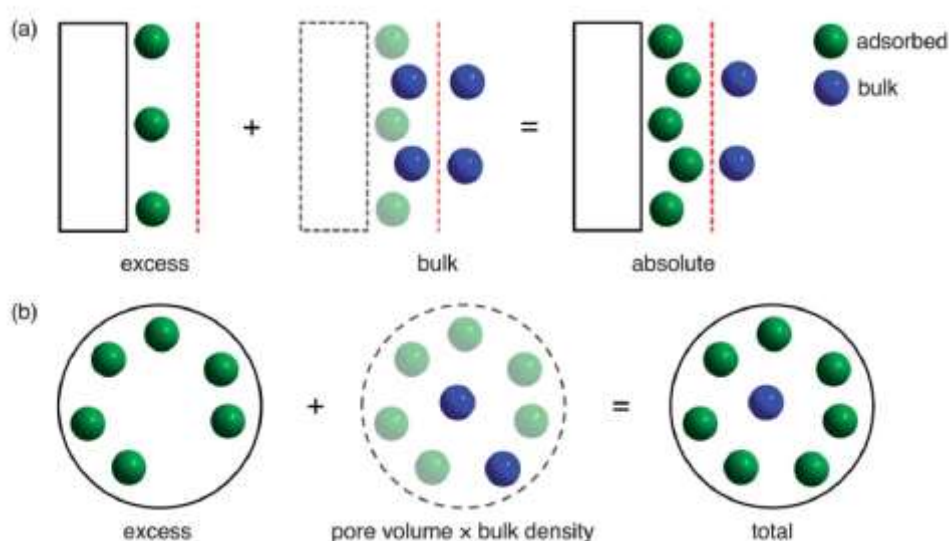


Figure 2.9 (a) Schematic view of the excess and absolute adsorption on a two-dimensional rectangular surface. (b) Total adsorption for porous materials.[50]

The design of the adsorption-based gas separation process is dependent on the capacity of the adsorbent in the operating temperature and pressure, the regeneration method such as PSA or TSA, the length of unused bed, and the product purities. Both high adsorption selectivity and high working capacity are desired for a good adsorbent. Regenerability which is the ratio of working capacity of the strongly adsorbed component to the amount of adsorbed gas is also important to assess the adsorption-based gas separation performance of materials. Several adsorbents including zeolites, carbon molecular sieves, activated carbons have been used in commercial adsorption-based gas separations to date.[76] In the past two

decades, we have witnessed the development of new porous materials, MOFs in gas separation and purification applications.[77] The very large number and variety of MOFs make them strong alternatives to other adsorbent materials in gas separation applications. MOFs are also able to overcome the main barriers of traditional adsorbents, high working capacity and high selectivity.[3] Due to their highly porous structures, MOFs offer high gas uptake capacity. In addition, tunable design of these materials provides superior functional properties which lead high gas affinity. For example, Arstad et al.[68] synthesized three different MOFs with and without uncoordinated amine functionalities and tested these materials as adsorbents for CO₂. Their results showed that amine-functionalized MOF adsorbents have significantly higher CO₂ adsorption capacities compared to non-functionalized MOFs due to high Van-der-Waals interaction of CO₂ with the amines. Similarly, Vaidhyanathan et al.[78] synthesized a three dimensional amine-functionalized porous MOF, Zn-aminotriazolato-oxalate (Zn-Atz) and showed that this MOF has a rapid CO₂ uptake at low pressures with complete reversibility and high enthalpy of adsorption for CO₂. The heat of adsorption exhibited by Zn-Atz (40.8 kJ/mol) was reported to be slightly lower than the highest value observed in zeolite NaX (48.2 kJ/mol) used in pressure swing adsorption devices.[78] This high adsorption energy was attributed to the strong CO₂-amine interactions and relatively small pores of the structure.

MOFs are widely used in carbon capture and storage applications (CCS) to reduce CO₂ emissions. Main CO₂ separations are pre-combustion capture (CO₂/H₂), post-combustion capture (CO₂/N₂) and natural gas purification (CO₂/CH₄). Since CO₂ has smaller kinetic diameter (3.3 Å) than those of N₂ (3.64 Å) and CH₄ (3.8 Å), many MOFs have high CO₂ selectivity over N₂ or CH₄ due to size or shape exclusion. For example, Liang and co-workers[79] compared the CO₂ separation performance of CuBTC with that of a benchmark zeolite-13X and reported that CuBTC exhibits higher CO₂/N₂ selectivity (~12) and CO₂/CH₄ selectivity (~4.5) than zeolite-13X (CO₂/N₂:~6 and CO₂/CH₄:~2.6). Chen et al.[77] reviewed a total of 27 promising MOF adsorbents for CO₂/N₂ and CO₂/CH₄ separations at room temperature. Based on their results, SIFSIX-2-Zn has the highest CO₂/N₂ selectivity (1818) and CO₂/CH₄ selectivity (231) at 1 bar.[77] This was attributed to narrow pore dimensions (3.84 Å) of SIFSIX-2-Zn. Mg-MOF-74 has also high CO₂/N₂ and CO₂/CH₄ selectivities due to the open metal sites of the framework which lead strong electrostatic interactions between

adsorbates and the framework. CO_2 ($13.4 \times 10^{-40} \text{ Cm}^2$) has higher quadrupole moment comparing to N_2 ($4.7 \times 10^{-40} \text{ Cm}^2$) or CH_4 (non-polar). Therefore, CO_2 molecules have strong electrostatic interactions with the framework which improve the CO_2 uptake capacity of MOFs. An et al.[46] synthesized a bio-compatible MOF, bio-MOF-11 and reported that this MOF exhibits a high selectivity (75) for CO_2/N_2 separations. An isoreticular series of bio-MOF-11 analogues was later synthesized by the same research group.[80] The CO_2 and N_2 adsorption isotherms up to 1 bar at 273 and 298 K were examined and high CO_2/N_2 selectivities were reported for bio-MOFs-11, -12, -13 and -14. Molecular simulations were also performed to understand gas adsorption behavior of these MOFs and IAST (Ideal Adsorbed Solution Theory) was used to predict adsorption selectivity for CO_2/N_2 mixtures. High CO_2/N_2 selectivities were reported as 43, 52 and 40 for bio-MOF-11, bio-MOF-12 and bio-MOF-13 at 1 bar and 298 K, respectively. It was also shown that as the aliphatic chain length increases (acetate, propionate, butyrate, and valerate chains for bio-MOFs-11, -12, -13 and -14, respectively), water stability of structures increases. Yaghi et al.[81] investigated the adsorption-based gas separation performance of ZIF-78, -79, -80, -81 and -82 and reported that ZIF-78 has the highest selectivity for CO_2/N_2 (50.1) and CO_2/CH_4 (10.6) separations due to strong electrostatic interactions and small pore diameter (7.1 Å) of ZIF-78. Long et al.[82] investigated CO_2/H_2 separation performance of different MOFs including MOF-177, Be-BTB, Cu-BTtri, Mg-MOF-74 and they reported that Mg-MOF-74 and Cu-BTtri exhibit high CO_2 selectivity over H_2 due to strong interactions between CO_2 molecules and the open metal sites of the frameworks. There are comprehensive reviews on CO_2 capture and separation in the literature.[3, 30, 77]

MOFs are also widely used in CH_4/H_2 separations. However, to best of our knowledge, there is no experimental CH_4/H_2 mixture adsorption data of MOFs in the literature. There is only ideal selectivity data in the literature. Ideal selectivity is estimated using single adsorption data of two different gas molecules. Details of ideal selectivity estimation can be found in Chapter 3. Since there is no experimental CH_4/H_2 mixture adsorption data of MOFs, computational methods are highly useful to determine the separation performance of each MOF. Recently, Basdogan et al.[25] estimated both ideal and mixture selectivities of a large number MOFs at a wide range of pressures. They found a good agreement between their predicted ideal selectivities and experimentally reported ideal selectivities. They also stated

that ideal selectivities can be only used at low pressures (≤ 1 bar) to compare the adsorption-based gas separation performance of MOFs. At higher pressures, ideal selectivity underestimated the mixture selectivity of MOFs because at high pressures, the gas molecules compete with each other for the same adsorption site and CH_4 molecules are adsorbed much strongly than H_2 molecules. For this reason, mixture selectivities were higher than the ideal selectivities. This result shows that multi-component effects play a significant role in determining separation performances of MOFs.

To date many computational studies were performed to determine the adsorption-based gas separation performance of MOFs.[25, 64, 83-86] Keskin's group[87-89] computed adsorption selectivities and delta loading capacities of many ZIFs, COFs and Cu-TDPAT for CH_4/H_2 , CO_2/H_2 , CO_2/N_2 and CO_2/CH_4 separations. Erucar and Keskin[90] assessed the performance of Zn-Atz in adsorption-based separations of CH_4/H_2 , CO_2/H_2 , CO_2/N_2 and CO_2/CH_4 mixtures calculated at an adsorption pressure of 10 bar and desorption pressure of 1 bar. Their results showed that Zn-Atz is a very promising adsorbent for CH_4/H_2 (CO_2/H_2) separations with a high CH_4 (CO_2) selectivity of 48 (886). The adsorption selectivity of Zn-Atz for CO_2/N_2 (98) is also high compared to that of traditional zeolites such as MOR, DDR, LTL and TON. Chen and Jiang[91] investigated separation performance of bio-MOF-11 for CO_2/N_2 and CO_2/H_2 mixtures using molecular simulations. The high adsorption selectivity (375) computed for CO_2/H_2 mixture at 298 K at 4 bar was attributed to the presence of Lewis-basic sites in adenine which improves the interactions with CO_2 molecules. They also showed that adsorption selectivity of bio-MOF-11 is not significantly affected from the humidity, suggesting that bio-MOFs can be efficiently used under industrial operating conditions. Wu et al.[84] investigated 105 MOFs for flue gas separations. They reported that in order to enhance gas adsorption selectivity of MOFs two strategies including increasing heat of adsorption and decreasing void fraction can be used.[84] Recently, Qiao et al.[85] screened 4764 MOFs for CO_2/N_2 and CO_2/CH_4 separations. They found that alkali-MOFs have the lowest separation performance but rare earth MOFs (Ln-MOFs) which have the moderate heat of adsorption values exhibit the highest separation performance. Wu et al.[86] screened a total 105 MOFs for adsorption-based CH_4/H_2 separations and they reported that three MOFs have high selectivity (>100) at low pressure (0.01 bar). Basdogan et al.[25] recently screened 250 different MOFs for adsorption based CH_4/H_2 separations and identified the top performing

material that exhibited the highest adsorption selectivity (204) for CH₄/H₂ separations. The high adsorption selectivity for CH₄ was attributed to narrow pore dimensions of the MOF (IPIDAN) (2.99/5.09 Å) which lead strong confinement of CH₄ molecules.[25] The current literature suggests that MOFs are promising adsorbents for adsorption-based gas separations.

2.3.2 Membrane-based Gas Separation

Membrane-based gas separation has become an attractive technology due to the lower energy requirement and ease of operation compared to the traditional gas separation methods such as distillation, extraction and adsorption. Polymeric membranes have been widely used in separation of gas mixtures in many industrial applications such as removal of CO₂ from natural gas, air separation, purification of alcohols from fermentation broths and H₂ recovery from hydrocarbon mixtures. Ease of fabrication and low cost are the advantages of polymeric membranes which make them widely preferable in gas separation processes. The key parameters used to assess the separation performance of a membrane are the gas permeability and selectivity. Permeability is defined as the transport rates of the components (permeates) through a membrane and selectivity is the ratio of the more permeable component's permeability to that of the less permeable one. Membranes having high gas permeability are economical since they require less surface area whereas membranes having high gas selectivity are efficient since they produce high purity gas streams. Therefore, both high gas permeability and high gas selectivity are desired for an effective membrane-based gas separation process.

Robeson[92] analyzed the gas separation characteristics of a large collection of polymeric membranes including polyimides, polysulfones, polyacetylenes, polypyrrolones, polymers of intrinsic microporosity (PIM) and set the upper bound on the selectivity vs. permeability performance of these polymeric membranes. The upper bound shows the trade-off between gas selectivity and permeability. Polymers having high permeability generally show low selectivity and polymers having high selectivity exhibit less permeability. Freeman et al.[93] demonstrated that the strong size sieving nature of the stiff chain glassy polymers is the main reason of the upper bound. Diffusion coefficients of gases increase with the increase in the fractional free volume of the polymers and rubbery polymers have molecular chain mobility. Therefore, permeability of the gas molecules is generally high in rubbery polymers but the sieving ability of these membranes is low since molecules can easily penetrate through

the flexible chains. On the other hand, glassy polymers have restricted chain motions which enable only the diffusion of small gas molecules through the chains. The selectivity of glassy polymers is high due to their strong size sieving ability. Developing membranes that can overcome the selectivity/permeability trade-off and exceed the Robeson's upper bound has been the main focus of membrane research for a long time.

MOFs have been recently used to fabricate defect-free, thin-film membranes and tested for gas separation applications. The first thin-film MOF membrane was fabricated using MOF-5 on a porous α -alumina substrate and high H_2 permeability was reported due to the large pores ($8 \text{ \AA} \times 15 \text{ \AA}$) of MOF-5.[94] There are many other experimental studies for MOF-5 membranes.[95-97] CuBTC membrane was also reported to exhibit high H_2 permeability and H_2 selectivity in separation of H_2/N_2 , H_2/CO_2 and H_2/CH_4 mixtures.[98] Following this study, several other CuBTC membranes were reported in the literature.[99-106] MOF-5, CuBTC, ZIF-8 and ZIF-90 were widely used to make thin-film MOF membranes. ZIF-8 membrane can be considered as the most widely studied MOF membrane and ZIF-8 was investigated in various separation applications such as H_2/CO_2 , H_2/CH_4 , C_2H_4/C_2H_6 , H_2/N_2 , CO_2/CH_4 . [107-109] ZIF-90 membrane was also widely studied in the literature. ZIF-90 was reported to exhibit high H_2/CH_4 selectivity (70.5) at 225 °C and 1 bar.[110] The high H_2 selectivity of ZIF-90 was attributed to narrow pore dimensions and inter-crystalline defects due to post-functionalization.[110] In a recent review, Adatoz et al.[111] discussed that only 29 different types of thin-film MOF membranes exist in the literature and they provided experimental gas permeability and selectivity measurements of these membranes together with their operating conditions. Among these MOF membranes, three of them are bio-MOF membranes, bio-MOF-1, bio-MOF-13 and bio-MOF-14. Bohrman and Carreon[112] fabricated the first bio-MOF membrane using bio-MOF-1 that exhibits CO_2/CH_4 selectivity of 2.7 at 1.38 bar and 298 K. Bio-MOF-13 and bio-MOF-14 have slightly higher CO_2/CH_4 selectivity (~ 4) than bio-MOF-11.[47]

Although there are thousands of different MOF structures that have been synthesized, only a few different types of thin-film MOF membranes have been fabricated to date because fabrication of pure MOF membranes has several limitations such as large scale production and defect-free membrane formation. High manufacturing cost is another barrier for the large-scale development of thin-film MOF membranes. The challenges experienced in making thin-

film MOF membranes and the trade-off problem of polymeric membranes have motivated researchers to design and develop alternative membranes known as mixed matrix membranes (MMMs) that show a great promise for short term commercial implementation.

MMMs are composite membranes that combine mechanical elasticity, easy processability and low cost of polymers with superior gas separation performance of nanoporous materials. They are formed by incorporation of selective nanoporous particles into polymer matrices as fillers.[113] The greatest advantage of this approach is to make membranes with relatively easy adaptation of existing commercial technology since fabrication of polymer membranes is well developed. There are three methods to prepare MMMs: (1)dispersion of the filler particles into the solvent and addition of the polymer to the filler solution, (2)preparation of the polymer solution and addition of the filler particles to the polymer solution, (3)preparation of the polymer solution and filler solution separately and combining these solutions.[114]

MOFs have been recently used as filler particles in MMM applications to improve the gas separation properties of pure polymers. Experimental efforts concluded that MOFs show better compatibility with the polymers compared to inorganic fillers such as zeolites and silicas since MOFs have organic linkers that enhance adhesion to the polymer phase.[115] Incorporation of MOFs within the polymers resulted in MOF-based MMMs that have better separation performance than the pure polymers. The very large number of MOFs and polymers represent an opportunity for fabrication of various MOF-based MMMs. Figure 2.10 shows the quick growth of number of publications on thin-film MOF membranes and MOF-based MMMs. Since fabrication of MOF-based MMMs is relatively easier than that of thin-film MOF membranes, the number of studies on MOF-based MMMs is higher than the one on pure MOF membranes.

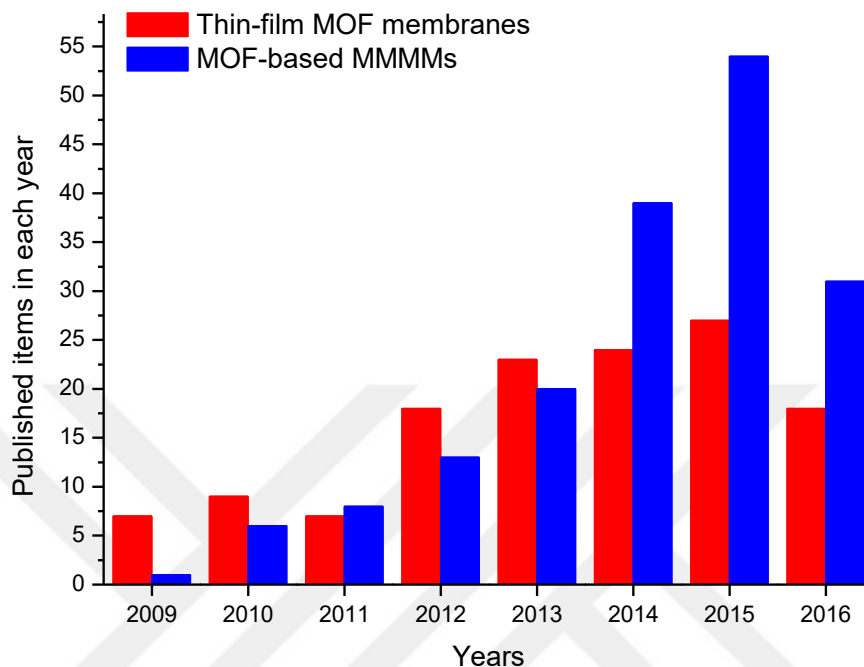


Figure 2.10 Number of publications featuring the terms "metal organic framework", "gas separation" in their topics and "membrane" in titles, Accessed: 2016-08-09 at Web of Science®

The first MOF-based MMM containing Cu(II)BPDC-TED (copper(II) biphenyl dicarboxylate triethylenediamine) in poly 3-acetoxyethylthiophene was synthesized by Yehia and co-workers.[116] They reported that CH₄ selectivity of MMMs having 20 and 30 wt% Cu(II)BPDC-TED increases whereas the CO₂ permeability and CO₂/CH₄ selectivity decrease. Zhang et al.[117] found similar results for the incorporation of Cu-BPY-HFS into Matrimid. They showed that Cu-BPY-HFS has the affinity towards CH₄ which makes this MOF suitable for CH₄ separation. The CO₂/CH₄ and H₂/CO₂ selectivities decreased while CH₄/N₂ selectivity slightly increased. Won and co-workers[118] embedded a MOF named [Cu₂(PF₆)(NO₃)(4,40-bpy)₄](PF₆)₂(H₂O)₂ into PSF (polysulfone) polymer up to 5 wt% and investigated the permeation of CH₄, N₂, He, H₂, O₂. They observed a remarkable decrease in CH₄ permeability of MMMs with increasing MOF loading due to the small pores of the MOF which restricted the motion of CH₄ molecules. This study underlined the importance of pore size in MOF selection. The first patent on MOF-based MMMs was reported by Liu and co-

workers[119] who incorporated IRMOF-1 (MOF-5) and HKUST-1 (CuBTC) into Ultem and Matrimid. They reported that H₂, CO₂ and CH₄ permeabilities were increased compared to the pure polymers. Selectivity of H₂ over CH₄ slightly decreased while CO₂ selectivity over CH₄ did not change. Similar results were found by Perez et al.[115] who also used MOF-5 as filler particles in Matrimid. They observed enhancements in permeability of H₂, O₂, CO₂, N₂ and CH₄ with very slight improvement in CH₄ selectivity for CO₂/CH₄ and N₂/CH₄ mixtures due to the larger solubility of CO₂ and N₂ in the polymer matrix. Diffusion of gas molecules were increased because of the high porosity of MOF-5 and higher permeabilities were observed in MOF-5/Matrimid MMMs compared to pure Matrimid. Car et al.[120] used CuBTC and Mn(HCOO)₂ as filler particles in PDMS (polydimethylsiloxane) and PSF for separation of CO₂ from N₂ and CH₄. They observed slight improvements in ideal selectivity of CO₂/N₂ and CO₂/CH₄ in addition to the increase in H₂ permeability and H₂/CH₄ selectivity compared to pure polymers. Similarly, Hu et al.[121] incorporated CuBTC into polyimide (PI) to obtain a hollow fiber MMM and reported a good compatibility between PI and CuBTC. They showed that both H₂ permeance and H₂ selectivity over CH₄, CO₂, O₂ and N₂ increase compared to those of pure polyimide and concluded that CuBTC/polyimide hollow fiber MMMs can be used for efficient H₂ separation applications. Adams et al.[122] synthesized CuTPA/polyvinyl acetate MMMs and reported improvements in CO₂ permeability and ideal selectivity of CO₂/N₂, CO₂/CH₄, O₂/N₂, He/CH₄ and N₂/CH₄ compared to pure polymer. They also observed a good contact between the polymer phase and CuTPA.

ZIF-8 was used as filler particles in most of the recent MOF-based MMM experiments. Ordonez et al.[123] fabricated ZIF-8/Matrimid MMMs and measured permeability of pure H₂, CO₂, O₂, N₂, CH₄, C₃H₈. They found that pure gas permeabilities increase with ZIF-8 because addition of ZIF-8 particles increase the distance between polymer chains and create a larger polymer free volume which result in enhanced gas permeability. Due to the nonselective gas permeation, the ideal selectivity did not change significantly. In MMMs where ZIF-8 loading is high (>40 wt%), gas molecules followed a more tortuous path around the ZIF-8 particles and their permeability decreased. The ideal selectivity increased specifically for CO₂/CH₄ and H₂/CH₄ pairs since ZIF-8 have small pore apertures that act as molecular sieves. Diaz et al.[124] reported the permeabilities of H₂, N₂, CO₂, CH₄, C₂H₆ and C₂H₂ in ZIF-8/poly(1,4-phenylenether-ether-sulfone) (PPEES) MMMs

and their results showed that permeability and diffusion coefficient of all gases increase as the ZIF-8 loading increases without any change in ideal selectivity. This result was attributed to the formation of large free volumes in the membrane by addition of ZIF-8, which agrees with the results of Ordonez et al.[123] and Merkel et al.[125] Similarly, Song et al.[126] measured the permeability of H₂, N₂, CO₂, CH₄ and O₂ across ZIF-8/Matrimid MMMs containing 0-0.3 weight fractions of ZIF-8 and reported that the permeability of all gases increase as the ZIF-8 loading increases compared to pure polymer membrane. The positron annihilation lifetime spectroscopy analyses confirmed that addition of ZIF-8 into Matrimid changed the molecular packing of the polyimide based membranes and led to an increase in the free volume and in gas permeability of ZIF-8/Matrimid membrane. Dai et al.[127] made asymmetric hollow fiber ZIF-8/Ultem membrane and observed an increase in separation performance of CO₂/N₂ gas pair for both pure gas and mixed gas feeds due to the good adhesion between the hollow fibers and ZIF-8 particles.

The MMMs containing ZIF-90 filler particles in Ultem, Matrimid and 6FDA-DAM polyimide were fabricated by Bae and coworkers.[128] Both pure and mixed gas permeabilities of CO₂ and CH₄ were measured. The best performance was observed for ZIF-90/6FDA-DAM membranes with high selectivity for CO₂/CH₄ and CO₂/N₂ separation since 6FDA-DAM polymer has high CO₂ permeability due to its large free volume and high CO₂ selectivity due to its size-sieving ability. These properties compared to Ultem and Matrimid allowed ZIF-90/6FDA-DAM membranes to exceed the upper bound. Yang and co-workers[129] embedded ZIF-7 into polybenzimidazole (PBI) polymer and obtained highly permeable and selective MMMs. These MMMs showed higher H₂ permeability and H₂/CO₂ selectivity than neat PBI and ZIF-7 membranes. The extra-introduced free volume due to the interactions between the PBI and ZIF-7 accelerated the transport of gases and the rigidified chains enhanced the molecular sieve effect.

Recent studies examined the effect of using two different types of filler particles or polymers in MMMs. For example, Zornoza et al.[130] used silicate-1 and CuBTC together in PSF to test if there are potential fillers that improve and stabilize filler dispersion when used together. Rigidity enhancement, restricted motion of the polymer, good dispersion and disaggregation of the fillers in the polymer matrix were achieved with the combination of silicalite-1 and CuBTC fillers. They measured CO₂/N₂, CO₂/CH₄, O₂/N₂ and H₂/CH₄ mixture

permeation and reported selectivity improvements for CO₂/CH₄ and CO₂/N₂ in the CuBTC/silicalite-1/PSF membranes. Basu et al.[131] incorporated CuBTC into PI/PSF for separation of binary gas mixtures, CO₂/CH₄ and CO₂/N₂. They observed that both CO₂ selectivity and CO₂ permeance of CuBTC/PI/PSF membranes are higher than those of unfilled polymers.

The literature survey summarized so far suggested that MOF-based MMMs exhibit promising gas separation performances. However, the high number of MOFs and polymers provides a fundamental challenge in this research: the appropriate choice of MOF/polymer pairs to achieve high efficiency for a specific gas separation. Practical fabrication of a single MMM takes several months and even if only one polymer is considered there are thousands of MOFs that could be potentially used to make MMMs. Given the very high number of MOF/polymer combinations, using computational screening methods to select the most promising MOF/polymer pairs before investigating a large amount of time and resources into MMM fabrication is crucial. Computational studies that can provide fundamental information for the separation performance of MOF-based MMMs prior to experiments are very helpful to identify the most promising MOF/polymer pairs for high efficiency gas separations. This type of computational studies predicts the material properties needed to characterize the performance of MMMs in advance and greatly accelerate the development of practical MOF-based MMMs.

Erucar and Keskin[90] recently reviewed molecular modeling studies of MOF-based MMMs. In computational studies, a good agreement between model predictions and experimentally reported gas permeabilities were found for IRMOF-1/Matrimid, CuBTC/Matrimid, CuBTC/PSF, CuBTC/PDMS, CuBTC/PI, Cu-BPY-HFS (Cu-4,4'-bipyridine-hexafluorosilicate)/Matrimid, ZIF-8/Matrimid, ZIF-8/Ultem, ZIF-8/PPEES, ZIF-90/Matrimid, ZIF-90/Ultem and ZIF-90/6FDA-DAM MMMs. The first computational methodology to estimate gas permeability through a MOF-based MMM was reported in 2010.[132] In that study, Matrimid was used as the polymer and permeability of gas molecules through Matrimid was taken from the experimental data. The filler was IRMOF-1 and gas permeabilities of IRMOF-1 were predicted using molecular simulations as described in Chapter 3.1. These permeability values were then inserted into the permeation models to predict P_{MMM} and predictions were in good agreement with the experimental data for IRMOF-

1/Matrimid MMM.[132] Erucar and Keskin[133] compared predictions of several permeation models with the available experimental data for single component CO₂ and CH₄ permeabilities in IRMOF-1/Matrimid MMMs and mixed-gas permeabilities of CO₂/CH₄:35/65 mixture in CuBTC/Matrimid MMMs. They found that the percentage average absolute relative error (AARE) values of the permeation models considering ideal morphology are in the following order: Pal>Bruggeman>Lewis-Nielson>Maxwell model. The AARE values for the models considering interfacial morphologies were in the following order: modified Maxwell>Felske>modified Felske model. Details of the permeation models were given in Chapter 3. Thornton et al.[134] predicted H₂/CO₂, H₂/N₂, O₂/N₂ separation performance of ZIF-8/Matrimid MMMs, CO₂/N₂ separation performance of ZIF-8/Matrimid and ZIF-90/6-FDA-DAM MMMs, CO₂/CH₄ separation performance of ZIF-90/Matrimid, ZIF-90/Ultem and ZIF-90/6-FDA-DAM MMMs. They used Bruggeman permeation model and considered ZIF fillers up to 60% volume fraction. At high volume fractions of the fillers, theoretical predictions deviated from the experimental measurements and this was attributed to the disruption of polymer chain packing at the ZIF-polymer interface. Erucar et al.[135] carried out MOF-based MMM calculations both with and without electrostatic interactions between adsorbates and MOFs for CO₂/CH₄, H₂/CO₂, CO₂/N₂ separations. Results showed that for rapid screening of MOF/polymer MMMs, the electrostatic interactions between adsorbates and MOFs can be neglected as a reasonable approximation if the MOF volume fraction is low in the MMM, less than 0.3. However, for higher MOF volume fractions, the electrostatic interactions should be included in the computational model. Zhang et al.[136] used fully atomistic simulations to study a MOF/polymer MMM. This is currently the only study in the literature to that models both the MOF and polymer at the atomic level. They studied H₂/CO₂ permeation in ZIF-7/PBI membranes using molecular simulations. They concluded that while there are some discrepancies between simulated and experimental results in neat PBI and ZIF-7, permeability and mechanical property of PBI membrane can be improved by adding ZIF-7. This method is expected to very helpful to study MMMs that include new polymers for which the gas permeability data is not available from the experimental studies. However, full atomic simulations of MOF-based MMM is challenging for several reasons:(i)large computational time and sources required to model the whole

system, (ii) lack of appropriate force fields to represent the MOF/polymer/interface system, (iii) representation of nonselective voids between MOF and polymer.

A review of current literature presented above suggests that although different types of MOFs studied in the literature, there is limited information about adsorption-based and membrane-based gas separations of bio-MOFs. In order to better evaluate adsorbent and membrane potential of bio-MOFs, their separation performances must be compared with well-known nanoporous materials considering adsorbent selectivity, working capacity, gas permeability and membrane selectivity. It is also important to note that molecular simulation studies mentioned above do not consider structural flexibility of bio-MOFs, in other words simulation of bio-MOFs at the atomic level was done using rigid framework assumption, by fixing crystallographic positions of the atoms. Rigid framework assumption saves tremendous computational time, however flexibility of structures may have significant effects on the gas adsorption and diffusion properties. Greathouse et al.[137] compared rigid and flexible force fields to compute H₂, Ar, Xe and Kr adsorption in IRMOF-1 at room temperature and showed that flexibility has negligible effect on adsorption of these gases. Flexibility is much more important in gas transport through nanoporous materials. Greathouse and Allendorf [138] showed that using a flexible force field results in good agreement with the experimental data of benzene diffusion in IRMOF-1. Zhang et al.[139] computed adsorption isotherms and diffusion coefficients of CO₂ and CH₄ molecules in ZIF-8 using both rigid and flexible force fields. They found negligible difference between the simulated adsorption isotherms in rigid and flexible ZIF-8 structures, which agreed well with the experimental data. However, significant difference between rigid and flexible simulations was found for gas diffusivities. They observed no diffusion behavior in rigid ZIF-8 for CO₂ and CH₄ whereas similar self-diffusion coefficients with the experimental data were obtained from flexible ZIF-8 simulations. These studies concluded that diffusion of gases is significantly affected from the structure flexibility especially if the pore size of the structure is close to the kinetic diameter of the gas molecule.

In this thesis, we performed grand canonical Monte Carlo (GCMC) and equilibrium molecular dynamics (EMD) simulations to investigate potential of ten different bio-MOFs in adsorption-based and membrane-based gas separations. In EMD simulations, flexibility of

bio-MOFs was considered and effects of structure flexibility on the predicted membrane performance of bio-MOFs were discussed.

2.4 Biomedical Applications of MOFs

MOFs have gained significant attention in the past decade and a large number of experimental and computational studies were conducted to assess gas storage and gas separation performance of MOFs.[31] One of the areas that MOFs recently started to appear is biomedical applications. Biomedical applications of MOFs include drug storage, drug delivery and imaging.[21, 31] Efficient drug storage is required to improve the drug bio-distribution, the biological half-life of the active species and therapeutic effect of the drug.[33] Lipids, polymeric nanoparticles, metal clusters and carbon structures have been tested as drug storage materials in the past.[33] However, these materials have several limitations such as low drug loading capacities (<5 wt%), rapid drug release and toxicity.[34] MOFs have been recently studied as alternative drug storage materials due to their large pore volumes.

The first group of MOFs which was investigated as potential candidates for drug storage was the MILs due to their large pore sizes (25-34 Å) and high surface areas (3100-5900 m²/g).[35] Horcajada and co-workers[140] investigated storage and release of an analgesic and anti-inflammatory drug, ibuprofen, in MIL-100(Cr) and MIL-101(Cr). They reported high ibuprofen loading in these materials, 0.35 g ibuprofen/g MIL-100(Cr) and 1.38 g ibuprofen/g MIL-101(Cr). They later investigated MIL-53(Cr) and MIL-53(Fe) for adsorption and delivery of ibuprofen and found out that both MOFs adsorb around 0.2 g ibuprofen/g MOF.[141] Figure 2.11 shows the ibuprofen delivery kinetics for different MOFs and mesoporous silica. Ibuprofen loading in MIL-101(Cr) (1.38 g/g) was reported to outperform mesoporous molecular sieves MCM-41 (0.34 g/g), MIL-100(Cr) (0.35 g/g) and MIL-53(Fe) (0.21 g/g). In other words, MIL-101(Cr) offered four times higher drug storage capacity than the mesoporous silica as shown in Figure 2.11. This result was attributed to the high surface area (4500 m²/g) of MIL-101(Cr) and formation of specific interactions between ibuprofen molecules and the Lewis acid metal sites and the organic moieties of the MOF.[34] However, practical usage of MIL-101(Cr) in drug storage and delivery is limited due to the presence of toxic Cr metal in the framework. This MOF is simply not biocompatible due to its toxic metal. By definition, biocompatibility means compatibility with a living system by not being

toxic. In order to decrease the toxic effects of organic linkers and metals, bio-molecules such as amino acids, nucleobases and sugars are used as linker molecules and bio-compatible metal cations are chosen to construct bio-MOFs.[36] In this way, bio-compatible MOFs may be reused in the body after administration. An and co-workers[37] reported that bio-MOF-1 shows promise for storage and release of cationic drug molecules due its anionic character. This was the first potential biomedical application of a MOF constructed with biomolecular building blocks.

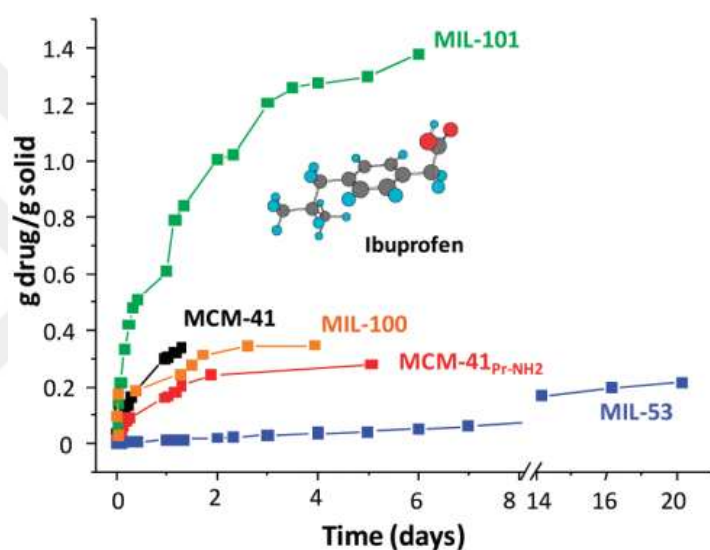


Figure 2.11 Ibuprofen delivery in several porous MOFs and MCM-41.[34]

Storage of antitumoral busulfan (Bu), doxorubicin (DOX) and antiviral azidothymidine triphosphate (AZT-Tp), cidofovir (CDV) is much more challenging because these drugs suffer from poor solubility and stability in the biological aqueous media in addition to short half-lives.[34] Current storage of Bu in liposomes or polymeric nanoparticles never exceeds 5-6 wt%.[142] As an alternative to these materials, Fe-based MOFs were tested for Bu storage. MIL-100(Fe) showed an unprecedented Bu uptake exceeding 25 wt% and MIL-53(Fe) was reported to show 13 wt% Bu uptake.[142] These results were explained by the lower pore volume of MIL-53(Fe) compared to that of MIL-100(Fe), but the reported Bu uptake of MIL-53(Fe) was still higher than that of traditional drug storage materials.[142] Anand et al.[143] showed controlled release of DOX incorporated into MIL-100(Fe) (9 wt%). For AZT-Tp and CDV storage, MIL-101-NH₂ showed high performance (42 wt%) exceeding any other nanoporous system.[144] The antitumor agent 5-fluorouracil (5-FU) was also

studied using Zn and Cu-based MOFs. Sun and co-workers[145] tested ZIF-8 (zeolitic imidazolate framework) for 5-FU storage and reported 45 wt% uptake. The same group achieved 50 wt% uptake of 5-FU in a Zn-MOF.[146] Lucena et al.[147] recently reported unprecedented 5-FU uptake (82 wt%) using CuBTC whereas Li et al.[148] synthesized a new Zn-based MOF and reported 23 wt% 5-FU uptake with highly controlled drug release. These pioneer experimental studies concluded that MOFs can be highly promising materials for drug storage and delivery.

Storage performances of MOFs were also tested for cosmetic molecules such as caffeine (lipo-reducer), urea (hydrating agent), benzophenone-3 and benzophenone-4 (UVA and UVB filters, respectively). Cunha and co-workers[149] studied caffeine uptake of UiO-66(Zr), MIL-53(Fe), MIL-100(Fe) and MIL-127(Fe). They reported caffeine uptake capacity of MIL-100(Fe) as 65.8 wt% using molecular simulations and 49.5 wt% using experimental methods. The discrepancy between simulations and experiments was explained by the pore structure of MIL-100(Fe). MIL-100(Fe) has spherical mesoporous cages connected by narrow pentagonal windows ($\sim 4.7 \text{ \AA} \times 5.5 \text{ \AA}$) and experimental studies showed that caffeine molecules ($\sim 7.6 \text{ \AA} \times 6.1 \text{ \AA}$) are adsorbed only in the large cavities of MIL-100(Fe). However, molecular simulations assumed that all windows of MIL-100(Fe) are accessible for caffeine molecules and therefore overestimated caffeine uptake. When caffeine uptake was considered only in the large cavities of MIL-100(Fe), simulated (46.4 wt%) and experimental (49.5 wt%) uptakes were found to be in good agreement. Horcajada et al.[144] also studied MIL-100(Fe) for storage of urea and reported the uptake value as 69.2 wt%. Liédana and co-workers[150] studied adsorption and release of caffeine in ZIF-8 and reported a lower uptake capacity (28 wt%) compared to Cunha et al.[149] for MIL-100(Fe) (49.5 wt%). However, caffeine uptake reported for ZIF-8 was still higher than that of mesoporous silica, SBA-15 (23 wt%) and non-ordered silicas (20.4 wt%).[80] The same group[151] recently carried out an efficient one-step encapsulation of caffeine in MOF NH_2 -MIL-88B(Fe) and compared their procedure to the traditional three-stage synthesis-activation-encapsulation procedure. They demonstrated a high guest loading (35 wt%) and controlled release. Devautour-Vinot et al.[152] studied caffeine uptake in a series of UiO-66(Zr)-type MOFs, functionalized with -Br, -2OH, - NH_2 and -H groups and reported caffeine uptakes of these materials as 9 wt%, 14 wt%, 22 wt% and 24 wt%, respectively.

Considering the very large number of available MOFs, it is not practical to test drug and cosmetic molecule uptake of each MOF using purely experimental manners. Computational methods that can predict drug storage capacity of MOFs prior to experimental studies would be highly useful to identify the materials with the highest performances. Molecular simulations can also provide molecular-level insights to guide the design and development of new drug carriers. However, the number of computational studies which investigated potential of MOFs in drug storage applications is very limited in the literature.[153-155] The main reason for this is that simulation of large guest molecules in MOFs is challenging because of the strong confinement of the guests by the host material. The first computational study was performed by Babarao et al.[153] who examined structural and dynamic behaviors of ibuprofen in MIL-101(Cr) and UMCM-1 (University of Michigan Crystalline Material). They used molecular simulations to determine uptake and mobility of ibuprofen in these two MOFs and found a good agreement between simulations and previously reported experiments[140] for maximum ibuprofen loading in MIL-101(Cr). They showed that ibuprofen has a stronger binding energy and lower mobility in MIL-101(Cr) than in UMCM-1. Bei and co-workers[154] also studied adsorption behavior of ibuprofen in bio-MOF-1, -11, -100 and UMCM-1. Their results showed that ibuprofen molecules are commonly adsorbed around the metal ions clusters of MOFs. The highest ibuprofen uptake was reported in bio-MOF-100 as 2.03 g ibuprofen/g MOF at 1 bar and 25 °C. They also examined diffusion of ibuprofen in bio-MOF-1, -11 and UMCM-1 and showed slow ibuprofen diffusion in all three MOFs. Bernini et al.[155] investigated different MOFs to determine their ibuprofen uptakes. They found that bio-MOF-100 has the highest ibuprofen uptake capacity (1975 mg/g) due to its high pore volume (2.9 cm³/g). They also reported that CD-MOF-1(CD:cyclodextrin), bio-MOF-100 and MOF-74 have very high potential energy of adsorption of ibuprofen suggesting that these materials can have long ibuprofen release times. In these simulation studies, the physiological body fluid was not considered. In a recent study, Bueno-Perez et al.[156] investigated adsorption of ibuprofen in HMOF-1(heterometal-organic framework), MIL-47(V) and MIL-53(Cr) in the liquid medium. Ibuprofen uptake in MIL-53(Cr) was found to be similar with the one reported by Bernini et al.[155] who did not consider water in their simulations. Therefore, it was concluded that water affects ibuprofen uptake at low pressure but it does not affect the saturation drug loading.

As we summarized above, almost all computational studies in the literature focused on ibuprofen adsorption in a limited number of MOFs, generally in MILs. There is almost no information about the drug/cosmetic molecule storage performances of different types of MOFs. This lack of information also limits understanding the relation between drug/cosmetic storage performances of MOFs and their structural properties. In this thesis, both adsorption and diffusion of representative drug and cosmetic molecules in various bio-compatible MOFs were studied.



Chapter 3

COMPUTATIONAL METHODS

"The underlying physical laws necessary for the mathematical theory of a large part of physics and the whole of chemistry are thus completely known, and the difficulty is only that the exact application of these laws leads to equations much too complicated to be soluble."

(P.A.M. Dirac, 1902-1984)

In this section, computational methods used to estimate gas permeability and gas selectivity of thin-film MOF membranes and MOF-based MMMs were discussed. In order to estimate the gas permeability and selectivity of the membranes, data for gas adsorption and diffusion in the pores of MOFs are required. Molecular simulations such as Grand Canonical Monte Carlo (GCMC), configurational bias Monte Carlo (CBMC) and Equilibrium Molecular Dynamics (EMD) methods were discussed to model gas/drug adsorption and diffusion in MOFs.

3.1 Theoretical Background of Molecular Simulations

In molecular simulations, the microscopic state of a system is defined in terms of positions and momenta of a set of particles. The Hamiltonian of the system can be expressed as a function of coordinates (q) and momenta (p) of the particles:

$$H(q, p) = K(p) + U(q) \quad (3.1)$$

where K is the kinetic energy of the system and U is the potential energy. The potential energy is dependent on the coordinates of individual atoms and pairs. Based on the molecular

mechanics, the classical molecular energy can be described as a Taylor expansion in bonds, bends and torsions, etc.[157]

$$U = \sum_{\text{bonds}} u_b(r) + \sum_{\text{bends}} u_\theta(\theta) + \sum_{\text{torsions}} u_\phi(\phi) + \sum_{\text{non-bonded}} u_{nb}(r) + \dots \quad (3.2)$$

In Eq. (3.2), u_b is the bond stretching potential which depends on the bond length (r), u_θ is the bending energy and it depends on the angle (θ) between two particles, u_ϕ is the torsional potential and ϕ represents the torsional angles and u_{nb} is the non-bonded energy which includes long-range intermolecular interactions between particles. Three-body and higher terms are neglected in most simulations because of the computational cost. In most GCMC simulations, it is reasonable to assume rigid framework therefore, the intramolecular interactions including bond stretching, angle bending and bond rotation can be neglected. However, checking the structural flexibility of MOFs using a sophisticated algorithm developed by Sarkisov et al.[158] can be an ideal methodology prior to neglecting the bonded terms to calculate the potential energy of the system.

The intermolecular interactions (non-bonded) between two particles are generally consisted of short-range van der Waals forces and long-range coulombic interactions. Lennard-Jones (LJ) 12-6 potential is widely used to consider non-bonded interactions.[159] The functional form of the LJ potential given in Eq.(3.3) is based on two parameters, σ , the size parameter and ϵ , the energy parameter.

$$U_{LJ} = 4\epsilon_{ij} \left[\left(\frac{\sigma_{ij}}{r_{ij}} \right)^{12} - \left(\frac{\sigma_{ij}}{r_{ij}} \right)^6 \right] \quad (3.3)$$

In Eq.(3.3), U_{LJ} is the intermolecular potential between two particles (i and j), r is the distance of separation from the center of one particle to the center of the other particle, ϵ_{ij} is the well depth and represents how strongly the two particles attract each other and σ_{ij} defines a molecular length scale related to the particle diameter and controls the scale of interaction.

Parameters of the LJ function are generally taken from the generic force fields which describe the same types of atoms in all MOFs with the same parameter.[160] The Universal Force Field (UFF)[161] and Dreiding[162] force field are commonly used as transferable force fields in molecular simulations of MOFs and the validity of the force fields is shown by many studies.[94, 163] For van der Waals terms, atom-based summation method is used and

the interactions between all pair of atoms which are further beyond the cut-off radius are neglected. Periodic boundary conditions are used in molecular simulations to eliminate the surface effects. Lorentz-Berthelot mixing rules are employed to calculate cross-interactions between two dissimilar LJ sites.[164, 165] Electrostatic potential energy (U_{ij}) of quadrupolar gas molecules such as CO_2 and N_2 are estimated using the Coulomb potential given in Eq.(3.4) where ϵ_0 , q_i and q_j represent the electric constant, partial atomic charges of i and j , respectively.

$$U_{ij} = \frac{1}{4\pi\epsilon_0} \frac{q_i q_j}{r_{ij}} \quad (3.4)$$

The partial charges of atoms are assigned using different methods from the literature such as CBAC (Connectivity Based Atomic Contribution) method,[166] EQeq (Extended Charge Equilibration Method)[16] and high-level quantum chemical calculation methods.[167] High-level quantum chemical calculations consider the electronic structure of atoms and calculations of the multi-electron wavefunctions are computationally costly. The CBAC and EQeq methods are used in molecular simulations especially for large-scale material screening purposes because these approximate methods provide a quick source for partial charges and the computational cost is lower compared to that of quantum chemical calculations. The CBAC method assumes that atoms with the same connectivity have the same charges in different MOFs and the accuracy of this method has been shown by calculating the CO_2 adsorption isotherms of different MOFs in the literature.[166] The EQeq method uses the ionization energies and electron affinities for every atom in the periodic table to calculate the partial charges of MOF atoms.[167]

Gas molecules are represented using different models in molecular simulations. For example, H_2 and CH_4 molecules are modeled as single spheres with united atom model. H_2 is generally represented using Buch potential[168] whereas TraPPE (transferable potentials for phase equilibria) force field[169] is used for CH_4 . CO_2 is represented as a rigid three site molecule with partial point charges located at the center of each site.[170] Similarly, N_2 molecule is modeled as a three site model with two sites located at two N atoms and the third one located at its center of mass (COM) with partial point charges.[171]

3.1.1 Grand Canonical Monte Carlo (GCMC) Simulations

In Monte Carlo simulations, the average behavior of a macroscopic system is predicted by the average of an infinite number of microstates in this system. This method is known as the ensemble averaging in statistical mechanics. For example, a mole of acetone can be considered as an ensemble with Avogadro's number of identical units of acetone molecules. In fact, the observable thermodynamic properties of a system can be found by using the average of the ensembles of all possible physical states of a system.[172]

In GCMC simulations, grand-canonical ensemble (μ , V , T) is used to predict the average number of particles in the system. In an adsorption experiment, the chemical potential (μ) and the temperature (T) of the gas inside and outside of the adsorbent must be equal at equilibrium. The reservoir is composed of the adsorbent in contact with the gas. Here, MOF is the adsorbent and gas molecules are the adsorbates. Since the reservoir imposes constant chemical potential and temperature by exchanging particles and energy, the knowledge of the temperature and the chemical potential of this reservoir is only required to predict the equilibrium concentration in the adsorbent.

The probability of finding an ensemble with an energy, $p(E_i)$ can be written as:

$$p(E_i) = \frac{W_i \cdot e^{-\beta E_i}}{\Omega} \quad (3.5)$$

where W_i is the number of states present at a given energy E_i and Ω is the quantity which is known as the canonical partition function and β is the reciprocal of the thermodynamic temperature of the system ($1/k_B T$). Here, k_B is the Boltzmann constant (1.38×10^{-23} J/K). Partition function (Ω) can be defined as follows:

$$\Omega = \sum_n e^{-\beta E_n} \quad (3.6)$$

where n is the index for the microstates of the system and E_n is the total energy of the system in the respective microstate. The molecular partition function (q) is dependent on the canonical partition function and can be expressed considering the distinguishable and indistinguishable particles (N), respectively in Eqs. (3.7) and (3.8).

$$\Omega = q^N \quad (3.7)$$

$$\Omega = \frac{q^N}{N!} \quad (3.8)$$

The molecular partition function can be estimated by considering molecular energy levels including translation (q_T), rotation (q_R), vibration (q_V) and electronic (q_E) components. Therefore, the total partition function can be expressed as follows:

$$q_{\text{Total}} = q_T \cdot q_R \cdot q_V \cdot q_E \quad (3.9)$$

Details of partition functions can be found in the literature.[172] The partition function of a combined system of N interacting particles in volume V and $M-N$ ideal gas molecules in volume V_0-V can be written for grand-canonical ensemble as follows:[173]

$$\Omega(N, M, V, V_0, T) = \frac{V^N (V_0 - V)^{M-N}}{\Lambda^{3M} N! (M-N)!} \int ds^{M-N} \int ds^N e^{-\beta U(s^N)} \quad (3.10)$$

where $\Lambda = \sqrt{h^2 / (2\pi m k_B T)}$ is the thermal de Broglie wavelength, m is the mass of a gas particle, h is the Planck constant, k_B is the Boltzmann constant and T is the temperature of the gas. It is important to note that the partition function defined in Eq. (3.10) is described using fractional coordinates (s) instead of the Cartesian coordinates (r) Therefore, an additional V^N is written in Eq. (3.10).

Figure 3.1 shows the exchange move of the $M-N$ particles in volume V_0-V with a N -particle system in volume V . The particles can interact in volume V but they cannot interact with each other in volume V_0-V . The potential energy function changes from $U(s^N)$ to $U(s^{N+1})$ when a molecule is transferred from the volume V_0-V to volume V .

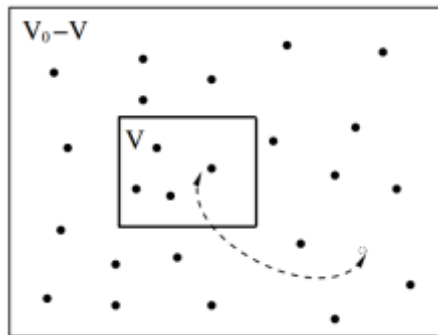


Figure 3.1 The schematic representations of exchange move[173]

The total partition function is then given for M particles over two separate volumes in Eq. (3.11).[173]

$$\Omega(M, V, V_0, T) = \sum_{N=0}^M \frac{V^N (V_0 - V)^{M-N}}{\Lambda^{3M} N! (M-N)!} \int ds^{M-N} \int ds^N e^{-\beta U(s^N)} \quad (3.11)$$

In GCMC simulations, acceptance rules for trial moves including particle displacement, particle insertion and deletion are performed. The probability for the acceptance of the particle displacement move is given as:[173]

$$\text{acc}(s \rightarrow s') = \min \left[1, \exp \left\{ -\beta \left(U(s'^N) - U(s^N) \right) \right\} \right] \quad (3.12)$$

The probability for the acceptance of the insertion move is given as:

$$\text{acc}(N \rightarrow N+1) = \min \left[1, \frac{V}{\Lambda^3(N+1)} \exp \left\{ \beta \left[\mu - U(N+1) + U(N) \right] \right\} \right] \quad (3.13)$$

The probability for the acceptance of the deletion move is given as:

$$\text{acc}(N \rightarrow N-1) = \min \left[1, \frac{\Lambda^3 N}{V} \exp \left\{ -\beta \left[\mu + U(N-1) - U(N) \right] \right\} \right] \quad (3.14)$$

After performing GCMC simulations, the configurational energy, pressure and density are calculated as ensemble averages.[174] The average number of adsorbed molecules is the main output of the GCMC simulations.[173]

$$\langle N \rangle = kT \left(\frac{\partial \ln \Omega}{\partial \mu} \right) \quad (3.15)$$

In order to compute adsorption isotherms, chemical potential (μ) must be converted to the pressure (P). At low pressures, the fugacity and the pressure can be assumed as equal because gas molecules behave ideally. However, at high pressures real gases deviate from the ideal gas law. Therefore, an equation of state of the mixture must be used. In molecular simulations, "widom test particle insertion method" is performed to estimate the chemical potential. In this method, a particle which has no interaction with the system is added into the system. The chemical potential of the system is related to the energy change due to the insertion of this particle.

$$\mu = k_B T \ln \left\{ \exp(-\beta \Delta U(s^{N+1})) \right\} \quad (3.16)$$

To analyze adsorption mechanisms in MOFs, a thermodynamic variable, namely isosteric heat of adsorption are commonly used. Isosteric heat of adsorption shows the average binding energy of an adsorbed molecule and can be calculated from the ensemble average fluctuations:[173]

$$Q_{st} = RT - \left(\frac{\langle U_{ads} \times N_{ads} \rangle - \langle U_{ads} \rangle \times \langle N_{ads} \rangle}{\langle N_{ads}^2 \rangle - \langle N_{ads} \rangle \times \langle N_{ads} \rangle} \right) \quad (3.17)$$

where Q_{st} is the isosteric heat of adsorption, T is the temperature, R is ideal gas constant, $\langle U_{ads} \rangle$ is the average potential energy of adsorbed phased and $\langle N_{ads} \rangle$ is the average number of molecules in the simulation system.

3.1.2 Equilibrium Molecular Dynamics (EMD) Simulations

EMD simulations are generally used to understand diffusion behavior of gas molecules in MOFs.[173] In EMD simulations, intermolecular and intramolecular interactions are used to compute the forces on the molecules. Then, Newton's equations of motion are solved numerically and positions and velocities of gas molecules are computed until the equilibrium is reached.[175] The self-diffusivities and corrected-diffusivities of gas species in MOFs' pores are computed from the results of EMD trajectories. The self-diffusivity ($D_{i,self}$) is described as the motion of individual tagged particles. In an isotropic three-dimensional medium, self-diffusivity is related to the mean-squared displacement (MSD) of the tagged particles by the Einstein relation,[176]

$$D_{i,self} = \lim_{t \rightarrow \infty} \frac{1}{dNt} \left\langle \left[\sum_{i=1}^N \left[\vec{r}_i(t) - \vec{r}_i(0) \right]^2 \right] \right\rangle \quad (3.18)$$

where $\vec{r}(t)$ is the position of the tagged particle at time t , N is the number of particles, d is the number of spatial dimension for diffusion ($d=2,4$ or 6 for one, two or three dimensions, respectively) and the angular brackets represent the ensemble average.

It is more convenient to define the transport diffusivity (D_t) for the macroscopic diffusion of gas molecules in MOFs. Transport diffusivity is calculated by using the corrected diffusivity (D_o) and the thermodynamic correction factor: [177]

$$D_t(c_i^{pure}) = D_o(c_i^{pure}) \cdot \frac{\partial \ln f_i^{pure}}{\partial \ln c_i^{pure}} \quad (3.19)$$

The thermodynamic correction factor ($\partial \ln f_i^{pure} / \partial \ln c_i^{pure}$) depends on the adsorbed concentration of gas (c) and fugacity (f) and it is fully defined once the single-component gas adsorption isotherm is known from the GCMC simulations. The corrected diffusivity (D_o)

includes information on the collective motion of multiple adsorbed molecules that is relevant to net mass transport and defined as follows:

$$D_{o,i} = \lim_{t \rightarrow \infty} \frac{1}{dNt} \left\langle \left(\sum_{l=1}^{N_i} [r_{il}(t) - r_{il}(0)] \right)^2 \right\rangle \quad (3.20)$$

In Eq.(3.20), $r_{il}(t)$ is the three dimensional position vector of molecule l of species i at time t . Well-developed approaches exist for calculating the corrected diffusion coefficient from MD simulations.[178] The self-diffusivity, transport diffusivity and corrected diffusivity are concentration dependent and only equal in the limit of zero concentration.[179] In some extreme cases, the self and corrected diffusivities may vary by orders of magnitude.[180]

3.2 Molecular Simulations of Thin-Film MOF Membranes

Selectivity is commonly used to assess gas separation performances of membranes. Gas selectivity of a thin-film MOF membrane depends on the ratio of gas permeabilities of each gas species through the membrane. Gas permeabilities can be estimated using both adsorption and diffusion data of gas molecules in the pores of MOFs. GCMC simulations are performed to obtain adsorption data whereas EMD simulations are required to provide the data for diffusion of gas molecules. Results obtained from GCMC and EMD simulations are then used to predict overall separation performances of MOF membranes.

Outcome of GCMC simulations is the adsorption amount of gases inside MOFs' pores. Once the GCMC simulations are performed for single-component gases, ideal adsorption selectivity (IAS) can be calculated. IAS is defined as the ratio of single-component adsorbed amount of different gases, c_i^{pure} and c_j^{pure} in MOFs:

$$IAS_{(i/j)} = \frac{c_i^{\text{pure}}}{c_j^{\text{pure}}} \quad (3.21)$$

Results obtained from mixture GCMC simulations are used to predict mixture adsorption selectivity (MAS) using adsorbed amounts of gas components i and j in their binary mixtures:

$$MAS_{(i/j)} = (c_i^{\text{mixture}}/c_j^{\text{mixture}})/(y_i/y_j) \quad (3.22)$$

In Eqs.(3.21) and (3.22), the subscripts i and j represent the strongly adsorbed component and the weakly adsorbed component, respectively. If the adsorption selectivities are greater than 1, the MOF is selective for component i over j .

Results obtained from EMD simulations can be used to calculate both single-component and mixture diffusion selectivities. Single-component diffusion is driven by the concentration gradient of the particular component and the ratio of single-component self-diffusivities gives the ideal diffusion selectivity (IDS):

$$\text{IDS}_{(i/j)} = \frac{D_{i,\text{self}}^{\text{pure}}}{D_{j,\text{self}}^{\text{pure}}} \quad (3.23)$$

In mixture diffusion, diffusion is dependent on both the concentration of the particular component and the other component in the mixture.[175] An equilibrated configuration obtained from a Monte Carlo run is the starting point of an EMD simulation and longer equilibration time is required for mixture components. Therefore, performing mixture EMD simulations is more challenging than that of single-component simulations. It is important to note that prior to EMD simulations, GCMC simulations are required to determine the equilibrium gas amount inside the MOF at the specified pressure and temperature. In order to predict mixture diffusion selectivity (MDS), the ratio of self-diffusivities of each gas species in their binary mixture is used:

$$\text{MDS}_{(i/j)} = \frac{D_{i,\text{self}}^{\text{mixture}}}{D_{j,\text{self}}^{\text{mixture}}} \quad (3.24)$$

In order to accelerate modeling of MOF membranes, membrane selectivity is approximated by the multiplication of adsorption and diffusion selectivities obtained from the GCMC and EMD simulations, respectively. Ideal membrane selectivity (IMS) is defined as follows:[181]

$$\text{IMS}_{(i/j)} = \text{IAS}_{(i/j)} \cdot \text{IDS}_{(i/j)} \quad (3.25)$$

Similarly, membrane's mixture selectivity (MMS) can be calculated as follows:

$$\text{MMS}_{(i/j)} = \text{MAS}_{(i/j)} \cdot \text{MDS}_{(i/j)} \quad (3.26)$$

Eqs.(3.25) and (3.26) assume that self-diffusivities of gases are estimated at the feed side of the membrane and the permeate side is kept under vacuum. Details of this approach can be found in the literature.[181] The validity of this approach was shown by comparing the results with the experiments.[25, 181] The CH₄/H₂ selectivity of MOF-5 membrane was accurately estimated using this approach but the predictions were reported to be less accurate for CuBTC membrane.[181] The validity of this approach was assessed for CH₄/H₂ separation

performance of NU-125, NU-140, MOF-5 and ZIF-8 membranes and results were found to be in good agreement with the experimental measurements.[25] It is important to note that experiments generally report ideal selectivity rather than mixture selectivity of membranes because of the challenges in measuring transport rates of gas mixtures through MOF membranes. In order to compare predictions of computational methods with the experimental measurements, ideal selectivity calculation as shown in Eq.(3.25) is commonly used. However, gas molecules exist in the form of mixtures in industrial processes. In order to examine the difference between ideal and mixture selectivities, both were calculated for 15 different ZIF membranes for separation of CO₂/CH₄, CO₂/N₂, CO₂/H₂ and CH₄/H₂. [182] Results showed that ideal selectivities calculated from single-component gas adsorption and diffusion data can be used to make initial predictions about the gas separation performances of materials if mixture data is not available. However, if one of the gas components is strongly favored over another in adsorption such as CO₂ in CO₂/H₂, multi-component effects between different species become important.[182] For example, strongly adsorbing gas species can reduce the diffusion rate of the other species in the mixture. These multi-component effects play a significant role in determining separation performance of membrane materials. As a result, ideal and mixture selectivities can be different especially at high gas loadings.[183] Therefore, performing GCMC and EMD simulations on the gas mixtures rather than single-component gases is required to assess the separation performance of MOFs under realistic conditions.

Permeability is also an important parameter to assess the gas separation performances of MOF membranes. Single-component gas permeabilities through a MOF membrane are calculated using the shell model[184] which assumes that diffusivities of the adsorbed components are constant throughout the membrane at the average concentration of the feed and permeate sites. Steady state flux (J) of a gas across a MOF membrane is calculated based on Fick's law,[185]

$$J_i = -D_t(c_i^{\text{ave}}) \cdot \nabla c_i \quad (3.27)$$

where ∇c_i is the concentration gradient of the adsorbed gas based on the difference between the feed and permeate pressures of the membrane. The shell model[184] assumes that the Fickian diffusivities are estimated at the average adsorbate loadings:

$$c_i^{ave} \cong (c_i^{permeate} + c_i^{feed}) / 2 \quad (3.28)$$

Steady state fluxes are then converted to single-component gas permeabilities (P) using the pressure drop (Δp) and membrane thickness (L):[186]

$$P_i^{pure} = J / \Delta p / L \quad (3.29)$$

Mixture gas permeabilities are calculated as follows,

$$P_i^{mixture} = \frac{\phi \cdot D_{i,self}^{mixture} \cdot c_i^{mixture}}{f_i^{mixture}} \quad (3.30)$$

where P_i is the permeability of species i , ϕ is the porosity of the MOF, $D_{i,self}$ is the self-diffusivity of species i in the mixture, c_i is the concentration of species i at the feed side of the membrane and f_i is the bulk phase fugacity of species i . [187] Gas permeabilities are generally reported in the unit of Barrers ($10^{-10} \text{ cm}^3 \text{ (STP) cm}/(\text{cm}^2 \text{ s cm Hg})$) in the literature. Once gas permeabilities are calculated, single-component and mixture selectivities can be also found using the ratio of single and mixture gas permeabilities, respectively and the results are same with Eqs.(3.25) and (3.26). Predicted gas permeabilities and selectivities can be compared with the experimental data to validate the accuracy of the molecular simulations. This computational methodology was tested both for mixture gas permeance through ZIF-69, ZIF-78, ZIF-90 and ZIF-95[87, 188] membranes and for single-component gas permeance through IRMOF-1, Ni-MOF-74 and MIL-53(Al) membranes.[188] Results showed that the predictions for both mixture and single-component gas permeance are in a good agreement with the experimental data.

3.3 Computational Modeling of MOF-based MMMs

Modeling of MOF-based MMMs requires the knowledge of the gas permeabilities in the polymer phase and dispersed phase (MOFs). Gas permeabilities of many polymeric membranes have been already reported in the literature,[92] however similar type of data is not available for MOF membranes. Therefore, predicting gas permeability of MOFs is a prerequisite for predicting permeability of MOF-based MMMs. Once the gas permeabilities of both MOF and polymer are known, theoretical permeation models can be used to predict the gas permeability of MOF-based MMMs. Selectivity of the MOF-based MMM can be then calculated as the ratio of the gas permeabilities of two different species.

Several theoretical permeation models are used to predict gas permeabilities of MMMs. These permeation models can be classified into two groups: models considering ideal morphology such as Maxwell,[189] Bruggeman,[190] Lewis-Nielson,[191] Pal[192] and models considering non-ideal morphology such as modified Maxwell,[113] Felske[193] and modified Felske.[192] Ideal morphology concept assumes that there are no defects, void formation or polymer rigidification around the particles at the polymer/filler interface. Non-ideal approach, on the other hand, considers all these deficiencies using additional parameters such as packing factor and the matrix rigidification factor. The predictions of different permeation models with the available experimental measurements for pure gas and mixed gas permeation of MOF-based MMMs were compared in order to determine the best predicting permeation model.[133] Results showed that the Maxwell model is the best predicting permeation model among the ones considering ideal morphology and modified Felske model is the best predicting model among the ones considering non-ideal morphology. Therefore, the Maxwell, modified Maxwell, Felske and modified Felske models were mainly discussed throughout this section. Detailed descriptions of the other permeation models are available in several review papers in the literature.[114, 194-196]

The Maxwell model[189] is widely used to estimate gas permeability of MMMs. Maxwell observed the close analogy between dielectrics and transport through membranes and assuming dilute dispersion of ellipsoids, Maxwell-Wagner-Sillars equation can be written for MOF-filled polymer membranes as follows,[197]

$$P_{\text{MMM}} = P_{\text{POLYMER}} \cdot \left[\frac{n \cdot P_{\text{MOF}} + (1-n) \cdot P_{\text{POLYMER}} + (1-n) \cdot (P_{\text{MOF}} - P_{\text{POLYMER}}) \cdot \phi}{n \cdot P_{\text{MOF}} + (1-n) \cdot P_{\text{POLYMER}} - n \cdot (P_{\text{MOF}} - P_{\text{POLYMER}}) \cdot \phi} \right] \quad (3.31)$$

where ϕ is the volume fraction of the MOF particles, n is the shape factor of the fillers, P_{MOF} is the MOF's permeability, P_{POLYMER} is the polymer's permeability and P_{MMM} is the permeability of the MOF/polymer MMM. The Maxwell model assumes that $n=1/3$ for random dispersion of the spherical filler particles and the equation reduces to the following where λ is defined as the permeability ratio, $P_{\text{MOF}}/P_{\text{POLYMER}}$:

$$P_{\text{MMM}} = P_{\text{POLYMER}} \left[\frac{2 \cdot (1-\phi) + (1+2\phi) \cdot \lambda}{(2+\phi) + (1-\phi) \cdot \lambda} \right] \quad (3.32)$$

The Maxwell model is valid for low filler volume fractions ($0 < \phi < 0.2$) since it assumes that a particle's flux pattern is not affected by the presence of nearby filler particles. This model does not consider packing limit of particles, the effect of particle size distribution, particle shape and aggregation of particles.

The modified Maxwell model[113] was developed to include interfacial voids, rigidified polymer layer and particle pore blockage. The model is based on the two-phase description, the polymer matrix is one phase and the combined insert and interphase is the other phase ('pseudo-insert phase'). The modified Maxwell model can be written as: [113]

$$P_{MMM} = P_{POLYMER} \cdot \left[\frac{P_{eff} + 2 \cdot P_{POLYMER} - 2 \cdot (\phi_d + \phi_I) \cdot (P_{POLYMER} - P_{eff})}{P_{eff} + 2 \cdot P_{POLYMER} + (\phi_d + \phi_I) \cdot (P_{POLYMER} - P_{eff})} \right] \quad (3.33)$$

$$P_{eff} = P_I \cdot \left[\frac{P_{MOF} + 2 \cdot P_I - 2\phi_s \cdot (P_I - P_{MOF})}{P_{MOF} + 2 \cdot P_I + \phi_s \cdot (P_I - P_{MOF})} \right] \quad (3.34)$$

$$\phi_s = \frac{\phi_d}{\phi_d + \phi_I} = \frac{r_d^3}{(r_d + l_I)^3} \quad (3.35)$$

Here, P_{eff} is the effective permeability of the pseudo-insert phase, P_I is the permeability of the interphase, ϕ_s is the volume fraction of the dispersed phase within the pseudo-insert phase, ϕ_d is the overall volume fraction in the membrane of the insert, ϕ_I is the overall volume fraction in the membrane of the interphase, r_d is the insert radius and l_I is the interphase thickness. The modified Maxwell model is valid for low to moderate values of ϕ like the Maxwell model.

The Felske model[193] assumes the dispersed particles as a core and the surrounding interfacial layer (rigidified interfacial layer or voids or particle pore blockage) as a shell. The model can be written as follows:

$$P_{MMM} = P_{POLYMER} \cdot \left[\frac{2 \cdot (1 - \phi) + (1 + 2\phi) \cdot (\beta / \gamma)}{(2 + \phi) + (1 - \phi) \cdot (\beta / \gamma)} \right] \quad (3.36)$$

$$\begin{aligned} \beta &= (2 + \delta^3) \cdot \lambda - 2 \cdot (1 - \delta^3) \cdot \lambda_{I/POLYMER} \\ \gamma &= (1 + 2\delta^3) - (1 - \delta^3) \cdot \lambda_{MOF/I} \end{aligned} \quad (3.37)$$

In these equations, $\lambda_{\text{I/POLYMER}} = P_{\text{INTERFACIAL SHELL}}/P_{\text{POLYMER}}$, $\lambda_{\text{MOF/I}} = P_{\text{MOF}}/P_{\text{INTERFACIAL SHELL}}$, $\lambda = P_{\text{MOF}}/P_{\text{POLYMER}}$ and δ is the ratio of outer radius of interfacial shell to the core radius. When $\delta=1$, this model reduces to the Maxwell model and it has the similar disadvantages.

The Modified Felske model[192] was developed by Pal to consider the morphology and packing factor of the filler particles,

$$P_{\text{MMM}} = P_{\text{POLYMER}} \cdot \left[\frac{1 + 2 \cdot ((\beta - \gamma)/(\beta + 2\gamma)) \cdot \phi}{1 - ((\beta - \gamma)/(\beta + 2\gamma)) \cdot \phi \cdot \varphi} \right], \quad \varphi = 1 + \left[\frac{(1 - \phi_m)}{(\phi_m)^2} \right] \cdot \phi \quad (3.38)$$

where ϕ_m is the maximum packing volume fraction of filler particles and assumed to be 0.64 for random close packing of uniform spheres.[114] This model reduces to the original Felske model when the maximum packing volume fraction of the core-shell particles is equal to 1 and it turns to the Lewis-Nielson model when $\delta=1$. If both parameters are equal to 1, the model reduces to the Maxwell model.

3.4 Molecular Simulations of Drug/Cosmetic Molecules

The first step in molecular simulations is to specify the positions of atoms or molecules in the system. The atomic positions of drug and cosmetic molecules were taken from the Zinc Database[198] and PubChem[199] libraries, respectively. Then geometry optimization was performed to determine the lowest energy configurations. This process is an iterative process, the energy and energy gradient (first derivative with respect to all geometric coordinates) were calculated considering the initial structure. Then, a new geometry was predicted until the following criteria was reached: the energy of the optimized structure must not be lower than a specified energy value, the energy gradient must approach zero and any geometrical parameter should not change by more than a specified value.[172] DMol³ module implemented in Materials Studio 8.0[200] software was used to optimize the geometries of ibuprofen, urea and caffeine molecules. An example configuration was shown for ibuprofen in Figure 3.2. The initial configuration was shown in left-hand side and after geometry optimization the configuration was changed as shown in right-hand side.

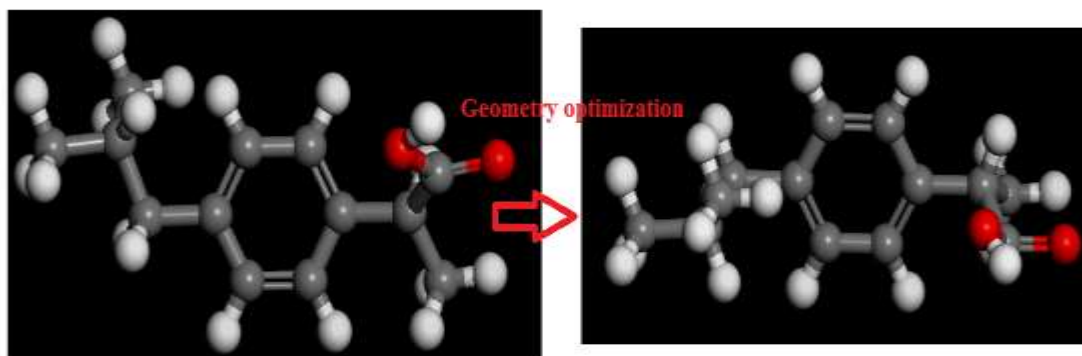


Figure 3.2 Geometry optimization of ibuprofen

Dmol³ calculations were based on quantum mechanics. In quantum mechanics calculations, it is required to define the time-independent and non-relativistic Schrödinger equation: [172]

$$H\Psi = E\Psi \quad (3.39)$$

where E is the total energy of the system, Ψ is the n -electron wave function which depends on the identities and positions of the nuclei and electrons and H is the Hamiltonian operator which provides the kinetic and potential energies for each particle in the system. Hamiltonian operator can be written as follows:[172]

$$H = -\frac{\hbar^2}{2m_e} \sum_i^{\text{electrons}} \nabla_i^2 - \frac{\hbar^2}{2} \sum_A^{\text{nuclei}} \frac{1}{M_A} \nabla_A^2 - \frac{e^2}{4\pi\epsilon_0} \sum_i^{\text{electrons}} \sum_A^{\text{nuclei}} \frac{Z_A}{r_{iA}} + \frac{e^2}{4\pi\epsilon_0} \sum_{i(i>j)}^{\text{electrons}} \sum_j^{\text{electrons}} \frac{1}{r_{ij}} + \frac{e^2}{4\pi\epsilon_0} \sum_{A(A>B)}^{\text{nuclei}} \sum_B^{\text{nuclei}} \frac{Z_A Z_B}{R_{AB}} \quad (3.40)$$

where Z_A is the nuclear charge, M_A is the mass of nucleus A , m_e is the mass of the electron (e), R_{AB} is the distance between nuclei A and B , r_{ij} is the distance between electrons i and j , r_{iA} is the distance between electron i and nucleus A , ϵ_0 is the permittivity of free space, and \hbar is the Planck constant divided by 2π .

In order to find a solution for Eq.(3.40), several assumptions must be done. The first assumption is based on Born-Oppenheimer approximation which assumes that the nuclei move much more slowly than electrons. Therefore, kinetic term for nuclei in Eq.(3.40) can be assumed as zero and coulombic term can be assumed as a constant. Born-Oppenheimer approximation leads to Eq. (3.41): [172]

$$H = -\frac{\hbar^2}{2m_e} \sum_i^{\text{electrons}} \nabla_i^2 - \frac{e^2}{4\pi\epsilon_0} \sum_i^{\text{electrons}} \sum_A^{\text{nuclei}} \frac{Z_A}{r_{iA}} + \frac{e^2}{4\pi\epsilon_0} \sum_{i(i>j)}^{\text{electrons}} \sum_j^{\text{electrons}} \frac{1}{r_{ij}} \quad (3.41)$$

However, solving Eq.(3.41) for many electron systems is still impossible. Therefore, different approaches can be used in the literature to solve this equation. One method is Hartree-Fock approximation assumes that electrons move independently of each other. A set of differential equations including the coordinates of a single electron can be written and solved numerically. This approximation also considers that molecular solutions are made up of atomic solution. The molecular orbitals are written as linear combinations of a basis set of prescribed functions namely, basis functions.[172]

The second method is density functional theory (DFT).[172] This method requires much lower computational cost compared to Hartree-Fock models. Therefore, DFT is widely used in the literature to investigate the electronic structure of many-body systems. DFT method is based on the electron density of the system rather than the many-body wave function. It is assumed that the total ground state energy of a many-electron system is a functional of the density. The partial charges of drug and cosmetic molecules were assigned after DFT calculations using electrostatic potential (ESP). Electronic energies were obtained by DFT using the B3LYP functional. DND basis set (basis file 3.5) was used as implemented in Materials Studio.

Electrostatic potential (ϵ_p) is the energy of interaction of a unit positive charge at some point in space, p with the nuclei and the electrons of a molecule. To estimate ESP charges, initially grid points covering the surface of the molecule were defined and then, electrostatic potential were calculated at each grid points. Using least-squares the best fit is done for the electrostatic potential at grid points and atom-centered charges, Q_A were calculated using the following equation:[172]

$$\epsilon_p^{\text{approx}} = \sum_A^{\text{nuclei}} \frac{e^2 Q_A}{4\pi\epsilon_0 R_{Ap}} \quad (3.42)$$

where R_{Ap} is the distance separating the point charges from the nuclei.

In the previous section (3.1), the general procedure for GCMC and MD simulations was discussed. Instead of conventional GCMC simulations, configurational bias-Monte Carlo

(CBMC) simulations were performed to determine the adsorbed number of ibuprofen, caffeine and urea molecules in MOFs at 1 bar and 37 °C. CBMC was developed for long-chain molecules. Since drug molecules are much bigger than gas molecules, CBMC algorithm was used to calculate the average adsorbed number of molecules in the system. GCMC simulations insert the molecule as a whole for specified moves which were previously mentioned. CBMC simulations, on the other hand insert molecules (chains) part by part biasing the growth process considering the energetically favorable configurations.[157] In order to apply this methodology k sets of trial positions are generated and one of these trial positions is selected with a probability:

$$P_i(j) = \frac{e^{-\beta U_i^{\text{ext}}(j)}}{\sum_{l=1}^k e^{-\beta U_i^{\text{ext}}(l)}} = \frac{e^{-\beta U_i^{\text{ext}}(j)}}{w(i)} \quad (3.43)$$

where U^{ext} is the external potential energy of each set of trial positions j of segment i and used to bias the selection of a set from the trial sets and $w(i)$ is known as the Rosenbluth factor. The bias is removed based on the acceptance rule. In this methodology, a molecule is grown segment by segment and for each segment a set of k trial configuration is generated based on the internal energy and the external energy of each set is computed. Herein, total potential energy is the sum of internal and external energies.

The trial position is then added to the chain repeatedly until the entire molecule is grown. This sampling method is known as Rosenbluth sampling and new Rosenbluth factor, W^{new} for newly grown molecule is calculated as:[157]

$$W^{\text{new}} = \prod_i w(i) \quad (3.44)$$

Prior to CBMC simulations torsional degrees of freedom were determined using Conformers module in Materials Studio.[200] Figure 3.3 shows the conformer analysis of the ibuprofen molecule.

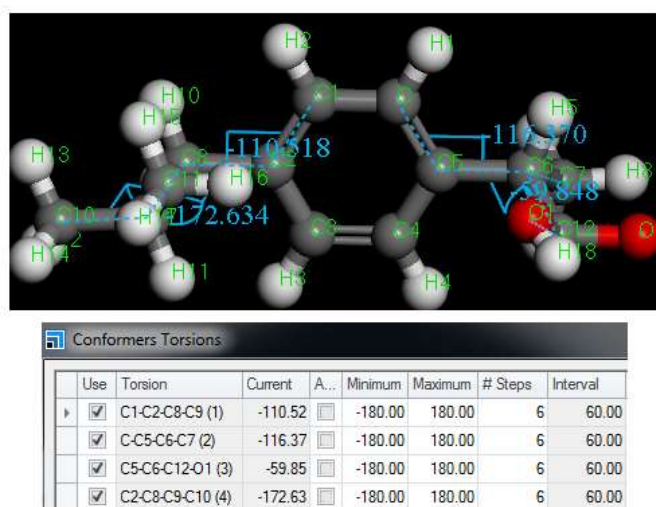


Figure 3.3 Conformer analysis for ibuprofen molecule.

Chapter 4

MODELING OF BIO-MOFS FOR GAS SEPARATIONS

This chapter evaluates the potential of bio-MOFs in energetic applications for CO₂ separation from CO₂/CH₄, CO₂/N₂ and CO₂/H₂ mixtures and H₂ separation from CH₄/H₂ mixture. Separation of these gas mixtures is economically, socially, environmentally significant for large-scale industrial applications. CO₂/CH₄ and CO₂/N₂ separations are important for natural gas purification and flue gas separation after post-combustion of the fuel. CO₂/H₂ and CH₄/H₂ separations are important for H₂ recovery from plants and refineries.

After showing the good agreement between experiments and molecular simulations for single-component adsorption isotherms of several gases in various bio-MOFs, adsorption selectivity and working capacity of these materials were predicted for CO₂/CH₄, CH₄/H₂, CO₂/H₂ and CO₂/N₂ separations. Membrane selectivity and gas permeability of bio-MOFs were computed considering flexibility of the structures in molecular simulations. Results showed that several bio-MOFs outperform widely studied MOFs and zeolites both in adsorption-based and membrane-based gas separations.

4.1 Modeling of Bio-MOFs for CO₂/CH₄ Separations

Separation of CO₂ from natural gas, which is mainly composed of CH₄ (75-90%), has significant importance in large-scale industrial applications since CO₂ causes pipeline corrosion and decreases energy content of the natural gas.[27] Therefore, developing new technologies for efficient CO₂ capture and separation has significant importance. A review of current literature discussed in Section 2 suggested that bio-MOFs are potential materials as adsorbents and membranes for gas separation applications, especially for CO₂/CH₄ separation.

In order to examine the separation performance of bio-MOFs, we performed GCMC and EMD simulations and compared CO₂ separation performances of bio-MOFs with those of various MOFs, zeolites, polymers.

4.1.1 Computational Details

Ten different bio-MOFs, bio-MOF-1, bio-MOF-11, bio-MOF-12, bio-MOF-13, bio-MOF-14, IZUMUM, NUDKON, OFUSAL, PESTUD and WODFOL were studied. The last five bio-MOFs were referred with the 'refcodes' taken from Cambridge Crystallographic Data Center (CCDC)[15] since they do not have common names such as bio-MOF-X. All crystal structures were taken from CCDC which includes experimentally reported structures. Solvent molecules were removed before simulations. Structural properties of bio-MOFs such as density, pore volume and pore sizes were computed and listed in Table 4.1. Atomistic representation of the bio-MOFs can be seen in Figure A.1 of Appendix. Li et al.[80] reported that bio-MOF-13 has two preferential configurations due to the configurations of butyrate chains. They modeled terminal ethyl group with partial occupancy at two positions resulting in configuration I and configuration II with probabilities of 42.6% and 57.4%, respectively. Following them, these two configurations were constructed and optimized prior to molecular simulations. The valerate chains in bio-MOF-14 were also modeled as configuration I, configuration II and configuration III with partial occupancies of 34.7%, 47.6% and 17.7%, respectively.[80] These configurations and unit cell representations of bio-MOF-13 and bio-MOF-14 are given in Figure 4.1 and Figure 4.2, respectively. In our molecular simulations, all configurations of bio-MOF-13 and bio-MOF-14 were used.

Table 4.1 Structural properties of bio-MOFs.

CCDC name	Organic linker and metals	Unit cell volume (Å ³)	Density (g/cm ³)	Pore volume (cm ³ /g)	PLD (Å)	LCD (Å)
NUDLAA (bio-MOF-1)	Adenine-Zn	16339.10	1.06	0.516	8.65	9.13
YUVSUE (bio-MOF-11)	Adenine-Co	5426.25	1.23	0.411	4.27	5.27
BEYSEF (bio-MOF-12)	Adenine-Co	5993.10	1.18	0.432	4.18	5.16
BEYSAB (bio-MOF-13)*	Adenine-Co	5564.72	1.34	0.323, 0.324	1.91, 3.23	4.84, 4.71
BEYRUU (bio-MOF-14)*	Adenine-Co	5615.59	1.25	0.222, 0.221, 0.234	0.99, 1.14, 0.95	2.8, 3.23, 3.79
IZUMUM	Adenine-Cu	5269.63	1.29	0.382	2.33	5.37
NUDKON	Adenine-Zn	9179.96	1.19	0.385	2.01	6.07
OFUSAL	Phosphaadamantane-Ag	1137.63	1.73	0.236	2.53	3.20
PESTUD	Aspartic acid-Ni	1169.00	1.52	0.243	3.26	4.02
WODFOL	Aspartic acid-Co	1180.60	1.51	0.247	3.20	4.15

Pore volume, PLD (pore limiting diameter) and LCD (largest cavity diameter) were calculated using Lev's algorithm.[201] *Pore volumes, PLDs and LCDs of all configurations (I, II for bio-MOF-13 and I, II, III for bio-MOF-14) were reported.

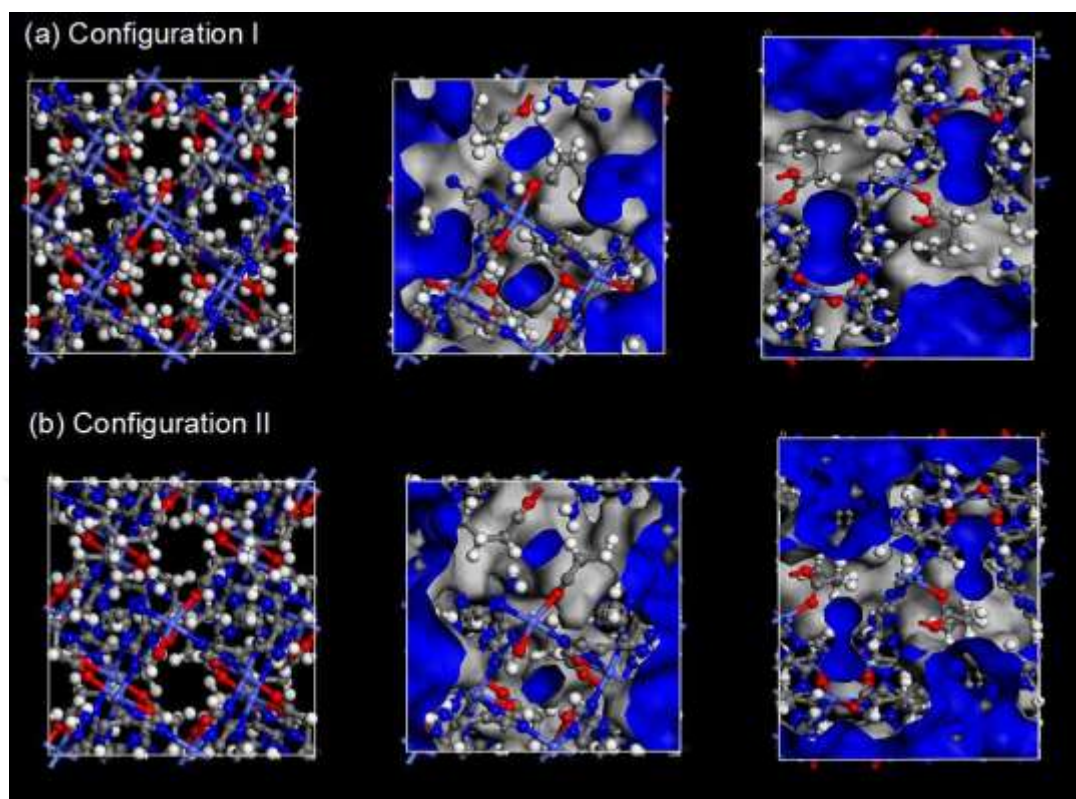


Figure 4.1 Configurations of bio-MOF-13. Connolly surface diagrams were prepared using 1 Å probe molecule. The inner (outer) surfaces of the cavities are shown in blue (gray).

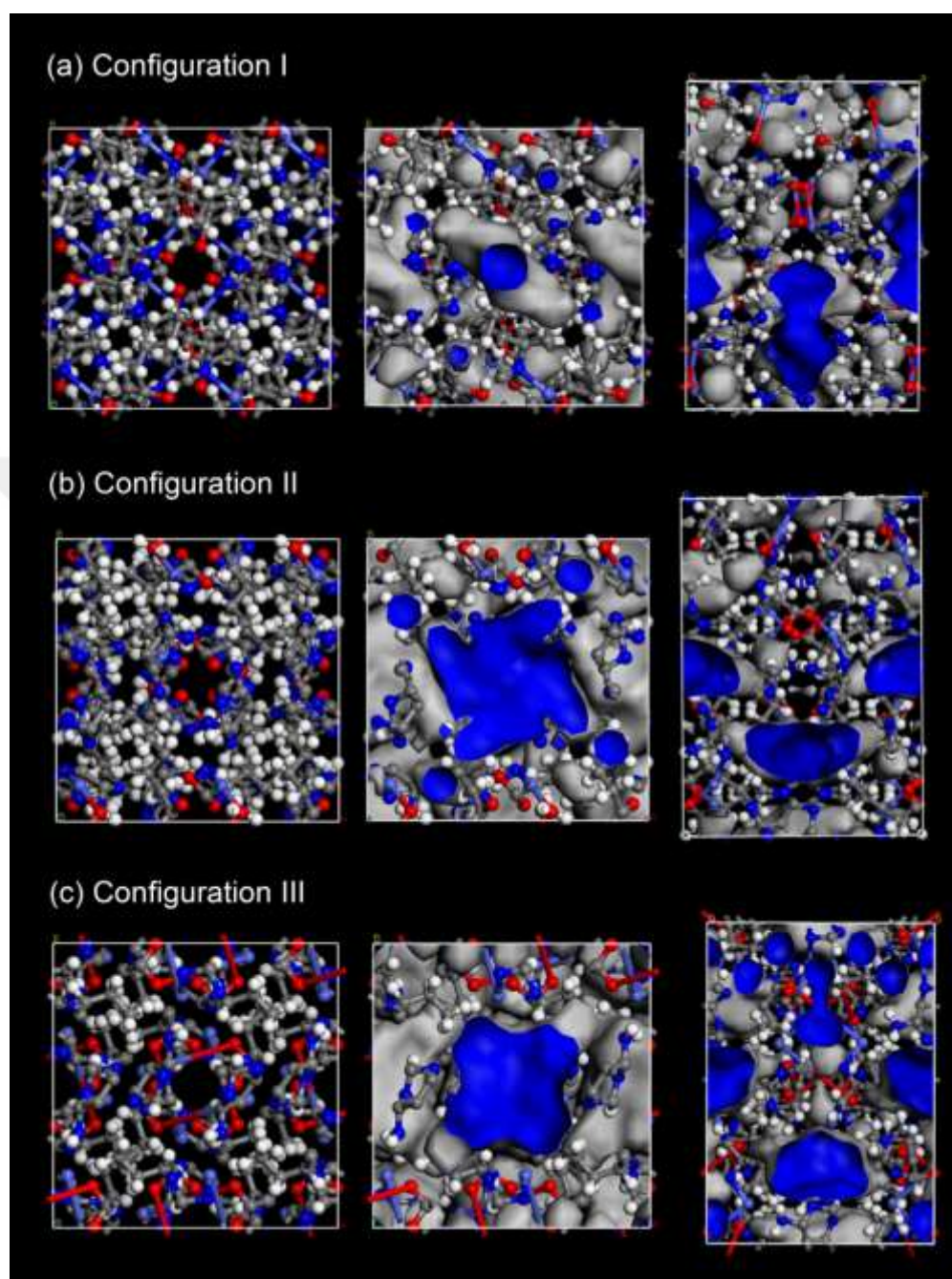


Figure 4.2 Configurations of bio-MOF-14. Connolly surface diagrams were prepared using 1 Å probe molecule. The inner (outer) surfaces of the cavities are shown in blue (gray).

Atomic models were used to compute the energetic interactions between atoms of bio-MOFs and gas molecules (CO₂, H₂, N₂ and CH₄).^[63] Lennard-Jones (LJ) 12-6 potential and Coulomb potential were used to model repulsion-dispersion forces and electrostatic interactions, respectively. The atomic charges of bio-MOFs were estimated using EQeq method.^[16] Both H₂ and CH₄ molecules were modeled as single spheres using united atom

model. H₂ was modeled with Buch potential[168] whereas TraPPE force field was used to model CH₄. [168, 169] CO₂ was modeled as a three site linear molecule with three charged LJ interaction sites located at each atom using the EPM2 potential.[170] Similarly, N₂ was modeled as a three site molecule with two sites located at two N atoms and the third one located at its center of mass (COM) with partial point charges.[171] The interaction potential parameters for gas molecules were given in Table 4.2. The universal force field (UFF)[161] LJ parameters were used for bio-MOF atoms.

Table 4.2 Interaction potential parameters used for gas molecules

Molecule	Atom	σ (Å)	ϵ/k_B (K)	q(e)
H ₂	H ₂	2.96	34.20	-
CH ₄	CH ₄	3.73	148.20	-
CO ₂	C	2.80	27.02	0.70
	O	3.05	79.01	-0.35
N ₂	N	3.32	36.40	-0.40
	COM	0.00	0.00	0.80

GCMC and EMD simulations were performed to obtain adsorption equilibria and self-diffusion coefficients of CO₂/CH₄ mixtures in bio-MOFs using Materials Studio 8.0 software.[200] We compared our simulation results with the experimental gas uptake data of bio-MOFs-11, -12, -13 and -14. By using sorption module, adsorption isotherms of CO₂ (298 K), H₂ (77 K and 87 K) and N₂ (298 K) were computed up to 1 bar. After validation of our simulation results as we will show below, we performed fixed pressure simulations at 300 K using sorption module at 1 bar and 10 bar for CO₂/CH₄:50/50 to obtain mixture adsorption data. Due to the anionic structure of bio-MOF-1, eight DMA (dimethylammonium) cations were added to the structure using fixed loading task in sorption module prior to fixed pressure simulations. Ewald and group summation method with 10⁻⁵ kcal/mol accuracy were used for calculation of electrostatic interactions. For van der Waals terms, atom based summation method was used with the cubic spline truncation. 12.5 Å was used as a cut off radius for van der Waals terms. Simulations were performed with trial configurations which consist of 2×10⁶ cycles for the equilibration and 1×10⁷ cycles for the production step. More

detailed information about Monte Carlo simulations of Materials Studio can be found elsewhere.[202]

Working capacity, (mol/kg), the difference between the uptake amounts at adsorption (10 bar) and desorption pressures (1 bar), was calculated using the GCMC results:

$$\Delta N_i = (N_i^{\text{ads}} - N_i^{\text{des}}) \quad (4.1)$$

Here, ΔN_i is the working capacity and N_i^{ads} (N_i^{des}) is the adsorption (desorption) amount of species i at 10 (1) bar.

The number of gas molecules per unit cell of bio-MOFs at 10 bar determined by the fixed pressure simulations (the grand canonical ensemble) was then packed into each MOF structure using fixed loading task (the canonical ensemble) in sorption module at 300 K. The lowest energy configuration was selected as the initial configuration of EMD simulations. Both rigid and flexible EMD simulations were performed using the forcite module of Materials Studio 8.0. In flexible simulations, we adopted Dreiding force field[162] for bond stretching, angle bending and dihedral torsions following Thornton et al.[134] who used Dreiding to measure the transport coefficients of several gases in ZIF membranes and confirmed their computational results with the experimental data. Geometry optimization steps were performed for each structure until the following convergence criteria were reached: 10^{-4} kcal/mol for energy, 5×10^{-3} kcal/mol Å for forces and 5×10^{-5} Å for displacement. The cell geometry was not allowed to change during the optimization step. After optimization steps, EMD simulations within the NVT ensemble were performed with a step size of 1 fs up to a total of 7 ns. Nose-Hoover-Langevin (NHL) thermostat[173] was used to keep temperature constant.

4.1.2 Validation of the Accuracy of Molecular Simulations

The results of molecular simulations were compared with the available experimental data of Li et al.[80] for single-component gas uptake in bio-MOFs-11, -12, -13 and -14. As expected for microporous materials, type I adsorption isotherm characteristics were observed for CO₂, H₂ and N₂. Figure 4.3(a) shows experimental and simulated adsorption isotherms of CO₂ at 298 K up to 1 bar. Two different experimental data for CO₂ uptake in bio-MOF-11 were reported in literature.[46, 203] The discrepancy in experimental CO₂ uptakes can be attributed to the differences in sample synthesis and activation procedures. The BET

(Brunauer-Emmett-Teller) surface area of bio-MOF-11 (1148 m²/g) synthesized in 2013 was reported to be higher than the surface area of bio-MOF-11 (1040 m²/g) synthesized in 2009, which is the reason of higher CO₂ uptake reported in 2013. Our molecular simulations gave better agreement with the experimental data reported in 2013. Simulation results do not agree well with the experimental CO₂ uptake measurements of bio-MOF-12. Simulations slightly overpredict CO₂ adsorption at high pressures but seem to underestimate the adsorption at very low pressures, in the Henry's law regime.

Two (three) different configurations of bio-MOF-13 (bio-MOF-14) were studied to examine the effects of chain configurations on CO₂ adsorption. The average adsorption amounts of CO₂ in bio-MOF-13 and bio-MOF-14 were computed as follows:

$$\begin{aligned} N_{\text{ave for bio-MOF-13}} &= P_1 \times n_1 + P_2 \times n_2 \\ N_{\text{ave for bio-MOF-14}} &= P_1 \times n_1 + P_2 \times n_2 + P_3 \times n_3 \end{aligned} \quad (4.2)$$

Here, n_i is the gas uptake computed using configuration i , P_i is the probability of configuration i reported by DFT calculations[80] and N_{ave} is the average gas uptake. Since the structure used to measure CO₂ uptake in experiments may contain both configuration, uptake calculated by Eq.(4.2) gave better agreement with the experiments for bio-MOF-13 as shown in Figure 4.3(a). However, for bio-MOF-14, simulations performed using possible configurations underpredicted experimental measurements. Our average simulated CO₂ uptake agreed well with the previous simulation data of Li et al.[80] although exact configuration of bio-MOF-14 that Li et al. used was not specified. Deviations between experimentally measured and simulated CO₂ uptakes can be attributed to the different chain configurations of bio-MOF-14 samples. Figure 4.3(a) also shows that changing the organic chain from acetate (bio-MOF-11) to valerate (bio-MOF-14) decreases CO₂ uptake due to the reduction in the pore volume. For example, CO₂ uptake in bio-MOF-11 was predicted as 4.4 mmol/g at 1 bar and 298 K whereas CO₂ uptake in bio-MOF-12 was predicted as 3.5 mmol/g under the same conditions. Average CO₂ uptakes of bio-MOF-13 and bio-MOF-14 were calculated as 2.1 mmol/g and 0.2 mmol/g, respectively at the same conditions due to their lower pore volumes.

Simulated H₂ isotherms at 77 K and 87 K up to 1 bar in bio-MOF-11 were compared with experiments in Figure 4.3(b) and results showed that simulations agree with the experiments. There is no reported experimental data for H₂ adsorption of other bio-MOFs. It is important to note that the only experimental input of our molecular simulations is the crystal structures of bio-MOFs and no force field parameter refining was used in our simulations. In Figure 4.3(c), experimental and simulated adsorption isotherms of N₂ in bio-MOFs-11, -12 and -13 were compared at 298 K. N₂ uptake of bio-MOF-14 was not included since we computed almost zero N₂ uptake (Figure A.2) in agreement with the experiments.[80] Our simulation results for N₂ agreed well with the experiments for bio-MOF-12 and bio-MOF-13 and slightly overestimated experimental data for bio-MOF-11. We were not able to compare the single component adsorption of CH₄ in bio-MOFs except bio-MOF-1 since there was not available experimental data for CH₄ adsorption in bio-MOFs. Our simulated CH₄ adsorption in bio-MOF-1 was found to be in good agreement with the experimental data measured at very low pressures as shown in Figure A.3. Comparison of Figures 4.3(a-c) indicated that CO₂ is more strongly adsorbed than H₂ and N₂ in bio-MOFs. This is due to the high interaction energy between CO₂ molecules and Lewis-basic nitrogen atoms of bio-MOFs.[80] CO₂ and N₂ also have electrostatic interactions with bio-MOFs which is absent for H₂. Since CO₂ has a much higher quadrupole moment (13.4 C·m²) than N₂ (4.7 C·m²), CO₂ is more strongly adsorbed than N₂ in all bio-MOFs.[204]

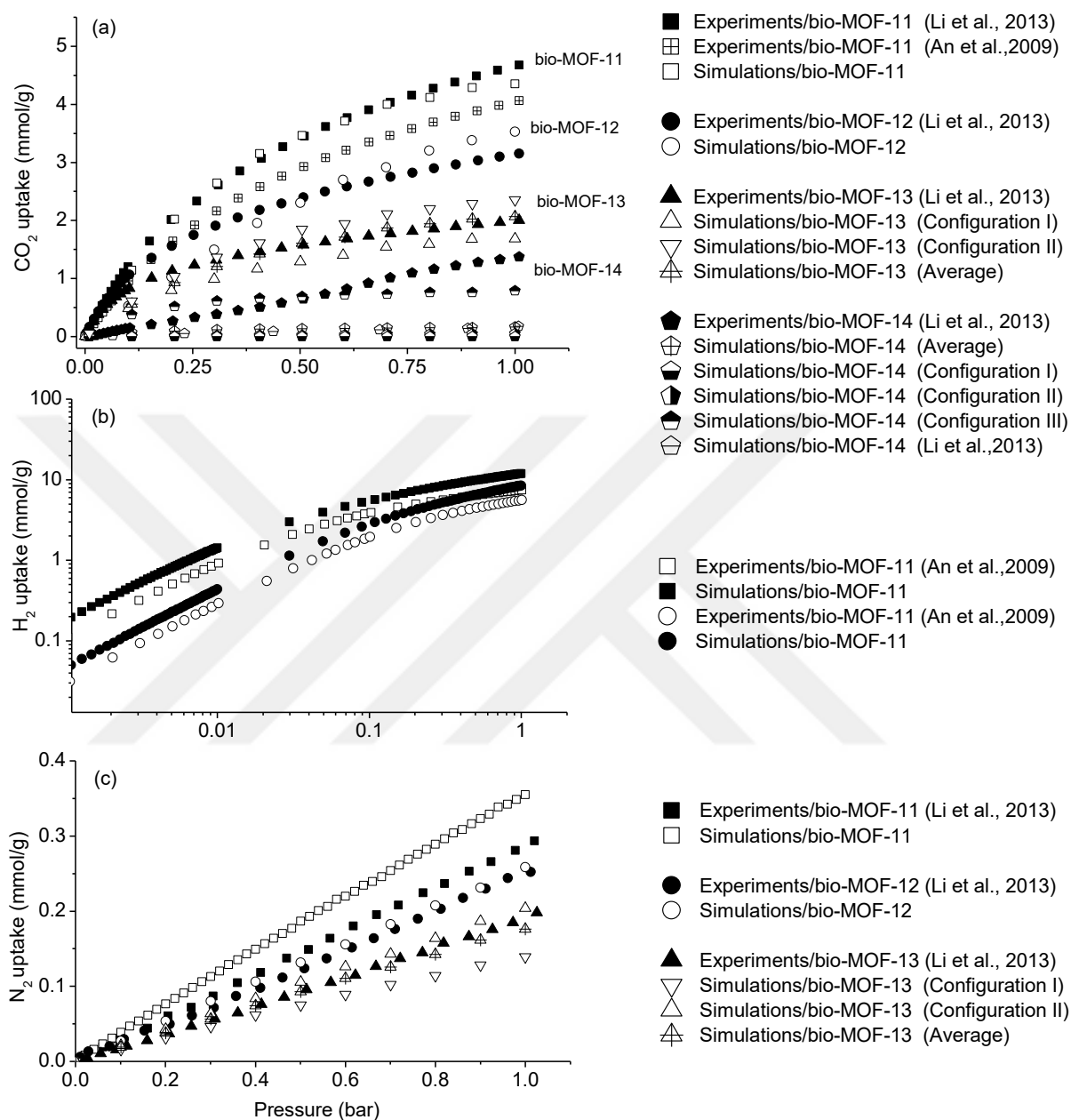


Figure 4.3 Comparison of experiments and our molecular simulations for single-component adsorption isotherm of (a)CO₂ at 298 K in bio-MOFs-11, -12, -13 and -14 (b)H₂ at 77 K (squares) and 87 K (circles) in bio-MOF-11 (c)N₂ at 298 K in bio-MOFs-11, -12 and -13.

4.1.3 Adsorption-based Gas Separation

Motivated from the good agreement between simulation results and experiments for single-component gas adsorption in bio-MOFs, adsorption isotherms of equimolar CO₂/CH₄ mixtures for ten different bio-MOFs were computed using molecular simulations. Adsorption selectivity and working capacity of these materials were computed. Figure 4.4 shows adsorption-based separation performances of bio-MOFs for CO₂/CH₄ mixtures calculated at an adsorption pressure of 10 bar and desorption pressure of 1 bar, at 300 K. In order to compare potential of bio-MOFs with other nanoporous adsorbents, data for several zeolites and other widely studied MOFs taken from the literature[205] were also shown in Figure 4.4. Both high adsorption selectivity and high working capacity are desired for a good adsorbent and an efficient adsorption-based separation process. Among ten bio-MOFs, OFUSAL has a very high CO₂/CH₄ adsorption selectivity (~185), but it suffers from low working capacity (0.4 mol CO₂/kg material). The high adsorption selectivity of OFUSAL can be explained by its cationic structure which strongly favors CO₂ over CH₄ similar to the zeolites having additional framework cations such as NaX, NaY and rho-ZMOF.[206] The low working capacity of this material is due to its low pore volume, which is the lowest among the bio-MOFs considered in this work (see Table 4.1). Working capacities of bio-MOFs decrease as the pore volumes of the materials decrease as can be seen from Figure 4.4. Bio-MOF-1 and bio-MOF-12 exhibit the highest CO₂ working capacities since they have the two largest pore volumes. Their adsorption selectivities are similar to other MOFs and zeolites. Therefore, bio-MOF-1 and bio-MOF-12 can be considered as the most promising adsorbents among the ones we studied since their working capacities (~3 mol CO₂/kg material) and adsorption selectivities (~8) are high. These two bio-MOFs outperform one of the most widely studied MOFs, ZIF-8, which has a CO₂ selectivity and working capacity of ~4 and ~3 mol CO₂/kg material, respectively.

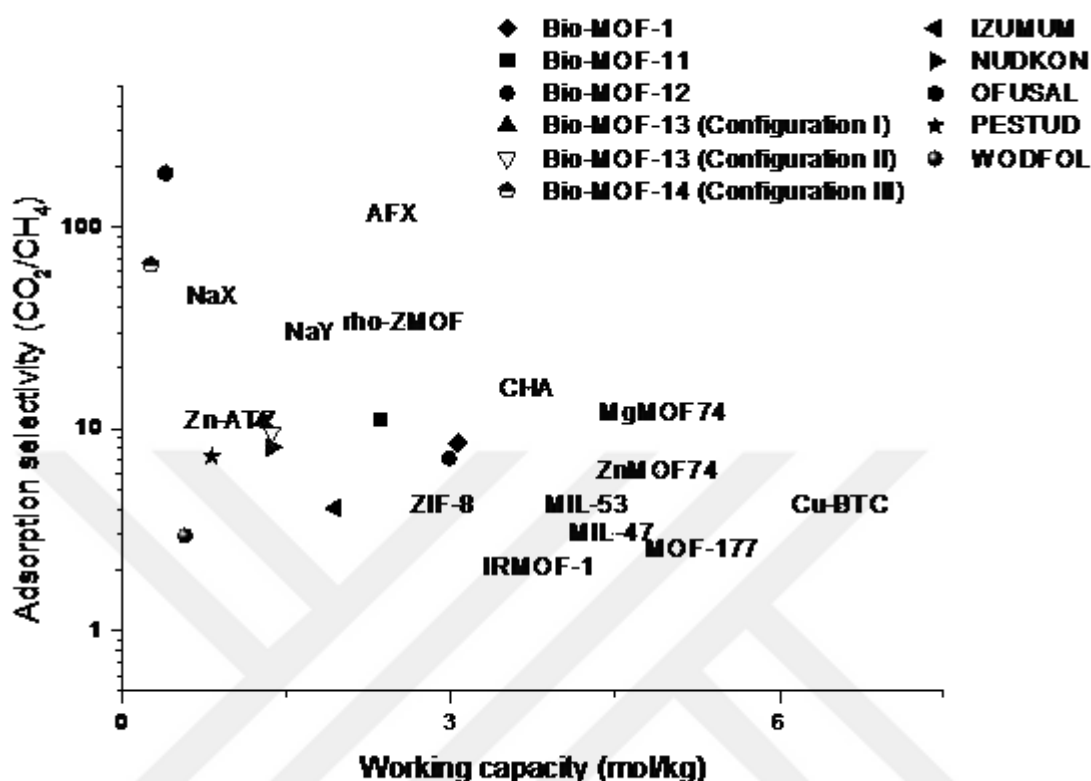


Figure 4.4 Comparison of adsorption selectivities and working capacities of bio-MOFs with other MOFs and zeolites for CO₂/CH₄:50/50 separation at 10 bar and 300 K

Simulation results for both configurations of bio-MOF-13 (I and II) were shown in Figure 4.4 and there is not a significant difference for adsorption selectivity and working capacity of two configurations. Results for configuration I and II of bio-MOF-14 were not shown in Figure 4.4 because none of the gases adsorbed in these configurations under the operating conditions we studied. The CH₄ uptake was almost zero for both configurations and CO₂ uptakes were very low, $\sim 10^{-4}$ mol CO₂/kg material for configuration I and ~ 0.2 mol CO₂/kg for configuration II. Among all configurations of bio-MOF-14, configuration III shows promising adsorption-based separation performance. The high adsorption selectivity (~ 65) of configuration III was attributed to very low CH₄ uptake (~ 0.014 mol CH₄/kg MOF) compared to CO₂ uptake (~ 0.925 mol CO₂/kg MOF). However, bio-MOF-14 suffers from low CO₂ working capacity. Configurations of the aliphatic chains in bio-MOF-13 have a weaker effect on the computed adsorption selectivity and CO₂ uptake compared to bio-MOF-14. This

result also agrees with the molecular simulation study of Li et al.[80] who showed that the chain configurations in bio-MOF-14 have a profound effect on CO₂ adsorption.

4.1.4 Membrane-based Gas Separation

Considering difficulties in the fabrication of defect-free and robust thin-film MOF membranes, molecular simulations play an important role in identifying promising membrane materials prior to experimental studies. Using GCMC and EMD simulations, CO₂/CH₄ permeation selectivity and CO₂ permeability of bio-MOF membranes were estimated and shown in Figure 4.5. The upper bound shown in Figure 4.5 represents the selectivity/permeability trade-off of polymeric membranes. Developing new membranes that can exceed the Robeson's upper bound[92] has been the main focus of membrane research over the last decade. Both high gas permeability and selectivity are desired for an efficient membrane-based gas separation process. High selectivity is required to obtain gases in high purity and high gas permeability decreases the required membrane area, hence capital cost. In order to examine the effect of structure flexibility on the membrane predictions of simulations, results from both rigid and flexible simulations were shown in Figure 4.5. Membrane predictions for OFUSAL were not shown because self-diffusion coefficient of CH₄ ($\sim 10^{-9}$ cm²/s) was found to be very low both in rigid and flexible simulations. CH₄ molecules cannot diffuse in the pores of OFUSAL since both pore limiting diameter (PLD) (2.5 Å) and largest cavity diameter (LCD) (3.2 Å) are smaller than the kinetic diameter of CH₄ (3.8 Å). Similarly, results from rigid EMD simulations of configuration III of bio-MOF-14 were not shown in Figure 4.5 because none of the gas molecules could move in the narrow pores (PLD:1.0 Å, LCD:3.8 Å) on the nanosecond time scales accessible using EMD ($< 10^{-8}$ cm²/s). Self-diffusion coefficients of CO₂ and CH₄, CO₂ permeability and CO₂/CH₄ permeation selectivity results both for rigid and flexible cases are given in Table 4.3. Examples of MSD (mean squared displacement) vs. time graphs together with error analysis of diffusion coefficients can be seen in Figure A.4 and Table A.1 of Appendix.

Table 4.3 Self-diffusion gas coefficients, CO₂ permeabilities and permeation selectivities of bio-MOFs.(CO₂/CH₄:50/50, at 10 bar and 300 K)

Bio-MOFs	D _{self} (cm ² /s) CH ₄		D _{self} (cm ² /s) CO ₂		Permeability of CO ₂ P _{CO₂} (Barrer/10 ⁴)		Permeation selectivity S _{CO₂/CH₄}	
	rigid	flexible	rigid	flexible	rigid	flexible	rigid	flexible
Bio-MOF-1	3.61×10 ⁻⁵	6.66×10 ⁻⁶	3.25×10 ⁻⁵	4.02×10 ⁻⁶	7.72	0.80	7.60	5.10
Bio-MOF-11	2.34×10 ⁻⁵	3.23×10 ⁻⁶	1.84×10 ⁻⁵	1.47×10 ⁻⁶	3.62	0.26	8.74	5.08
Bio-MOF-12	8.11×10 ⁻⁶	2.24×10 ⁻⁶	1.06×10 ⁻⁵	1.57×10 ⁻⁶	1.92	0.27	9.31	5.01
Bio-MOF-13 (configuration I)	< 10 ⁻⁹	1.67×10 ⁻⁸	< 10 ⁻⁹	2.23×10 ⁻⁷	1.48×10 ⁻⁴	0.02	*	189.12
Bio-MOF-13 (configuration II)	6.70×10 ⁻⁷	2.40×10 ⁻⁷	2.40×10 ⁻⁶	7.40×10 ⁻⁷	0.24	0.07	34.33	29.55
Bio-MOF-14 (configuration III)	< 10 ⁻⁹	6.00×10 ⁻⁸	< 10 ⁻⁹	1.00×10 ⁻⁷	2.07×10 ⁻⁴	0.002	*	6.67
IZUMUM	8.17×10 ⁻⁶	1.26×10 ⁻⁵	1.11×10 ⁻⁵	2.16×10 ⁻⁵	1.35	2.55	5.47	6.90
NUDKON	6.60×10 ⁻⁷	4.00×10 ⁻⁸	3.50×10 ⁻⁷	9.00×10 ⁻⁸	0.04	0.01	4.30	18.23
OFUSAL	< 10 ⁻⁸	< 10 ⁻⁹	9.00×10 ⁻⁸	7.00×10 ⁻⁸	0.012	0.01	*	*
PESTUD	3.80×10 ⁻⁷	3.10×10 ⁻⁷	1.24×10 ⁻⁶	9.40×10 ⁻⁷	0.11	0.08	23.83	22.15
WODFOL	1.20×10 ⁻⁷	1.45×10 ⁻⁷	4.85×10 ⁻⁵	1.87×10 ⁻⁶	2.80	1.08	1189.31	37.94

* Permeation selectivities were not reported since CH₄ and/or CO₂ diffusivities were found to be very slow.

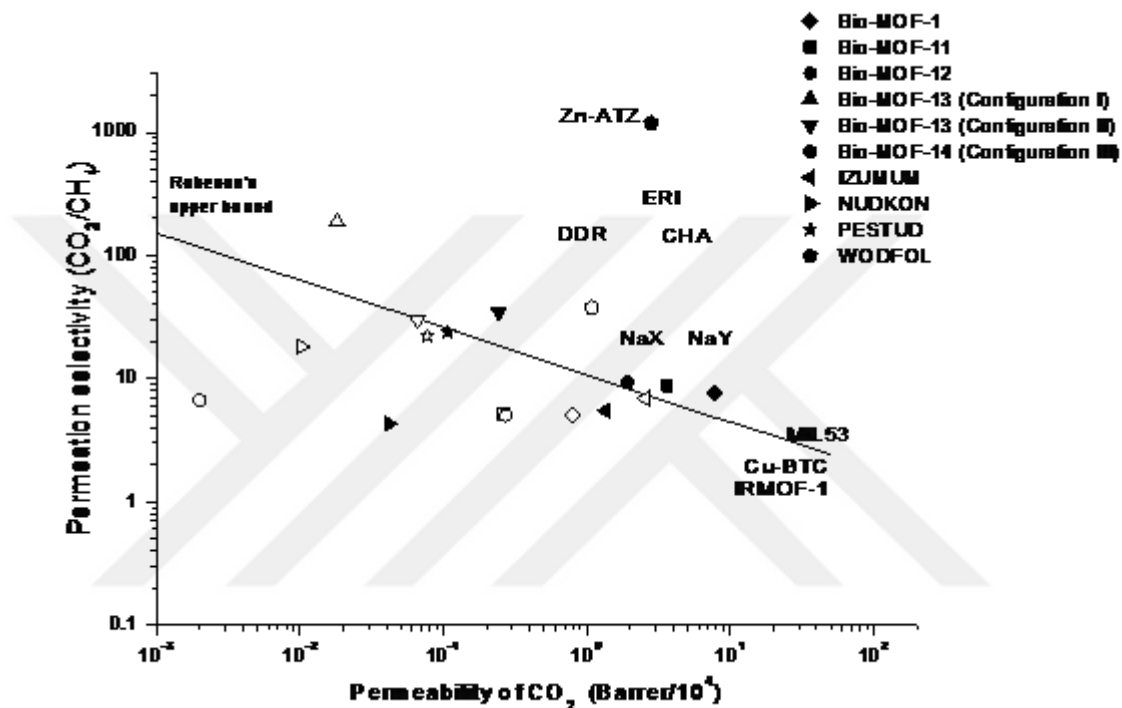


Figure 4.5 Comparison of CO₂/CH₄ permeation selectivity and CO₂ permeability of bio-MOFs with other MOFs and zeolites at 10 bar and 300 K. (CO₂/CH₄:50/50) Closed (open) symbols represent the results of rigid (flexible) EMD simulation.

Results of rigid molecular simulations showed that among ten bio-MOFs, five bio-MOFs, WODFOL, bio-MOF-1, -11, -12, -13 (configuration II) exceed the upper bound established for CO₂/CH₄ separation. WODFOL exhibits very high membrane selectivity (1189). This high CO₂ selectivity is due to very slow diffusion of CH₄ ($\sim 10^{-8}$ cm²/s) compared to CO₂ ($\sim 10^{-5}$ cm²/s). In other words, high membrane selectivity of WODFOL is driven by the high diffusion selectivity. WODFOL outperforms well-known zeolite and MOF membranes such as NaX, DDR, ERI, CHA, Cu-BTC, IRMOF-1 and MIL-53 because of its high CO₂ selectivity. Bio-MOFs-1, -11 and -12 are also located above the Robeson's upper bound due to their high CO₂ permeabilities. Since these three bio-MOFs have the largest free volumes among the ones we considered in this work, their CO₂ permeabilities are very high ($>10^4$ Barrer). Permeation selectivity of these three materials are similar (~ 9) and higher than the three widely studied MOF membranes, IRMOF-1, Cu-BTC and MIL-53. The high CO₂ permeation selectivity of bio-MOF-1, -11 and -12 is driven from the high adsorption selectivity for CO₂ (~ 8 for bio-MOF-1, ~ 11 for bio-MOF-11 and ~ 7 for bio-MOF-12). The self-diffusivities of CO₂ and CH₄ are similar in the pores of bio-MOFs-1, -11 and -12. Therefore, diffusion selectivity does not strongly favor one gas over other and becomes ~ 1 . Bio-MOF-13 (configuration II) also exceeds the Robeson's upper bound due to its high CO₂ selectivity (34.3), resulted from high adsorption and diffusion selectivity for CO₂ over CH₄ (9.6 and 3.6, respectively).

One of the important findings from Figure 4.5 is that chain configurations in bio-MOF-13 have an important effect on the membrane's performance. In Figure 4.4, we showed that chain configurations of bio-MOF-13 have negligible effect on the CO₂ adsorption. However, Figure 4.5 and Table 4.3 show that chain configurations become important for diffusion of gases. Considering configuration I of rigid bio-MOF-13, we estimated very low CO₂ and CH₄ diffusivities ($<10^{-8}$ cm²/s). Higher CO₂ and CH₄ diffusivities ($\sim 10^{-6}$ cm²/s and $\sim 10^{-7}$ cm²/s, respectively) were obtained for configuration II of rigid bio-MOF-13. As Figure 4.1 shows cavities in configuration II of bio-MOF-13 are interconnected which allow diffusion of gas

molecules from one cage to another whereas cavities in configuration I are isolated from each other and hinder gas diffusion. Higher gas diffusivities in configuration II resulted in higher gas permeabilities as can be seen from Figure 4.5. Li et al.[80] also discussed connection of cavities in bio-MOF-13 in their experimental study showing that interconnected cavities of configuration II allow passage of N₂ molecules. We also validated this result in Figure 4.3(a) and (c) where we showed that configuration II of bio-MOF-13 adsorbs more CO₂ and N₂ molecules compared to configuration I.

Molecular simulations were repeated considering flexibility of bio-MOF structures and the results were compared with rigid simulations in Figure 4.5 to examine the effects of structural flexibility on the predicted membrane performance of materials. For all bio-MOFs, except IZUMUM, structure flexibility decreased diffusion coefficient of CO₂ and hence CO₂ permeability. For example, self-diffusion coefficient of CO₂ in rigid (flexible) bio-MOF-1 was predicted as 3.25×10^{-5} cm²/s (4.02×10^{-6} cm²/s). Observing a decrease in self-diffusion coefficient of gases in nanoporous materials when flexibility of the material is taken into account is an expected outcome. Smit and Maesen[207] discussed that diffusion coefficients in flexible zeolites can be either lower or higher than those in rigid zeolites depending on the system. For example, Dubbeldam et al.[208] found an increase of energy barrier for propane in flexible zeolite, ERI, suggesting a decrease of the diffusion coefficient compared to case of a rigid ERI. In order to understand the decrease in self-diffusion coefficients of gases when bio-MOF flexibility was included in our molecular simulations, total free volumes of structures were analyzed during EMD simulations by estimating van der Waals (vdW) surfaces using Materials Studio 8.0. VdW surface is the surface that intersects with the vdW radii of the atoms in the framework. This analysis can be done by setting the Connolly probe radius or solvent probe radius to zero in Connolly surface or solvent surface estimation, respectively. For this analysis, we simply relaxed all bio-MOF structures with geometry optimization using UFF and performed EMD simulations up to 100 ps without gas molecules. As can be seen from Figure A.5, total free volumes of bio-MOFs decreased when flexibility of structures were taken into account. Only for IZUMUM, we observed that permeability

slightly increases although the pore volume of the structure decreases on a small scale when the flexibility was considered. In order to understand this, we examined the change in pore sizes of this structure. As shown in Figure A.6, LCD of IZUMUM increases in flexible simulations and therefore, CO₂ molecules move faster through the cavities. Pore size analysis for the remaining bio-MOFs is also shown in Figures A.6-A.8. For bio-MOF-1, -12, -13, NUDKON, OFUSAL and WODFOL, both PLDs and LCDs decreased when flexibility was taken into account, in agreement with the decreasing diffusion coefficients of gases. The pore sizes did not change significantly for PESTUD, therefore self-diffusivities and permeabilities of gases did not change in this material as can be seen from Figure 4.5. For bio-MOF-14, PLDs were slightly increased in all three configurations when flexibility was included (see Figure A.8). However, these PLDs were still too low (~ 1 Å) for diffusion of any gas molecules. Figure 4.5 shows that lower membrane selectivities were found for all bio-MOFs except NUDKON when structural flexibility was accounted for in molecular simulations. In the case of NUDKON, the decrease in CH₄ diffusivity was much more pronounced compared to the decrease in CO₂ diffusivity. Therefore, a slight increase in CO₂ selectivity was obtained for NUDKON. Considering both rigid and flexible simulation results, WODFOL, bio-MOFs-1, -11 and -12 were identified as promising membrane materials for natural gas purification since they are located well above the upper bound established for CO₂/CH₄ separation.

The predictions obtained from molecular simulations were finally compared with the experimentally fabricated bio-MOF-1 membrane in Figure 4.6.[112] CO₂ permeability and CO₂/CH₄ selectivity of this membrane were computed using rigid and flexible molecular simulations under the same conditions with the experiments, at 298 K and a feed pressure of 2.38 bar. Figure 4.6 shows that flexible EMD simulations of bio-MOF-1 agree well with the experimental data. Experiments reported CO₂ permeability of 5.7×10^4 Barrer and CO₂/CH₄ selectivity of 2.5 whereas flexible simulations predicted CO₂ permeability of 5.4×10^4 Barrer and CO₂/CH₄ selectivity of 2.6. Rigid simulation results gave higher CO₂ permeability (2.7×10^5 Barrer) and selectivity (8.5) compared to flexible simulation results in agreement

with our discussion above. These results showed that accounting for flexibility of the structure is important for accurate prediction of membrane properties.

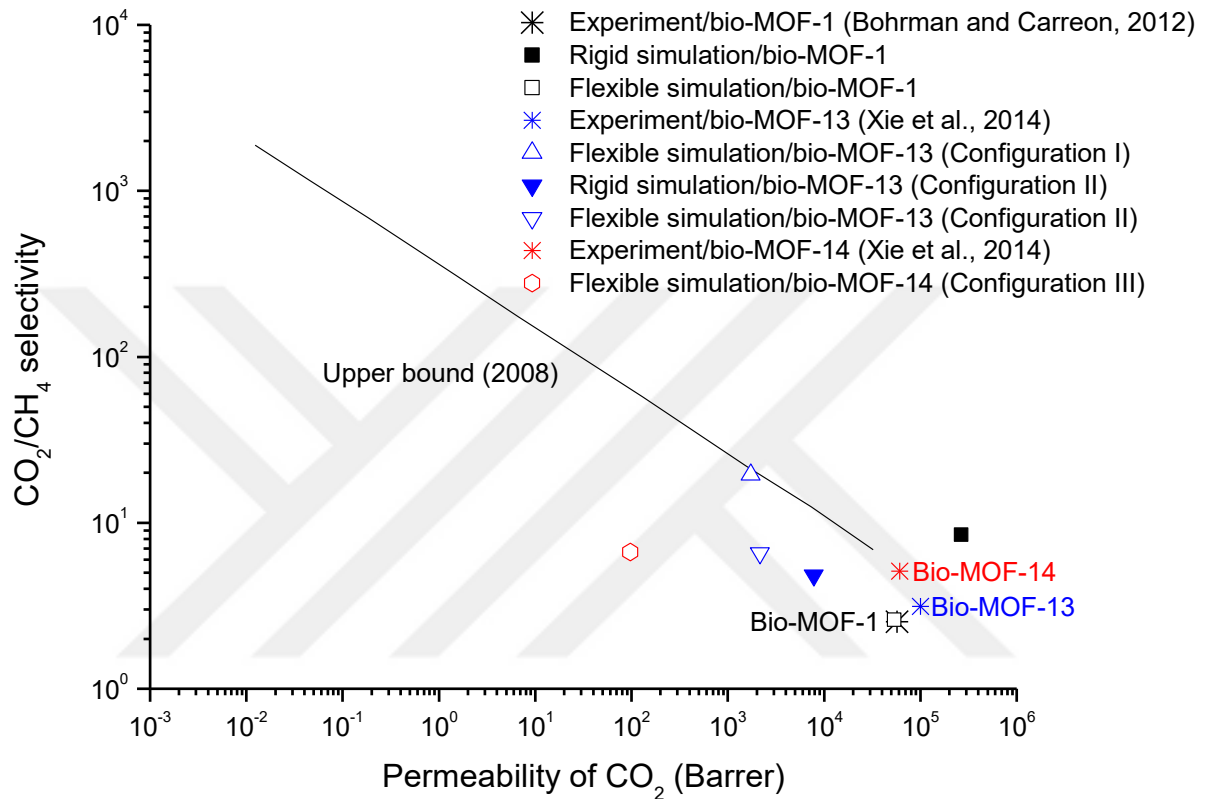


Figure 4.6 Comparison of experiments and molecular simulations for bio-MOF-1, bio-MOF-13 and bio-MOF-14 membranes in CO₂/CH₄ (50/50) separation. Feed pressure is 2.4 bar and temperature is 298 K for bio-MOF-1, 295 K for bio-MOFs-13 and -14. Simulation results for rigid bio-MOF-13 (configuration I) and rigid bio-MOF-14 (configuration III) were not shown since gas diffusion was not measurable in these materials.

As this work was in preparation, two other bio-MOF membranes, bio-MOF-13 and -14, were also fabricated.[47] For bio-MOF-13 and bio-MOF-14, molecular simulations of different configurations did not agree well with the experimental data. The discrepancy between molecular simulations and experiments can be attributed to inappropriateness of the force field used in the molecular simulations and/or possible defects in the fabricated membrane. As shown in Figure 4.3, our molecular simulations well predicted CO₂ adsorption in bio-MOF-13 which validates the accuracy of the force field. Since CO₂ permeability is

calculated based on adsorption and diffusion of CO₂ (see Eq.3.30) and our predictions for CO₂ adsorption agreed well with experiments for bio-MOF-13, the difference between simulated and experimentally measured CO₂ permeability must be due to the diffusion. Therefore, we compared CO₂ self-diffusivities obtained from simulations and experiments. Since experiments did not directly report CO₂ diffusivity, we computed it using experimentally reported permeance data as $\sim 10^{-5}$ cm²/s.[47] Molecular simulations predicted one order of magnitude lower diffusion coefficient ($\sim 10^{-6}$ cm²/s) for rigid configuration II of bio-MOF-13 compared to experiments, which is the main reason behind the discrepancy between simulated and measured CO₂ permeability.

This disagreement can be discussed from two perspectives: (1) The force field that well describes CO₂ adsorption in bio-MOF-13 may be less accurate to describe CO₂ diffusion in the same material. Development of structure-specific force fields that describes intramolecular interactions with a high accuracy from quantum mechanical calculations can be useful. However, this process is very time consuming and challenging. The idea of molecular simulations is to use generic force fields to provide an initial estimate about the materials' properties. (2) The high CO₂ permeability reported by experiments may be due to the defects in the microstructure of the intergrown thin-films since defects associated with grain boundaries can allow significant fluxes of gases through the membrane. The high concentration of non-MOF (unselective) pores in bio-MOF-13 and -14 membranes may lead to higher permeances. It is also important to note that in contrast to single-crystals used in our molecular simulations, fabricated membrane layer is polycrystalline where grain boundaries may contribute to an unknown mass transport. This discussion is also valid for bio-MOF-14. The discrepancy between experimental and simulated CO₂ permeance of bio-MOF-14 is due to the underestimation of molecular simulations not only for diffusion but also for adsorption of CO₂. As we discussed in Figure 4.3, molecular simulations performed by us and by Li et al.[80] underestimated CO₂ adsorption in bio-MOF-14.

Bio-MOFs-13 and -14 have two and three chain configurations, respectively and it is not possible to identify which configuration was dominant in the fabricated membranes.

Therefore, simulations considering only a single chain configuration may give different results than the actual experiments. It is important to note that we found a good agreement between molecular simulations and experiments for bio-MOF-1 membrane which does not exhibit different chain configurations. This result suggests that molecular simulations described in this work can be used to make accurate predictions about the membrane performances of bio-MOFs if the material has a single chain configuration. In fact, most of the MOFs synthesized to date are reported to have a single chain configuration,[15] which means molecular simulation methods can be used to have an initial estimate about the membrane-based gas separation performance of most MOFs prior to extensive experimental efforts.

Finally, it is important to note that selectivity is not the only criteria for a membrane material selection. A material can have a very high selectivity, exceeding the Robeson upper bound, but in the actual process it may lead to very large membrane areas. A trade-off exists between membrane area and permeate CO₂ concentration as discussed by Merkel et al.[209] A lower selectivity does not produce a good separation whereas a higher selectivity uses much more membrane area with little additional improvement in CO₂ purity.

4.2 Evaluation of Bio-MOFs for Other Gas Separations

The gas mixtures we considered in this study are very important for a number of large-scale industrial separation applications. CO₂/H₂ separation is important for H₂ recovery from plants and refineries during pre-combustion of fossil fuels whereas CO₂/N₂ separation is essential for flue gas separation after post-combustion of fuel. We also investigated H₂ separation from CH₄ since obtaining pure H₂ after steam reforming of natural gas is critical.

The separation performance of bio-MOFs for CO₂/H₂, CO₂/N₂ and CH₄/H₂ mixtures were assessed and the effects of temperature and pressure on gas selectivity were also investigated. The filler performance of bio-MOFs which were previously identified as promising membranes were finally investigated for MMM applications.

4.2.1 Adsorption-based and Membrane-based Gas Separations

The potential of bio-MOFs in adsorption based separation processes were initially investigated for CO₂/H₂, CO₂/N₂ and CH₄/H₂ mixtures. Figures 4.7-4.9 show the performance of bio-MOFs in adsorption-based separations of CH₄/H₂, CO₂/H₂ and CO₂/N₂ mixtures calculated at an adsorption pressure of 10 bar and desorption pressure of 1 bar. The data of several zeolites and MOFs from the literature were included to compare the potential of bio-MOFs with the traditional adsorbents. Figure 4.7 demonstrates that bio-MOF-11, bio-MOF-12 and IZUMUM show higher CH₄/H₂ separation performance compared to other MOFs and traditional zeolites such as CHA, TSC and ITQ-29. The adsorption selectivity of CH₄/H₂ and CH₄ delta loading capacities (working capacities) of bio-MOF-11 (41.7 and 2.13 mol/kg, respectively) and IZUMUM (48.2 and 2.06 mol/kg, respectively) are similar since IZUMUM has the identical structure of bio-MOF-11 with the only exception of metal ions. IZUMUM has Cu and bio-MOF-11 has Co metal centers connected by adenine linkers.

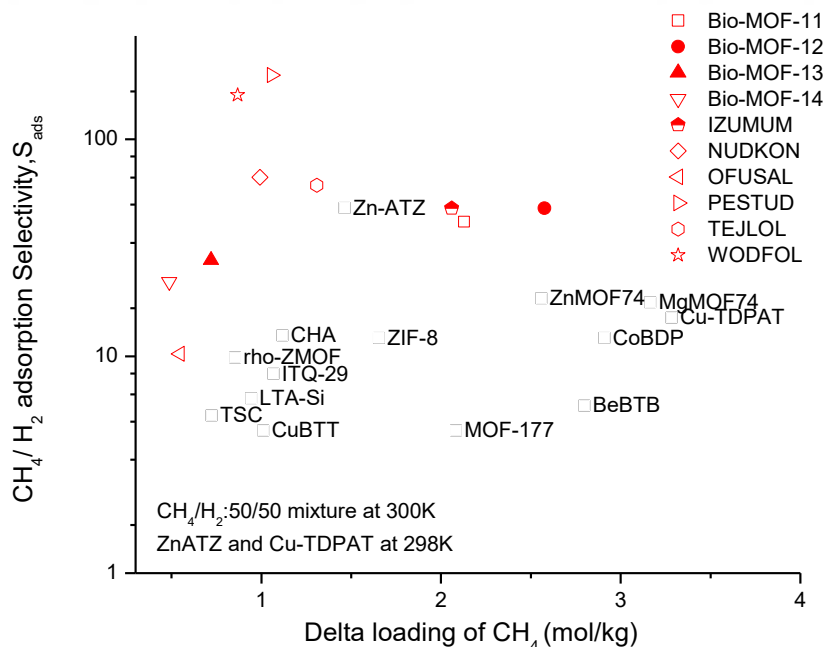


Figure 4.7 Comparison of adsorption selectivities and delta loading capacities of MOFs and zeolites for CH₄/H₂ separation. (Delta loading is also known as working capacity.)

In Figure 4.8, CO₂/H₂ separation performances of bio-MOFs are shown. As can be seen, none of the bio-MOFs can outperform NaX due to its high CO₂/H₂ selectivity. This was attributed to strong electrostatic interactions between CO₂ molecules and non-framework cations, Na⁺. [205] Bio-MOF-11 and bio-MOF-12 again represent similar performances. Since electrostatic interactions become important for CO₂ mixtures, the separation performances of IZUMUM and bio-MOF-11 start to show dissimilar trends. In all mixtures, bio-MOF-11 outperforms IZUMUM due to its higher CO₂ selectivity and higher CO₂ working capacity. Chen and Jiang [91] discussed that high CO₂ uptake capacity of bio-MOF-11 can be attributed to the narrow channels and the Lewis basic sites which are an amino group and a pyrimidine nitrogen atom that coordinates to metal ions. Since CO₂ molecules have quadrupole moments, electrostatic interactions have significant importance. Apart from the adsorbent-CO₂ interactions, several other reasons of higher CO₂ selectivity of bio-MOF-11 compared to IZUMUM can be different charge methods used for these MOFs structures, higher PLD, surface area and pore volume of bio-MOF-11 compared to IZUMUM.

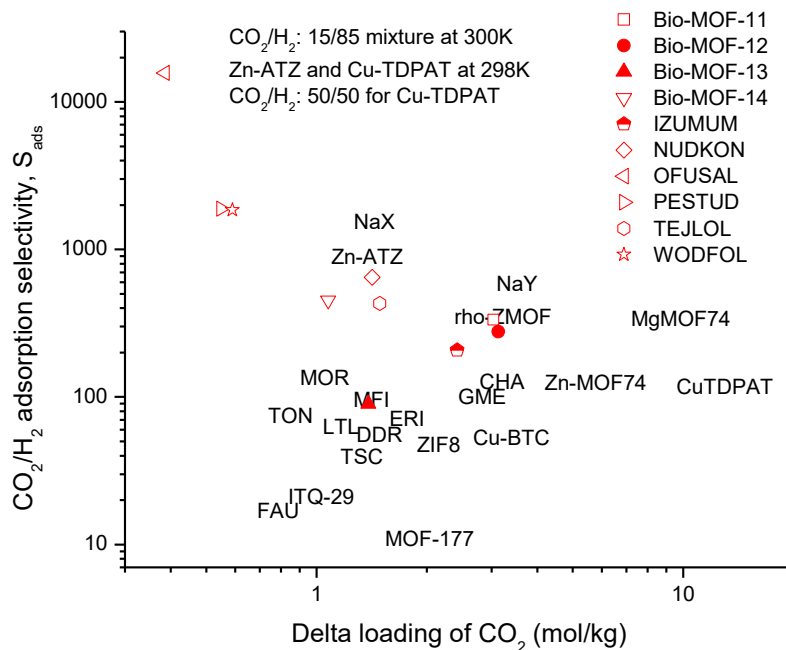


Figure 4.8 Comparison of adsorption selectivities and delta loading capacities of MOFs and zeolites for CO₂/H₂ separation.

Figure 4.9 shows the CO₂/N₂ separation performance of bio-MOFs. OFUSAL has very high CO₂ selectivity (4829) but it has the lowest working capacities (0.45 mol/kg) due to its narrow pore dimensions (2.53Å×3.20Å). Bio-MOF-13, bio-MOF-14, NUDKON and TEJLOL have similar performances for separation of CO₂/N₂ mixtures. These bio-MOFs have the same organic linker, adenine, but their metal centers are different. Similarly, PESTUD and WODFOL show similar performances since they also have the same organic linker, aspartic acid.

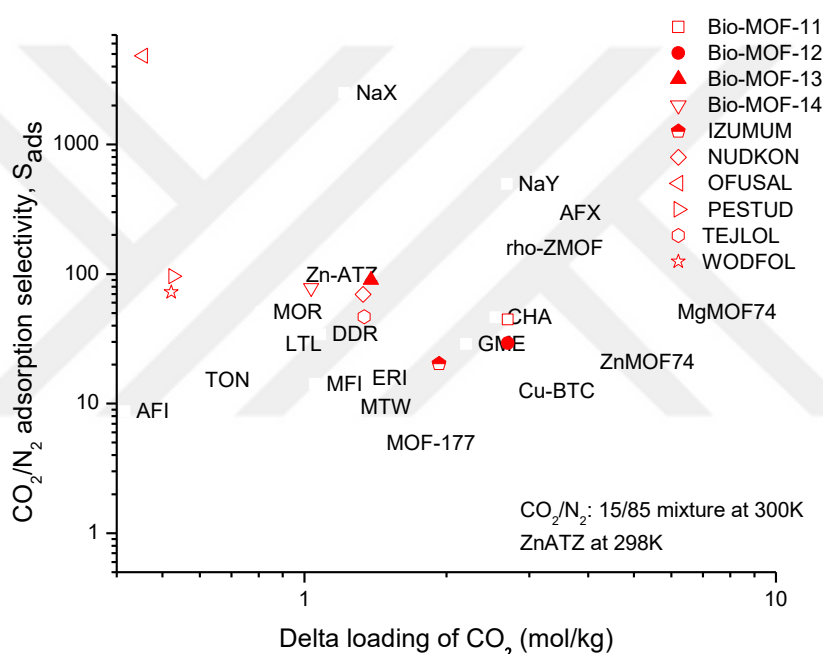


Figure 4.9 Comparison of adsorption selectivities and delta loading capacities of MOFs and zeolites for CO₂/N₂ separation

The results of GCMC and EMD simulations were then used to estimate the permeation selectivity of bio-MOFs as explained in Chapter 3. As can be seen from Figure 4.10, PESTUD and WODFOL have higher permeation selectivities (200.05 and 447.25, respectively) for CH₄/H₂ mixture. All bio-MOFs outperform MOFs such as ZIF-8, Zn-ATZ and traditional zeolites such as LTA and CHA. Similar analysis can be done for CO₂/H₂ separation in Figure 4.11. The high separation performances of PESTUD and WODFOL can be attributed to the high adsorption selectivity of CO₂ over H₂. The strong interactions of CO₂ molecules between the framework atoms enhance the adsorption of CO₂. Bio-MOFs that were studied in this research can be used as promising membranes for CO₂/H₂ separations due to

their high CO₂ permeabilities and high CO₂/H₂ permeation selectivities. For CO₂/N₂ mixtures shown in Figure 4.12, WODFOL and bio-MOF-11 have promising performances compared to other bio-MOFs and traditional zeolites such as TON, GME, MFI and LTA. In Figure 4.12, the line represents the Robeson's upper bound[92] for polymer membranes. As can be seen, five bio-MOFs, bio-MOF-11, IZUMUM, PESTUD, TEJLOL and WODFOL can exceed this upper bound and among them WODFOL exhibits high CO₂ permeability and high CO₂ selectivity over N₂.

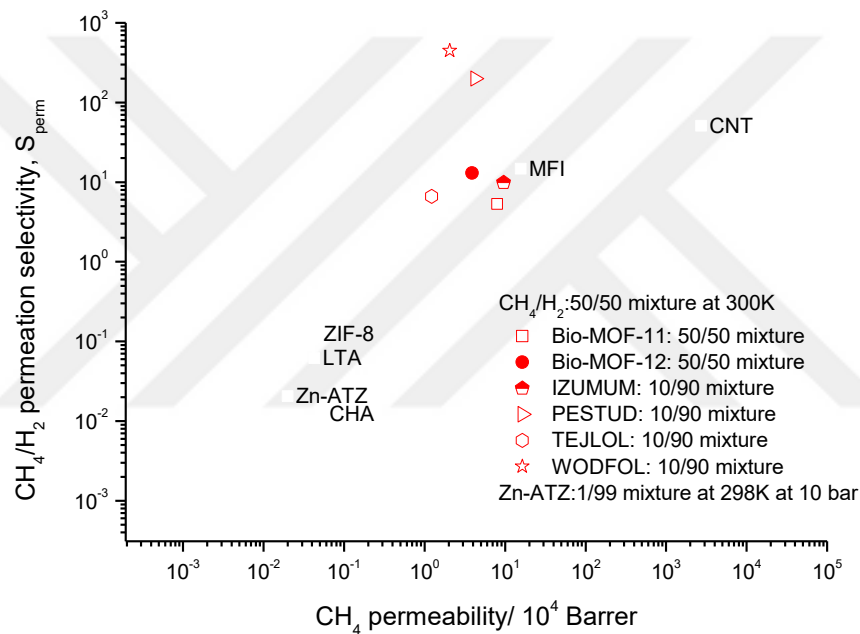


Figure 4.10 Comparison of permeation selectivities and CH₄ permeabilities of MOFs and zeolites for CH₄/H₂ separation.

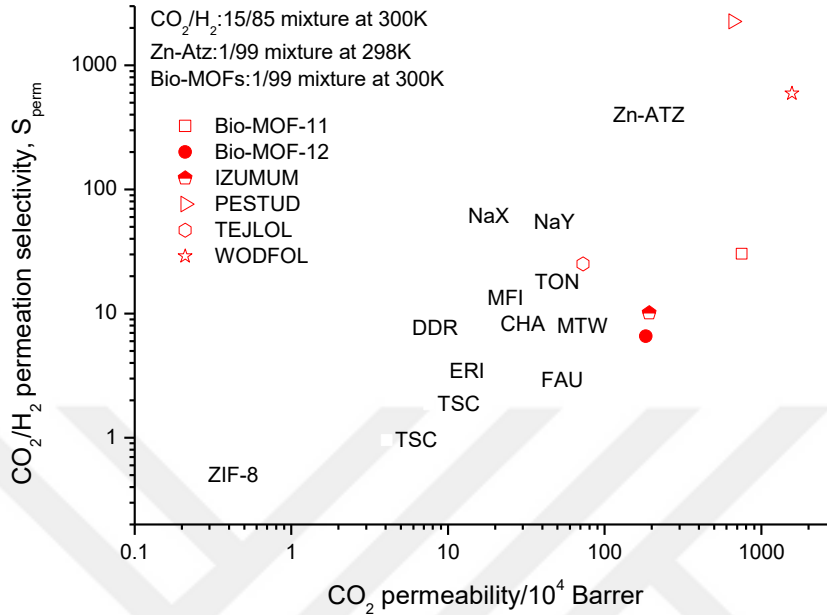


Figure 4.11 Comparison of permeation selectivities and CO₂ permeabilities of MOFs and zeolites for CO₂/H₂ separation.

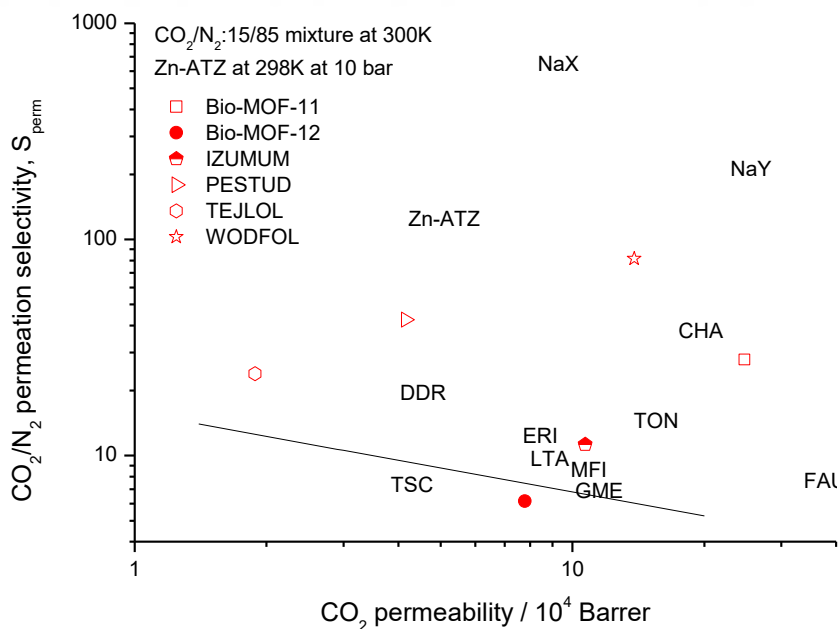


Figure 4.12 Comparison of permeation selectivities and CO₂ permeabilities of MOFs and zeolites for CO₂/N₂ separation.

4.2.2 Investigation of Temperature and Pressure Effects

Bio-MOF-11 and WODFOL were identified as promising adsorbents for industrially important gas separations in Section 4.2.1. Therefore, the influence of temperature and pressure on gas selectivity of these two MOFs were further examined. Figure 4.13 shows the effect of temperature and pressure on the gas selectivity of bio-MOF-11. Since adsorption is an exothermic process, when the temperature is increased, gas uptakes decrease. Therefore, gas selectivities are decreased as shown in Figure 4.13(a-d). Adsorption selectivity strongly favors CH₄ in CH₄/H₂ mixture and CO₂ in CO₂/CH₄, CO₂/H₂ and CO₂/N₂ mixtures. In the pressure range we studied, the adsorption selectivity for CO₂/H₂ is the highest. For example, at 10 bar and 298 K adsorption selectivity for CO₂ over H₂ was predicted to be around 357. This is expected since CO₂ is more strongly adsorbed than H₂ due to high interaction energy between polar CO₂ and adenine linkers of bio-MOF-11 and strong confinement of CO₂ molecules in the narrow pores of bio-MOF-11.

For CH₄/H₂ mixture shown in Figure 4.13(a), adsorption selectivity slightly increases until 5 bar and then decreases. The energetic effects favor CH₄ adsorption and selectivity enhances until 5 bar whereas at higher pressures, packing effects come into play and smaller H₂ molecules can find available space for adsorption. As a result, selectivity decreases. The lowest adsorption selectivities were found for CO₂/CH₄ mixtures as shown in Figure 4.13(b). This can be explained by the similar inter-molecular interactions and size effects of gas molecules. Figures 4.13(c-d) show that CO₂ is strongly adsorbed in both CO₂/H₂ and CO₂/N₂ mixtures. Adsorption selectivity for CO₂ over N₂ is much lower than the selectivity for CO₂ over H₂ because both CO₂ and N₂ have electrostatic interactions which enhance the gas uptake. Additionally, due to a size-selective molecular sieving effect, CO₂ is much preferentially adsorbed over H₂.

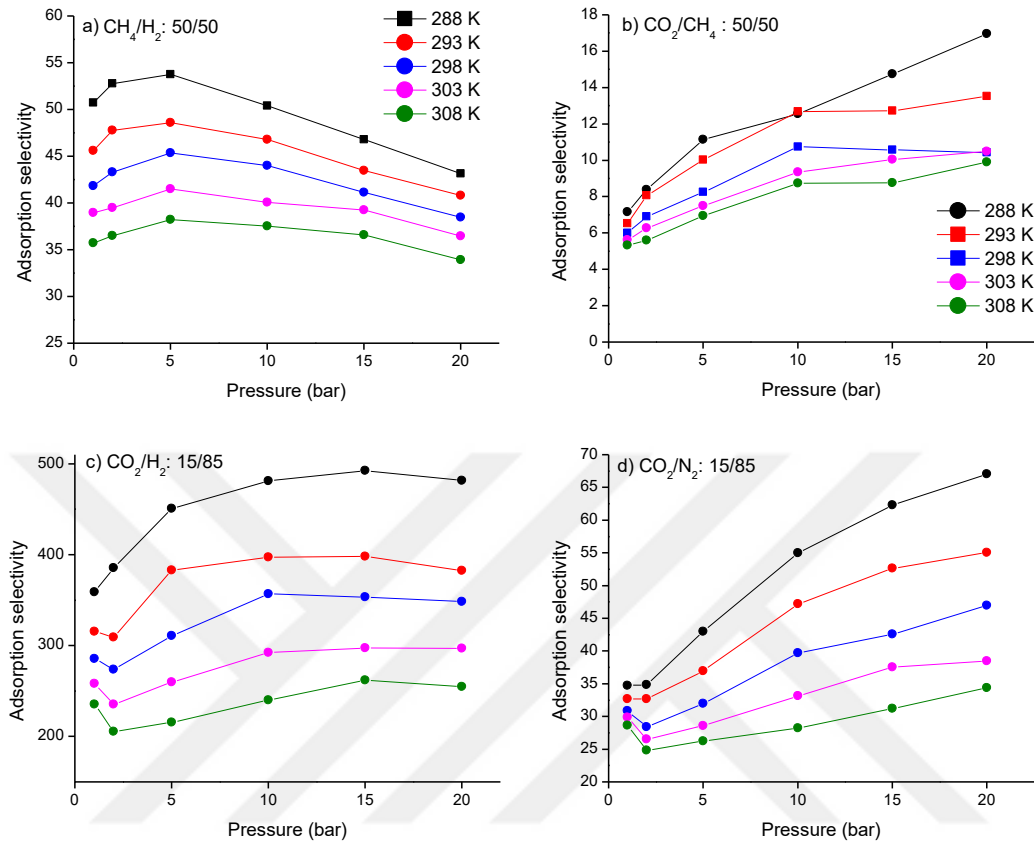


Figure 4.13 Investigation of temperature and pressure effects on (a)CH₄/H₂, (b)CO₂/CH₄, (c)CO₂/H₂ and (d)CO₂/N₂ selectivities of bio-MOF-11.

Since WODFOL was identified as one of the most promising materials for gas separation applications, the influence of temperature and pressure on its gas selectivity was also investigated. Figure 4.14 shows the adsorption selectivities of WODFOL for CH₄/H₂, CO₂/CH₄, CO₂/H₂ and CO₂/N₂ mixtures. Similar to the bio-MOF-11, the highest (the lowest) selectivity was found for CO₂/H₂ (CO₂/CH₄) mixtures. The adsorption selectivity trends were found to be similar for CH₄/H₂ and CO₂/H₂ mixtures. In both mixtures, adsorption selectivity decreases with increasing pressure and temperature. Due to the very low pore volume and narrow pore sizes of WODFOL, H₂ molecules can only fit into available channels and therefore selectivity sharply decreases with increasing pressure. The disordered curves shown in Figures 5.8(b) and (d) demonstrate that WODFOL has already reached to saturation loading of CO₂ at very low pressures. Therefore, negligible effect of pressure on gas selectivity was observed.

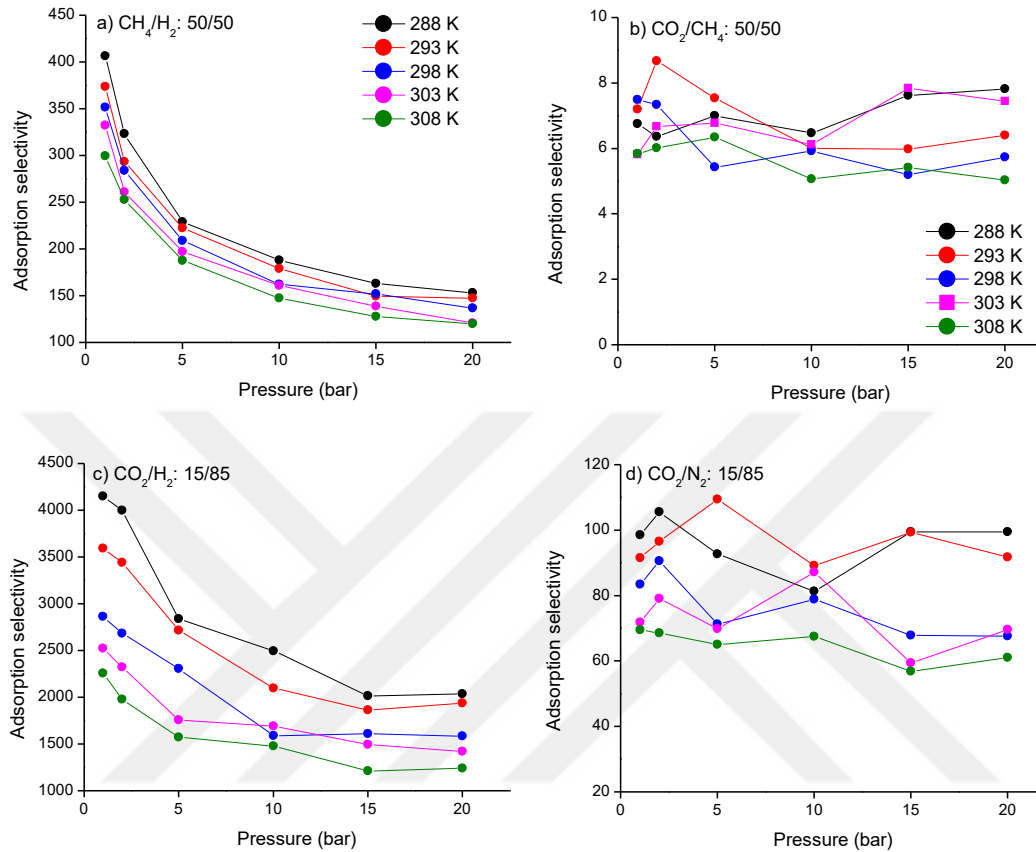


Figure 4.14 Investigation of temperature and pressure effects on (a)CH₄/H₂, (b)CO₂/CH₄, (c)CO₂/H₂ and (d)CO₂/N₂ selectivities of WODFOL.

4.2.3 Investigation of Bio-MOFs for MMM Applications

The gas separation performances of bio-MOF-11-filled membranes and WODFOL-filled membranes were investigated. Initially, gas permeabilities and selectivities were estimated for pure bio-MOF-11 and WODFOL membranes at 298 K and 10 bar. CH₄ and CO₂ are more strongly adsorbed in CO₂/H₂ and CH₄/H₂ mixtures. Therefore, the compositions of the bulk gases were set to 99/1 for H₂/CH₄ and H₂/CO₂ to compute the self-diffusivity of the less adsorbed component (H₂) with better statistical accuracy. The Maxwell model was then used to calculate the gas permeabilities through MOF-based MMMs.

Tables 4.4, 4.5, 4.6, and 4.7 show the data of pure bio-MOF-11 and WODFOL membranes for H₂/CH₄, CO₂/CH₄, H₂/CO₂ and CO₂/N₂ separations, respectively. At that point, it is important to highlight that both selectivity and permeability of polymeric

membranes have been reported for H₂ in the literature since polymeric membranes selectively separate H₂ from CH₄ or CO₂. [92] In order to be consistent with the literature data, we used H₂/CH₄ and H₂/CO₂ selectivity of MOF membranes in Tables 4.4 and 4.6, respectively.

Table 4.4 Permeability and selectivity data of pure MOF membranes for H₂/CH₄ separation

H ₂ /CH ₄ : 99/1 T= 298 K	Permeability of CH ₄ (Barrer)	Permeability of H ₂ (Barrer)	Selectivity H ₂ /CH ₄
Bio-MOF-11	1.59×10 ⁵	2.63×10 ⁴	0.17
WODFOL	1.31×10 ⁵	4.97×10 ³	0.04

Table 4.5 Permeability and selectivity data of pure MOF membranes for CO₂/CH₄ separation

CO ₂ /CH ₄ : 50/50 T= 298 K	Permeability of CO ₂ (Barrer)	Permeability of CH ₄ (Barrer)	Selectivity CO ₂ /CH ₄
Bio-MOF-11	3.47×10 ⁴	1.09×10 ⁴	3.19
WODFOL	9.10×10 ⁴	3.23×10 ³	28.13

Table 4.6 Permeability and selectivity data of pure MOF membranes for H₂/CO₂ separation

H ₂ /CO ₂ : 99/1 T= 298 K	Permeability of CO ₂ (Barrer)	Permeability of H ₂ (Barrer)	Selectivity H ₂ /CO ₂
Bio-MOF-11	3.03×10 ⁴	2.40×10 ⁴	0.79
WODFOL	2.33×10 ⁶	5.73×10 ³	0.003

Table 4.7 Permeability and selectivity data of pure MOF membranes for CO₂/N₂ separation

CO ₂ /N ₂ : 15/85 T= 298 K	Permeability of CO ₂ (Barrer)	Permeability of N ₂ (Barrer)	Selectivity CO ₂ /N ₂
Bio-MOF-11	7.48×10 ⁴	8.17×10 ³	9.15
WODFOL	1.97×10 ⁵	2.32×10 ³	84.96

Table 4.4 shows that both bio-MOF-1 and WODFOL are CH₄ selective membranes. Since CH₄ is energetically preferred over H₂, CH₄ (H₂) is the strongly (weakly) adsorbed component in these MOFs. Therefore, adsorption selectivities favor CH₄ over H₂ (CH₄/H₂ selectivity >1). Diffusion selectivities favor H₂ (CH₄/H₂ selectivity <1) in all MOFs since H₂ molecules diffuse faster than CH₄ molecules. H₂ molecules are lighter, smaller and weakly adsorbed into the pores of MOFs which leads to faster diffusion of H₂ than CH₄. Therefore, using these materials for CH₄ separation will be more efficient. Table 4.5 demonstrates the permeability/selectivity data of pure MOF membranes for CO₂/CH₄ separation. Bio-MOF-11 (~10) and WODFOL (~6) are CO₂ selective in adsorption. In bio-MOF-11, CH₄ molecules

(6×10^{-5} cm²/s) diffuse slightly faster than CO₂ molecules (2×10^{-5} cm²/s). This can be explained by the high adsorption affinity for CO₂. Since diffusion selectivity slightly favors CH₄ in bio-MOF-11, membrane selectivity (3.19) is much lower than adsorption selectivity (10). On the other hand, membrane selectivity of WODFOL (28.13) is much higher than its adsorption selectivity (6) since in WODFOL, both adsorption and diffusion strongly favors CO₂. Due to the narrow pore dimensions of WODFOL, the self-diffusivity of CH₄ ($\sim 10^{-5}$ cm²/s) is one order of magnitude lower than the self-diffusivity of CO₂ ($\sim 10^{-4}$ cm²/s). Therefore, diffusion selectivity strongly favors CO₂ over CH₄ and this MOF become a CO₂ selective membrane.

Tables 4.6 and 4.7 also show that these two MOFs are CO₂ selective. The same discussion for H₂/CH₄ separation is valid for H₂/CO₂ separation. H₂ molecules diffuse much faster than CO₂ molecules in both bio-MOF-11 and WODFOL. Therefore, diffusion selectivity favors H₂ whereas adsorption selectivity strongly favors CO₂ in these MOFs. Therefore, they become CO₂ selective membranes. For example, the diffusion selectivity of bio-MOF-11 for H₂ is 242, but the adsorption selectivity of bio-MOF-11 for the same gas is 0.0033 and the membrane selectivity of bio-MOF-11 becomes 0.79 for H₂/CO₂ separation. In Table 4.7, permeabilities of CO₂ and N₂ were given for bio-MOF-1 and WODFOL. WODFOL was identified as a promising membrane because both adsorption and diffusion favor CO₂ in this separation.

Since H₂ selectivities of bio-MOF-11 and WODFOL are below 1, we only consider CO₂ separations for MMM applications. Figure 4.15 shows the CO₂ permeabilities and membrane selectivities of pure MOF membranes, pure Matrimid and MOF-based MMMs for CO₂/CH₄ and CO₂/N₂ separations. Herein, bio-MOF-11 and WODFOL were considered as filler particles in one of the widely studied commercial polymer, Matrimid. The black solid lines in Figures 4.15(a) and (b) represent the famous Robeson's upper bounds[92] for CO₂/CH₄ and CO₂/N₂ separations, respectively. Polymeric membranes are located below these upper bounds. Since MOFs are highly porous materials, the CO₂ permeabilities of MOF membranes are significantly higher than the CO₂ permeabilities of the polymers. The permeabilities of polymeric membranes are in the range of 10^2 - 10^4 Barrers whereas MOF membranes exhibit CO₂ permeabilities in the range of 10^3 - 10^6 Barrers.

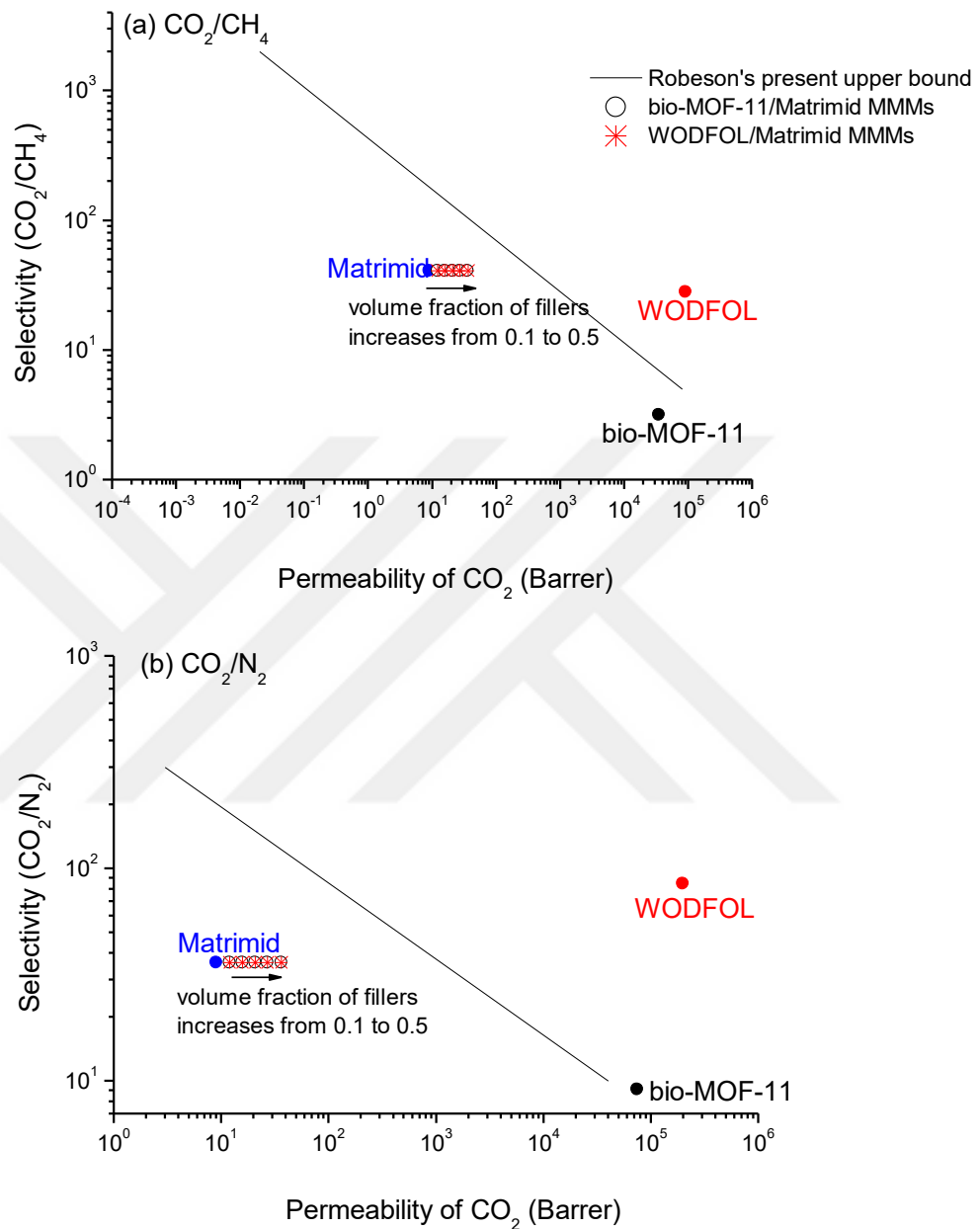


Figure 4.15 Comparison of membrane selectivity and CO₂ permeability of MOF membranes with polymeric membranes for (a)CO₂/CH₄ and (b)CO₂/N₂ separations. The data of pure MOF membrane and matrimid were also shown.

As shown in Figures 4.15(a) and (b), both WODFOL and bio-MOF-11 enhanced the CO₂ permeability of pure Matrimid without changing its CO₂ selectivity. Since both WODFOL and bio-MOF-11 have lower CO₂ selectivities than Matrimid, the selectivity of MMMs did not change when the MOF filler particles are incorporated into Matrimid. As

shown in Figure 4.15, Matrimid has very low CO₂ permeability. Therefore, addition of highly permeable fillers is not enough to achieve high-performance membranes that will exceed Robeson's upper bound. If a very permeable but low selective polymer was used, the identity of MOF used in MMMs would be very important. This analysis shows the importance of MOF/polymer matching to achieve high gas selectivity and permeability.



Chapter 5

EFFICIENT STORAGE OF DRUG AND COSMETIC MOLECULES IN BIO-MOFS

In this chapter, molecular simulations were used to investigate storage and release of an analgesic and anti-inflammatory drug, ibuprofen and two cosmetic molecules, caffeine (lipo-reducer) and urea (hydrating agent) in bio-compatible MOFs. The results of our molecular simulations were compared with the experimentally available data for ibuprofen, caffeine and urea uptakes of MOFs. Motivated from the good agreement between molecular simulations and experiments, molecular simulations were extended to 24 different bio-compatible MOFs and ibuprofen, caffeine and urea storage performances of these bio-MOFs were predicted. Bio-MOF-100 and MOF-74 material series were identified as promising candidates for drug/cosmetic molecule storage. These bio-compatible MOFs outperformed widely studied drug storage materials such as MIL-53(Fe), MIL-100(Fe), MIL-101(Cr), zeolites and mesoporous silica (MCM-41). Diffusion of drug molecules in MOFs were also investigated using molecular dynamics simulations that consider flexibility of the MOF structures. Results showed slow diffusion of drug molecules in MOFs' pores suggesting that MOFs can be strong alternatives to traditional nanoporous materials for drug storage and delivery.

5.1 Computational Details

In this study, various bio-compatible MOFs were examined for adsorption and diffusion of drug and cosmetic molecules. These bio-compatible MOFs are bio-MOFs, CD-MOFs and MOF-74 material series. Bio-MOFs are consisted of endogenous or therapeutically active ligands such as amino acids, peptides, nucleotides, γ -cyclodextrin or bioactive molecules.[33] CD-MOFs are known as edible MOFs which have γ -cyclodextrin building units linked by potassium ions.[210] MOF-74 materials are known to be promising in drug storage[211] due

to their extremely large pore volumes and non-toxic Mg^{2+} cations.[212] They have very large pore apertures ranging from 16 to 54 Å, which make them promising for storage of large guest molecules. In order to make comparisons between our computational predictions and experimentally available drug storage data, several MILs were also studied. As a result, 24 MOFs (bio-MOFs: bio-MOF-1, -11, -12, -100, -101, -102, IZUMUM, NUDKON, MILs: MIL-53(Fe), MIL-100(Fe), MIL-101(Cr), CD-MOFs: CD-MOF-1, -2, -3 and MOF-74 (VOGTIV) and its family: RAVXIX, RAVXET, RAVWUI, RAVXAP, RAVWIW, RAVWOC, RAVWES, RAVWAO, RAVVUH) were investigated in this work. Crystal structures of all MOFs were taken from Cambridge Crystallographic Data Center (CCDC).[15] Solvent molecules, if present, were removed before performing molecular simulations. Stability of the MOFs after solvent removal was confirmed from the corresponding experimental synthesis studies.[36, 74, 141, 212-216] Pore volumes, pore limiting diameters (PLD), largest cavity diameters (LCD) and accessible surface areas of MOFs were calculated using Zeo++ software.[217] These structural properties were reported in the Table B.1 in addition to the information about the type of organic linkers and metals in the framework. Unit cell representations of MOFs were also provided in Table B.1.

Configurational bias-Monte Carlo (CBMC) simulations were performed using fixed pressure task in sorption module of Materials Studio 8.0[200] to determine the adsorbed number of ibuprofen, caffeine and urea molecules in MOFs at 1 bar and 37 °C. Structure of ibuprofen was taken from Zinc Database[198] and structures of caffeine and urea were taken from PubChem.[199] DMol3 was used to optimize the geometries of ibuprofen, urea and caffeine molecules and ESP (ElectroStatic Potential) charges were assigned to all guest molecules. Torsion degrees of freedom for each guest molecule were defined prior to CBMC simulations. The interactions of ibuprofen, caffeine and urea with MOFs were modeled using Lennard-Jones (LJ) 12-6 and Coulomb potentials. LJ parameters were taken from the Universal Force Field (UFF)[161] both for MOFs and guest molecules. For van der Waals terms, atom-based summation method was used with the cubic spline truncation. 12.5 Å was used as a cut off radius for van der Waals terms. The atomic charges of MOFs were estimated using EQeq (Extended Charge Equilibration) method.[16] Ewald summation method with 10^{-5} kcal/mol accuracy was used for the calculation of electrostatic interactions. Due to the anionic structure of bio-MOF-1, -100, -101 and -102, DMA cations were added into the

frameworks using fixed loading task in sorption module prior to CBMC simulations. Simulations were performed with trial configurations consisting of 1×10^6 cycles for the equilibration and 1×10^6 cycles for the production step. More detailed information about CBMC simulations can be found elsewhere.[218]

After performing CBMC simulations, drug uptake capacities of each MOF were calculated at 1 bar and three promising MOFs, bio-MOF-100, -102 and RAVXIX were selected for further investigation of drug delivery. Molecular dynamics (MD) simulations play a significant role in understanding drug delivery systems. MD simulations were used to study the diffusion of drug/cosmetic molecules and examined the interactions between guest molecules and MOFs. One molecule of ibuprofen/caffeine/urea was located in MOFs using CBMC simulations before performing MD simulations. The lowest energy configurations of MOFs were used as the initial configuration of the MD simulations. Drug release is a dynamic process and considering mobility of both guest molecules and MOFs is important to mimic the real systems. Moreover, previous studies showed that considering flexibility of a MOF in simulations is essential if the size of the guest molecule is similar to the pore size of the MOF material.[219] Therefore, we performed MD simulations both with rigid and flexible MOFs using the forcite module of Materials Studio. In flexible simulations, UFF was used for bond stretching, angle bending and dihedral torsions as implemented in Materials Studio. Geometry optimization steps were performed for rigid MOF structures until the following convergence criteria were reached: 10^{-4} kcal/mol for energy, 5×10^{-3} kcal/mol Å for forces and 5×10^{-5} Å for displacement. For the flexible MD simulations, geometry optimizations were performed until the energy convergence (0.002 kcal/mol) was reached. The cell geometry was not allowed to change during the optimization step. After optimization, MD simulations within the NVT ensemble were performed with a step size of 1 fs up to a total of 1 ns at 37°C. Nose-Hoover thermostat[173] was used to keep the temperature constant.

Diffusion of guest molecules was examined by the mean square displacement (MSD) using Eq.(5.1) where N is the number of guest molecules and $r_j(t)$ is the position of the j^{th} guest molecule at time t :

$$\text{MSD}(t) = \frac{1}{N} \sum_{j=1}^N \left\langle \left[\vec{r}_j(t) - \vec{r}_j(0) \right]^2 \right\rangle \quad (5.1)$$

The MSD of guest molecules was calculated using the average of at least three independent MD simulations. We also investigated radial distribution functions (RDF) which show the probability of finding an atom at a spherical shell of certain thickness at a distance (r) from the reference atom which is generally located at the origin. RDF analysis is useful to study the interaction of specified atoms with other atoms present in the system using the position and distribution of these atoms. The RDF, $g_{ij}(r)$, is expressed as follows:

$$g_{ij}(r) = \frac{N_{ij}(r, r + \Delta r) \cdot V}{4\pi r^2 \cdot \Delta r \cdot N_i \cdot N_j} \quad (5.2)$$

Here, $N_{ij}(r, r + \Delta r)$ is the number of atom j around i within a shell from r to $r + \Delta r$, V is the system volume, N_i and N_j are the number of atoms i and j , respectively. RDF analyses were carried out using 1000 trajectory frames that were saved every 1 ps of MD simulations.

Since drug release experiments are generally conducted in a liquid environment, the effect of presence of water on the diffusion of guest molecules were also investigated. It is not currently possible to mimic the full physiological environment of body fluid using current computational methods.[220] Therefore, water as a representative of an aqueous solvent was used in our molecular simulations. Water molecules were packed into the MOF structures using amorphous cell module of Materials Studio. Bueno-Perez et al.[156] investigated the effect of water on ibuprofen adsorption considering ibuprofen/water:1/99 (molar) in the system. We used guest/water:5/95 (molar) composition in our MD simulations. This composition was found to be an optimal one for computational efficiency since most MOFs examined in this work have large pore volumes and require significant computational time for the time dependent behavior of large guest molecules.

5.2. Comparison of Simulations with the Experimental Data

In order to validate the accuracy of our computational approach, the results of our molecular simulations were first compared with the available experimental data for ibuprofen uptake in MIL-53(Fe),[144] MIL-100(Fe),[144] MIL-101(Cr).[33] The results were demonstrated in Figure 5.1 and numerical data were tabulated in Table B.2. We reported drug/cosmetic molecule storage values as mg (drug/cosmetic molecule)/g MOF following the literature.[140] Our molecular simulations for ibuprofen uptake of MILs are in good agreement with the experimentally reported data.[140, 144] We also included the results of

recent computational studies of Bernini et al.,[155] Bei et al.[154] and Babarao et al.[153] for ibuprofen uptakes in MIL-101(Cr), MIL-100(Fe), MIL-53(Fe), MOF-74, CD-MOF-1, bio-MOFs-1, -11 and -100 in Figure 5.1. All our simulations were performed at 1 bar and body temperature, 37 °C. Bernini et al.[155] reported ibuprofen uptake at the saturation loading at 37 °C, Bei et al.[154] and Babarao et al.[153] reported at 1 bar and room temperature, 25 °C. There is a good agreement between our simulations and Bernini et al.[155] for ibuprofen uptake in MOF-74, CD-MOF-1, MIL-53(Fe), MIL-100(Fe) and MIL-101(Cr). Both Bernini et al.'s[155] and our molecular simulations overestimated experimentally reported ibuprofen uptake in MIL-100(Fe). This can be explained with the following discussion: In molecular simulations the entire void volume of the MOF, accessible for ibuprofen molecules or not, is taken into account. However, experiments showed that ibuprofen molecules ($\sim 10 \text{ \AA} \times 5 \text{ \AA}$) preferentially fill into the larger cages ($\sim 8.5 \text{ \AA} \times 29 \text{ \AA}$) instead of narrow windows ($\sim 4.7 \text{ \AA} \times 5.5 \text{ \AA}$) of MIL-100(Fe).[144] Therefore, molecular simulations generally overestimated ibuprofen uptake in MIL-100(Fe). Bernini et al.[155] repeated their simulations by blocking adsorption of ibuprofen in the smaller mesoporous cavities, but they still found higher uptake (403 mg/g) than the experiments (330 mg/g).[144] This result indicated that non-accessibility of the cavities may affect ibuprofen adsorption but it is still not enough to explain the discrepancy between simulations and experiments for this particular MOF. At that point it is also important to note that the differences between simulations and experiments may also result from the experimental issues such as activation of the MOF samples.

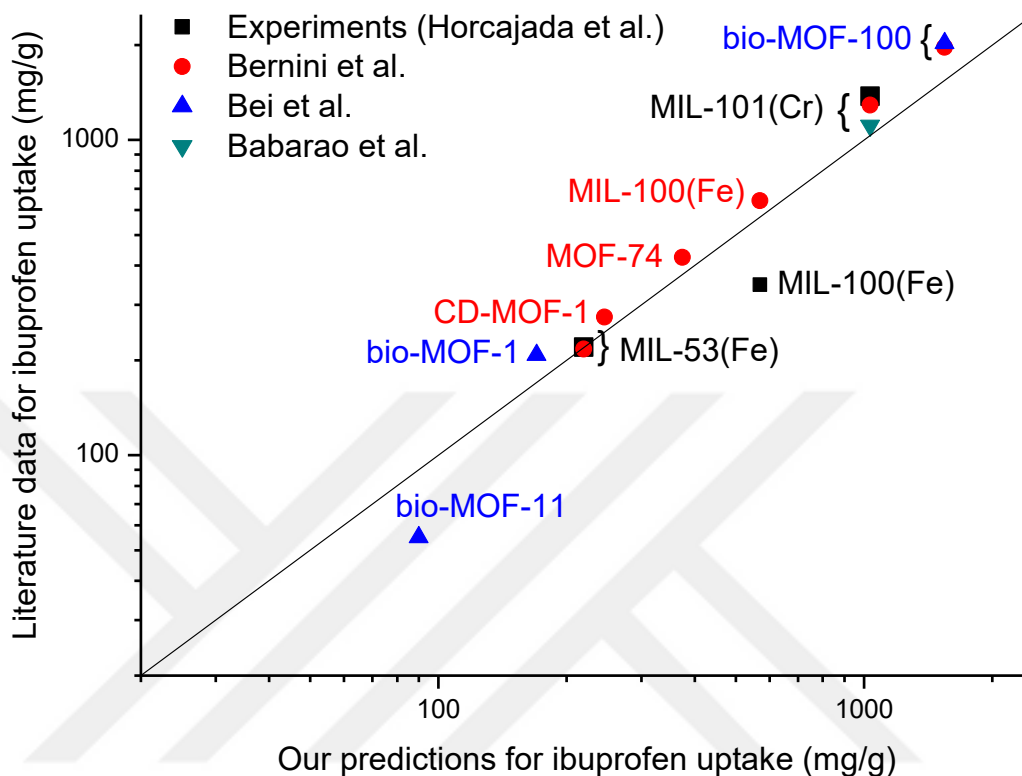


Figure 5.1 Comparison of our predicted ibuprofen uptake with the experiments[140, 144] and other simulation data[153-155] available in the literature.

There is a good agreement between different simulation studies for ibuprofen uptake in MIL-101(Cr) although there are differences in the models used in molecular simulations of different groups. For example, we used the same potential model with Babarao et al.[153] for MIL-101(Cr) but they did not consider fluorine atoms of the MOF in their simulations. We used the same structure and force field for MIL-101(Cr) with Bernini et al.[155] but they modeled ibuprofen molecule using a different force field. Our simulations also agree with Bei et al.[154] for ibuprofen uptakes in bio-MOF-1 and -100. We predicted higher ibuprofen uptake in bio-MOF-11 than Bei et al.[154] This can be explained by the narrow pores of bio-MOF-11 which make it difficult to accurately predict uptake of tightly fitted guest molecules in the material.

Our predictions were also compared with the available experimental data for caffeine[144, 149, 150] and urea[144] uptakes in different MOFs in Figure 5.2. A good agreement between our predictions and experimental data were found for caffeine uptake in

ZIF-8 and urea uptake in MIL-100(Fe). Our simulation results were also in good agreement with the simulations of Cunha et al.[149] for caffeine uptakes in MIL-100(Fe) and UiO-66(Zr). For MIL-100(Fe), UiO-66(Zr) and MIL-53(Fe), we repeated our simulations at 100 bar and room temperature to compare our results under the same conditions with Cunha et al.[149] The caffeine uptakes of MOFs did not change when the pressure was increased from 1 to 100 bar suggesting that saturation of guest molecules has already reached at 1 bar. Similar to the previous discussion made for ibuprofen, simulations overestimated caffeine uptake of MIL-100(Fe) because of the full accessibility of all the windows. Cunha and coworkers[149] estimated caffeine uptake assuming that small cages are not available for caffeine adsorption and reported that experiments (49.5 wt%) and simulations (46.4 wt%) are in good agreement in this case. For urea uptake in MIL-100(Fe), simulations were found to be in very good agreement with the experiments. Due to the small size of urea ($4.1 \times 3.1 \text{ \AA}$), both cages of MIL-100(Fe) were fully accessible in this case. We used the open form of MIL-53(Fe)[221] in our simulations and reported a larger surface area ($1593 \text{ m}^2/\text{g}$) compared to Cunha et al.[149] ($1000 \text{ m}^2/\text{g}$) which explains our slightly higher prediction for caffeine uptake in this MOF. Overall, Figures 5.1 and 5.2 suggest that the computational approach that was described above can be used to make accurate predictions about ibuprofen, caffeine and urea uptakes of various bio-compatible MOFs.

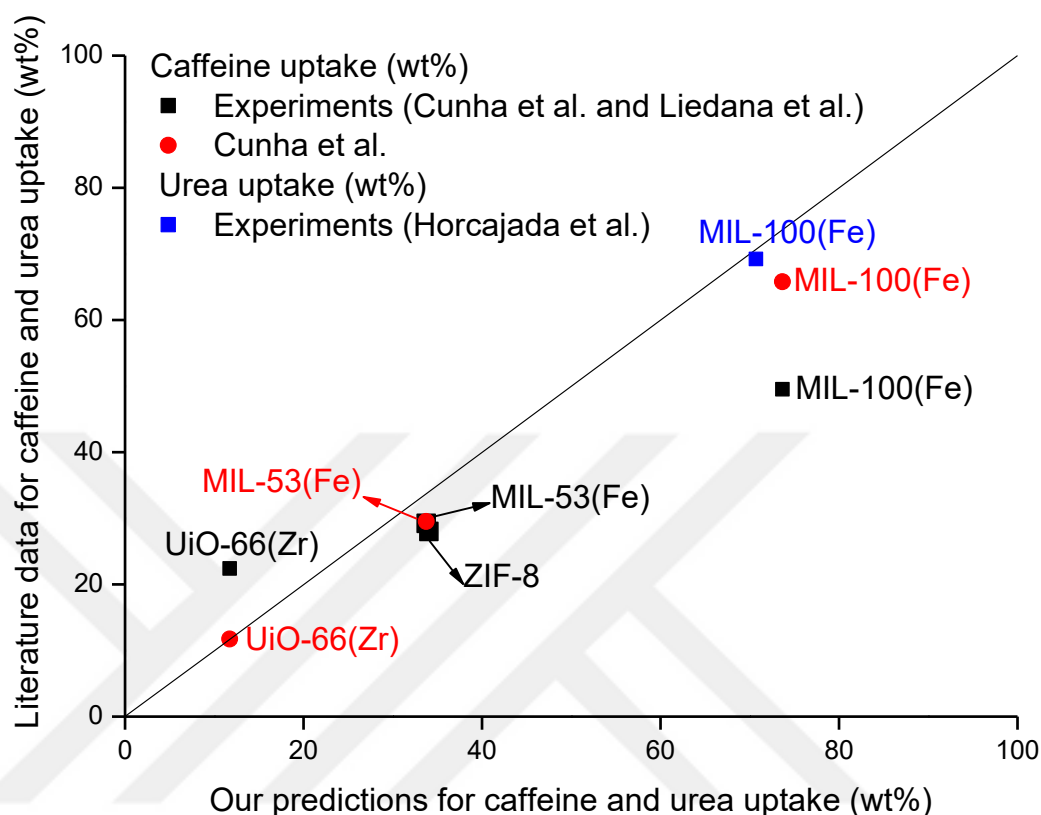


Figure 5.2 Comparison of our predicted caffeine and urea uptakes with the experiments[144, 149, 150] and other simulation data[149] available in the literature.

5.3 Ibuprofen, Caffeine and Urea Uptake and Diffusion in Bio-Compatible MOFs

After validating the accuracy of our computational approach, the same methodology was used to investigate ibuprofen/caffeine/urea uptakes of different bio-compatible MOFs for which experimental data is not available. Figure 5.3 shows our predicted ibuprofen uptake results in 24 different bio-compatible MOFs. The dashed line in this figure represents the current upper limit for ibuprofen storage, 1376 mg/g, which belongs to MIL-101(Cr).[140] Our predictions suggest that bio-MOF-100, -102 and several materials from MOF-74 series (RAVWIW, RAVWUI, RAVXAP, RAVXET and RAVXIX) are highly promising for ibuprofen storage. Most of these MOFs have large pore volumes and large surface areas as shown in Table B.1. The most promising MOF among the ones we studied is RAVXIX which shows ibuprofen storage of 2559 mg/g. This high capacity can be attributed to its extremely large pore apertures ($>53 \text{ \AA}$) and high pore volume ($3.7 \text{ cm}^3/\text{g}$). These results suggest that

several MOFs, especially bio-MOF-100 series (1110-1961 mg ibuprofen/g) and MOF-74 series (RAVVUH-RAVXIX) (863-2559 mg ibuprofen/g), can outperform traditional drug storage materials such as mesoporous silica MCM-41 (340 mg ibuprofen/g), MCM-41-NH₂ (220 mg ibuprofen/g) and zeolite FAU (160 mg ibuprofen/g) by exceeding the current limits for storage of ibuprofen.[34]

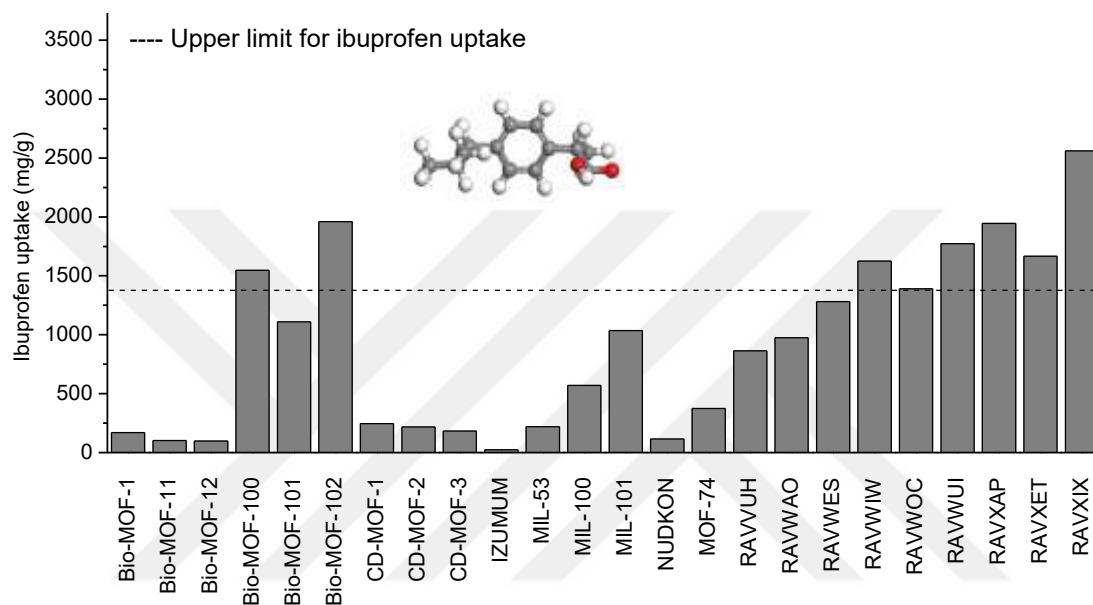


Figure 5.3 Predicted ibuprofen uptake of MOFs. Current limit was set based on experimental ibuprofen uptake of MIL-101(Cr).[140]

The effects of structural properties such as pore volume and pore diameter on ibuprofen adsorption in MOF-74 materials were also investigated. These materials have the same topology but different organic linkers. Therefore, it is appropriate to examine the effects of pore properties on the guest uptake capacities of these materials. The pore volumes and LCDs for the isorecticular series of MOF-74 structures range from 0.7 cm³/g to 3.7 cm³/g and from 11.6 Å to 53.6 Å, respectively. Figure 5.4 shows the linear correlations between predicted ibuprofen uptakes in MOF-74 series and their calculated pore volumes and LCDs. Results showed that ibuprofen uptake increases as the pore volume and LCD of materials increase as expected. For example, MOF-74 has the lowest ibuprofen uptake (~375 mg/g) due to its lowest pore volume (0.7 cm³/g) and smallest LCD (11.6 Å). RAVVUH and RAVWAO have similar ibuprofen uptakes (863-976 mg/g) since they have similar LCDs (~17 Å) and pore volumes (~1 cm³/g). The ibuprofen uptake increases from 1281 mg/g (RAVWES) to 1666 mg/g (RAVXET) as the pore volume and LCD of MOFs (RAVWES-RAVXET) increase

from 1.8 to 2.5 cm³/g and from 24 to 38 Å, respectively. RAVXIX has the highest ibuprofen uptake (2559 mg/g) since it has the highest pore volume (3.7 cm³/g) and LCD (~54 Å). Snapshots taken from adsorption simulations of MOF-74 and RAVWES can be seen in Figure B.1. These results suggest that it is possible to design new materials with enhanced ibuprofen storage capacities by changing the organic linkers used in the synthesis of MOF-74 series.

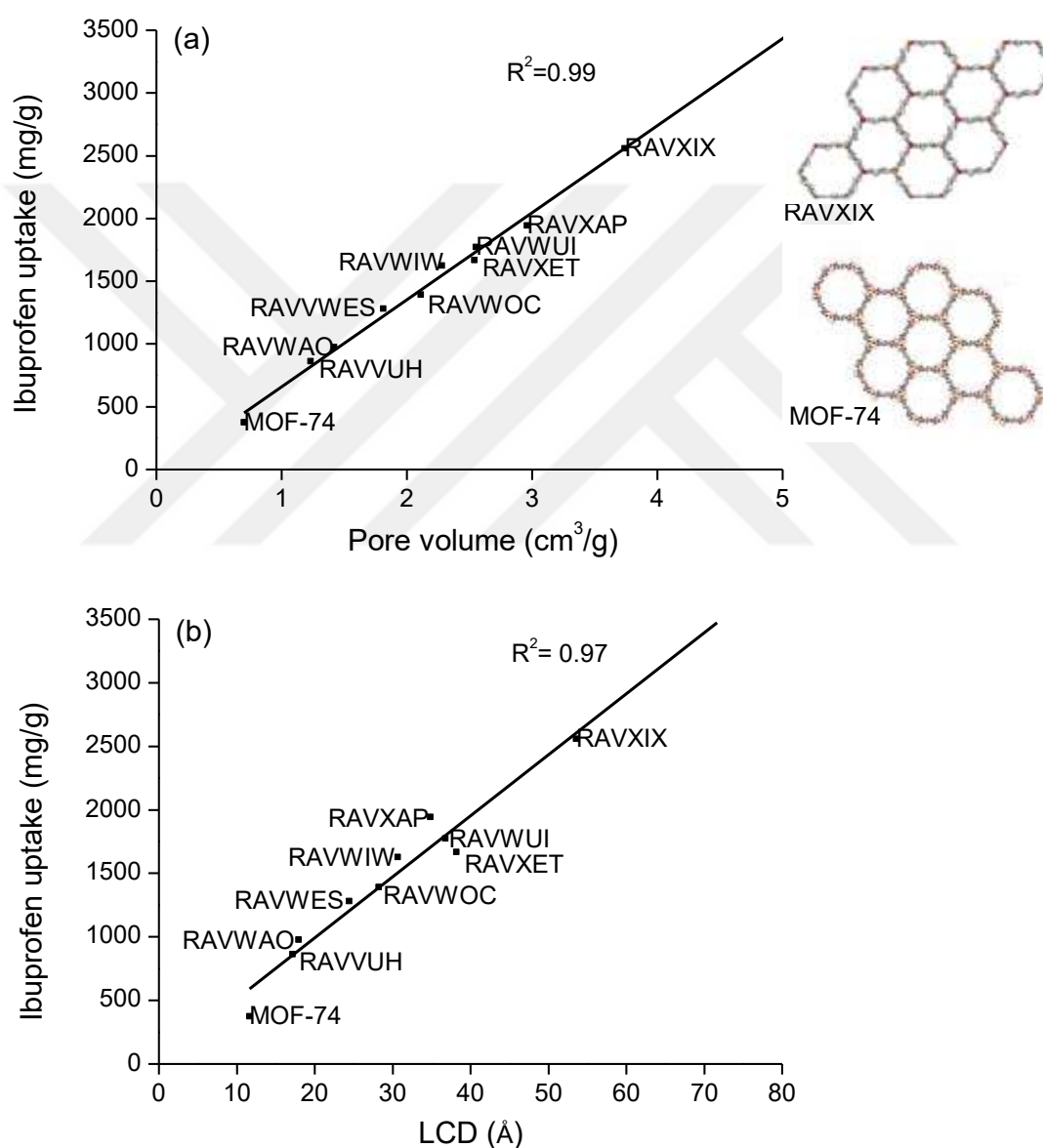


Figure 5.4 Correlations between predicted ibuprofen uptakes of MOF-74 series and their calculated (a) pore volumes (b) largest cavity diameters (LCDs).

Caffeine and urea uptakes of MOFs were examined and the results were shown in Figure 5.5 and Figure 5.6, respectively. Current upper limits for caffeine and urea uptakes are defined as 495 mg/g[149] and 692 mg/g,[144] both for MIL-100(Fe). All MOF-74 materials were found to be promising for storage of caffeine and urea with uptakes >529 mg/g and >655 mg/g, respectively. Bio-MOF-100, -101 and -102 showed high caffeine and urea uptakes. Due to the small pore sizes of IZUMUM ($\sim 4.6 \times 5.6 \text{ \AA}$) and NUDKON ($\sim 2.3 \times 6.4 \text{ \AA}$), no caffeine molecule ($\sim 7.6 \times 6.1 \text{ \AA}$) was able to enter into their pores, therefore we did not show the results for these two structures in Figure 5.5. Our results showed that especially bio-MOF-100 series (1413-2520 mg caffeine/g) and MOF-74 series (RAVVUH-RAVXIX) (1016-3258 mg caffeine/g) can outperform traditional caffeine storage materials such as mesoporous silica, SBA-15 (230 mg caffeine/g) and non-ordered silica (204 caffeine mg/g).[80] In the case of urea uptake, MIL-101(Cr) ($\sim 1425 \text{ mg urea/g}$), bio-MOF-100 series (1400-2141 mg urea/g) and MOF-74 series (RAVVUH-RAVXIX) (1048-2938 mg urea/g) can outperform MIL-100(Fe) which has the current highest experimental urea uptake (692 mg/g).[144]

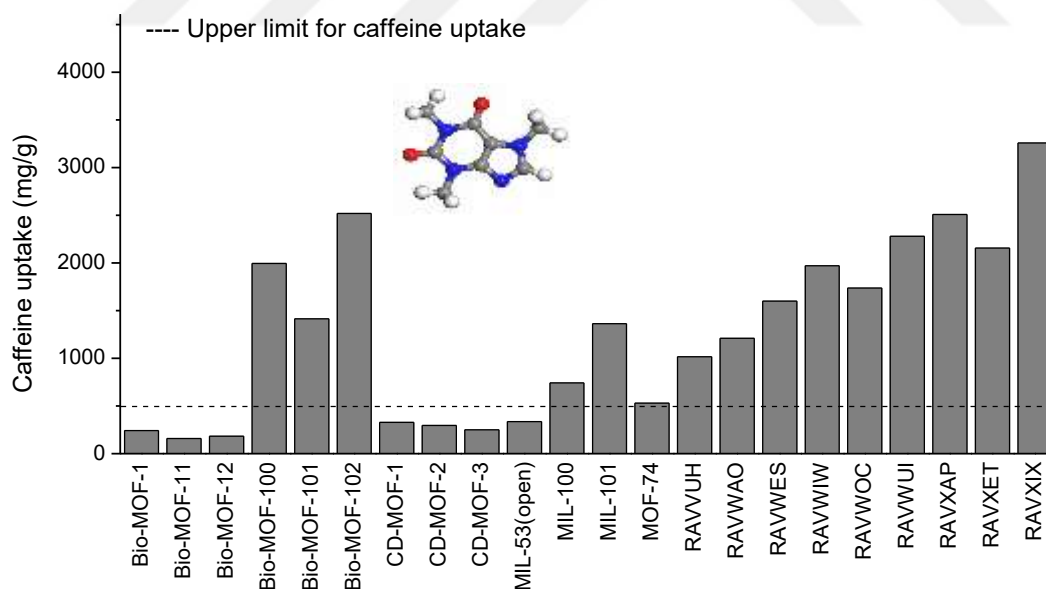


Figure 5.5 Predicted caffeine uptake in MOFs. Current limit was set based on experimental caffeine uptake of MIL-100(Fe).[149]

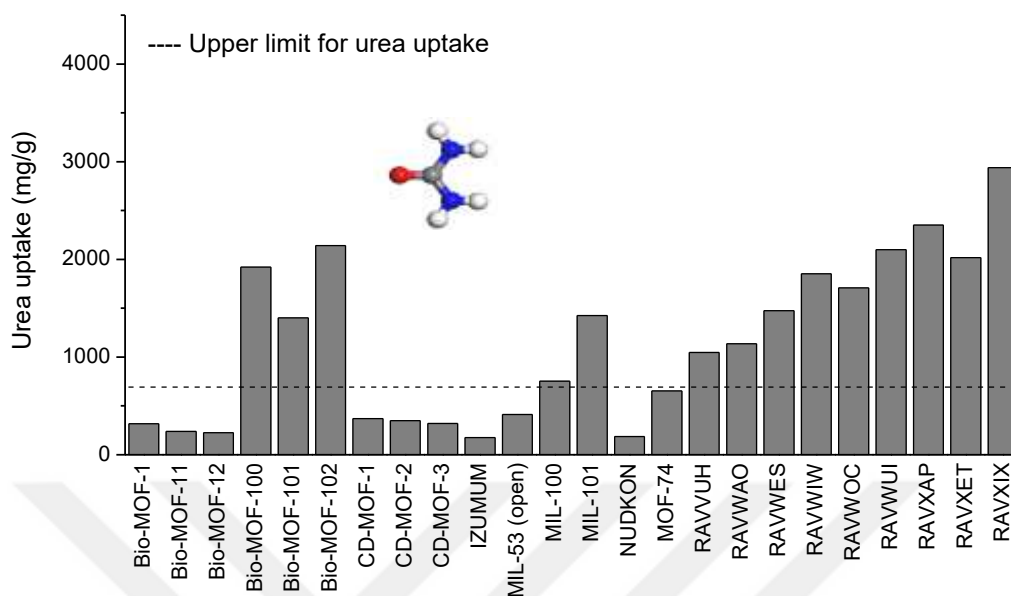


Figure 5.6 Predicted urea uptake in MOFs. Current limit was set based on experimental urea uptake of MIL-100(Fe).[144]

After identifying the top promising MOFs for drug/cosmetic molecule storage, the diffusion of guest molecules in these MOFs were examined using MD simulations. As discussed before, there were only two studies[153] in the literature that examined ibuprofen diffusion in MOFs. Our simulations were initially compared with these simulations for ibuprofen diffusion in MIL-101(Cr) and bio-MOF-11. MD simulations were performed at the same conditions with the literature considering only 1 ibuprofen molecule in one unit cell of the MOF. Figure 5.7 represents the mean square displacements (MSDs) of ibuprofen in rigid and flexible MIL-101(Cr) structures and the dotted line shows the cell boundary of MIL-101(Cr). Consistent with Babarao et al.[153, 154] we showed that ibuprofen diffusion is very slow in MIL-101(Cr) both for rigid and flexible frameworks. When the flexibility of the structure was considered, diffusion of ibuprofen was slightly enhanced but it was still very slow. This enhancement can be explained by the coordination bond formation between oxygen atom of carboxyl group of ibuprofen and Cr atoms of MIL-101(Cr). Figure B.2 demonstrates the favorable conformation of ibuprofen in MIL-101(Cr). As can be seen from this figure, oxygen atom of carboxyl group of ibuprofen heads toward to Cr atom of MIL-101(Cr). The radial distribution function (RDF) analysis were also carried out to examine the most favorable interaction sites between ibuprofen and MIL-101(Cr). Figure 5.7(b) shows the RDF for oxygen atom of carboxyl group of ibuprofen and metal atom of MIL-101(Cr). The

first peak is located at 2.03 Å, which is very close to the experimentally reported Cr-O distance (1.9-2.0 Å),[153] indicating the formation of a coordination bond between ibuprofen and MIL-101(Cr). Diffusion of ibuprofen in bio-MOF-11 were also computed and the results were compared with the previously reported simulation data[154] in Figure B.3. Our simulation results are in a good agreement with those of Bei et al.[154] for diffusion of ibuprofen in rigid bio-MOF-11. Simulations showed that ibuprofen molecule is very slow through the narrow pores of bio-MOF-11 in rigid simulations. Similar to MIL-101(Cr), diffusion of ibuprofen molecule was slightly increased when the flexibility of the framework was considered. However, it was still far away from the cell boundary indicating slow delivery of ibuprofen in bio-MOF-11 as desired for a drug delivery system.

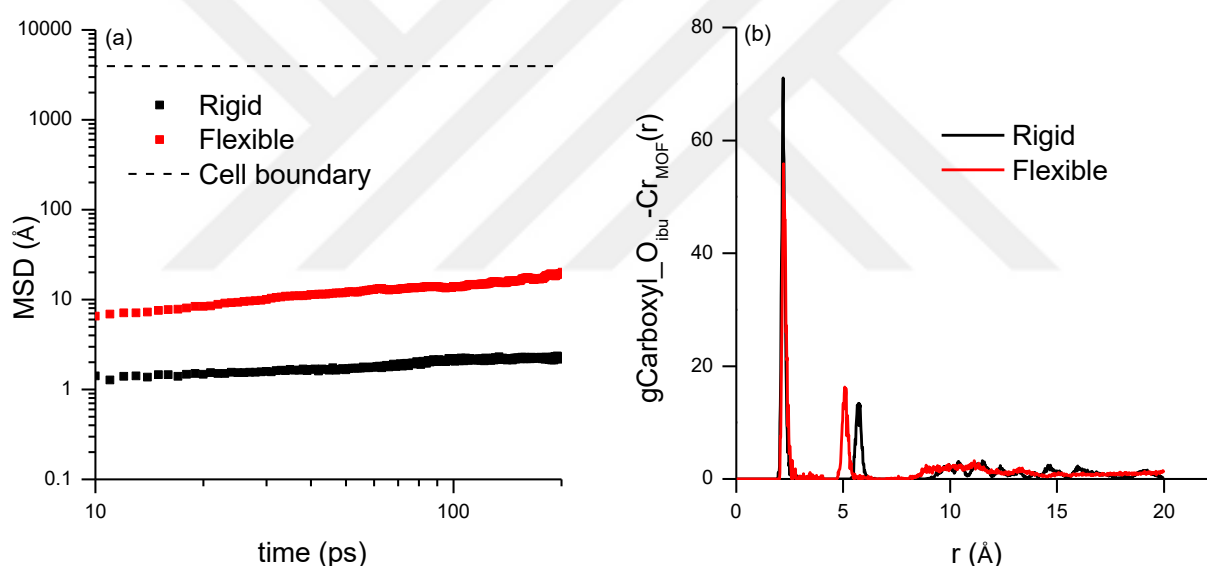


Figure 5.7 (a)MSD and (b)RDF analyses of ibuprofen diffusion in MIL-101(Cr).

Ibuprofen diffusion in bio-MOF-100 was then examined since this MOF was one of the most promising materials for storage of ibuprofen, caffeine and urea as discussed above. Bio-MOF-100 is a prototype of isoreticular bio-MOF-10X series and understanding diffusion in this MOF will enable us to infer the diffusion behavior of other bio-MOF-10X materials. There is currently no study in the literature that examines mobility of guest molecules in the pores of bio-MOF-100. This lack of information encouraged us to examine drug diffusion in bio-MOF-100. Figure 5.8 shows the MSDs of ibuprofen, caffeine and urea in rigid and

flexible bio-MOF-100 structures. As can be seen from this figure, none of the guest molecules can surpass the cell boundary of cubic bio-MOF-100, suggesting that guest mobility is very slow in this material as desired for drug delivery. Different diffusion trends were observed for each guest molecule. Ibuprofen is the slowest and urea is the fastest diffusing molecule in bio-MOF-100. This can be explained by the size and weight differences of the molecules. Ibuprofen is heavier (206.3 g/mol) and larger ($\sim 10 \text{ \AA} \times 5 \text{ \AA}$) than caffeine (194.2 g/mol, $\sim 6.1 \text{ \AA} \times 7.6 \text{ \AA}$) molecule. Therefore, ibuprofen diffuses slower than caffeine. Urea has the smallest size ($\sim 4.1 \text{ \AA} \times 3.1 \text{ \AA}$) and the lowest weight (60.1 g/mol) hence its diffusion is faster than ibuprofen and caffeine.

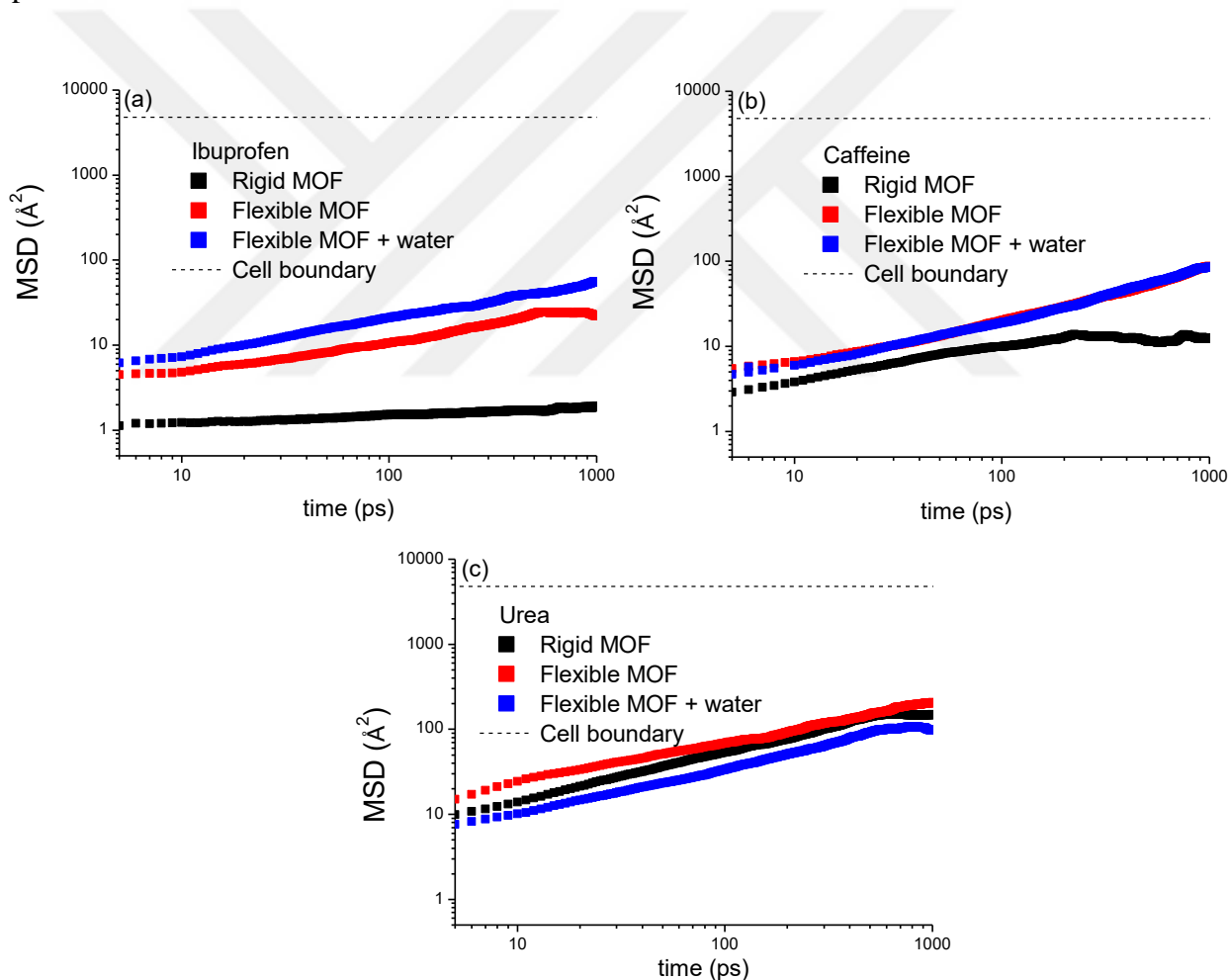


Figure 5.8 MSD of (a) ibuprofen, (b) caffeine and (c) urea in bio-MOF-100.

Figure 5.8(a) shows that diffusion of ibuprofen was slightly increased when the flexibility of MOF was considered. To further understand the increased diffusion in flexible

simulations, we relaxed bio-MOF-100 with geometry optimization and performed MD simulations without guest molecules to examine the change in pore sizes of the MOF. Details of this methodology can be found in our previous study.[222] Figure B.4 shows the change in pore sizes of bio-MOF-100 during MD simulations. Since both small and large pore sizes of the MOF were increased in flexible simulations, diffusion of ibuprofen was enhanced. Presence of water molecules in the system slightly increased the diffusion of ibuprofen as shown in Figure 5.8(a). MD results showed that one water molecule gets close to the hydroxyl group of ibuprofen whereas other water molecules push the hydrophobic carboxylate part of ibuprofen further apart. These competing interactions between water molecules and ibuprofen caused an increase in ibuprofen mobility. Caffeine diffusion in bio-MOF-100 is shown in Figure 5.8(b). Similar to ibuprofen, diffusion of caffeine was also slightly increased when the flexibility of the MOF was taken into account. The presence of water molecules does not significantly affect the diffusion of caffeine since it is an amphiphilic molecule. Figure 5.8(c) shows that there is no significant difference between rigid and flexible simulation results for urea diffusion in bio-MOF-100 because this molecule is very small compared to the pore sizes of the MOF. It is well-known that flexibility of the MOF does not affect the diffusion of small guest molecules in large pores.[219] Diffusion of urea decreased in the presence of water due to the hydrophilic character of urea. MD simulations showed that water molecules get close to urea molecule as shown in Figure B.5 and slowed down its diffusion due to the steric hindrance effects.

In order to better understand the interactions between guest molecules and MOF, RDF analyses were carried out for bio-MOF-100. In RDF calculations, we specifically focused on the interaction between guest molecules and metal atoms of MOFs since metal sites in MOFs are generally the primary adsorption sites for guests.[223] The interaction between oxygen atoms of (carboxyl and hydroxyl groups) of ibuprofen and metal atom of bio-MOF-100 was first investigated. Rigid simulation results showed that $g_{\text{carboxyl_Oibu-ZnMOF}}(r)$ has an intense peak at 2.97 Å while $g_{\text{hydroxyl_Oibu-ZnMOF}}$ has an intense peak at 4.17 Å as shown in Figures B.6(a,b). When flexible and water-filled flexible MOFs were studied, the intense peaks of $g_{\text{carboxyl_Oibu-ZnMOF}}(r)$ were observed at 8.51 Å and 4.45 Å, respectively. That means the interaction between the oxygen atom of carboxyl group of ibuprofen and Zn atom of bio-MOF-100 was weakened in the flexible and water-filled simulations. Similar results were also

found for oxygen atoms of hydroxyl groups of ibuprofen and Zn atom of bio-MOF-100. When flexible and water-filled flexible MOFs were studied, the intense peaks of $g_{\text{hydroxyl_Oibu-ZnMOF}}(r)$ were observed at 4.27 Å and 4.59 Å, respectively. These results indicate weaker interaction between ibuprofen and bio-MOF-100 supporting the increase in ibuprofen diffusion as shown in Figure 5.8(a).

Figure B6(c) shows the interactions between oxygen atoms of caffeine molecule and metal atoms of bio-MOF-100. The sharp peaks are located at 2.83 Å for rigid MOF, 4.07 Å for flexible MOF and 5.49 Å in the water-filled MOF. The interactions between oxygen atoms of caffeine and Zn atom of bio-MOF-100 were weakened when the flexibility was included in the simulations and this caused to faster diffusion of caffeine as supported by the results shown in Figure 5.8(b). Similar to ibuprofen, diffusion of caffeine molecule was also increased when flexible bio-MOF-100 was considered. We observed no significant effect of water on the diffusion of caffeine in the pores of flexible bio-MOF-100. Figure B6(d) indicates that oxygen atom of hydrophilic urea molecule has favorable interaction with Zn atoms of bio-MOF-100 since the first peak was observed at 2.29 Å for rigid MOF, 2.05 Å for flexible MOF and 2.13 Å in water-filled MOF. There is no significant difference in the peak intensities of rigid, flexible and water-filled MOF as shown in Figure B6(d) suggesting that the structural arrangement of oxygen atoms of urea molecule and Zn atoms of bio-MOF-100 does not change. This result indicates similar diffusion trends for urea in rigid, flexible and water-filled MOF as supported by Figure 5.8(c). Strong adsorption of ibuprofen, caffeine and urea in bio-MOF-100 leads to slow diffusion of these molecules, making this material promising for drug delivery. High isosteric heat of adsorption energies of bio-MOF-100 (~31 kcal/mol for ibuprofen, ~20 kcal/mol for caffeine and ~10 kcal/mol for urea) are also evidences for strong adsorption of the guest molecules. Snapshots of simulations showing adsorption conformations of ibuprofen, caffeine and urea molecules in bio-MOF-100 are given in Figures B.7-B.9 of Appendix.

In order to understand the effects of pore volume and pore size on the drug diffusion in MOFs, ibuprofen diffusion in two MOFs with similar structures, bio-MOF-100 and -102 was studied. Ibuprofen diffusion in RAVXIX was also investigated since this MOF has the highest drug/cosmetic molecule storage as shown in Figures 5.3, 5.5 and 5.6. Figure 5.9 shows the MSD data of ibuprofen in bio-MOF-100, -102 and RAVXIX. Bio-MOF-100 and -102 are the

two MOFs that have the same topology but different organic linkers. Diffusion of ibuprofen in all two cases (rigid and flexible) was slower in bio-MOF-100 compared to that of in bio-MOF-102. When two MOFs have the same topology and similar interactions with a guest molecule, diffusion may be simply explained by the available pore volumes. Since bio-MOF-100 has a smaller pore volume ($2.6 \text{ cm}^3/\text{g}$) compared to bio-MOF-102 ($3.2 \text{ cm}^3/\text{g}$), diffusion of ibuprofen is much slower in the former. Bio-MOF-100 also exhibits higher isosteric heat of adsorption (31 kcal/mol) for ibuprofen than bio-MOF-102 (27 kcal/mol) explaining the slow diffusion of ibuprofen in the pores of bio-MOF-100.

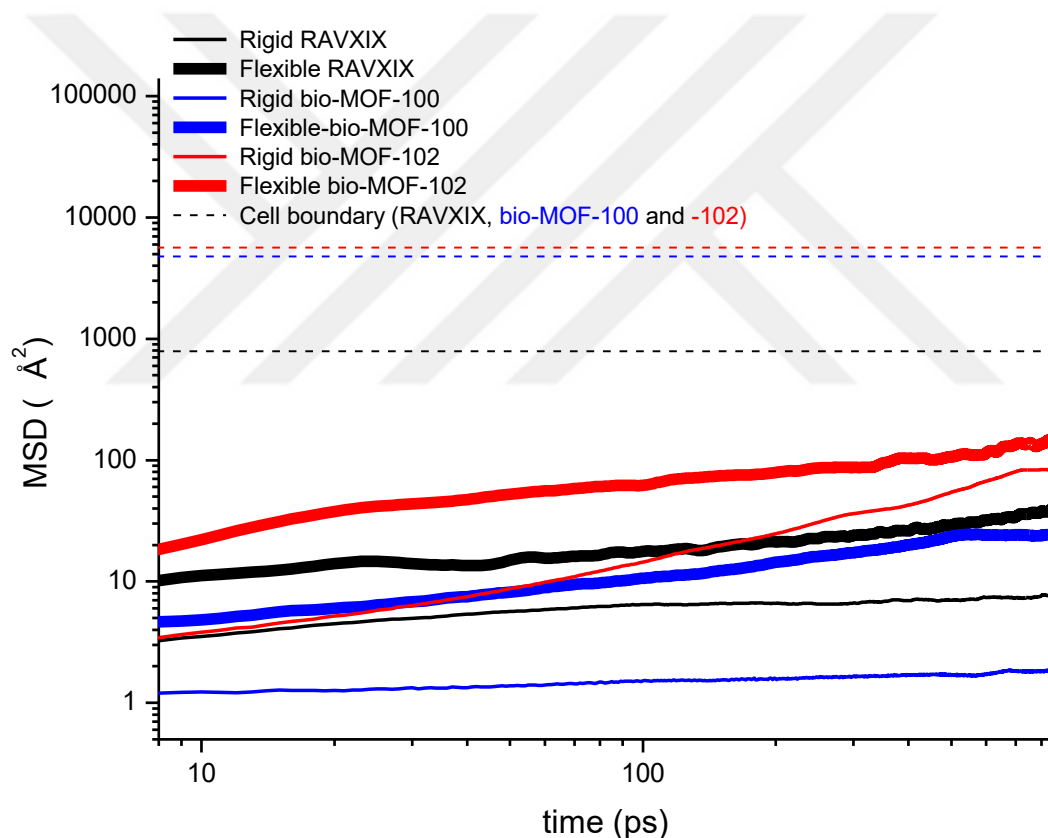


Figure 5.9 Comparison of ibuprofen diffusion in bio-MOF-100, -102 and RAVXIX.

In the case of RAVXIX, we cannot simply discuss ibuprofen diffusion by comparing the pore volumes of MOFs because RAVXIX has a completely different chemical topology. Chemical composition and topology of MOFs strongly affect the affinity of materials for specific guest molecules. Although RAVXIX has the highest pore volume ($3.7 \text{ cm}^3/\text{g}$) among the materials we studied, diffusion of ibuprofen was found to be very slow in this MOF

supported by the high isosteric heat of adsorption energy for ibuprofen (30 kcal/mol). When the flexibility was included in simulations, diffusion of ibuprofen slightly increased in all three MOFs but it was still too slow to surpass the cell boundaries. This analysis showed that both physical properties such as pore volume and chemical properties such as topology affect the diffusion of guest molecules.



Chapter 6

CONCLUSION

The main aim of this thesis is to assess the performance of a new group of nanoporous materials, bio-compatible metal organic frameworks (bio-MOFs), which are constructed from biomolecules and metal cations, in energy and biomedical applications. These materials have gained significant attention due to their superior properties including permanent porosity, chemical functionality and structure-tunability. The research on bio-MOFs has been currently starting and there is no computational study which investigates and compares the performance of bio-MOFs with other well-known porous materials both in energy and biomedical applications. Therefore, the outcome of this research significantly contributes to design and development of bio-compatible materials for different applications.

The first part of this research focused on energy applications of bio-MOFs for CO₂ separation from CO₂/CH₄, CO₂/N₂ and CO₂/H₂ mixtures and H₂ separation from CH₄/H₂ mixtures. Molecular simulations were performed to evaluate adsorption-based and membrane-based gas separation performances of ten different bio-MOF structures. Bio-MOF-1, bio-MOF-11 and bio-MOF-12 were identified as promising adsorbents and membranes for natural gas purification. A bio-MOF named as WODFOL exhibited high membrane selectivity for CO₂/CH₄ separation compared to the widely studied MOFs. Results showed that bio-MOFs-1, -11 and -12 outperform ZIF-8, Zn-ATZ and IRMOF-1 in adsorption-based separation of CO₂/CH₄ mixtures due to their high CO₂ working capacity and high CO₂ selectivity. Bio-MOF-14 (configuration III) and OFUSAL showed high adsorption selectivity for CO₂ over CH₄ but their working capacities were found to be low compared to other bio-MOFs. Five

bio-MOFs, named as bio-MOF-1, -11, -12, -13 (configuration II) and WODFOL exceeded the Robeson's upper bound and outperformed Cu-BTC, IRMOF-1 and MIL-53 membranes. Membrane selectivity and gas permeability of bio-MOFs were recomputed considering the flexibility of the structures in molecular simulations. The CO₂ permeability of all bio-MOFs except one (IZUMUM) decreased when flexibility was considered due to the decrease in the pore volumes and pore sizes of the materials. Our results also showed that chain configurations may have significant effect on the gas diffusion whereas negligible effect on the CO₂ adsorption of bio-MOF-13. Finally, results showed that molecular simulations can be used to make accurate predictions about the membrane performances of bio-MOFs having a single configuration such as bio-MOF-1.

The potential of bio-MOFs in adsorption-based and membrane-based separations was also investigated for CO₂/N₂, CO₂/H₂ and CH₄/H₂ mixtures. WODFOL and bio-MOF-11 were identified as promising adsorbents especially for CO₂ separations. The temperature and pressure effects on gas selectivities were investigated for these two MOFs. Results showed that when the temperature is increased, gas selectivities decreased due to the exothermic nature of the adsorption process. Adsorption selectivity strongly favored CH₄ in CH₄/H₂ mixtures and CO₂ in CO₂/CH₄, CO₂/N₂ and CO₂/H₂ mixtures. The highest adsorption selectivity in both MOFs was obtained for CO₂/H₂ mixtures because of the strong interactions between CO₂ molecules and framework atoms. Different selectivity-pressure trends were observed for each MOF. For example, adsorption selectivity of bio-MOF-11 for CH₄/H₂ mixtures slightly increased until 5 bar and then decreased. At low pressures, the energetic effects favored CH₄ adsorption and selectivity increased whereas at high pressures packing effects (entropic effects) came into play and favored H₂ adsorption. As a result, CH₄ selectivity decreased. On the other hand, the increase in selectivity at low pressures was not observed for WODFOL. This was attributed to the very low pore volume and narrow pore sizes of WODFOL. This analysis shows that physical properties of materials such as pore volume and pore dimensions have strong effects on the adsorption-based gas separation performances of materials.

Using molecular simulations and the Maxwell permeation model, gas separation performances of bio-MOF-11 and WODFOL-based MMMs were investigated and results were compared with those of polymeric membranes. When WODFOL and bio-MOF-11 were

added into the widely studied polymer, Matrimid, the CO₂ permeability of Matrimid increased without any change in the selectivity because bio-MOF-11 and WODFOL have higher CO₂ permeability compared to Matrimid. However, MOF-based MMMs did not exceed the upper bound because of the low CO₂ permeability of Matrimid. Results showed that careful selection of MOF/polymer pairs is important because the performance of MOF-based MMMs depends on the identity of both MOFs and polymers.

The second part of this research investigated the potential of bio-MOFs in biomedical applications. The storage performances of different bio-compatible MOFs for drug and cosmetic molecules were assessed using molecular simulations. Comparison of the simulated storage capacities and experimentally reported values was consistent for several MOFs that have different structural properties. Motivated from this high consistency, our computational approach was applied to examine ibuprofen, caffeine and urea storage potentials of 24 bio-compatible MOFs. Results showed that bio-MOF-100 series and MOF-74 series (RAVVUH-RAVXIX) are promising materials for storage of ibuprofen, caffeine and urea molecules. These materials were identified to outperform traditional drug storage materials such as zeolite and mesoporous silica (MCM-41). The correlations between the pore volume and pore sizes of MOFs were also investigated. Results showed that ibuprofen uptake is highly correlated with the pore volume and pore size of MOFs having similar chemical topologies. Diffusions of ibuprofen, caffeine and urea were studied in representative MOFs, bio-MOF-100, -102 and RAVXIX. Slow diffusion of guest molecules was observed due to strong interaction between guests and MOFs as desired for drug delivery.

Results of this thesis showed that bio-MOFs have strong potential in gas storage/separation and drug storage/delivery applications. The computational methodology used in this study will be helpful to identify the most promising MOFs for both energetic and drug storage applications prior to extensive experimental efforts. It is also important to state the assumptions associated with our molecular simulations to accurately judge the performances of these materials in practical applications:

- *MOFs*: In all molecular simulations, perfect MOF crystals with no defects were assumed. However, this may not be the case in real synthesized materials. Our simulations do not provide any information about the stability of these materials for long term industrial gas separation applications. It is also important to note that

molecular simulations provide an initial estimate about the gas separation performance of bio-MOF membranes. The real performance of the fabricated bio-MOF membranes may not be as good as the well-known robust zeolite membranes for gas separations due to experimental challenges. In fact, fabricated bio-MOF-1, -13 and -14 membranes showed decent separation performance for CO₂/CH₄ separation but this performance is not close to zeolite membranes.

- *Drug storage and delivery:* Molecular simulations do not provide the release kinetics and degradation mechanisms of drug incorporated bio-MOF materials in body environment. In addition, molecular simulations do not provide any information about the toxicity of the materials. All these issues are likely to be examined by experiments.
- *Gas mixtures:* Molecular simulations were performed for binary gas separations. For example, for natural gas purification molecular simulations considered binary mixture of CH₄ and CO₂. However, other gas species such as water, SO_x and NO_x also exist in the real mixtures and these impurities may affect predicted separation performance of MOF membranes. It will be helpful to study multi-component gas mixtures in molecular simulations to evaluate the realistic separation performance of MOF membranes.
- *Force fields:* Generic force fields were used in this study to provide an initial estimate about the materials' performance for gas separation and drug storage applications. Using structure-specific force fields that describe intramolecular interactions with a high accuracy from quantum mechanical calculations can be useful. However, this process is very time consuming and challenging.
- *Mixed matrix membranes (MMMs):* In order to estimate the gas permeabilities through MOF-based MMMs, the gas permeability of MOFs obtained from molecular simulations and the gas permeability of polymers taken from experimental data were used. A fully atomistic approach can be used to predict the realistic performance of MOF-based MMMs and also this methodology can be used to better understand the compatibility between the MOF and polymer and to design high quality MOF/polymer membranes because separation performance of MMMs is dependent on the compatibility between the filler and polymer phases.

Considering the quick development of the computational techniques, much progress on this exciting field is expected in the future. The major opportunities in this research area can be discussed as follows:

- *Investigation of the synergistic effects of drugs in MOFs:* Combination therapy which means the use of more than one drug for the same disease is an effective way for cancer treatment. To the best of our knowledge, there is no molecular simulation study which investigates MOFs as potential multi-carriers of drugs. Computational studies which aim to understand co-adsorption and co-delivery processes of multi-component systems in bio-compatible MOFs will be highly beneficial for the development of therapeutic cargoes with different functional properties.
- *Development of quantitative structure-property (QSPR) relationships:* This type of analysis is very useful to quickly predict the performance of a material using its structural characteristics before performing extensive experiments. Developing QSPR models for large number of MOF membranes will be useful to unlock structure-performance relations and to provide guidelines to experimentalist for the design of high-performance MOF membranes.
- *Molecular simulations of chiral bio-MOFs:* Recently chiral bio-MOFs (non-superimposable with their mirror image) have been synthesized. Chiral separation is very important in drug development, pharmacology and environmental science. Chiral MOFs are promising for enantioselective separation of racemic organic molecules. However, the research on chiral bio-MOFs is still rare in the literature. Computational studies can be useful to provide molecular insights about the separation mechanisms in these special MOFs.
- *Development of advanced simulation techniques:* More sophisticated algorithms are required to simulate the body environment for biomedical applications of MOFs. The modeling of drug transport in a bio-MOF membrane will be groundbreaking to understand the solution-diffusion mechanisms of drug molecules in a liquid environment.

BIBLIOGRAPHY

- [1] G. Ozin, Nanochemistry- When It Rains It Pores (Accessed: 2016-08-01) <http://www.materialsviews.com/nanochemistry-when-it-rains-it-pores/>.
- [2] M.E. Davis, Ordered Porous Materials for Emerging Applications, *Nature*, **2002**, *417*, 813.
- [3] J.-R. Li, J. Sculley, H.-C. Zhou, Metal-Organic Frameworks for Separations, *Chem. Rev.*, **2011**, *112*, 869.
- [4] R.J. Kuppler, D.J. Timmons, Q.-R. Fang, J.-R. Li, T.A. Makal, M.D. Young, D. Yuan, D. Zhao, W. Zhuang, H.-C. Zhou, Potential Applications of Metal-Organic Frameworks, *Coord. Chem. Rev.*, **2009**, *253*, 3042.
- [5] G.Q. Lu, X.S. Zhao, Nanoporous Materials: Science and Engineering, Imperial College Press: London, 2004.
- [6] Z.-A. Qiao, S.-H. Chai, K. Nelson, Z. Bi, J. Chen, S.M. Mahurin, X. Zhu, S. Dai, Polymeric Molecular Sieve Membranes via in Situ Cross-Linking of Non-Porous Polymer Membrane Templates, *Nat. Commun.*, **2014**, *5*, 1.
- [7] S. Sircar, T.C. Golden, M.B. Rao, Activated Carbon for Gas Separation and Storage, *Carbon*, **1996**, *34*, 1.
- [8] S. Morooka, K. Kusakabe, Microporous Inorganic Membranes for Gas Separation, *MRS Bull.*, **1999**, *24*, 25.
- [9] R.M. de Vos, H. Verweij, Improved Performance of Silica Membranes for Gas Separation, *J. Membr. Sci.*, **1998**, *143*, 37.
- [10] A.F. Ismail, L.I.B. David, A Review on the Latest Development of Carbon Membranes for Gas Separation, *J. Membr. Sci.*, **2001**, *193*, 1.
- [11] H. Li, M. Eddaoudi, M. O'Keeffe, O.M. Yaghi, Design and Synthesis of an Exceptionally Stable and Highly Porous Metal-Organic Framework, *Nature*, **1999**, *402*, 276.
- [12] H. Frost, T. Düren, R.Q. Snurr, Effects of Surface Area, Free Volume, and Heat of Adsorption on Hydrogen Uptake in Metal-Organic Frameworks, *J. Phys. Chem. B*, **2006**, *110*, 9565.
- [13] G. Sethia, A. Sayari, Activated Carbon with Optimum Pore Size Distribution for Hydrogen Storage, *Carbon*, **2016**, *99*, 289.

- [14] M. Eddaoudi, J. Kim, N. Rosi, D. Vodak, J. Wachter, M. O'Keeffe, O.M. Yaghi, Systematic Design of Pore Size and Functionality in Isorecticular MOFs and Their Application in Methane Storage, *Science*, **2002**, 295, 469.
- [15] F.H. Allen, The Cambridge Structural Database: a Quarter of a Million Crystal Structures and Rising, *Acta Crystallogr., Sect. B: Struct. Sci.*, **2002**, 58, 380.
- [16] C.E. Wilmer, K.C. Kim, R.Q. Snurr, An Extended Charge Equilibration Method, *J. Phys. Chem. Lett.*, **2012**, 3, 2506.
- [17] M. Eddaoudi, H. Li, O. Yaghi, Highly Porous and Stable Metal-Organic Frameworks: Structure Design and Sorption Properties, *J. Am. Chem. Soc.*, **2000**, 122, 1391.
- [18] S. Ma, H.-C. Zhou, Gas Storage in Porous Metal-Organic Frameworks for Clean Energy Applications, *Chem. Commun.*, **2010**, 46, 44.
- [19] S. Keskin, T.M. van Heest, D.S. Sholl, Can Metal-Organic Framework Materials Play a Useful Role in Large-Scale Carbon Dioxide Separations?, *ChemSusChem*, **2010**, 3, 879.
- [20] I. Erucar, S. Keskin, Efficient Storage of Drug and Cosmetic Molecules in Bio-Compatible MOFs: A Molecular Simulation Study, *Ind. Eng. Chem. Res.*, **2016**, 55, 1929.
- [21] J. Della Rocca, D. Liu, W. Lin, Nanoscale Metal-Organic Frameworks for Biomedical Imaging and Drug Delivery, *Acc. Chem. Res.*, **2011**, 44, 957.
- [22] M.D. Allendorf, V. Stavila, Crystal Engineering, Structure-Function Relationships, and the Future of Metal-Organic Frameworks, *CrystEngComm*, **2015**, 17, 229.
- [23] W. Li, Y. Zhang, Q. Li, G. Zhang, Metal-Organic Framework Composite Membranes: Synthesis and Separation Applications, *Chem. Eng. Sci.*, **2015**, 135, 232.
- [24] Z.R. Herm, R. Krishna, J.R. Long, CO₂/CH₄, CH₄/H₂ and CO₂/CH₄/H₂ Separations at High Pressures Using Mg₂(dobdc), *Microporous Mesoporous Mater.*, **2012**, 151, 481.
- [25] Y. Basdogan, K.B. Sezginel, S. Keskin, Identifying Highly Selective Metal Organic Frameworks for CH₄/H₂ Separations Using Computational Tools, *Ind. Eng. Chem. Res.*, **2015**, 54, 8479.
- [26] I. Erucar, S. Keskin, Computational assessment of MOF membranes for CH₄/H₂ separations, *J. Membr. Sci.*, **2016**, 514, 313.
- [27] S.R. Venna, M.A. Carreon, Metal Organic Framework Membranes for Carbon Dioxide Separation, *Chem. Eng. Sci.*, **2015**, 124, 3.

- [28] K. Sumida, D.L. Rogow, J.A. Mason, T.M. McDonald, E.D. Bloch, Z.R. Herm, T.-H. Bae, J.R. Long, Carbon Dioxide Capture in Metal-Organic Frameworks, *Chem. Rev.*, **2012**, *112*, 724.
- [29] J. Caro, Are MOF Membranes Better in Gas Separation than those Made of Zeolites?, *Curr. Opin. Chem. Eng.*, **2011**, *1*, 77.
- [30] J.-R. Li, R.J. Kuppler, H.-C. Zhou, Selective Gas Adsorption and Separation in Metal-Organic Frameworks, *Chem. Soc. Rev.*, **2009**, *38*, 1477.
- [31] S. Keskin, S. Kızılel, Biomedical Applications of Metal Organic Frameworks, *Ind. Eng. Chem. Res.*, **2011**, *50*, 1799.
- [32] C.-Y. Sun, C. Qin, X.-L. Wang, Z.-M. Su, Metal-Organic Frameworks as Potential Drug Delivery Systems, *Expert Opin. Drug Delivery*, **2013**, *10*, 89.
- [33] C. Tamames-Tabar, A. García-Márquez, M.J. Blanco-Prieto, C. Serre, P. Horcajada, MOFs in Pharmaceutical Technology, in: *Bio- and Bioinspired Nanomaterials*, Wiley-VCH Verlag GmbH & Co. KGaA, **2014**.
- [34] P. Horcajada, R. Gref, T. Baati, P.K. Allan, G. Maurin, P. Couvreur, G. Férey, R.E. Morris, C. Serre, Metal-Organic Frameworks in Biomedicine, *Chem. Rev.*, **2011**, *112*, 1232.
- [35] G. Férey, C. Mellot-Draznieks, C. Serre, F. Millange, J. Dutour, S. Surblé, I. Margiolaki, A Chromium Terephthalate-Based Solid with Unusually Large Pore Volumes and Surface Area, *Science*, **2005**, *309*, 2040.
- [36] I. Imaz, M. Rubio-Martinez, J. An, I. Sole-Font, N.L. Rosi, D. Maspoch, Metal-Biomolecule Frameworks (MBioFs), *Chem. Commun.*, **2011**, *47*, 7287.
- [37] J. An, S.J. Geib, N.L. Rosi, Cation-Triggered Drug Release from a Porous Zinc-Adeninate Metal-Organic Framework, *J. Am. Chem. Soc.*, **2009**, *131*, 8376.
- [38] A.C. McKinlay, R.E. Morris, P. Horcajada, G. Férey, R. Gref, P. Couvreur, C. Serre, BioMOFs: Metal-Organic Frameworks for Biological and Medical Applications, *Angew. Chem., Int. Ed.*, **2010**, *49*, 6260.
- [39] E.A. Tomic, Thermal Stability of Coordination Polymers, *J. Appl. Polym. Sci.*, **1965**, *9*, 3745.
- [40] O.M. Yaghi, M. O'Keeffe, N.W. Ockwig, H.K. Chae, M. Eddaoudi, J. Kim, Reticular Synthesis and The Design of New Materials, *Nature*, **2003**, *423*, 705.
- [41] H.-C. Zhou, J.R. Long, O.M. Yaghi, Introduction to Metal-Organic Frameworks, *Chem. Rev.*, **2012**, *112*, 673.

- [42] C.-C. Wang, Y.-S. Ho, Research Trend of Metal-Organic Frameworks: A Bibliometric Analysis, *Scientometrics*, **2016**, 1,1.
- [43] J.L.C. Rowsell, O.M. Yaghi, Metal-Organic Frameworks: A New Class of Porous Materials, *Microporous and Mesoporous Mater.*, **2004**, 73, 3.
- [44] R. Liu, T. Yu, Z. Shi, Z. Wang, The Preparation of Metal-Organic Frameworks and Their Biomedical Application, *Int. J. Nanomed.*, **2016**, 11, 1187.
- [45] M. Giménez-Marqués, T. Hidalgo, C. Serre, P. Horcajada, Nanostructured Metal-Organic Frameworks and their Bio-Related Applications, *Coord. Chem. Rev.*, **2016**, 307, Part 2, 342.
- [46] J. An, S.J. Geib, N.L. Rosi, High and Selective CO₂ Uptake in a Cobalt Adeninate Metal-Organic Framework Exhibiting Pyrimidine- and Amino-Decorated Pores, *J. Am. Chem. Soc.*, **2009**, 132, 38.
- [47] Z. Xie, T. Li, N.L. Rosi, M.A. Carreon, Alumina-Supported Cobalt-Adeninate MOF Membranes for CO₂/CH₄ Separation, *J. Mater. Chem. A*, **2014**, 2, 1239.
- [48] M. Beckner, A. Dailly, Hydrogen and Methane Storage in Adsorbent Materials for Automotive Applications, *Int. J. Energy Res.*, **2016**, 40, 91.
- [49] R. Zou, A.I. Abdel-Fattah, H. Xu, Y. Zhao, D.D. Hickmott, Storage and Separation Applications of Nanoporous Metal-Organic Frameworks, *CrystEngComm*, **2010**, 12, 1337.
- [50] J.A. Mason, M. Veenstra, J.R. Long, Evaluating Metal-Organic Frameworks for Natural Gas Storage, *Chem. Sci.*, **2014**, 5, 32.
- [51] Y. He, W. Zhou, G. Qian, B. Chen, Methane Storage in Metal-Organic Frameworks, *Chem. Soc. Rev.*, **2014**, 43, 5657.
- [52] M.P. Suh, H.J. Park, T.K. Prasad, D.-W. Lim, Hydrogen Storage in Metal-Organic Frameworks, *Chem. Rev.*, **2011**, 112, 782.
- [53] J. Sculley, D. Yuan, H.-C. Zhou, The Current Status of Hydrogen Storage in Metal-Organic Frameworks-Updated, *Energy Environ. Sci.*, **2011**, 4, 2721.
- [54] L.J. Murray, M. Dinca, J.R. Long, Hydrogen Storage in Metal-Organic Frameworks, *Chem. Soc. Rev.*, **2009**, 38, 1294.
- [55] Y.H. Hu, L. Zhang, Hydrogen Storage in Metal-Organic Frameworks, *Adv. Mater.*, **2010**, 22.
- [56] H.W. Langmi, J. Ren, B. North, M. Mathe, D. Bessarabov, Hydrogen Storage in Metal-Organic Frameworks: A Review, *Electrochim. Acta*, **2014**, 128, 368.

- [57] Y. Basdogan, S. Keskin, Simulation and Modelling of MOFs for Hydrogen Storage, *CrystEngComm*, **2015**, *17*, 261.
- [58] S.S. Han, W.Q. Deng, W.A. Goddard, Improved Designs of Metal-Organic Frameworks for Hydrogen Storage, *Angew. Chem.*, **2007**, *119*, 6405.
- [59] P. Ryan, L.J. Broadbelt, R.Q. Snurr, Is Catenation Beneficial for Hydrogen Storage in Metal-Organic Frameworks?, *Chem. Commun.*, **2008**, 4132.
- [60] V. Menon, S. Komarneni, Porous Adsorbents for Vehicular Natural Gas Storage: A Review, *J. Porous Mater.*, **1998**, *5*, 43.
- [61] Y. Peng, V. Krungleviciute, I. Eryazici, J.T. Hupp, O.K. Farha, T. Yildirim, Methane Storage in Metal-Organic Frameworks: Current Records, Surprise Findings, and Challenges, *J. Am. Chem. Soc.*, **2013**, *135*, 11887.
- [62] K. Konstas, T. Osl, Y. Yang, M. Batten, N. Burke, A.J. Hill, M.R. Hill, Methane storage in metal organic frameworks, *J. Mater. Chem.*, **2012**, *22*, 16698.
- [63] R.B. Getman, Y.-S. Bae, C.E. Wilmer, R.Q. Snurr, Review and Analysis of Molecular Simulations of Methane, Hydrogen, and Acetylene Storage in Metal-Organic Frameworks, *Chem. Rev.*, **2011**, *112*, 703.
- [64] C.E. Wilmer, M. Leaf, C.Y. Lee, O.K. Farha, B.G. Hauser, J.T. Hupp, R.Q. Snurr, Large-Scale Screening of Hypothetical Metal-Organic Frameworks, *Nat. Chem.*, **2012**, *4*, 83.
- [65] Y.J. Colon, R.Q. Snurr, High-Throughput Computational Screening of Metal-Organic Frameworks, *Chem. Soc. Rev.*, **2014**, *43*, 5735.
- [66] M. Fernandez, T.K. Woo, C.E. Wilmer, R.Q. Snurr, Large-Scale Quantitative Structure-Property Relationship (QSPR) Analysis of Methane Storage in Metal-Organic Frameworks, *J. Phys. Chem. C*, **2013**, *117*, 7681.
- [67] Y.G. Chung, J. Camp, M. Haranczyk, B.J. Sikora, W. Bury, V. Krungleviciute, T. Yildirim, O.K. Farha, D.S. Sholl, R.Q. Snurr, Computation-Ready, Experimental Metal-Organic Frameworks: A Tool To Enable High-Throughput Screening of Nanoporous Crystals, *Chem. Mater.*, **2014**, *26*, 6185.
- [68] B. Arstad, H. Fjellvåg, K. Kongshaug, O. Swang, R. Blom, Amine Functionalised Metal Organic Frameworks (MOFs) as Adsorbents for Carbon Dioxide, *Adsorption*, **2008**, *14*, 755.
- [69] J.-R. Li, Y. Ma, M.C. McCarthy, J. Sculley, J. Yu, H.-K. Jeong, P.B. Balbuena, H.-C. Zhou, Carbon Dioxide Capture-Related Gas Adsorption and Separation in Metal-Organic Frameworks, *Coord. Chem. Rev.*, **2011**, *255*, 1791.

- [70] S. Keskin, T.M.V. Heest, D.S. Sholl, Can Metal-Organic Framework Materials Play a Useful Role in Large-Scale Carbon Dioxide Separations?, *ChemSusChem*, **2010**, *3*, 879.
- [71] A. Schoedel, Z. Ji, O.M. Yaghi, The Role of Metal-Organic Frameworks in A Carbon-Neutral Energy Cycle, *Nat. Energy*, **2016**, *1*, 16034.
- [72] R. Babarao, J. Jiang, Molecular Screening of Metal-Organic Frameworks for CO₂ Storage, *Langmuir*, **2008**, *24*, 6270.
- [73] R. Babarao, J. Jiang, Exceptionally High CO₂ Storage in Covalent-Organic Frameworks: Atomistic Simulation Study, *Energy Environ. Sci.*, **2008**, *1*, 139.
- [74] D. Liu, C. Zheng, Q. Yang, C. Zhong, Understanding the Adsorption and Diffusion of Carbon Dioxide in Zeolitic Imidazolate Frameworks: A Molecular Simulation Study, *J. Phys. Chem. C*, **2009**, *113*, 5004.
- [75] A.I. Skoulidas, D.S. Sholl, Self-Diffusion and Transport Diffusion of Light Gases in Metal-Organic Framework Materials Assessed Using Molecular Dynamics Simulations, *J. Phys. Chem. B*, **2005**, *109*, 15760.
- [76] R.T. Yang, Gas Separation by Adsorption Processes, Butterworth-Heinemann, 2013.
- [77] B. Li, H. Wang, B. Chen, Microporous Metal-Organic Frameworks for Gas Separation, *Chem. - Asian J.*, **2014**, *9*, 1474.
- [78] R. Vaidhyanathan, S.S. Iremonger, K.W. Dawson, G.K.H. Shimizu, An Amine-Functionalized Metal Organic Framework for Preferential CO₂ Adsorption at Low Pressures, *Chem. Commun.*, **2009**, *35*, 5230.
- [79] Z. Liang, M. Marshall, A.L. Chaffee, CO₂ Adsorption-Based Separation by Metal Organic Framework (Cu-BTC) versus Zeolite (13X), *Energy Fuels*, **2009**, *23*, 2785.
- [80] N. Liédana, E. Marín, C. Téllez, J. Coronas, One-Step Encapsulation of Caffeine in SBA-15 Type and Non-Ordered Silicas, *Chem. Eng. J.*, **2013**, *223*, 714.
- [81] A. Phan, C.J. Doonan, F.J. Uribe-Romo, C.B. Knobler, M. O'keeffe, O.M. Yaghi, Synthesis, Structure, and Carbon Dioxide Capture Properties of Zeolitic Imidazolate Frameworks, *Acc. Chem. Res*, **2010**, *43*, 58.
- [82] Z.R. Herm, J.A. Swisher, B. Smit, R. Krishna, J.R. Long, Metal-Organic Frameworks as Adsorbents for Hydrogen Purification and Precombustion Carbon Dioxide Capture, *J. Am. Chem. Soc.*, **2011**, *133*, 5664.
- [83] L.-C. Lin, A.H. Berger, R.L. Martin, J. Kim, J.A. Swisher, K. Jariwala, C.H. Rycroft, A.S. Bhowm, M.W. Deem, M. Haranczyk, In Silico Screening of Carbon-Capture Materials, *Nat. Mater.*, **2012**, *11*, 633.

- [84] D. Wu, Q. Yang, C. Zhong, D. Liu, H. Huang, W. Zhang, G. Maurin, Revealing the Structure-Property Relationships of Metal-Organic Frameworks for CO₂ Capture from Flue Gas, *Langmuir*, **2012**, 28, 12094.
- [85] Z. Qiao, K. Zhang, J. Jiang, In Silico Screening of 4764 Computation-Ready, Experimental Metal-Organic Frameworks for CO₂ Separation, *J. Mater. Chem. A*, **2016**, 4, 2105.
- [86] D. Wu, C. Wang, B. Liu, D. Liu, Q. Yang, C. Zhong, Large-Scale Computational Screening of Metal-Organic Frameworks for CH₄/H₂ Separation, *AIChE J.*, **2012**, 58, 2078.
- [87] E. Atci, S. Keskin, Understanding the Potential of Zeolite Imidazolate Framework Membranes in Gas Separations Using Atomically Detailed Calculations, *The Journal of Physical Chemistry C*, **2012**, 116, 15525.
- [88] S. Keskin, Gas Adsorption and Diffusion in a Highly CO₂ Selective Metal-Organic Framework: Molecular Simulations, *Mol. Sim.*, **2013**, 39, 14.
- [89] S. Keskin, Adsorption, Diffusion, and Separation of CH₄/H₂ Mixtures in Covalent Organic Frameworks: Molecular Simulations and Theoretical Predictions, *J. Phys. Chem. C*, **2011**, 116, 1772.
- [90] I. Erucar, S. Keskin, High CO₂ Selectivity of an Amine-Functionalized Metal Organic Framework in Adsorption-Based and Membrane-Based Gas Separations, *Ind. Eng. Chem. Res.*, **2013**, 52, 3462.
- [91] Y. Chen, J. Jiang, A Bio-Metal-Organic Framework for Highly Selective CO₂ Capture: A Molecular Simulation Study, *ChemSusChem*, **2010**, 3, 982.
- [92] L.M. Robeson, The Upper Bound Revisited, *J. Membr. Sci.*, **2008**, 320, 390.
- [93] B.D. Freeman, Basis of Permeability/Selectivity Tradeoff Relations in Polymeric Gas Separation Membranes, *Macromolecules*, **1999**, 32, 375.
- [94] S. Keskin, J. Liu, J.K. Johnson, D.S. Sholl, Atomically Detailed Models of Gas Mixture Diffusion Through CuBTC Membranes, *Microporous and Mesoporous Mater.*, **2009**, 125, 101.
- [95] Y. Yoo, Z. Lai, H.-K. Jeong, Fabrication of MOF-5 Membranes using Microwave-Induced Rapid Seeding and Solvothermal Secondary Growth, *Microporous and Mesoporous Mater.*, **2009**, 123, 100.
- [96] Z. Zhao, X. Ma, A. Kasik, Z. Li, Y.S. Lin, Gas Separation Properties of Metal Organic Framework (MOF-5) Membranes, *Ind. Eng. Chem. Res.*, **2013**, 52, 1102.
- [97] Z. Zhao, X. Ma, Z. Li, Y.S. Lin, Synthesis, Characterization and Gas Transport Properties of MOF-5 Membranes, *J. Membr. Sci.*, **2011**, 382, 82.

- [98] H. Guo, G. Zhu, I.J. Hewitt, S. Qiu, "Twin Copper Source" Growth of Metal–Organic Framework Membrane: $\text{Cu}_3(\text{BTC})_2$ with High Permeability and Selectivity for Recycling H_2 , *J. Am. Chem. Soc.*, **2009**, *131*, 1646.
- [99] J. Nan, X. Dong, W. Wang, W. Jin, N. Xu, Step-by-step Seeding Procedure for Preparing HKUST-1 Membrane on Porous α -Alumina Support, *Langmuir*, **2011**, *27*, 4309.
- [100] V.V. Guerrero, Y. Yoo, M.C. McCarthy, H.-K. Jeong, HKUST-1 Membranes on Porous Supports Using Secondary Growth, *J. Mater. Chem.*, **2010**, *20*, 3938.
- [101] M.N. Shah, M.A. Gonzalez, M.C. McCarthy, H.-K. Jeong, An Unconventional Rapid Synthesis of High Performance Metal–Organic Framework Membranes, *Langmuir*, **2013**, *29*, 7896.
- [102] Y. Mao, W. Cao, J. Li, Y. Liu, Y. Ying, L. Sun, X. Peng, Enhanced Gas Separation through well-intergrown MOF Membranes: Seed Morphology and Crystal Growth Effects, *J. Mater. Chem. A*, **2013**, *1*, 11711.
- [103] F. Cao, C. Zhang, Y. Xiao, H. Huang, W. Zhang, D. Liu, C. Zhong, Q. Yang, Z. Yang, X. Lu, Helium Recovery by a Cu-BTC Metal–Organic-Framework Membrane, *Ind. Eng. Chem. Res.*, **2012**, *51*, 11274.
- [104] T. Ben, C. Lu, C. Pei, S. Xu, S. Qiu, Polymer-Supported and Free-Standing Metal–Organic Framework Membrane, *Chem. - Eur. J.*, **2012**, *18*, 10250.
- [105] D. Nagaraju, D.G. Bhagat, R. Banerjee, U.K. Kharul, In Situ Growth of Metal–Organic Frameworks on a Porous Ultrafiltration Membrane for Gas Separation, *J. Mater. Chem. A*, **2013**, *1*, 8828.
- [106] N. Hara, M. Yoshimune, H. Negishi, K. Haraya, S. Hara, T. Yamaguchi, Metal–Organic Framework Membranes with Layered Structure Prepared within the Porous Support, *RSC Adv.*, **2013**, *3*, 14233.
- [107] Y. Liu, N. Wang, L. Diestel, F. Steinbach, J. Caro, MOF Membrane Synthesis in the Confined Space of a Vertically Aligned LDH Network, *Chem. Commun.*, **2014**, *50*, 4225.
- [108] H. Bux, C. Chmelik, R. Krishna, J. Caro, Ethene/Ethane Separation by the MOF Membrane ZIF-8: Molecular Correlation of Permeation, Adsorption, Diffusion, *J. Membr. Sci.*, **2011**, *369*, 284.
- [109] H. Bux, C. Chmelik, J.M. van Baten, R. Krishna, J. Caro, Novel MOF-Membrane for Molecular Sieving Predicted by IR-Diffusion Studies and Molecular Modeling, *Adv. Mater.*, **2010**, *22*, 4741.

- [110] A. Huang, N. Wang, C. Kong, J. Caro, Organosilica-Functionalized Zeolitic Imidazolate Framework ZIF-90 Membrane with High Gas-Separation Performance, *Angew. Chem., Int. Ed.*, **2012**, *51*, 10551.
- [111] E. Adatoz, A.K. Avci, S. Keskin, Opportunities and Challenges of MOF-based Membranes in Gas Separations, *Sep. Purif. Technol.*, **2015**, *152*, 207.
- [112] J.A. Bohrman, M.A. Carreon, Synthesis and CO₂/CH₄ separation performance of Bio-MOF-1 membranes, *Chem. Commun.*, **2012**, *48*, 5130.
- [113] T.T. Moore, R. Mahajan, D.Q. Vu, W.J. Koros, Hybrid Membrane Materials Comprising Organic Polymers with Rigid Dispersed Phases, *AIChE J.*, **2004**, *50*, 311.
- [114] M.A. Aroon, A.F. Ismail, T. Matsuura, M.M. Montazer-Rahmati, Performance Studies of Mixed Matrix Membranes for Gas Separation: A Review, *Sep. Purif. Technol.*, **2010**, *75*, 229.
- [115] E.V. Perez, K.J. Balkus, J.P. Ferraris, I.H. Musselman, Mixed-Matrix Membranes Containing MOF-5 for Gas Separations, *J. Membr. Sci.*, **2009**, *328*, 165.
- [116] H. Yehia, T. Pisklak, J. Ferraris, K. Balkus, I. Musselman, Methane Facilitated Transport Using Copper (II) Biphenyl Dicarboxylate-Triethylenediamine/Poly (3-acetoxyethylthiophene) Mixed Matrix Membranes, *Polym. Prepr.*, **2004**, *45*, 35.
- [117] Y. Zhang, I.H. Musselman, J.P. Ferraris, K.J. Balkus Jr, Gas Permeability Properties of Matrimid® Membranes Containing the Metal-Organic Framework Cu-BPY-HFS, *J. Membr. Sci.*, **2008**, *313*, 170.
- [118] J. Won, J.S. Seo, J.H. Kim, H.S. Kim, Y.S. Kang, S.J. Kim, Y. Kim, J. Jegal, Coordination Compound Molecular Sieve Membranes, *Adv. Mater.*, **2005**, *17*, 80.
- [119] C. Liu, B. McCulloch, S.T. Wilson, A.I. Benin, M.E. Schott, Metal organic framework--polymer mixed matrix membranes, in, US7637983, 2009.
- [120] Anja Car, Chrtomir Stropnik, K.-V. Peinemann, Hybrid Membrane Materials with Different Metal-Organic Frameworks (MOFs) for Gas Separation, *Desalination*, **2006**, *200*, 424.
- [121] J. Hu, H. Cai, H. Ren, Y. Wei, Z. Xu, H. Liu, Y. Hu, Mixed-Matrix Membrane Hollow Fibers of Cu₃(BTC)₂ MOF and Polyimide for Gas Separation and Adsorption, *Ind. Eng. Chem. Res.*, **2010**, *49*, 12605.
- [122] R. Adams, C. Carson, J. Ward, R. Tannenbaum, W. Koros, Metal Organic Framework Mixed Matrix Membranes for Gas Separations, *Microporous and Mesoporous Mater.*, **2010**, *131*, 13.

- [123] M.J.C. Ordoñez, K.J. Balkus Jr, J.P. Ferraris, I.H. Musselman, Molecular Sieving Realized with ZIF-8/Matrimid® Mixed-Matrix Membranes, *J. Membr. Sci.*, **2010**, *361*, 28.
- [124] K. Díaz, M. López-González, L.F. del Castillo, E. Riande, Effect of Zeolitic Imidazolate Frameworks on the Gas Transport Performance of ZIF8-poly(1,4-phenylene ether-ether-sulfone) Hybrid Membranes, *J. Membr. Sci.*, **2011**, *383*, 206.
- [125] T.C. Merkel, B.D. Freeman, R.J. Spontak, Z. He, I. Pinnau, P. Meakin, A.J. Hill, Ultraporous, Reverse-Selective Nanocomposite Membranes, *Science*, **2002**, *296*, 519.
- [126] Q. Song, S.K. Nataraj, M.V. Roussanova, J.C. Tan, D.J. Hughes, W. Li, P. Bourgoïn, M.A. Alam, A.K. Cheetham, S.A. Al-Muhtaseb, E. Sivaniah, Zeolitic Imidazolate Framework (ZIF-8) based Polymer Nanocomposite Membranes for Gas Separation, *Energy Environ. Sci.*, **2012**, *5*, 8359.
- [127] Y. Dai, J.R. Johnson, O. Karvan, D.S. Sholl, W.J. Koros, Ultem®/ZIF-8 Mixed Matrix Hollow Fiber Membranes for CO₂/N₂ Separations, *J. Membr. Sci.*, **2012**, *401–402*, 76.
- [128] T.-H. Bae, J.S. Lee, W. Qiu, W.J. Koros, C.W. Jones, S. Nair, A High-Performance Gas-Separation Membrane Containing Submicrometer-Sized Metal-Organic Framework Crystals, *Angew. Chem., Int. Ed.*, **2010**, *49*, 9863.
- [129] T. Yang, Y. Xiao, T.-S. Chung, Poly-/Metal-Benzimidazole Nano-Composite Membranes for Hydrogen Purification, *Energy Environ. Sci.*, **2011**, *4*, 4171.
- [130] B. Zornoza, B. Seoane, J.M. Zamaro, C. Téllez, J. Coronas, Combination of MOFs and Zeolites for Mixed-Matrix Membranes, *ChemPhysChem*, **2011**, *12*, 2781.
- [131] S. Basu, A. Cano-Odena, I.F.J. Vankelecom, Asymmetric Matrimid®/[Cu₃(BTC)₂] Mixed-Matrix Membranes for Gas Separations, *J. Membr. Sci.*, **2010**, *362*, 478.
- [132] S. Keskin, D.S. Sholl, Selecting Metal Organic Frameworks as Enabling Materials in Mixed Matrix Membranes for High Efficiency Natural Gas Purification, *Energy Environ. Sci.*, **2010**, *3*, 343.
- [133] I. Erucar, S. Keskin, Screening Metal-Organic Framework-Based Mixed-Matrix Membranes for CO₂/CH₄ Separations, *Ind. Eng. Chem. Res.*, **2011**, *50*, 12606.
- [134] A.W. Thornton, D. Dubbeldam, M.S. Liu, B.P. Ladewig, A.J. Hill, M.R. Hill, Feasibility of Zeolitic Imidazolate Framework Membranes for Clean Energy Applications, *Energy Environ. Sci.*, **2012**, *5*, 7637.
- [135] I. Erucar, T.A. Manz, S. Keskin, Effects of Electrostatic Interactions on Gas Adsorption and Permeability of MOF Membranes, *Mol. Sim.*, **2014**, *40*, 557.

- [136] L. Zhang, Z. Hu, J. Jiang, Metal-Organic Framework/Polymer Mixed-Matrix Membranes for H₂/CO₂ Separation: A Fully Atomistic Simulation Study, *J. Phys. Chem. C*, **2012**, *116*, 19268.
- [137] J.A. Greathouse, T.L. Kinnibrugh, M.D. Allendorf, Adsorption and Separation of Noble Gases by IRMOF-1: Grand Canonical Monte Carlo Simulations, *Ind. Eng. Chem. Res.*, **2009**, *48*, 3425.
- [138] J.A. Greathouse, M.D. Allendorf, Force Field Validation for Molecular Dynamics Simulations of IRMOF-1 and Other Isoreticular Zinc Carboxylate Coordination Polymers, *J. Phys. Chem. C*, **2008**, *112*, 5795.
- [139] L. Zhang, G. Wu, J. Jiang, Adsorption and Diffusion of CO₂ and CH₄ in Zeolitic Imidazolate Framework-8: Effect of Structural Flexibility, *J. Phys. Chem. C*, **2014**, *118*, 8788.
- [140] P. Horcajada, C. Serre, M. Vallet-Regí, M. Sebban, F. Taulelle, G. Férey, Metal-Organic Frameworks as Efficient Materials for Drug Delivery, *Angew. Chem.*, **2006**, *118*, 6120.
- [141] P. Horcajada, C. Serre, G. Maurin, N.A. Ramsahye, F. Balas, M. Vallet-Regí, M. Sebban, F. Taulelle, G. Férey, Flexible Porous Metal-Organic Frameworks for a Controlled Drug Delivery, *J. Am. Chem. Soc.*, **2008**, *130*, 6774.
- [142] T. Chalati, P. Horcajada, P. Couvreur, C. Serre, M. Ben Yahia, G. Maurin, R. Gref, Porous Metal Organic Framework Nanoparticles to Address the Challenges Related to Busulfan Encapsulation, *Nanomedicine*, **2011**, *6*, 1683.
- [143] R. Anand, F. Borghi, F. Manoli, I. Manet, V. Agostoni, P. Reschiglian, R. Gref, S. Monti, Host-Guest Interactions in Fe(III)-Trimesate MOF Nanoparticles Loaded with Doxorubicin, *J. Phys. Chem. B*, **2014**, *118*, 8532.
- [144] P. Horcajada, T. Chalati, C. Serre, B. Gillet, C. Sebban, T. Baati, J.F. Eubank, D. Heurtaux, P. Clayette, C. Kreuz, Porous Metal-Organic-Framework Nanoscale Carriers as a Potential Platform for Drug Delivery and Imaging, *Nat. Mater.*, **2010**, *9*, 172.
- [145] C.-Y. Sun, C. Qin, X.-L. Wang, G.-S. Yang, K.-Z. Shao, Y.-Q. Lan, Z.-M. Su, P. Huang, C.-G. Wang, E.-B. Wang, Zeolitic Imidazolate Framework-8 as Efficient pH-Sensitive Drug Delivery Vehicle, *Dalton Trans.*, **2012**, *41*, 6906.
- [146] C.Y. Sun, C. Qin, C.G. Wang, Z.M. Su, S. Wang, X.L. Wang, G.S. Yang, K.Z. Shao, Y.Q. Lan, E.B. Wang, Chiral Nanoporous Metal-Organic Frameworks with High Porosity as Materials for Drug Delivery, *Adv. Mater.*, **2011**, *23*, 5629.
- [147] F.R.S. Lucena, L.C. de Araújo, M.d.D. Rodrigues, T.G. da Silva, V.R. Pereira, G.C. Militão, D.A. Fontes, P.J. Rolim-Neto, F.F. da Silva, S.C. Nascimento, Induction of

- Cancer Cell Death by Apoptosis and Slow Release of 5-Fluoracil from Metal-Organic Frameworks Cu-BTC, *Biomed. Pharmacother.*, **2013**, 67, 707.
- [148] Q.-L. Li, J.-P. Wang, W.-C. Liu, X.-Y. Zhuang, J.-Q. Liu, G.-L. Fan, B.-H. Li, W.-N. Lin, J.-H. Man, A New (4,8)-Connected Topological MOF as Potential Drug Delivery, *Inorg. Chem. Commun.*, **2015**, 55, 8.
- [149] D. Cunha, M. Ben Yahia, S. Hall, S.R. Miller, H. Chevreau, E. Elkaïm, G. Maurin, P. Horcajada, C. Serre, Rationale of Drug Encapsulation and Release from Biocompatible Porous Metal-Organic Frameworks, *Chem. Mater.*, **2013**, 25, 2767.
- [150] N. Liédana, A. Galve, C.s. Rubio, C. Téllez, J. Coronas, CAF@ ZIF-8: One-Step Encapsulation of Caffeine in MOF, *ACS Appl. Mater. Interfaces*, **2012**, 4, 5016.
- [151] N. Liedana, P. Lozano, A. Galve, C. Tellez, J. Coronas, The Template Role of Caffeine in its One-Step Encapsulation in MOF NH₂-MIL-88B(Fe), *J. Mater. Chem. B*, **2014**, 2, 1144.
- [152] S. Devautour-Vinot, C. Martineau, S. Diaby, M. Ben-Yahia, S. Miller, C. Serre, P. Horcajada, D. Cunha, F. Taulelle, G. Maurin, Caffeine Confinement into a Series of Functionalized Porous Zirconium MOFs: A Joint Experimental/Modeling Exploration, *J. Phys. Chem. C*, **2013**, 117, 11694.
- [153] R. Babarao, J. Jiang, Unraveling the Energetics and Dynamics of Ibuprofen in Mesoporous Metal-Organic Frameworks, *J. Phys. Chem. C*, **2009**, 113, 18287.
- [154] L. Bei, L. Yuanhui, L. Zhi, C. Guangjin, Molecular Simulation of Drug Adsorption and Diffusion in Bio-MOFs, *Acta Chim. Sinica*, **2014**, 72, 942.
- [155] M.C. Bernini, D. Fairen-Jimenez, M. Pasinetti, A.J. Ramirez-Pastor, R.Q. Snurr, Screening of Bio-Compatible Metal-Organic Frameworks as Potential Drug Carriers Using Monte Carlo Simulations, *J. Mater. Chem. B*, **2014**, 2, 766.
- [156] R. Bueno-Perez, A. Martin-Calvo, P. Gomez-Alvarez, J.J. Gutierrez-Sevillano, P.J. Merkling, T.J.H. Vlugt, T.S. van Erp, D. Dubbeldam, S. Calero, Enantioselective Adsorption of Ibuprofen and Lysine in Metal-Organic Frameworks, *Chem. Commun.*, **2014**, 50, 10849.
- [157] D. Dubbeldam, A. Torres-Knoop, K.S. Walton, Monte Carlo Codes, Tools And Algorithms, *Mol. Simul.*, **2013**, 39, 1253.
- [158] L. Sarkisov, R.L. Martin, M. Haranczyk, B. Smit, On the Flexibility of Metal-Organic Frameworks, *J. Am. Chem. Soc.*, **2014**, 136, 2228.
- [159] B. Smit, Phase Diagrams of Lennard-Jones Fluids, *J. Chem. Phys.*, **1992**, 96, 8639.
- [160] F.-X. Coudert, A.H. Fuchs, Computational Characterization and Prediction of Metal-Organic Framework Properties, *Coord. Chem. Rev.*, **2016**, 307, 211.

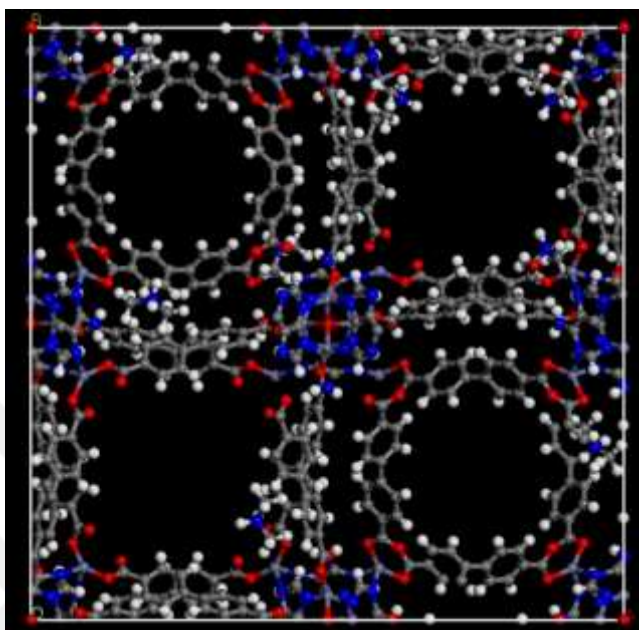
- [161] A.K. Rappe, C.J. Casewit, K.S. Colwell, W.A. Goddard, W.M. Skiff, UFF, A Full Periodic Table Force Field for Molecular Mechanics and Molecular Dynamics Simulations, *J. Am. Chem. Soc.*, **1992**, *114*, 10024.
- [162] S.L. Mayo, B.D. Olafson, W.A. Goddard, Dreiding: A Generic Force Field for Molecular Simulations, *J. Phys. Chem.*, **1990**, *94*, 8897.
- [163] H.-c. Guo, F. Shi, Z.-f. Ma, X.-q. Liu, Molecular Simulation for Adsorption and Separation of CH₄/H₂ in Zeolitic Imidazolate Frameworks, *J. Phys. Chem. C*, **2010**, *114*, 12158.
- [164] H. Lorentz, Ueber die Anwendung Des Satzes vom Virial in der Kinetischen Theorie der Gase, *Ann. Phys. (Berlin, Ger.)*, **1881**, *248*, 127.
- [165] D. Berthelot, Sur le Melange des Gaz, *C. R. Hebd. Seanc. Acad. Sci. (Paris)*, **1898**, *126*, 1703.
- [166] Q. Xu, C. Zhong, A General Approach for Estimating Framework Charges in Metal-Organic Frameworks, *J. Phys. Chem. C*, **2010**, *114*, 5035.
- [167] Q. Yang, D. Liu, C. Zhong, J.-R. Li, Development of Computational Methodologies for Metal-Organic Frameworks and Their Application in Gas Separations, *Chem. Rev.*, **2013**, *113*, 8261.
- [168] V. Buch, Path Integral Simulations of Mixed Para-D₂ and Ortho-D₂ Clusters: The Orientational Effects, *J. Chem. Phys.*, **1994**, *100*, 7610.
- [169] M.G. Martin, J.I. Siepmann, Transferable Potentials for Phase Equilibria. 1. United-Atom Description Of n-Alkanes, *J. Phys. Chem. B*, **1998**, *102*, 2569.
- [170] J.J. Potoff, J.I. Siepmann, Vapor-Liquid Equilibria of Mixtures Containing Alkanes, Carbon Dioxide, and Nitrogen, *AIChE J.*, **2001**, *47*, 1676.
- [171] K. Makrodimitris, G.K. Papadopoulos, D.N. Theodorou, Prediction of Permeation Properties Of CO₂ and N₂ through Silicalite via Molecular Simulations, *J. Phys. Chem. B*, **2001**, *105*, 777.
- [172] T. Engel, P.J. Reid, W. Hehre, Physical Chemistry, Pearson: Glenview, 2013.
- [173] D. Frenkel, B. Smit, Understanding Molecular Simulation: From Algorithms to Applications, Academic press: London, 2002.
- [174] M.P. Allen, D.J. Tildesley, Computer Simulation of Liquids, Oxford University Press: Bristol, 1989.
- [175] B. Smit, T.L.M. Maesen, Molecular Simulations of Zeolites: Adsorption, Diffusion, and Shape Selectivity, *Chem. Rev.*, **2008**, *108*, 4125.

- [176] A. Einstein, On the Theory of the Brownian Movement, *Ann. Phys. (Berlin, Ger.)*, **1906**, *4*, 371.
- [177] L.S. Darken, Diffusion, Mobility and Their Interrelation Through Free Energy in Binary Metallic Systems, *Trans. Aime*, **1948**, *175*, 184.
- [178] F.J. Keil, R. Krishna, M.-O. Coppens, Modeling of Diffusion in Zeolites, *Rev. Chem. Eng.*, **2000**, *16*, 71.
- [179] A.I. Skoulidas, D.S. Sholl, Molecular Dynamics Simulations of Self-Diffusivities, Corrected Diffusivities, and Transport Diffusivities of Light Gases in Four Silica Zeolites To Assess Influences of Pore Shape and Connectivity, *J. Phys. Chem. A*, **2003**, *107*, 10132.
- [180] D.M. Ackerman, A.I. Skoulidas, D.S. Sholl, J. Karl Johnson, Diffusivities of Ar and Ne in Carbon Nanotubes, *Mol. Simul.*, **2003**, *29*, 677.
- [181] S. Keskin, D.S. Sholl, Efficient Methods for Screening of Metal Organic Framework Membranes for Gas Separations Using Atomically Detailed Models, *Langmuir*, **2009**, *25*, 11786.
- [182] G. Yilmaz, A. Ozcan, S. Keskin, Computational Screening of ZIFs for CO₂ Separations, *Mol. Simul.*, **2015**, *41*, 713.
- [183] S. Keskin, D.S. Sholl, Assessment of a Metal-Organic Framework Membrane for Gas Separations Using Atomically Detailed Calculations: CO₂, CH₄, N₂, H₂ Mixtures in MOF-5, *Ind. Eng. Chem. Res.*, **2009**, *48*, 914.
- [184] J. Wesselingh, R. Krishna, Mass Transfer in Multicomponent Mixtures, Delft University Press: Delft, 2000.
- [185] A. Fick, V. On Liquid Diffusion, *The London, Edinburgh, and Dublin Philos. Mag. (1841-1944)*, **1855**, *10*, 30.
- [186] R.E. Kesting, A. Fritzsche, Polymeric Gas Separation Membranes, John Wiley & Sons, Inc.: New York, 1993.
- [187] R. Krishna, J.M. van Baten, In Silico Screening of Zeolite Membranes for CO₂ Capture, *J. Membr. Sci.*, **2010**, *360*, 323.
- [188] E. Adatoz, S. Keskin, Application of MD Simulations to Predict Membrane Properties of MOFs, *J. Nanomater.*, **2015**, *2015*.
- [189] J.C. Maxwell, A Treatise on Electricity and Magnetism, Dover Publications, New York, 1954.

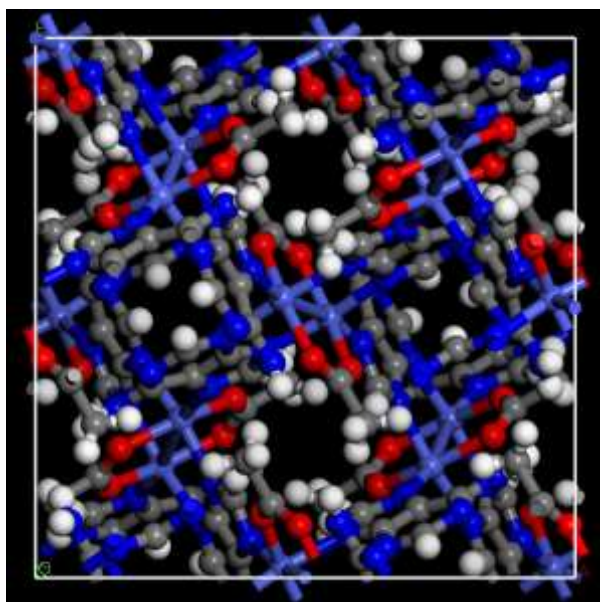
- [190] V.D. Bruggeman, Berechnung Verschiedener Physikalischer Konstanten von Heterogenen Substanzen. I. Dielektrizitätskonstanten und Leitfähigkeiten der Mischkörper aus Isotropen Substanzen, *Ann. Phys.(Leipzig)* **1935**, 416, 636.
- [191] T. Lewis, L. Nielsen, Dynamic Mechanical Properties of Particulate-Filled Composites, *J. Appl. Polym. Sci.*, **1970**, 14, 1449.
- [192] R. Pal, New Models for Thermal Conductivity of Particulate Composites, *J. Reinf. Plast. Compos.*, **2007**, 26, 643.
- [193] J. Felske, Effective Thermal Conductivity of Composite Spheres in a Continuous Medium with Contact Resistance, *Int. J. Heat Mass Transfer*, **2004**, 47, 3453.
- [194] I. Erucar, S. Keskin, Molecular Modeling of MOF-based Mixed Matrix Membranes, *Curr. Org. Chem.*, **2014**, 18, 2364.
- [195] I. Erucar, G. Yilmaz, S. Keskin, Recent Advances in Metal-Organic Framework-Based Mixed Matrix Membranes, *Chem. - Asian J.*, **2013**, 8, 1692.
- [196] H. Vinh-Thang, S. Kaliaguine, Predictive Models for Mixed-Matrix Membrane Performance: A Review, *Chem. Rev.*, **2013**, 113, 4980.
- [197] R. Bouma, A. Checchetti, G. Chidichimo, E. Drioli, Permeation Through a Heterogeneous Membrane: The Effect of the Dispersed Phase, *J. Membr. Sci.*, **1997**, 128, 141.
- [198] J.J. Irwin, B.K. Shoichet, ZINC-a Free Database of Commercially Available Compounds for Virtual Screening, *J. Chem. Inf. Model.*, **2005**, 45, 177.
- [199] E.E. Bolton, Y. Wang, P.A. Thiessen, S.H. Bryant, PubChem: Integrated Platform of Small Molecules and Biological Activities, *Annu. Rep. Comput. Chem.*, **2008**, 4, 217.
- [200] C. Materials Studio v8.0; Biovia Software Inc.: San Diego, 2007.
- [201] L. Sarkisov, A. Harrison, Computational Structure Characterisation Tools in Application to Ordered and Disordered Porous Materials, *Mol. Sim.*, **2011**, 37, 1248.
- [202] R.L. Akkermans, N.A. Spenley, S.H. Robertson, Monte Carlo methods in materials studio, *Mol. Sim.*, **2013**, 39, 1153.
- [203] T. Li, D.-L. Chen, J.E. Sullivan, M.T. Kozlowski, J.K. Johnson, N.L. Rosi, Systematic modulation and enhancement of CO₂ : N₂ selectivity and water stability in an isorecticular series of bio-MOF-11 analogues, *Chem. Sci.*, **2013**, 4, 1746.
- [204] Y.-S. Bae, O.K. Farha, J.T. Hupp, R.Q. Snurr, Enhancement of CO₂/N₂ selectivity in a metal-organic framework by cavity modification, *J. Mater. Chem.*, **2009**, 19, 2131.

- [205] R. Krishna, J.M. Van Baten, In Silico Screening of Metal-Organic Frameworks in Separation Applications, *Phys. Chem. Chem. Phys.*, **2011**, *13*, 10593.
- [206] R. Babarao, J. Jiang, Unprecedentedly High Selective Adsorption of Gas Mixtures in rho Zeolite-like Metal–Organic Framework: A Molecular Simulation Study, *J. Am. Chem. Soc.*, **2009**, *131*, 11417.
- [207] B. Smit, T.L.M. Maesen, Molecular Simulations of Zeolites: Adsorption, Diffusion, and Shape Selectivity, *Chem. Rev.*, **2008**, *108*, 4125.
- [208] D. Dubbeldam, S. Calero, T.L. Maesen, B. Smit, Incommensurate Diffusion in Confined Systems, *Phys. Rev. Lett.*, **2003**, *90*, 245901.
- [209] T.C. Merkel, H. Lin, X. Wei, R. Baker, Power Plant Post-Combustion Carbon Dioxide Capture: An Opportunity for Membranes, *J. Membr. Sci.*, **2010**, *359*, 126.
- [210] R.A. Smaldone, R.S. Forgan, H. Furukawa, J.J. Gassensmith, A.M. Slawin, O.M. Yaghi, J.F. Stoddart, Metal-Organic Frameworks From Edible Natural Products, *Angew. Chem., Int. Ed.*, **2010**, *49*, 8630.
- [211] Q. Hu, J. Yu, M. Liu, A. Liu, Z. Dou, Y. Yang, A Low Cytotoxic Cationic Metal–Organic Framework Carrier for Controllable Drug Release, *J. Med. Chem.*, **2014**, *57*, 5679.
- [212] H. Deng, S. Grunder, K.E. Cordova, C. Valente, H. Furukawa, M. Hmadeh, F. Gándara, A.C. Whalley, Z. Liu, S. Asahina, H. Kazumori, M. O’Keeffe, O. Terasaki, J.F. Stoddart, O.M. Yaghi, Large-Pore Apertures in a Series of Metal-Organic Frameworks, *Science*, **2012**, *336*, 1018.
- [213] J. Ahmad, M.-B. Hägg, Preparation and Characterization of Polyvinyl Acetate/Zeolite 4A Mixed Matrix Membrane for Gas Separation, *J. Membr. Sci.*, **2013**, *427*, 73.
- [214] S. Pérez-Yáñez, G. Beobide, O. Castillo, J. Cepeda, A. Luque, A.T. Aguayo, P. Román, Open-Framework Copper Adeninate Compounds with Three-Dimensional Microchannels Tailored by Aliphatic Monocarboxylic Acids, *Inorg. Chem.*, **2011**, *50*, 5330.
- [215] J. An, R.P. Fiorella, S.J. Geib, N.L. Rosi, Synthesis, Structure, Assembly, and Modulation of the CO₂ Adsorption Properties of a Zinc-Adeninate Macrocyclic, *J. Am. Chem. Soc.*, **2009**, *131*, 8401.
- [216] P. Horcajada, S. Surblé, C. Serre, D.-Y. Hong, Y.-K. Seo, J.-S. Chang, J.-M. Greneche, I. Margiolaki, G. Férey, Synthesis and Catalytic Properties of MIL-100(Fe), an Iron (III) Carboxylate with Large Pores, *Chem. Commun.*, **2007**, 2820.
- [217] T.F. Willems, C.H. Rycroft, M. Kazi, J.C. Meza, M. Haranczyk, Algorithms and Tools for High-Throughput Geometry-Based Analysis of Crystalline Porous Materials, *Microporous and Mesoporous Mater.*, **2012**, *149*, 134.

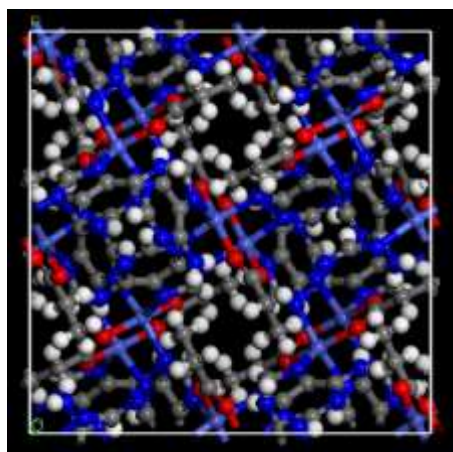
- [218] R.L. Akkermans, N.A. Spenley, S.H. Robertson, Monte Carlo Methods in Materials Studio, *Mol. Simul.*, **2013**, *39*, 1153.
- [219] E. Haldoupis, T. Watanabe, S. Nair, D.S. Sholl, Quantifying Large Effects of Framework Flexibility on Diffusion in MOFs: CH₄ and CO₂ in ZIF-8, *ChemPhysChem*, **2012**, *13*, 3449.
- [220] S.A. Adcock, J.A. McCammon, Molecular Dynamics: Survey of Methods for Simulating the Activity of Proteins, *Chem. Rev.*, **2006**, *106*, 1589.
- [221] T. Devic, P. Horcajada, C. Serre, F. Salles, G. Maurin, B. Moulin, D. Heurtaux, G. Clet, A. Vimont, J.-M. Grenèche, B.L. Ouay, F. Moreau, E. Magnier, Y. Filinchuk, J. Marrot, J.-C. Lavalley, M. Daturi, G. Férey, Functionalization in Flexible Porous Solids: Effects on the Pore Opening and the Host-Guest Interactions, *J. Am. Chem. Soc.*, **2010**, *132*, 1127.
- [222] I. Erucar, S. Keskin, Computational Modeling of Bio-MOFs for CO₂/CH₄ Separations, *Chem. Eng. Sci.*, **2015**, *130*, 120.
- [223] A. Uzun, S. Keskin, Site Characteristics in Metal Organic Frameworks for Gas Adsorption, *Prog. Surf. Sci.*, **2014**, *89*, 56.

APPENDIX A: Modeling of Bio-MOFs for Gas Separations

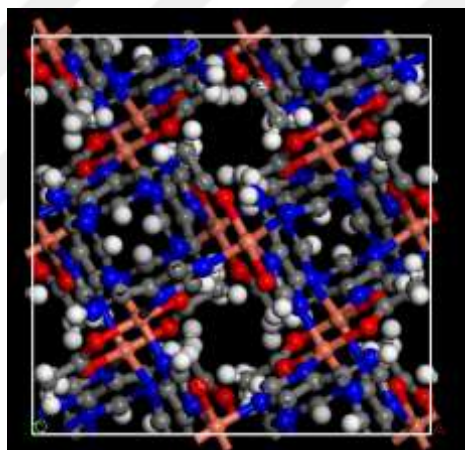
(a) Unit cell structure of Bio-MOF-1. Carbon: grey, Hydrogen: white, Oxygen: red, Zinc: purple, Nitrogen: blue.



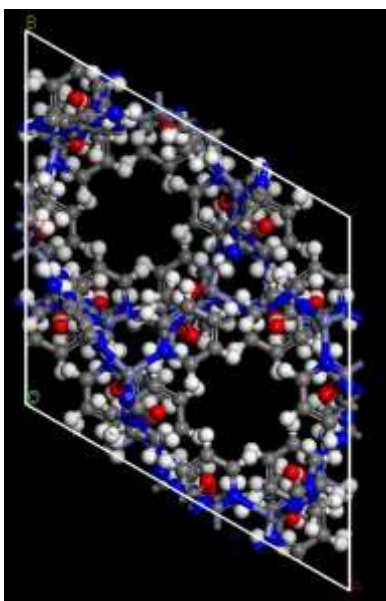
(b) Unit cell structure of Bio-MOF-11. Carbon: grey, Hydrogen: white, Oxygen: red, Zinc: purple, Nitrogen: blue.



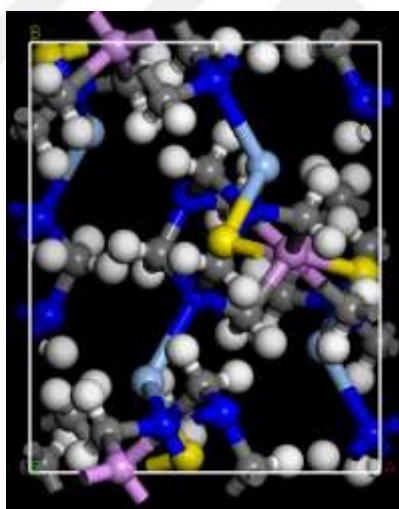
(c) Unit cell structure of Bio-MOF-12. Carbon: grey, Hydrogen: white, Oxygen: red, Zinc: purple, Nitrogen: blue.



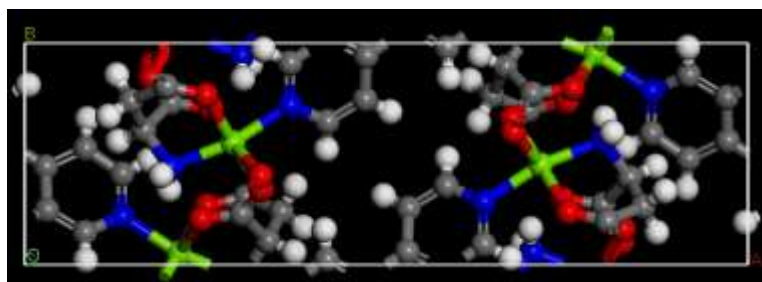
(d) Unit cell structure of IZUMUM. Carbon: grey, Hydrogen: white, Oxygen: red, Copper: orange, Nitrogen: blue.



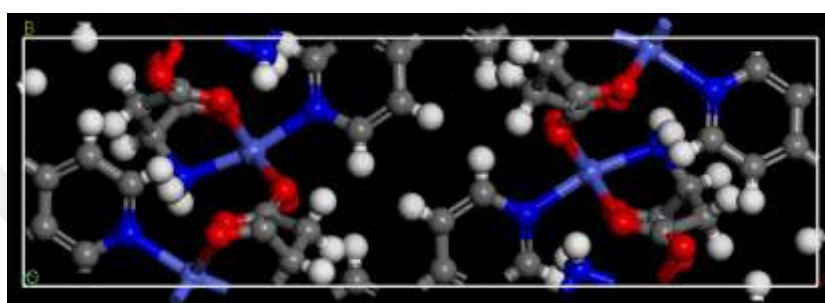
(e) Unit cell structure of NUDKON. Carbon: grey, Hydrogen: white, Oxygen: red, Zinc: purple, Nitrogen: blue.



(f) Unit cell structure of OFUSAL. Carbon: grey, Hydrogen: white, Oxygen: red, Phosphorous: pink, Nitrogen: blue, Sulfur: yellow, Silver: light blue.



(g) Unit cell structure of PESTUD. Carbon: grey, Hydrogen: white, Oxygen: red, Nickel: yellow, Nitrogen: blue.



(h) Unit cell structure of WODFOL. Carbon: grey, Hydrogen: white, Oxygen: red, Cobalt: Purple, Nitrogen: blue.

Figure A.1 (a-h) Unit cell structures of bio-MOFs given A along X, B in XY plane

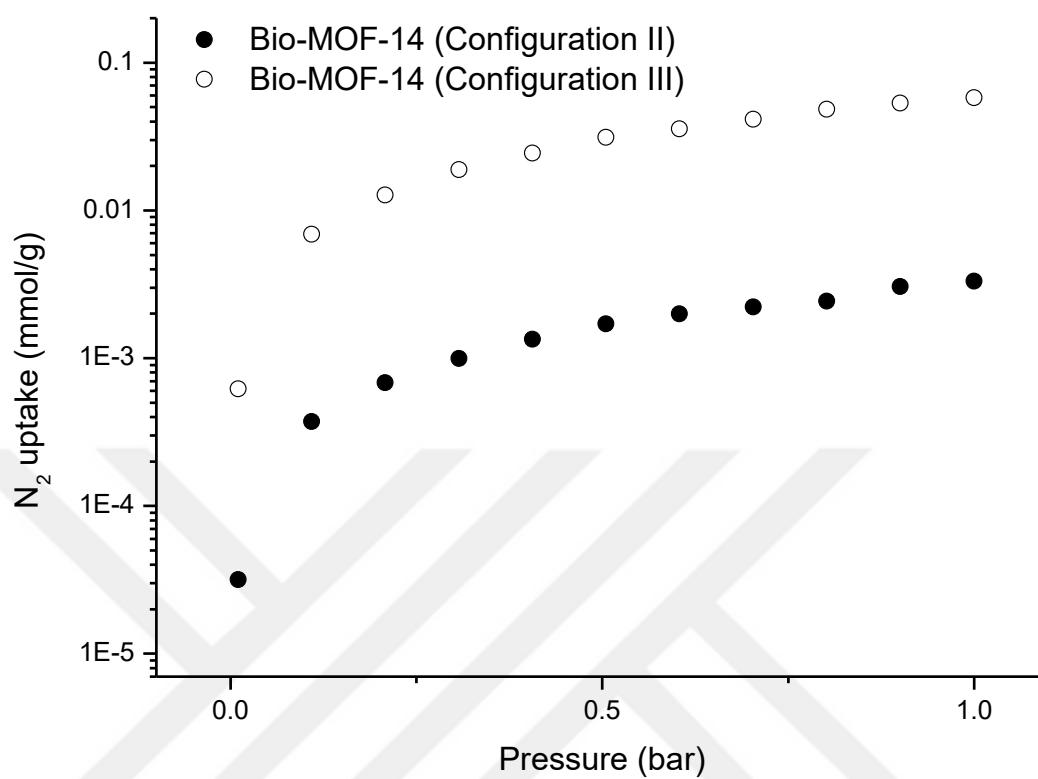


Figure A.2 N₂ uptakes in bio-MOF-14. (No N₂ adsorption was observed for configuration I.)

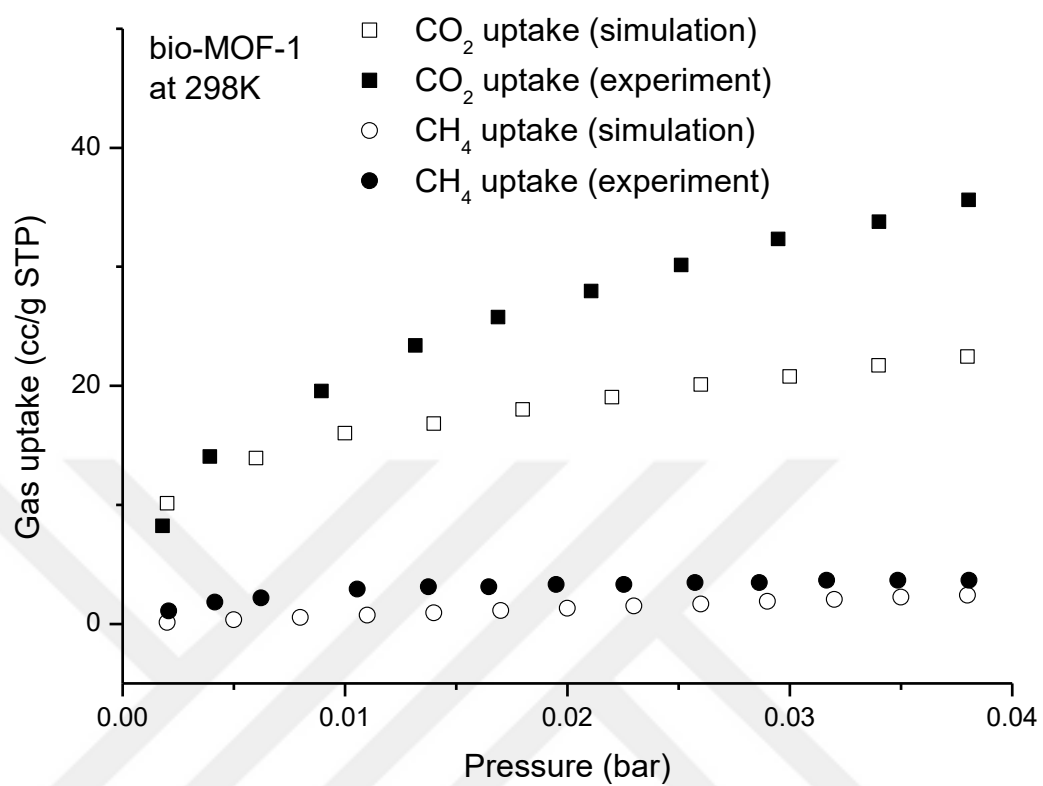


Figure A.3 CO₂ and CH₄ uptakes in bio-MOF-1.

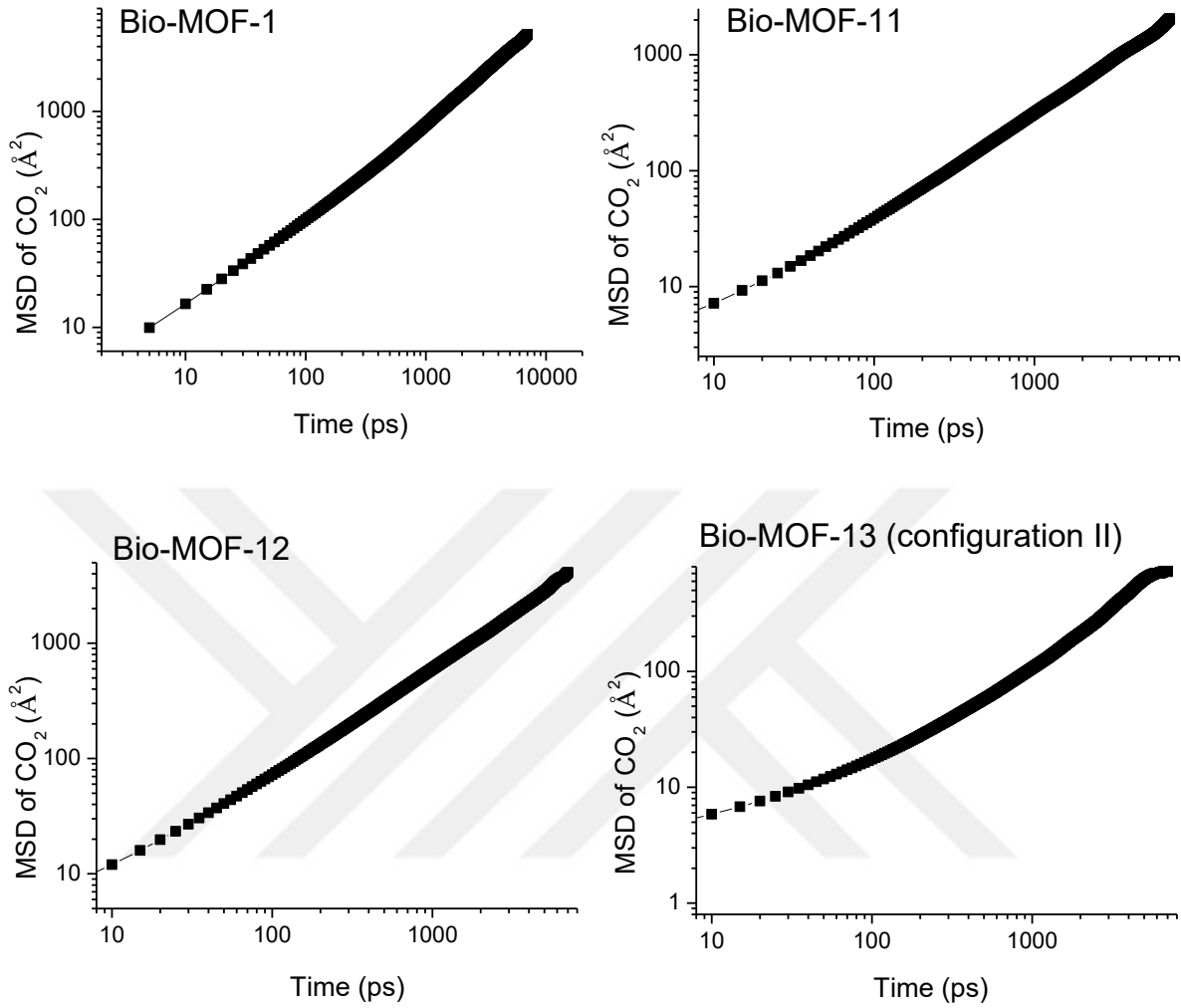
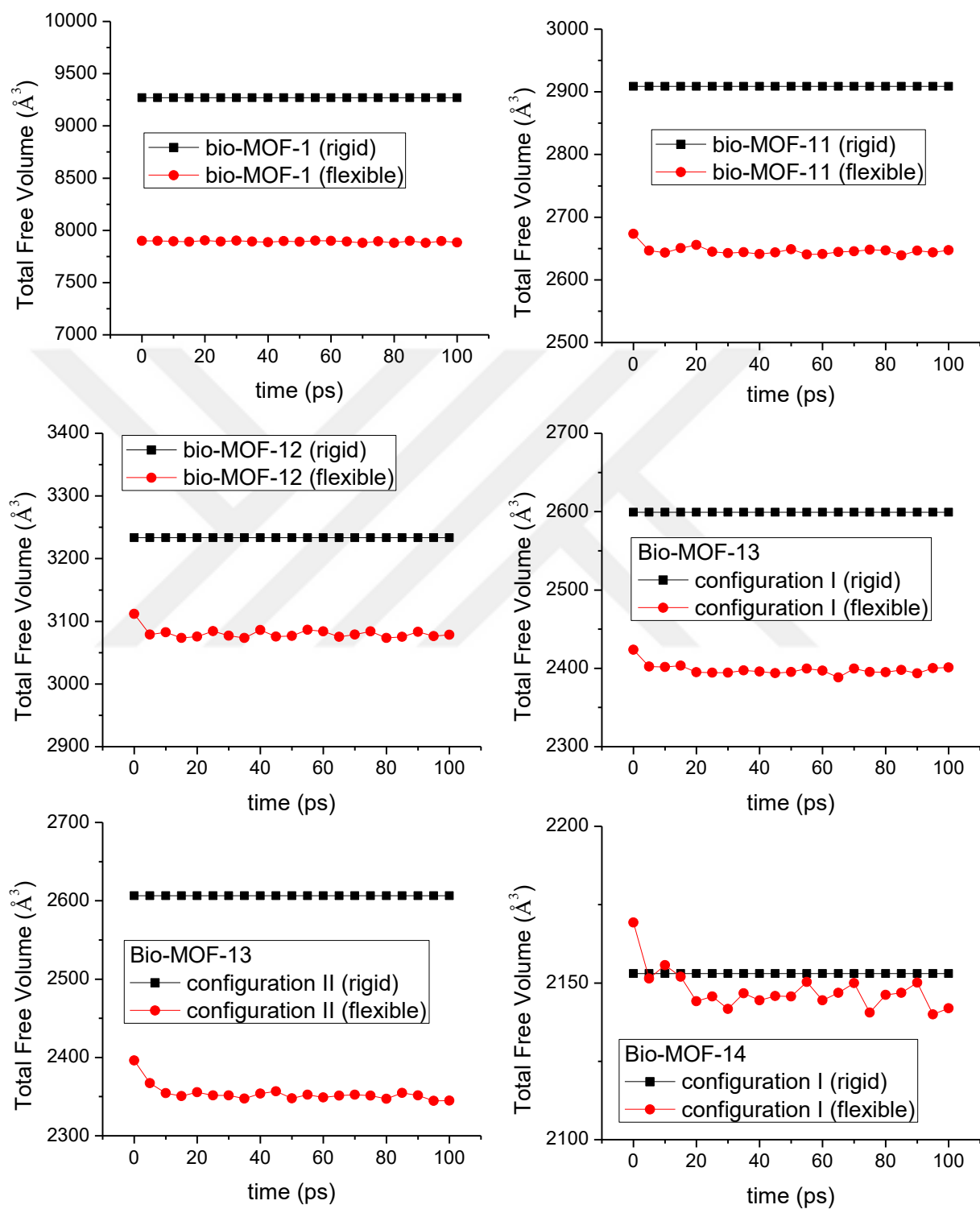
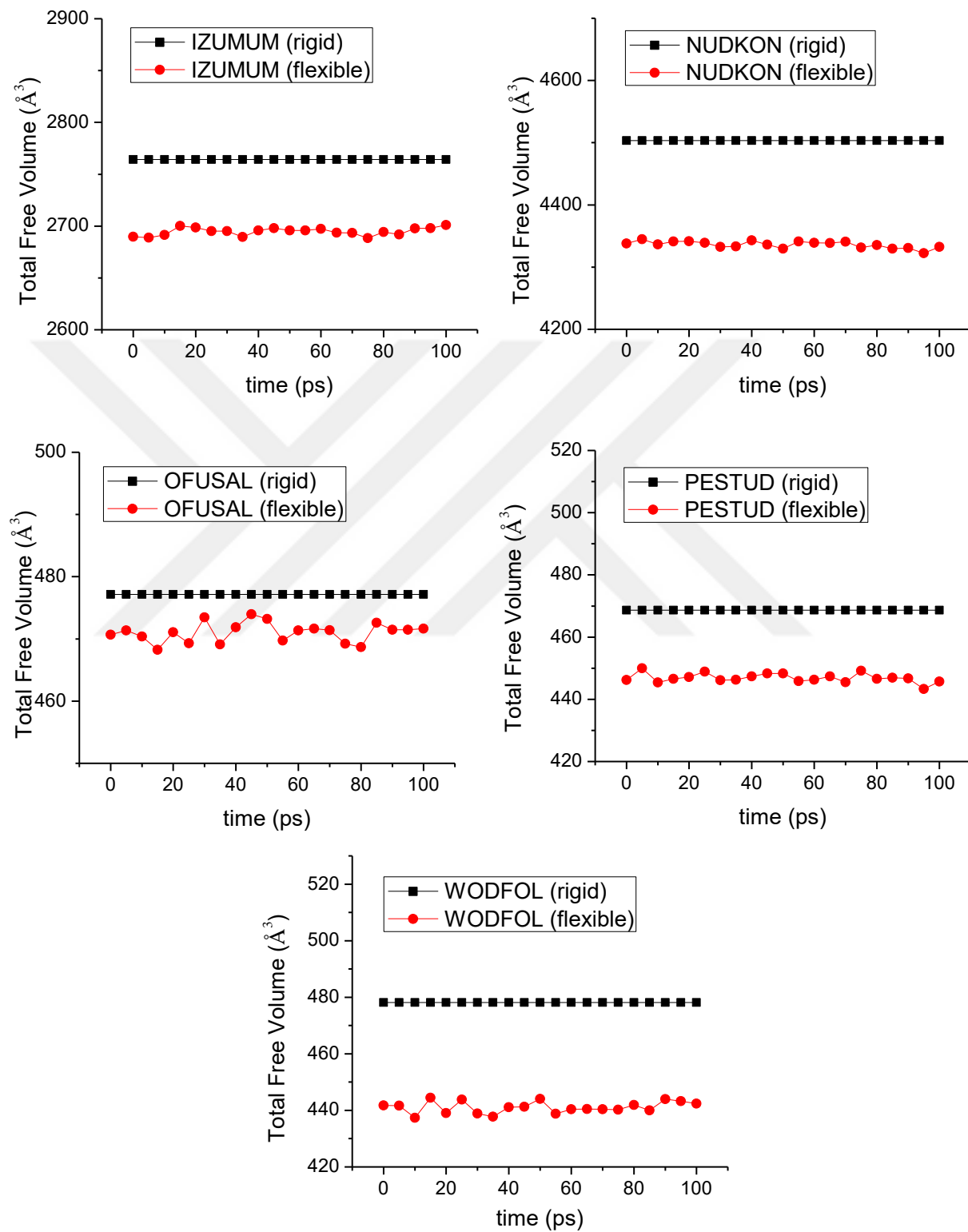


Figure A.4 Mean square displacements (MSD) vs. t graphs for rigid bio-MOF-1, -11, -12 and -13 (configuration II).

Table A.1 Diffusion coefficients of CO₂ for rigid bio-MOF-1, -11, -12 and -13.

Bio-MOFs	$D_{\text{self}} \text{ CO}_2$ (cm ² /s)	Uncertainty of $D_{\text{self}} \text{ CO}_2$ (cm ² /s)
Bio-MOF-1	3.25×10^{-5}	9.18×10^{-6}
Bio-MOF-11	1.84×10^{-5}	2.96×10^{-6}
Bio-MOF-12	1.06×10^{-5}	3.50×10^{-6}
Bio-MOF-13 (configuration II)	2.40×10^{-6}	6.23×10^{-7}



**Figure A.5** Total free volume analysis of bio-MOFs

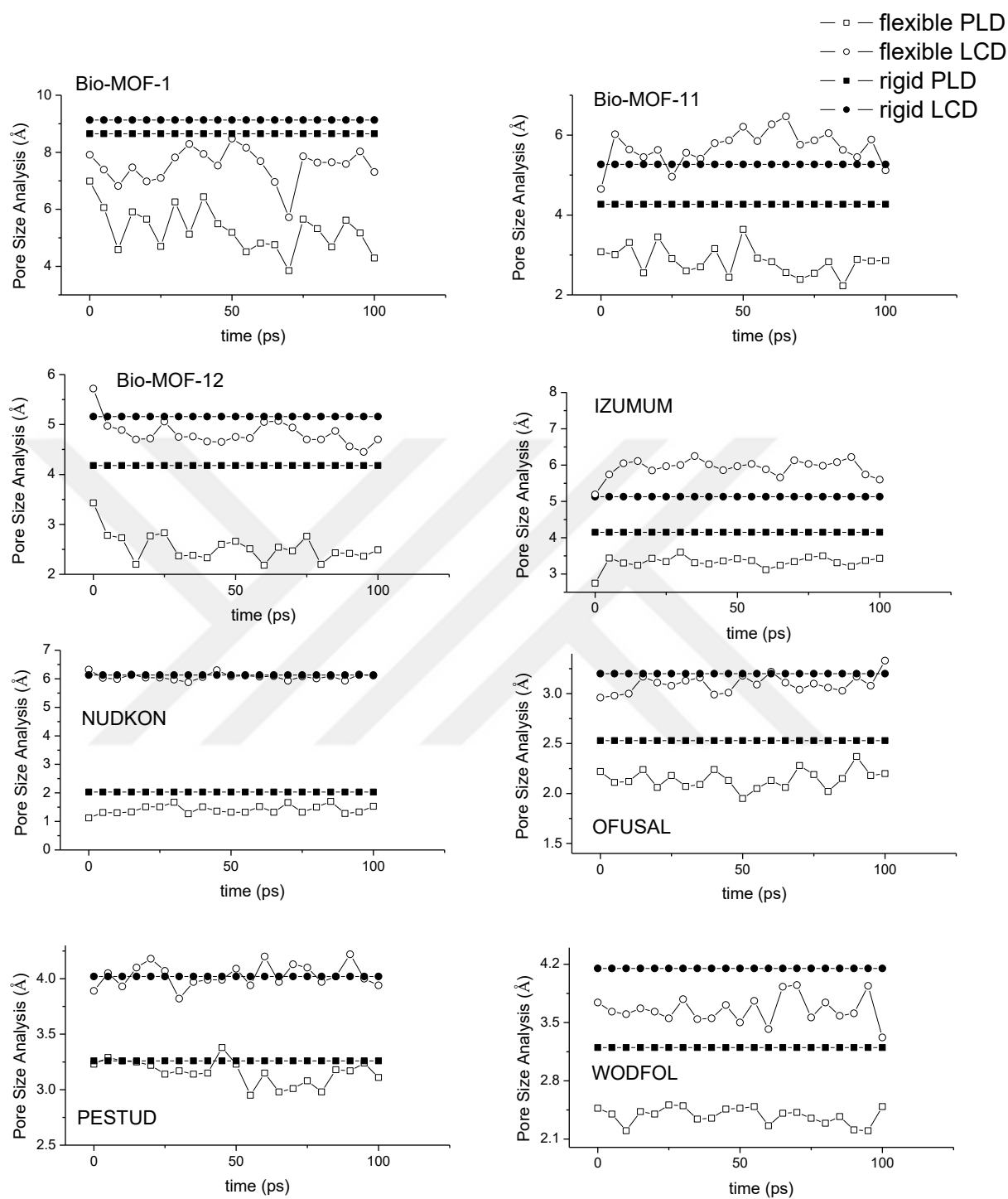


Figure A.6 Pore size analysis of bio-MOFs-1, -11, -12, IZUMUM, NUDKON, OFUSAL, PESTUD and WODFOL.

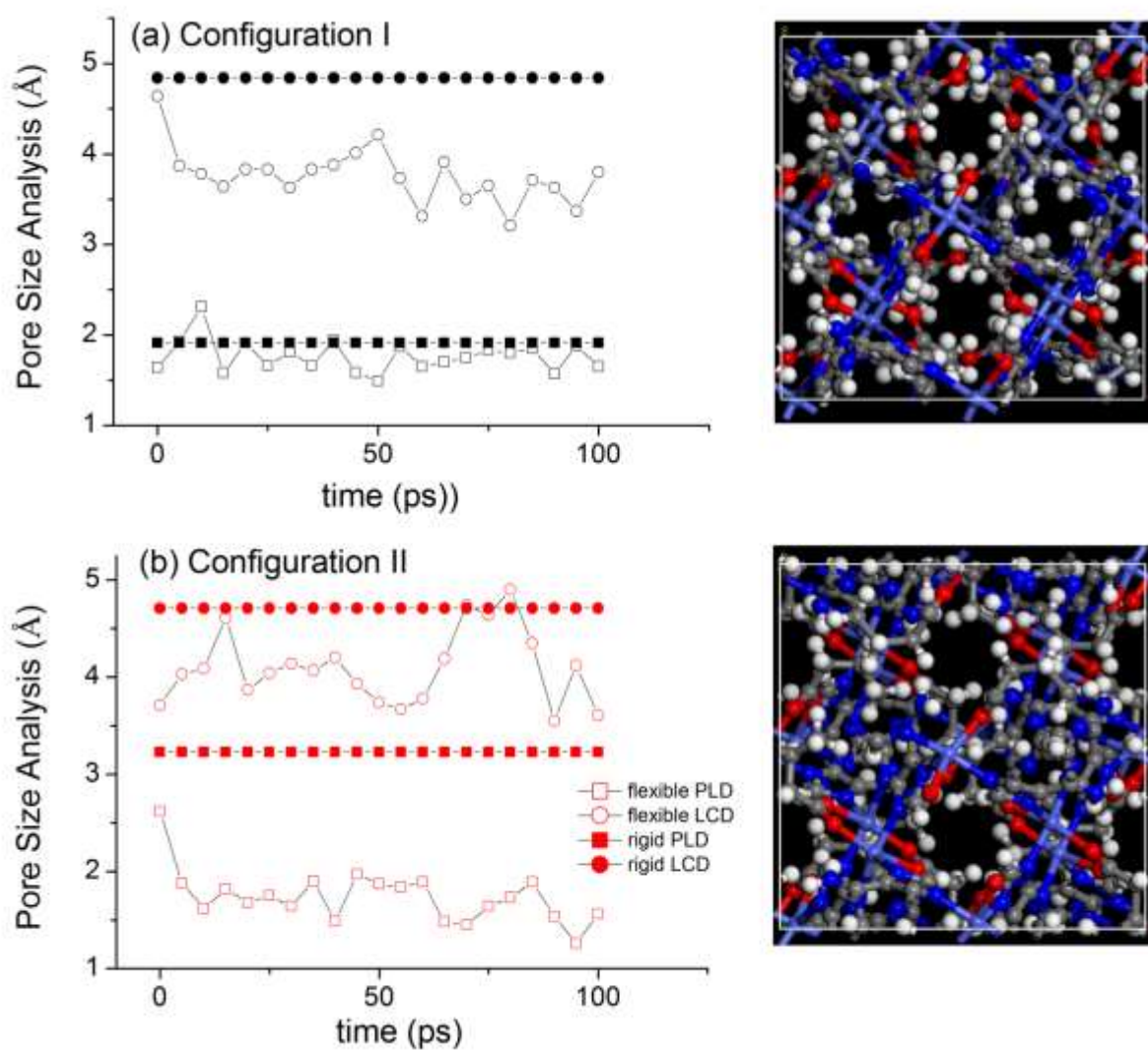


Figure A.7 Pore size analysis of bio-MOF-13.

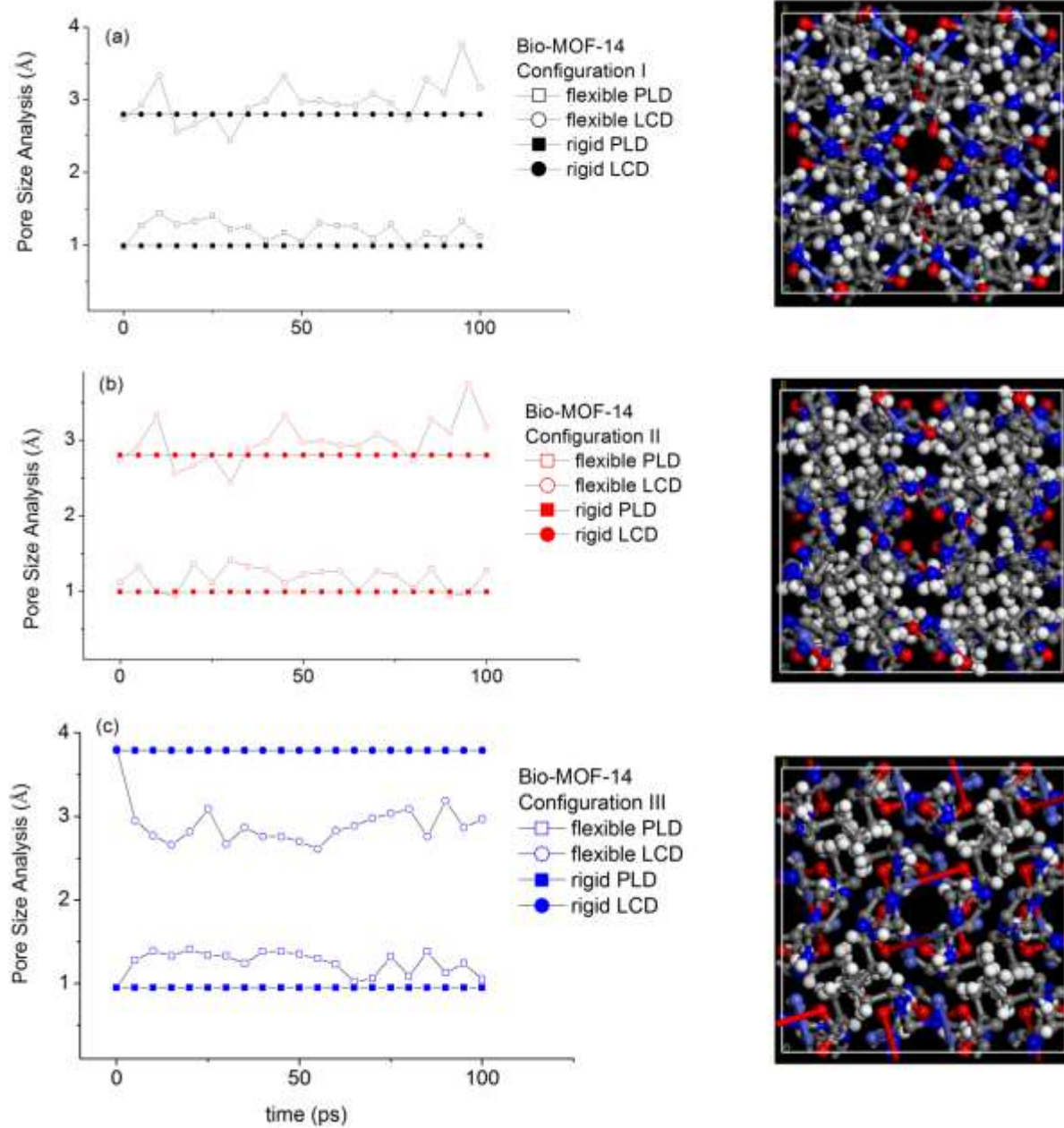
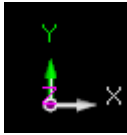
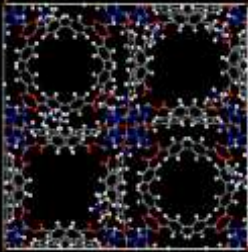
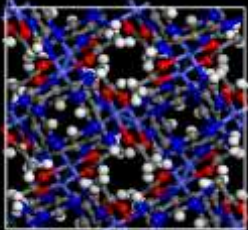
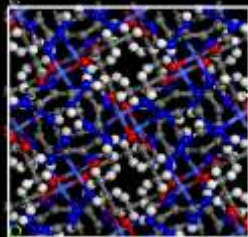



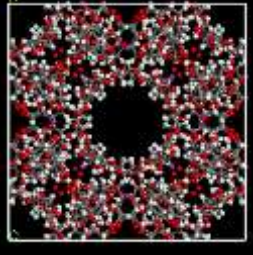
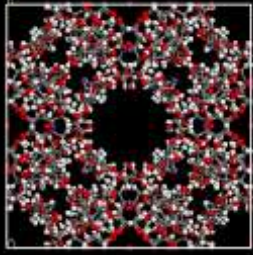
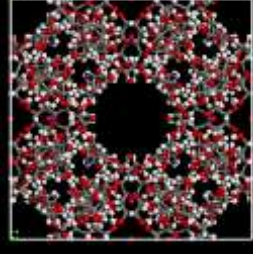
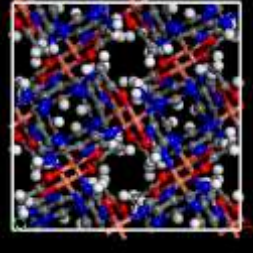


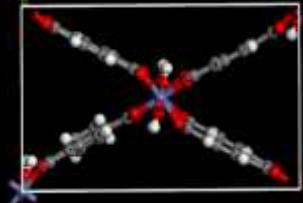
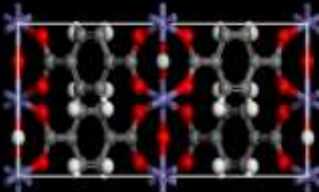
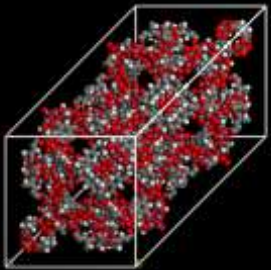
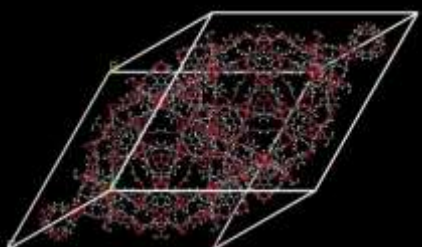
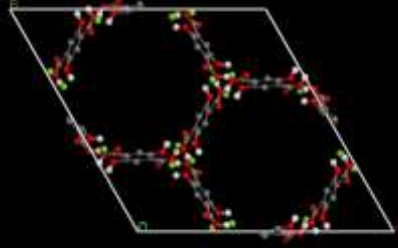
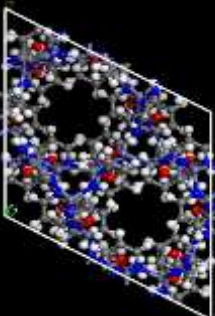
Figure A.8 Pore size analysis of bio-MOF-14.

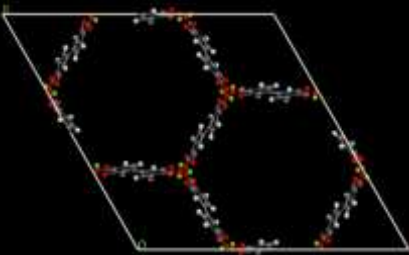
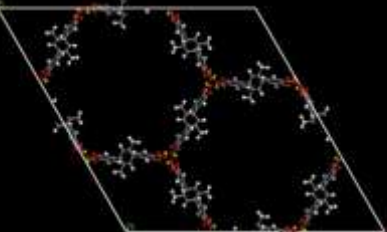
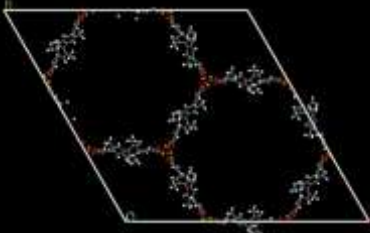
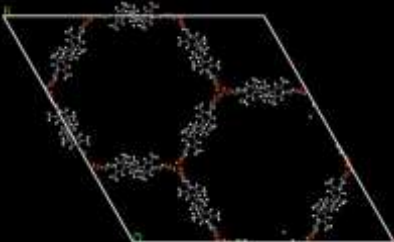
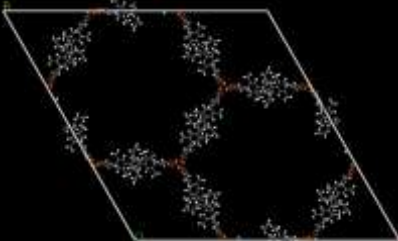
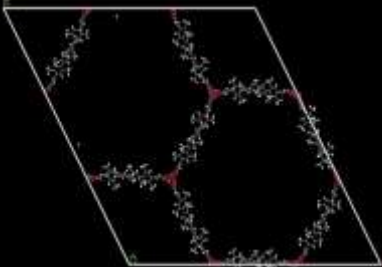
APPENDIX B: Efficient storage of drug/cosmetic molecules in bio-compatible MOFs

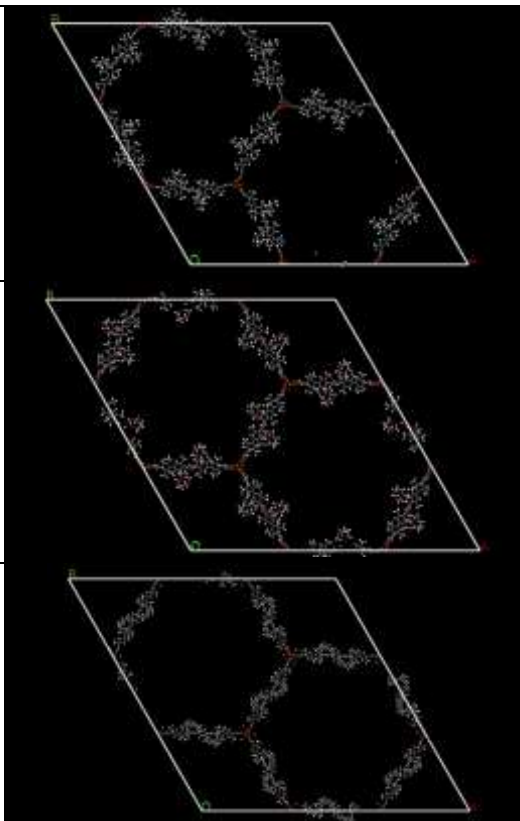
Table B.1 Structural properties of bio-compatible MOFs[†]

MOF name	Organic linker and metals	Pore volume (cm ³ /g)	Surface area (m ² /g)	PLD (Å)	LCD (Å)	3D structures 
Bio-MOF-1	Adenine Zn	0.55	1069	4.75	5.62	
Bio-MOF-11	Adenine Co	0.44	860	4.59	5.76	
Bio-MOF-12	Adenine Co	0.46	1001	4.75	5.62	
Bio-MOF-100	Adenine Zn	2.64	3673	14.72	20.23	

Bio-MOF-101	Adenine Zn	2.15	2754	19.56	24.09	
Bio-MOF-102	Adenine Zn	3.21	3465	26.28	31.40	
CD-MOF-1	Cyclodextrin K	0.59	1130	7.17	16.85	
CD-MOF-2	Cyclodextrin Rb	0.59	1085	7.14	16.84	
CD-MOF-3	Cyclodextrin Cs	0.54	948	6.68	16.15	
IZUMUM	Adenine Cu	0.42	776	4.64	5.58	

MIL-53	Fe terephthalate	0.53	1096	5.64	6.13	
MIL-53-open ¹	Fe terephthalate	0.64	1593	7.33	7.83	
MIL-100	Fe carboxylate	0.99	1748	9.04	27.91	
MIL-101	Cr terephthalate	1.96	3158	14.05	36.15	
MOF-74	DOT* Mg	0.70	1621	10.76	11.64	
NUDKON	Adenine Zn	0.43	178	2.34	6.44	

RAVVUH	DOT* Mg	1.23	2228	16.38	17.18	
RAVWAO	DOT* Mg	1.42	2621	17.51	17.93	
RAVWES	DOT* Mg	1.81	2759	23.63	24.44	
RAVWIW	DOT* Mg	2.28	3018	30.14	30.70	
RAVWOC	DOT* Mg	2.11	2916	27.56	28.22	
RAVWUI	DOT* Zn	2.55	2893	36.43	36.79	

RAVXAP	DOT* Mg	2.96	3360	34.36	34.86	
RAVXET	DOT* Mg	2.54	2809	38.07	38.23	
RAVXIX	DOT* Mg	3.74	3036	53.26	53.58	

†Physical properties, such as pore volume, pore-limiting diameter (PLD), largest cavity diameter (LCD), surface area (gravimetric surface area) were calculated using zeo++ software.² Surface area calculations were performed using a probe radius of 1.86Å. For pore volume calculations, probe radius was set to zero. Measurements were done for bio-MOF-1, -100, -101 and -102 considering dimethylammonium (DMA) cations inside the cell. *DOT: dioxidoterephthalate. Surface area and pore volume of bio-MOF-102 and surface area of NUDKON were estimated using Materials Studio 8.0 software.

Table B.2 Data for comparison of our predicted ibuprofen uptake with the experiments[140, 144] and other simulation data[153-155] available in the literature.

MOF name	Our data	Experiments	Ibuprofen uptake (mg/g)		
			Bernini et al.[155]	Bei et al.[154]	Babarao et al. [153]
Bio-MOF-1	170			208	
Bio-MOF-11	90			55	
Bio-MOF-100	1547		1969	2030	
CD-MOF-1	246		274		
MIL-53(Fe)	220	220	217		
MIL-100(Fe)	570	347	641		
MIL-101(Cr)	1035	1376	1289		1110
MOF-74	375		425		

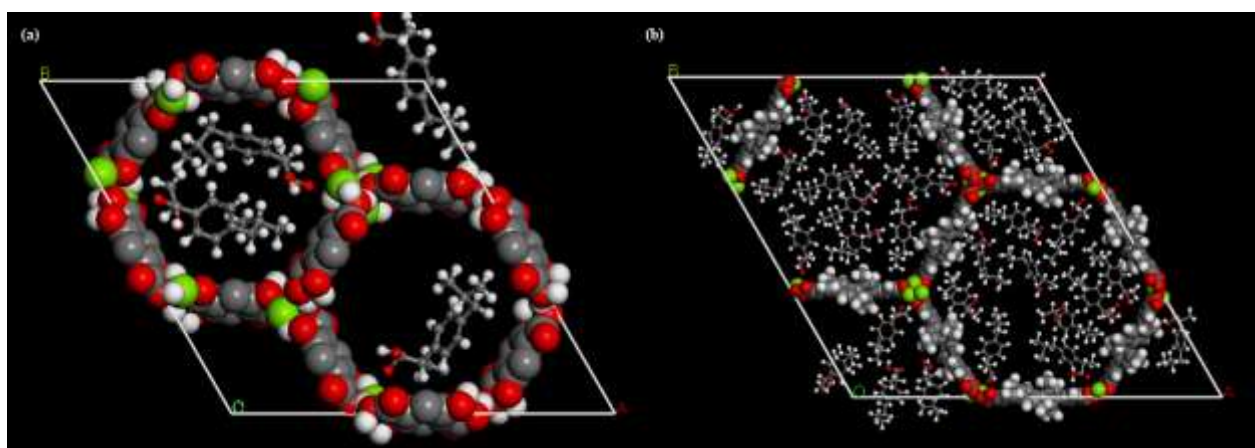


Figure B.1 Conformation of ibuprofen molecules in (a)MOF-74 and (b)RAVWES.

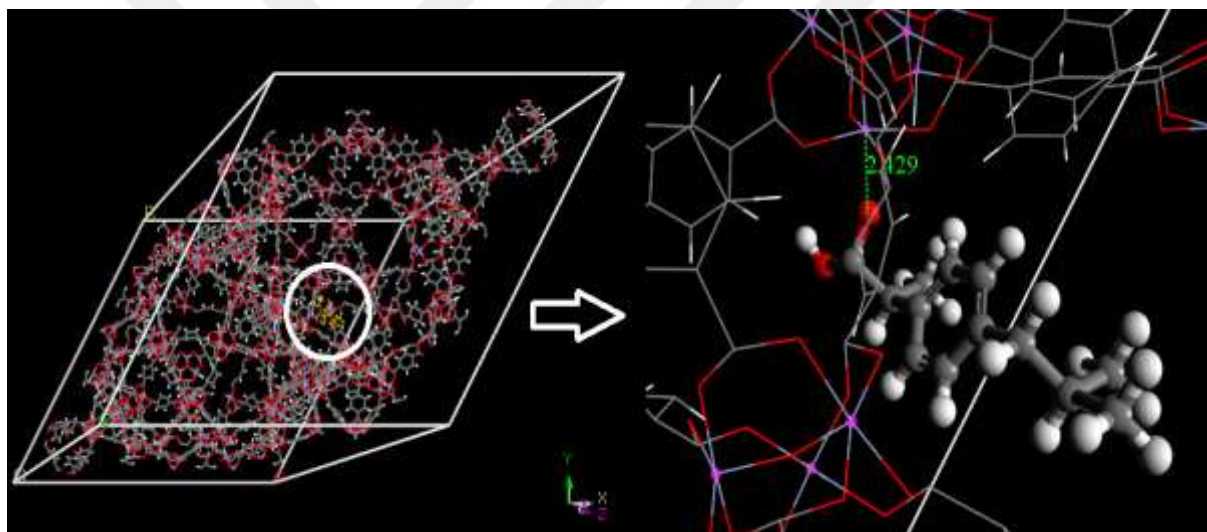


Figure B.2 Conformation of ibuprofen in MIL-101(Cr).

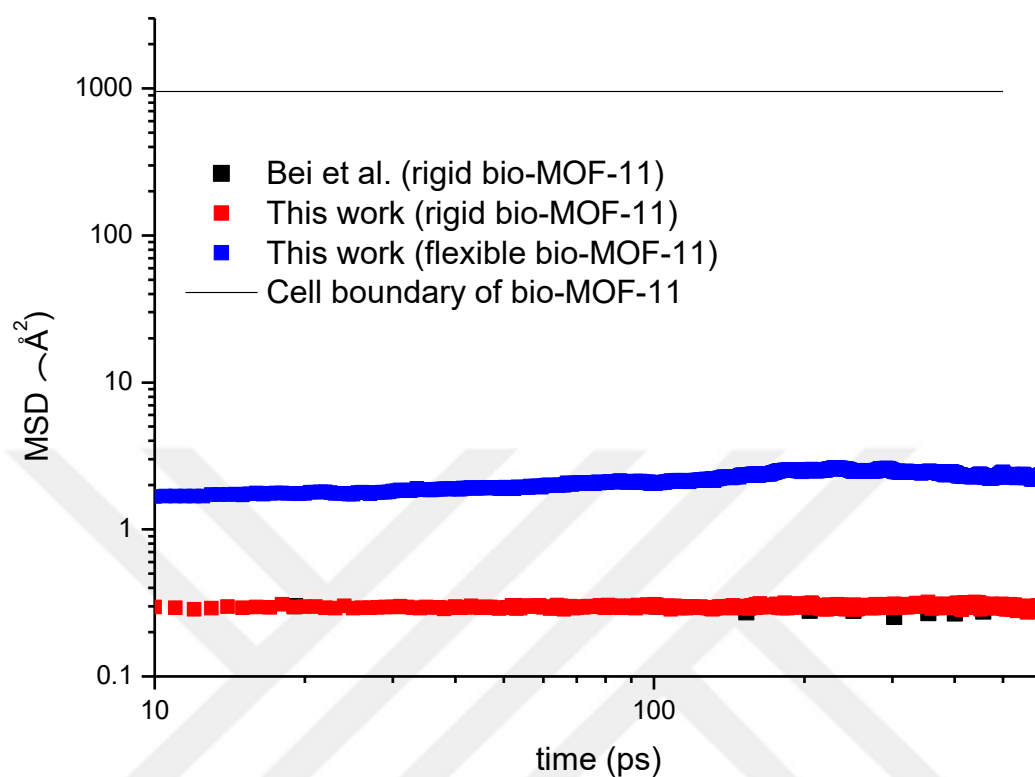


Figure B.3 MSDs of ibuprofen in bio-MOF-11. Data for Bei et al.[154] is taken from the literature. (Cell boundaries were estimated considering the smallest unit cell parameters.)

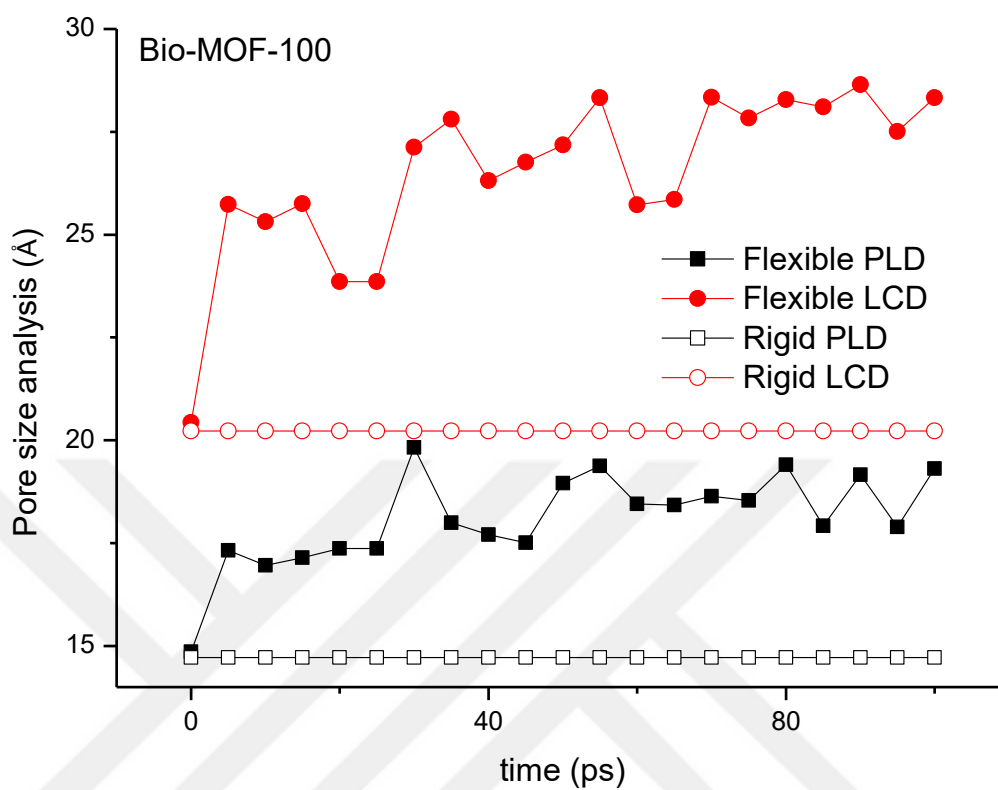


Figure B.4 Pore size analysis of bio-MOF-100 during MD simulations.

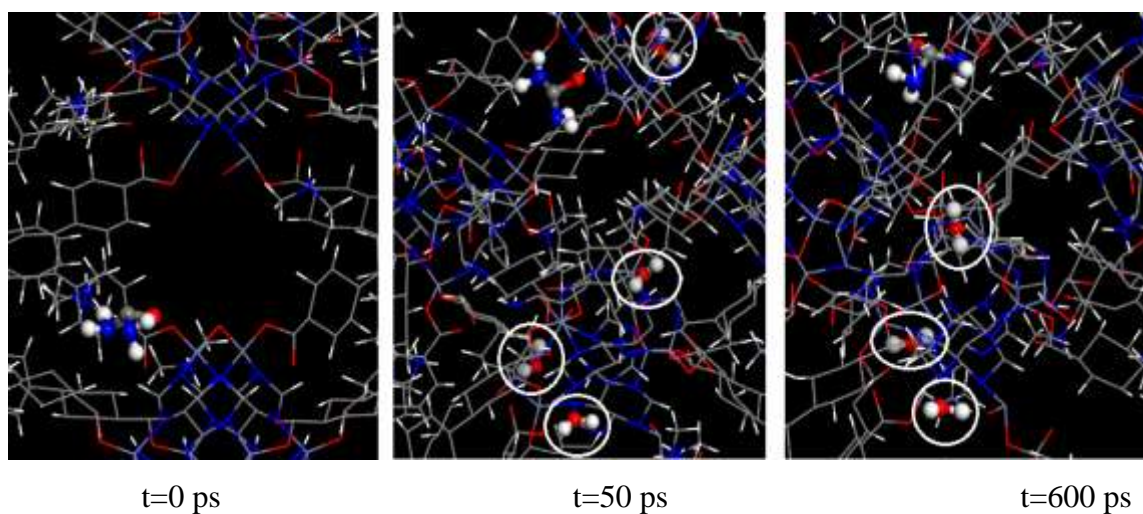


Figure B.5 MD snapshots of urea diffusion in bio-MOF-100 in the presence of water.

Water molecules are shown in white circles.

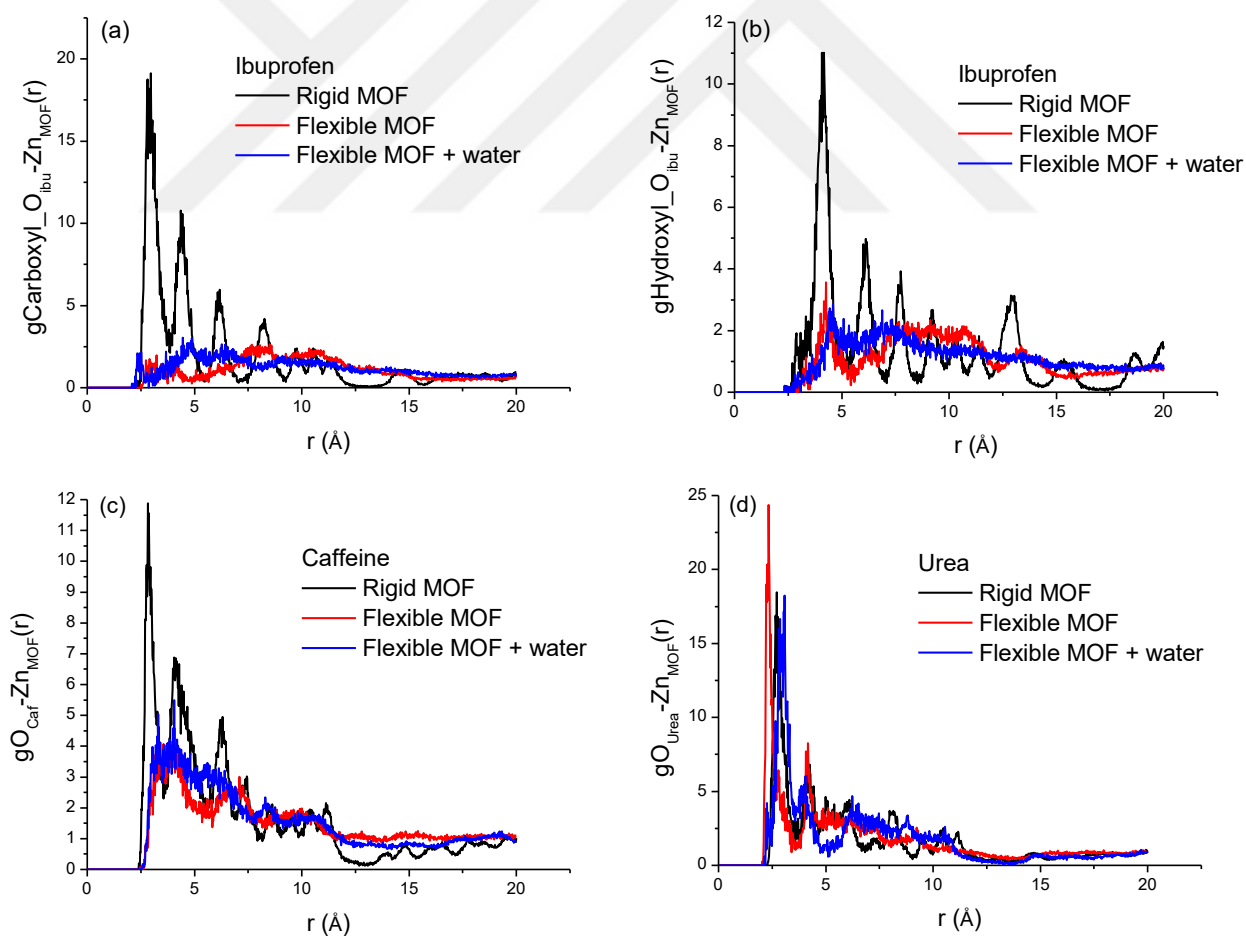


Figure B.6 RDF analyses of (a,b)ibuprofen, (c)caffeine and (d)urea in bio-MOF-100.

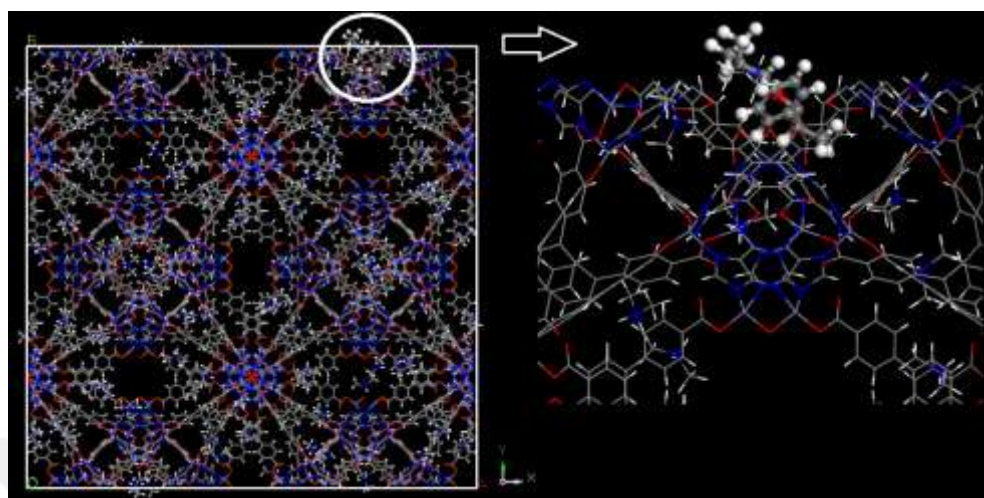


Figure B.7 Conformation of ibuprofen in bio-MOF-100.

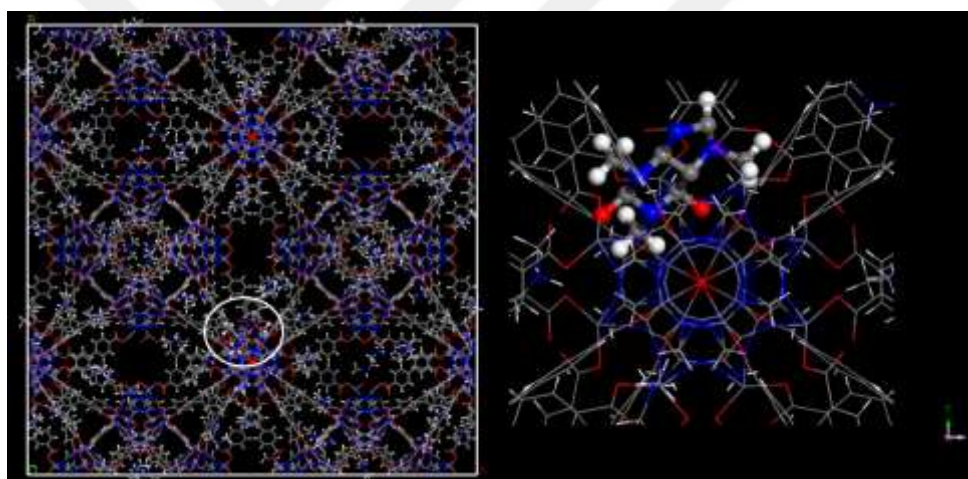


Figure B.8 Conformation of caffeine in bio-MOF-100.

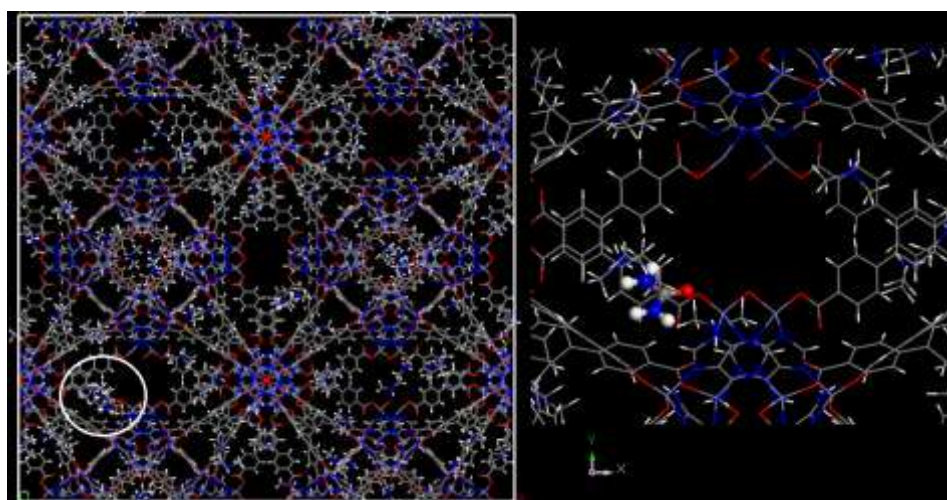


Figure B.9 Conformation of urea in bio-MOF-100.

VITA

İlknur Erucar was born in Istanbul, on July 24, 1987. She received her BS degree in Chemical Engineering from Yıldız Technical University in 2009. She completed her M.Sc. degree at Koc University, Department of Computational Sciences & Engineering in 2012. She is currently completing a Ph.D at the Chemical & Biological Engineering Department of Koc University. She received the scholarship from TUBITAK (“2211-C Öncelikli Alanlara Yönelik Yurt İçi Doktora Bursu”) and She is the first person who has been awarded by this scholarship in Engineering Department of Koc University.

List of Publications:

Publications in Peer-Reviewed International Journals:

1. Erucar I. and Keskin S. "Computational Assessment of MOF Membranes for CH₄/H₂ Separations" *Journal of Membrane Science* 514, 313-321 (2016).
2. Erucar I. and Keskin S. "Efficient storage of drug and cosmetic molecules in bio-compatible MOFs: A molecular simulation study" *Industrial & Engineering Chemistry Research* 55(7), 1929-1939 (2016).
3. Erucar I. and Keskin S. "Computational Methods for MOF/Polymer Membranes" *The Chemical Record* 16(2), 703-718 (2016).
4. Erucar I. and Keskin S. "Computational Modeling of Bio-MOFs for CO₂/CH₄ Separations" *Chemical Engineering Science* 130, 120-128 (2015).
5. Erucar I. and Keskin S. "Molecular Modeling of MOF-based Mixed Matrix Membranes" *Current Organic Chemistry* 18 (18), 2364-2380 (2014).
6. Erucar I., Manz T., Keskin S. "Effects of Electrostatic Interactions on Gas Adsorption and Permeability of MOF Membranes" *Molecular Simulation* 40, 557-570 (2014).
7. Erucar I., Yilmaz G., Keskin S. "Recent Advances in Metal Organic Framework-based Mixed Matrix Membranes" *Chemistry - An Asian Journal* 8, 1692-1704 (2013). (Invited review paper)
8. Erucar I. and Keskin S. "High CO₂ Selectivity of an Amine-Functionalized Metal Organic Framework in Adsorption-based and Membrane-based Gas Separations" *Industrial & Engineering Chemistry Research* 52(9), 3462-3472 (2013).
9. Ulker Z., Erucar I., Keskin S. and Erkey C. "Novel nanostructured composites of silica aerogels with a metal organic framework" *Microporous Mesoporous Materials* 170, 352-358 (2013).
10. Erucar I. and Keskin S. "Computational Screening of Metal Organic Frameworks for Mixed Matrix Membrane Applications" *Journal of Membrane Science* 407-408, 221-230 (2012).
11. Erucar I. and Keskin S. "Screening Metal Organic Framework-based Mixed Matrix Membranes for CO₂/CH₄ Separations" *Industrial & Engineering Chemistry Research* 50(22), 12606-2616 (2011).

12. Erucar, I. and Keskin S. "Separation of CO₂ Mixtures Using Zn(bdc)(ted)_{0.5} Membranes and Composites: A Molecular Simulation Study" *Journal of Physical Chemistry C* 15(28), 13637-13644 (2011).
13. Atci E., Erucar I., Keskin S. "Adsorption and Transport of CH₄, CO₂, H₂ Mixtures in a Bio-MOF Material from Molecular Simulations" *Journal of Physical Chemistry C* 115(14), 6833-6840 (2011).

Note: Chapters 4 and 5 published in peer-reviewed journals. (2nd and 4th articles listed above)

The published articles were also used in Chapters 2 and 3.

